NASA/TM–2019-220289

CASPEr: An Approach to Characterize the Performance of Onboard Airplane Energy State and Automation Mode Prediction Functions

Wilfredo Torres-Pomales
Langley Research Center, Hampton, Virginia

July 2019

NASA STI Program . . . in Profile

Since its founding, NASA has been dedicated to the advancement of aeronautics and space science. The NASA scientific and technical information (STI) program plays a key part in helping NASA maintain this important role.

The NASA STI program operates under the auspices of the Agency Chief Information Officer. It collects, organizes, provides for archiving, and disseminates NASA's STI. The NASA STI program provides access to the NTRS Registered and its public interface, the NASA Technical Reports Server, thus providing one of the largest collections of aeronautical and space science STI in the world. Results are published in both non-NASA channels and by NASA in the NASA STI Report Series, which includes the following report types:

- TECHNICAL PUBLICATION. Reports of completed research or a major significant phase of research that present the results of NASA Programs and include extensive data or theoretical analysis. Includes compilations of significant scientific and technical data and information deemed to be of continuing reference value. NASA counter-part of peer-reviewed formal professional papers but has less stringent limitations on manuscript length and extent of graphic presentations.

- TECHNICAL MEMORANDUM. Scientific and technical findings that are preliminary or of specialized interest, e.g., quick release reports, working papers, and bibliographies that contain minimal annotation. Does not contain extensive analysis.

- CONTRACTOR REPORT. Scientific and technical findings by NASA-sponsored contractors and grantees.

- CONFERENCE PUBLICATION. Collected papers from scientific and technical conferences, symposia, seminars, or other meetings sponsored or co-sponsored by NASA.

- SPECIAL PUBLICATION. Scientific, technical, or historical information from NASA programs, projects, and missions, often concerned with subjects having substantial public interest.

- TECHNICAL TRANSLATION. English-language translations of foreign scientific and technical material pertinent to NASA's mission.

Specialized services also include organizing and publishing research results, distributing specialized research announcements and feeds, providing information desk and personal search support, and enabling data exchange services.

For more information about the NASA STI program, see the following:

- Access the NASA STI program home page at http://www.sti.nasa.gov

- E-mail your question to help@sti.nasa.gov

- Phone the NASA STI Information Desk at 757-864-9658

- Write to:
  NASA STI Information Desk
  Mail Stop 148
  NASA Langley Research Center
  Hampton, VA 23681-2199

NASA/TM–2019-220289

CASPEr: An Approach to Characterize the Performance of Onboard Airplane Energy State and Automation Mode Prediction Functions

Wilfredo Torres-Pomales
Langley Research Center, Hampton, Virginia

National Aeronautics and
Space Administration

Langley Research Center
Hampton, Virginia 23681-2199

July 2019

Acknowledgments

The work presented in this report was supported by the Technologies for Airplane State Awareness (TASA) Project under the Airspace Operations and Safety Program (AOSP) of the Aeronautics Research Mission Directorate (ARMD). I would like to express my gratitude to Dr. Steve Young, who posed the challenge that motivated this work and has continued to support it with technical guidance and funding. Michael M. Madden and James R. Barnes were involved in the initial planning of CASPEr-1 and provided valuable guidance and information about the prediction functions, terminal area operations, cockpit avionics and procedures, and the simulation infrastructure available to implement the test plan. Paul C. Sugden was in charge of implementing the test plan; his comments, questions, and suggestions were critical in refining the test plan and ensuring a successful implementation. Laura J. Smith and Yamira Santiago-Espada have contributed to the planning, data analysis, and the development of an assessment approach for airplane state and automation mode prediction functions. I am appreciative of everyone who has made possible the work described herein.

Available from:

NASA STI Program / Mail Stop 148
NASA Langley Research Center
Hampton, VA 23681-2199
Fax: 757-864-6500

Abstract

The Commercial Aviation Safety Team (CAST) has identified a set of safety enhancements to mitigate the risks of loss of control in-flight (LOC-I) accidents and incidents involving commercial transport airplanes. In support of this, NASA has been developing technologies intended to enhance flight crew awareness of airplane systems, attitude, and energy state. This report describes preliminary ideas for a methodology to assess the goodness of onboard airplane energy state and automation mode prediction functions. The methodology is intended to contribute to the goal of moving these prediction technologies to the readiness level required for transition to industry and reduce the technology certification risks. In addition, this report describes a simulation-based approach named CASPEr (Characterization of Airplane State Prediction Error) to characterize the performance of these predictive functions over a wide range of operational conditions. The first exploratory version of this approach is described. The bulk of the report documents the initial results of tests to characterize the performance of an airplane trajectory prediction function. Future reports will give additional performance characterization results for this function and a complete description of the proposed methodology to assess such functions.

Table of Contents

Acronyms and Abbreviations

3D	Three Dimensions
4D	Four Dimensions
absMax	Maximum Absolute Value (same as maxAbs)
AFS	Auto-Flight System
AIME	Automation and Information Management Experiment
AP	Auto-Pilot
AT	Auto-Throttle
ATC	Air Traffic Control
CAS	Calibrated Airspeed
CASPEr	Characterization of Airplane State Prediction Error
CAST	Commercial Aviation Safety Team
CDU	Control Display Unit
DOE	Design Of Experiments
EICAS	Engine Indicating and Crew Alerting System
FAA	Federal Aviation Administration
FAF	Final Approach Fix
FMC	Flight Management Computer
FMS	Flight Management System
HITL	Human In The Loop
IAF	Initial Approach Fix
IAS	Indicated Airspeed
IC	Initial Conditions
IQR	Inter-Quartile Range
KMEM	Memphis International Airport
Kt	Knots
LOC-I	Loss Of Control In-flight
maxAbs	Maximum Absolute Value
MCP	Mode Control Panel
MHP/PAE	Multiple Hypothesis Prediction function with Predictive Alerting
NaN	Not A Number
ND	Navigation Display
RMS	Root Mean Square
RMSE	Root-Mean-Square Error
RW	Runway (same as RWY)
RWY	Runway
SA	Sensitivity Analysis
SE	Safety Enhancement
STAR	Standard Terminal Arrival Route
TAS	True Airspeed
TFMS	Tactical Flight Management System
TOD	Top Of Descent
TP	Trajectory Prediction
TPS	Trajectory Prediction System
TRL	Technology Readiness Level
UQ	Uncertainty Quantification
VSD	Vertical Situation Display

1. Background

In 2010 the Commercial Aviation Safety Team (CAST) sponsored a study to analyze a set of loss of control in flight (LOC-I) accidents and incidents involving commercial transport airplanes in which the flight crew lost awareness of the airplane's state (i.e., attitude and energy) [1] [2]. This study identified recurring themes in the analyzed LOC-I events and suggested a number of wide ranging intervention strategies to mitigate the risks associated with the identified problems. Among the identified interventions were changes to current and future aircraft designs in areas such as flight envelope protection, improved alerting, automation design, and energy state management display and prediction systems.

Subsequent analysis and assessment activities by CAST yielded a set of specific safety enhancement (SE) recommendations and detailed implementation plans. The SE recommendations included research and development (R&D) in technologies that address open issues in areas such as alerting, distraction, automation confusion, and system knowledge. Of these, R&D SE 207 and 208 are intended to enhance flight crew awareness of airplane systems, attitude, and energy state [3] [4].

NASA R&D activities related to SE 207 and 208 include high-fidelity human-in-the-loop (HITL) simulation experiments to address or achieve outputs defined by CAST:

- SE-207, Output 3: Systems that predict the future aircraft energy state and/or autoflight configuration if the current course of action is continued, and provide appropriate alerting [3]
- SE-208, Output 1a: Displays that present in an intuitive manner the current and future state of automated systems [4]
- SE-208, Output 1b: Displays that present in an intuitive manner the aircraft flight-critical data systems in use by autoflight system, flight control laws, and primary instruments [4]

These R&D experiments, called AIME (Automation and Information Management Experiment), are intended to raise the technology readiness level (TRL) for selected new technologies, discover design characteristics requiring refinement, and assess their usability [5]. The technologies being evaluated include, among others, a Trajectory Prediction function (TP) [6] [7] and a Multiple Hypothesis Prediction function with Predictive Alerting (MHP/PAE) [8]. These technologies provide information to the flight crew on the cockpit Navigation Display (ND), the Vertical Situation Display (VSD), the Engine Indicating and Crew Alerting System (EICAS), and a Synoptics display.

2. Problem

The work presented in this report was motivated by the question of how to assess the "goodness" of airplane energy state prediction and alerting functions such as TP and MHP/PAE. We are interested in a general approach to assess such functions, and we want to demonstrate the application of the approach to these particular functions. The assessment approach should be comprehensive, objective, and feasible. Given that these technologies are part of CAST-proposed design SEs for commercial transport airplanes, the assessment approach should contribute to the R&D goals of moving the technology to the readiness level required for transition to industry and reduce the technology certification risks.

There are additional considerations in the development of this technology assessment approach.

- The "goodness" of the airplane energy state prediction and alerting functions refers to the fitness or suitability of these functions for their intended purpose, which is to reduce the risk of accidents and incident by enhancing the situational awareness of the flight crew [9], in particular awareness of the airplane energy state and automation mode, in commercial transport airplanes. Figure 1 illustrates an abstract model of situation awareness in context.

- These state prediction and alerting functions are sources of information to contribute to the situational awareness of the crew in flight. Data quality parameters such as accuracy, resolution, assurance, traceability, timeliness, completeness, and format, as defined in aviation standard DO-200B [10], are relevant to the assessment of these functions.

- It is expected that the operational envelope of these airplane energy state prediction and alerting functions covers the full envelope of airplane performance and automation capabilities. This is a large multi-dimensional space that needs to be explored. As a result, the definition of scenarios may be one of the more complex aspects of an assessment.

- As these are cockpit technologies, they have two major aspects: the "softer" (i.e., more qualitative and subjective) human factors in the interaction between the functions and the flight crew, and the "harder" (i.e., more quantitative and objective) technical design of the functions. AIME [5] and other HITL experiments [6] [7] are the main sources of data to evaluate the human-factors aspect of these technologies.

- Based on a brief high-level safety analysis [11] [12], it is expected that for these prediction and alerting functions a "loss of function" failure condition in flight would be classified as "minor" severity, in part because there should be alternative data sources available to the flight crew.

However, a "misleading or malfunction without warning" failure condition could have effects of higher severity (i.e., "major" or higher).

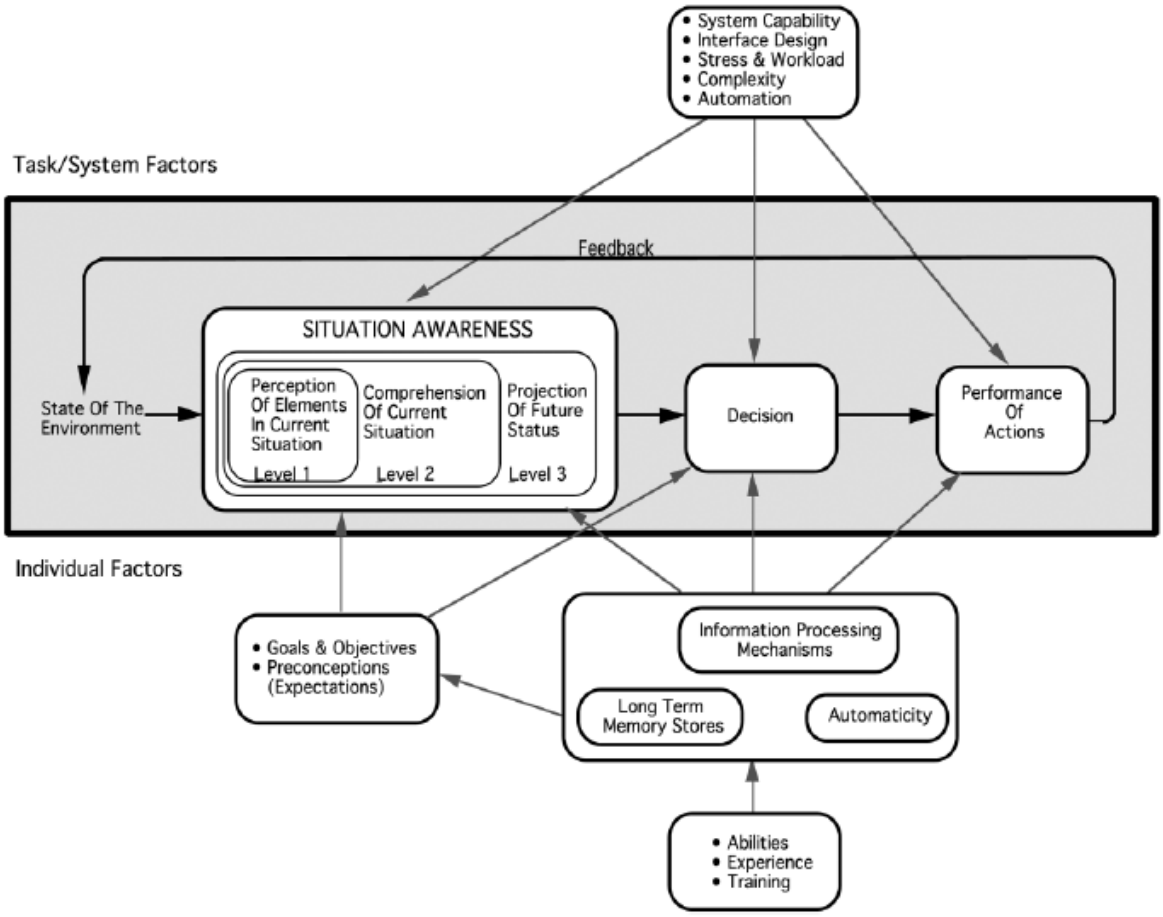

Figure 1: High-Level Model of Situational Awareness [9]

- As these are predictive functions, their assessment should be based, to the extent possible, on quantitative measures of performance, especially the accuracy of the predictions and the rates of false positive and false negative alerting.
- The development of the assessment approach should consider that the primary purpose is independent assessment of the technologies, rather than being an integral part of their design process. The assessment should generate data and provide insights about how good the functions are for their intended purpose and operational context, but the approach and its results may not necessarily be adequate to troubleshoot undesired behavior of the functions.

- These technologies are implemented in software intended to run on existing avionics systems. Standard software test, evaluation, and assurance approaches should be considered. Aviation standards for software approval, such as DO-178 [13], are relevant to the assessment of these technologies.

- These technologies are under development and it is expected that they will require multiple cycles of refinement and parameter tuning before they are sufficiently mature to transition to industry. Likewise, the technologies will have to be assessed repeatedly during their development. The cost and complexity of the assessment approach itself are important considerations.

Taking all this into considerations, we can identify four broad aspects of the technology that should be part of an assessment:

- **Capability**: This is the ability to perform or achieve certain actions or outcomes. This is the function (or behavior) and performance (e.g., accuracy, timeliness, resolution) of the state prediction and alerting functions.

- **Dependability**: From a computing perspective, this the ability to deliver service that can justifiably be trusted; or alternatively, it is defined as the ability to avoid service failures that are more frequent or more severe than is acceptable [14]. The relevant threats to dependable service are unintentional events and actions. This concept encompasses the attributes of:

    - **Integrity**: delivery of proper or correct service;

    - **Reliability**: perform a required function under specified conditions, without failure, for a specified period of time;

    - **Availability**: readiness for correct service at any given point in time; and

    - **Safety**: acceptable risk (i.e., combination of severity and frequency) of harm to people or property.

- **Security**: This encompasses the attributes of integrity, availability, and confidentiality (i.e., absence of unauthorized disclosure) [14]. The relevant threats to secure service are intentional events and actions.

- **Assurance**: This is related to the confidence and evidence that requirements are satisfied, and is defined as the planned and systematic actions necessary to provide adequate confidence and evidence that a product or process satisfies given requirements [12].

All of these aspects are important to the development of the state prediction and alerting technologies, especially as the readiness level advances and the focus shifts toward handoff to industry and implementation in the context of transport aircraft and system development. The development of a comprehensive approach to assess the goodness of the state prediction and alerting technologies is ongoing and it is expected that the assessment will leverage relevant existing standards and recommended practices. The proposed assessment approach will be documented in a future report.

Given that these state prediction and alerting technologies are currently at low to medium readiness level, the immediate focus should be on assessing the performance and integrity of the predictive functions over a wide range of conditions. Thus, the near-term problem of interest is the evaluation of performance over selected operational scenarios. The following section describes a concept for these performance evaluations.

3. CASPEr: Concept

Figure 2 on the next page illustrates the concept for the chosen simulation-based approach to test and analyze the performance of the predictive functions. The concept is called the Characterization of Airplane State Prediction Error (CASPEr). This concept leverages the high-fidelity simulation infrastructure developed for the AIME experiments, but it uses a software model of pilot behavior rather than a real pilot, thus eliminating some of the limitations and cost of human-in-the-lop (HITL) experiments. However, this simulation-based approach is intended to complement rather than supplant HITL experiments as the Pilot Software Model cannot fully capture the complexity of real pilot behavior. The proposed approach enables high observability and controllability of the test conditions, flexibility to configure and evolve the simulation capability as needed, and the possibility of faster-than-real-time simulations, which enables the collection of large amounts of performance data.

The major elements of CASPEr are the Definition of Scenarios, the Simulation, the Prediction Performance Analysis, and the generation of a Prediction Performance Report. As in AIME, the simulation is based on a high-fidelity model of a commercial transport airplane. As mentioned in the previous section, it is assumed that the operating envelope of the predictive functions covers the full envelope of airplane performance and automation capability. Automation here refers primarily to the Flight Management System (FMS) and the Auto-Flight System (AFS). The central element of the FMS is the Flight Management Computer (FMC) with its Control Display Unit (CDU) interface. The AFS

consists of the Auto-Pilot (AP) and the Auto-Throttle (AT) with the Mode Control Panel (MCP) interface. The Pilot Behavior Model interacts with both the FMS and the AFS as needed for the defined scenarios.

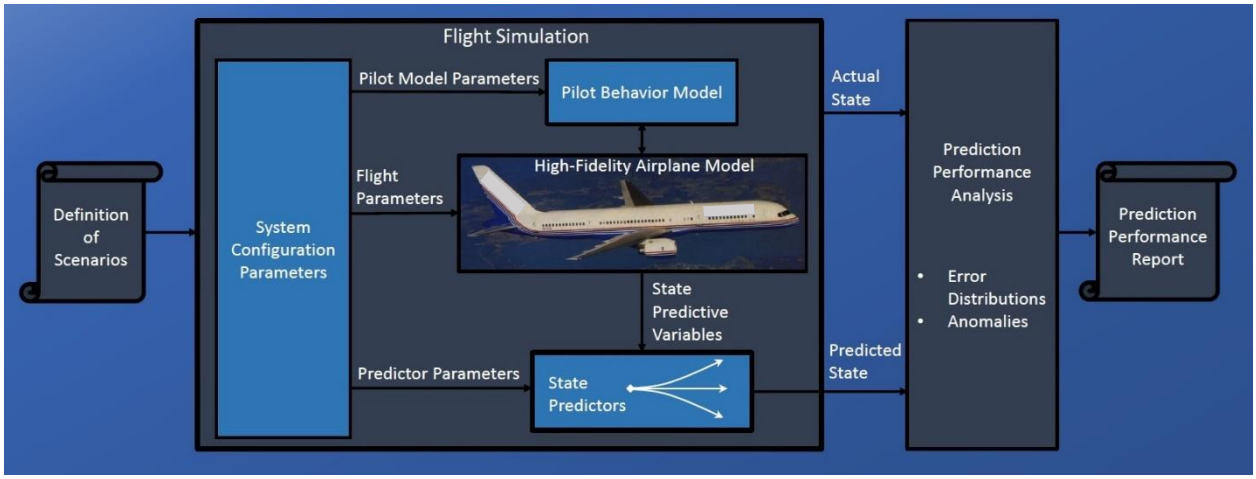

Figure 2: High-Level Concept Graphic for Prediction Performance Evaluation

The CASPEr concept reflects the view that, although the predictive functions are implemented in software, their performance characterization can be more meaningful and effective if based on operation-level scenarios. Unit tests are necessary and useful during design, but the definition of test scenarios at the unit level and the analysis of coverage and representativeness for inputs and output effects may be complex and based on dependency abstractions and judgments which are difficult to assess. An operation-level approach inherently generates valid inputs and propagates output effects. This approach can effectively leverage existing domain expertise to define test scenarios, analyze performance, and interpret results.

The TP function predicts the airplane 4D path and the automation mode. The airplane translational motion state consists of its 3D position (latitude, longitude, and altitude) and speed. The rotational state of the airplane (pitch, roll, and yaw) is not an output of this system, although a maneuver envelope technology was tested in an earlier iteration of the AIME experiments [5]. The airplane energy management issues that motivate this work are related primarily to translational energy (i.e., potential and kinetic energy), not rotational energy. Taking this into consideration and the fact that the automation mode has a causal relation to the airplane translational state, in CASPEr we are interested mainly in the translational state of the airplane, with the automation mode being of interest as a way to understand and explain observed translational state (i.e., trajectory) predictions.

The output in CASPEr is an analysis of performance and behavior for the predictive functions. The main performance criterion is accuracy in the prediction of airplane energy state and automation mode. Accuracy is measured in terms of distribution statistics for the prediction error, which is the difference

between the predicted state and the observed state of the airplane. The behavior of the prediction functions is also of interest, as attributes such as frequency of invalid outputs (in some sense) and missed output updates reflect on the quality of the software implementation and how much it can be trusted. In CASPEr, the goodness of the predictive functions has an inverse relation with the prediction error (Figure 3) and also with the frequency and severity of invalid or missing outputs.

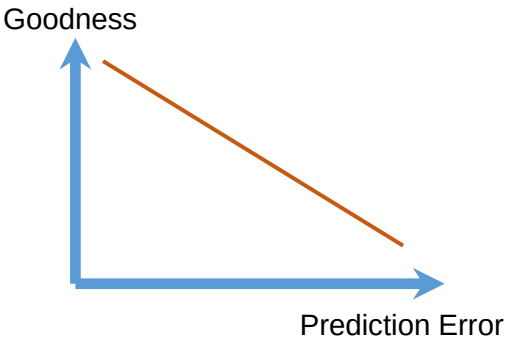

Figure 3: General relation between Goodness and Prediction Error

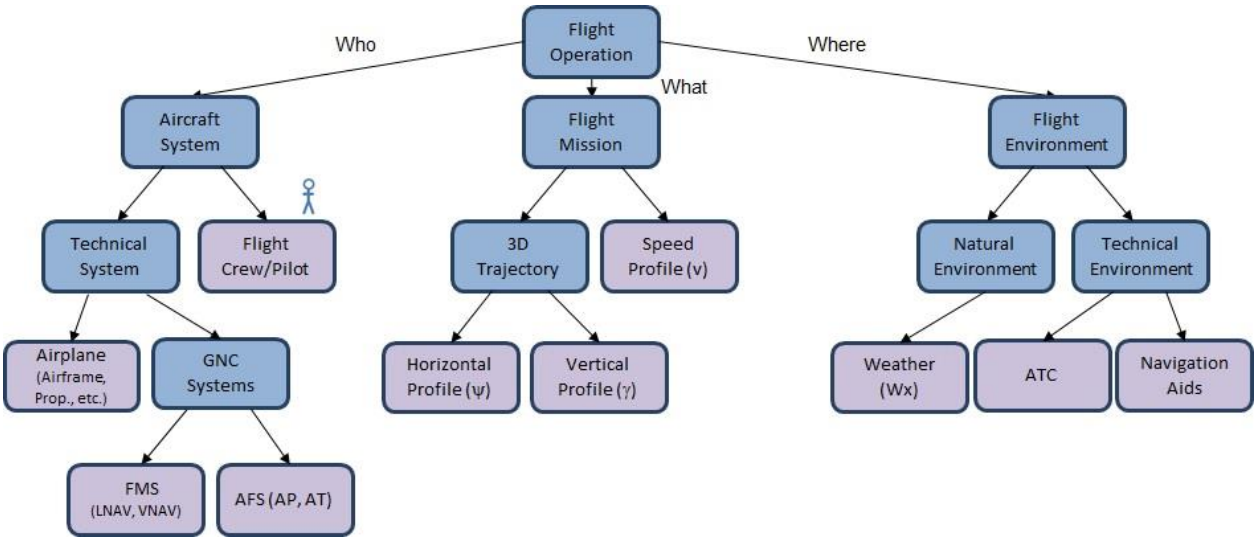

Figure 4: Structural Decomposition of a Flight Operation

Figure 4 illustrates a structural decomposition of a flight operation. The three top level branches capture who is performing the flight operation (i.e., the aircraft system, including the airplane and the flight crew), what the flight mission is (i.e., the trajectory to be flown), and technical and natural environments where the mission is to be carried out. The leaves of this decomposition are the variables (or factors) to be specified in the definition of scenarios. Each of these factors may be decomposed further as needed to properly specify the desired scenarios. Also, there may be relations and

dependencies between the factors. These relations may be traceable to aspects such as airplane performance and limitations, automation capability, and safety constraints. An operation-level definition of scenarios enables to easily capture such relations.

Figure 5 is a simple illustration of the operation of the airplane under the control of the (simulated) pilot and the automation. The state history of the airplane is influenced by the performance of the vehicle, the natural environment in which it is operating, the characteristics of the navigation aids in the operating environment, the performance of the sensors on the airplane, the capabilities of the automation (FMS, AP, and AT), and the inputs from the pilot. The pilot is responsible for programming the desired flight trajectory into the FMS and selecting appropriate flight modes and targets for the AP and AT. The pilot is also responsible for controlling the deployment of wing flaps and extending or retracting the landing gear. Strategic trajectory settings are entered in the FMS through the CDU, and tactical trajectory selections are made in the MCP. Such tactical pilot inputs (or interventions) can simulate air traffic control (ATC) clearances for route, heading, altitude, and speed.

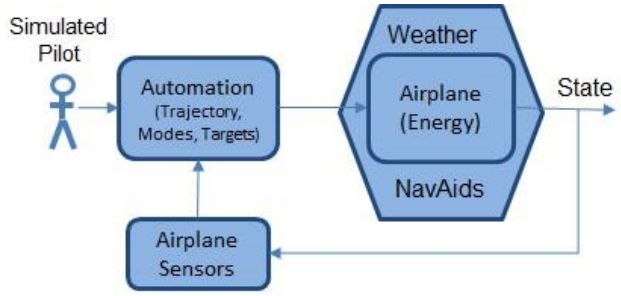

Figure 5: Simple Abstract Closed-Loop Model of Airplane Operation

The CASPEr approach enables high-fidelity simulation experiments for uncertainty quantification (UQ) and sensitivity analysis (SA) [15] of prediction performance over a large scenario space. Design of experiments (DOE) theory [16] can be used in the definition of scenarios as combinations of flight operation variables. With this simulation-based approach it is easy to set the parameters of dynamic random variables (for example, wind gusts and pilot reaction time) and also manipulate parameters of variables that are constant for a given flight operation but can vary between flight operations (for example, airplane weight and wind speed and direction).

4. CASPEr-1

CASPEr-1 is the first application of the CASPEr approach for performance evaluation of the predictive technologies with fully automated high-fidelity flight simulations. The goal of CASPEr-1 is an

initial evaluation of performance and anomalous behavior for the predictive functions operating under different types of conditions. Here we only tested the performance of the TP function for airplane state prediction. The PAE alerting function will be tested in future simulation experiments. All the flight operations were in the Memphis International Airport (code KMEM) terminal airspace flying published arrival routes (STAR, Standard Terminal Arrival Route) and approaches to selected runways. Airport information and instrument flight procedures for KMEM are publically available from the FAA [17].

4.1. Airport: Memphis International Airport (KMEM)

Figure 6 on the next page shows the layout of the airport, including the runways. The airport elevation is around 340 feet. KMEM was the airport used in the first AIME HITL experiment [5], so selecting KMEM for CASPEr-1 helped to maximize reuse of the simulation infrastructure developed for AIME and to minimize the cost and uncertainties of programming and simulating terminal area operations.

4.1.1. Runways

The runway layout at KMEM enables landing in each cardinal point direction. The airport has four runways, each with two landing directions. Figure 7 shows the selected runways for CASPEr-1. The north direction is up in this figure. The red markers are waypoints marking the locations of the landing ends of the runways. The landing directions for runways 09, 18C, 27, and 36C are east (heading of 90 degrees), south (180 degrees), west (270 degrees), and north (360 degrees), respectively.

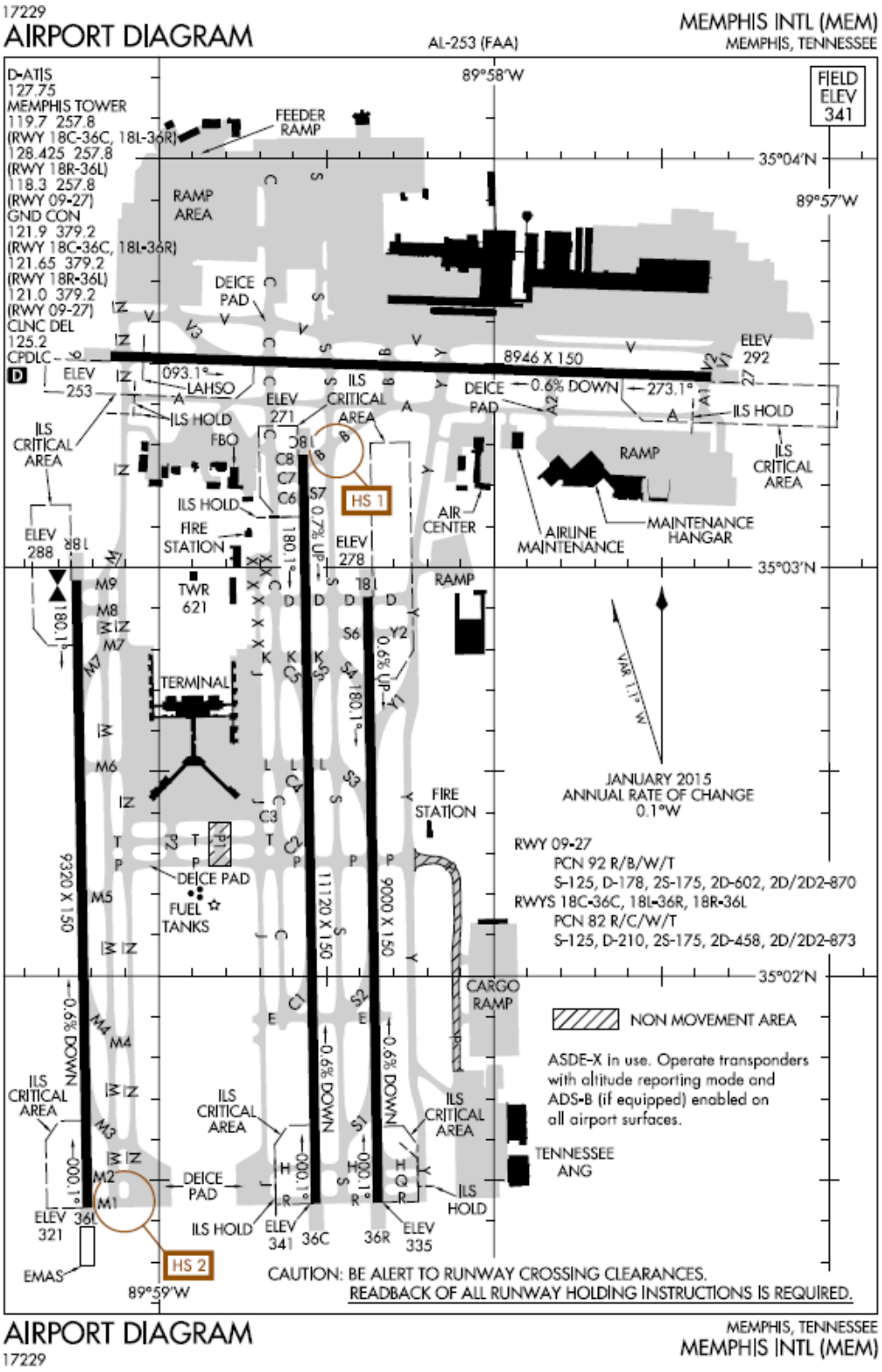

Figure 6: Airport Diagram for Memphis International Airport (KMEM)

Figure 7: Selected Runways at KMEM

4.1.2. Arrival Routes

Seven STAR procedures were chosen for CASPEr-1. These were divided into two groups based on the direction from which the airplane arrives at the airport. Corner-point STARs named BLUZZ, VANZE, HOBRK, and BRBBQ, as shown in Figure 8, arrive from "corner" directions: northeast, southeast, southwest, and northwest. Cardinal-point STARs, shown in Figure 9, arrive from cardinal point directions: west, north, and east. The cardinal-point STARs are CONDR, HYTHR, and MONAA.

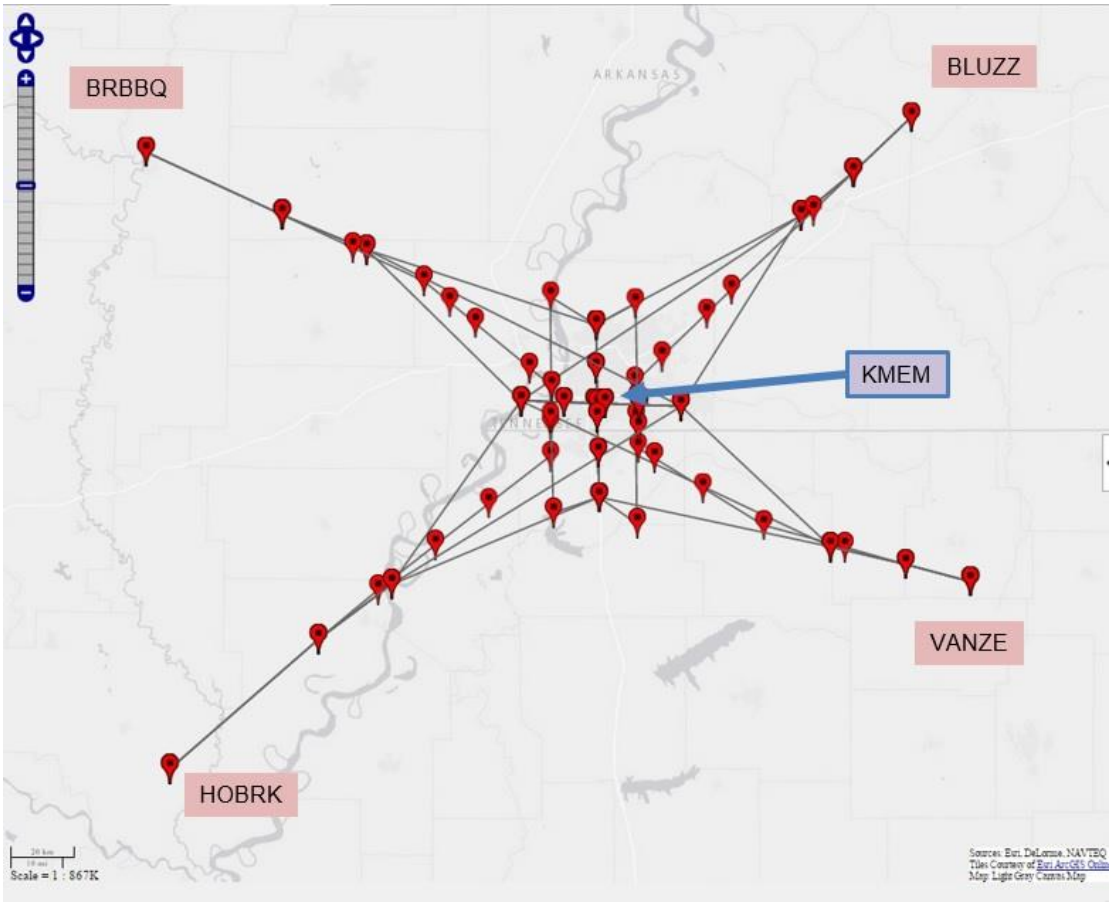

Figure 8: Selected Corner-Point STARs at KMEM

It is possible to reach any of the four runways from any of the seven arrival routes. This gives a total of twenty-eight STAR-and-Runway combinations available for testing. The chosen set of STAR-and-Runway combination routes has both variety, which can be leveraged to test and explore a significant range of flight conditions, and also structure and symmetry, which can be used to compare and contrast routes in terms of their effects on predictive function performance and behavior. This enables testing to determine whether the landing direction alone or in combination with other factors has a significant effect on the performance and behavior of the prediction function.

Additional information about the arrival routes and runways is given in Appendix B.

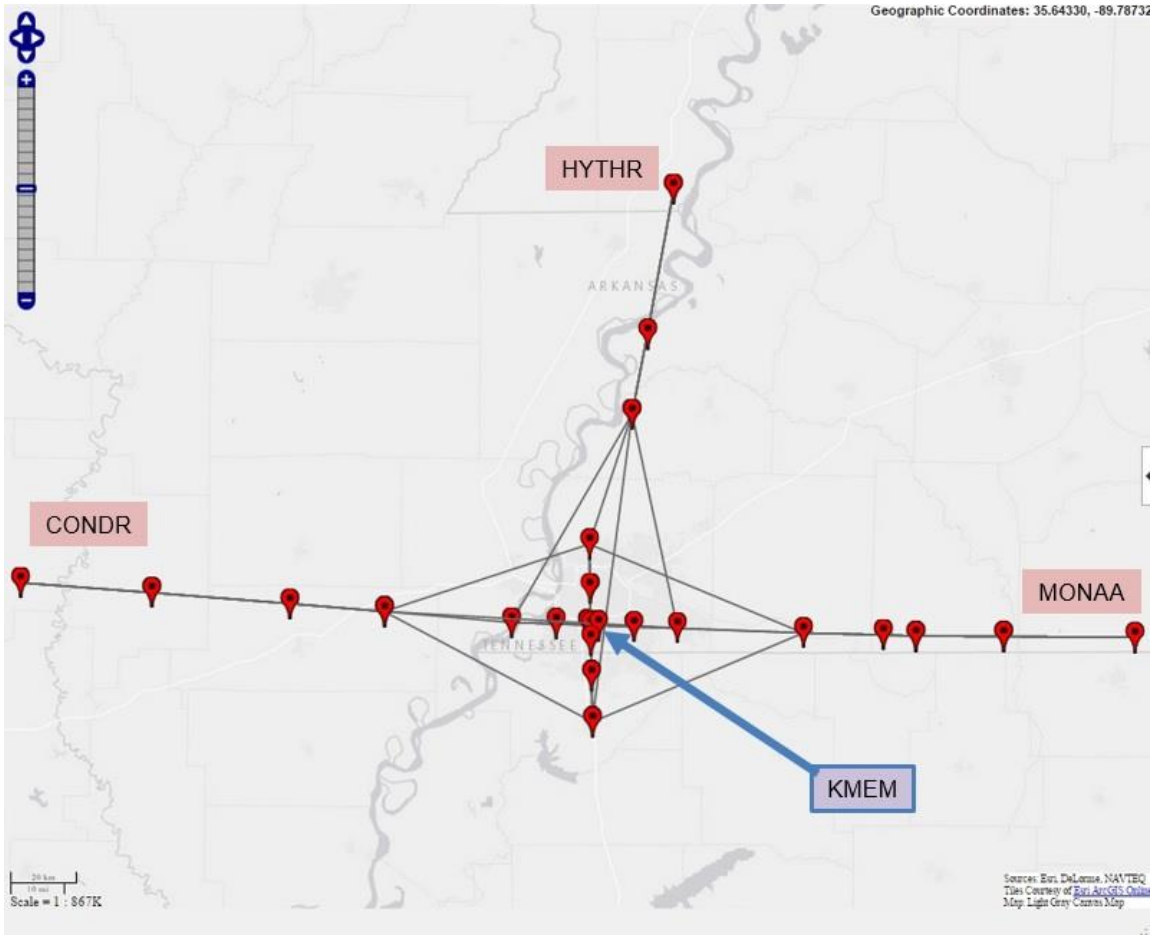

Figure 9: Selected Cardinal-Point STARs at KMEM

4.2. Performance Metrics

The goal of CASPEr-1 is to evaluate the performance of the TP prediction function. The predicted airplane state of primary interest is the translational state, which includes the horizontal position and the energy state. The prediction of automation mode is of secondary interest as a means to understand and explain observed translational state predictions. However, CASPEr is not intended as a means to diagnose the performance of the prediction function, which would require a more granular decomposition of operational factors and deep insight into the input-output relations and internal behavior of the prediction function. Instead, we are interested in the relation between the flight operation factors and the performance of the prediction function.

The translational state variables of the airplane include the horizontal position given in terms of latitude and longitude, and the energy state given in terms of altitude, airspeed, and total energy. The unit

of measure for latitude and longitude is degrees (deg or °); for altitude the unit is feet (ft); airspeed is measured in knots (kt). The predicted airspeed is the indicated airspeed V_{IAS}, which is the speed indicated by the pressure-based speed measuring instruments on the airplane and is used in communications between pilots and air traffic controllers [18]. The calibrated airspeed V_{CAS} is the airspeed corrected for instrument and altitude measurement errors. The true airspeed V_{TAS} is the actual speed of the airplane relative to undisturbed air. V_{CAS} and V_{TAS} are related by a complex mathematical relation with parameters of air density, pressure, and temperature. In the simulation environment used for CASPEr, V_{IAS} and V_{CAS} are equal since instrument and altitude measurement errors are not modeled.

The total translational energy of the airplane (denoted E_{Total}) is equal to the potential energy (E_P) plus the kinetic energy (E_K):

$$E_{Total} = E_P + E_K = m_a g h + m v_{TAS}^2/2$$

where m_a denotes the mass of the airplane, g denotes the gravitational acceleration (in m/s^2), h denotes the altitude (in m), and v_{TAS} denotes the true airspeed (in m/s) [19]. The specific energy, or energy height, of the airplane is given by:

$$H_e = E_{Total}/w = h + v_{TAS}^2/2g$$

where w = mg, the weight of the airplane. H_e is an altitude-equivalent measure of energy and it has units of distance, given in meters or converted to feet. The energy height is used here as a single measure of energy that combines both altitude and airspeed.

From a computing perspective, the prediction function provides a real-time service to other entities, either computing functions or the flight crew, that depend on its output. This service consists of a sequence of (service) items, each characterized by a value (or content) and a time of generation [14], which are required to satisfy specified real-time timing constraints such as the update rate (or update period) . The behavior of the prediction function is its sequence of outputs in time [20].

For CASPEr-1, the update rate for the TP prediction function is 1 Hz. The output of interest at time t (i.e., the service item at time t) consists of the predicted values of airplane state variables for look-ahead times τ ranging from 0 to 299 seconds (i.e., almost 5 minutes). Let $x_{Pred}(t, \tau)$ denote the predicted value of state variable x generated at time t for look-ahead time τ, i.e., the predicted value of the state for time t + τ. Since the predicted airplane state variables are real-valued, we can measure prediction performance based on the following simple definitions of absolute and relative prediction errors at time t for look-ahead τ:

$$e_{Pred,Abs}(t, \tau) = x_{Pred}(t, \tau) - x_{Obs}(t + \tau)$$

$$e_{Pred,Rel}(t, \tau) = [x_{Pred}(t, \tau) - x_{Obs}(t + \tau)]/x_{Obs}(t + \tau)$$

where x_{Pred} and x_{Obs} denote predicted and observed state values, respectively. Notice that for each observed state variable x at real-time T, i.e., $x_{Obs}(T)$, the prediction function generates 300 predictions starting with the predicted state value at time t = T – 299 (i.e., $\tau = 299$) until time t = T (i.e., $\tau = 0$) when the output is an estimate of the current state.

A simulated test flight generates a sequence of prediction errors for each airplane state variable which are auto-correlated, rather than independent random samples, as these errors are based on predictive models of a physical system (i.e., the airplane). This implies that the prediction performance analysis should not be based on statistical measures intended for independent sample sets if such measures could be misleading. Instead the prediction errors are viewed as time-sampled signals or time series and applied conventional measures for signal characteristics. Let L denote the number of outputs (i.e., service items) generated by the prediction function during a simulated flight, where each service item consists of a vector of 300 prediction values (one for each look-ahead time) for each predicted state variable. As an example, for a simulated flight of 15 minutes, there are 15 min x 60 sec/min x 300 predictions/sec = 270,000 prediction error data values for each predicted state variable. Conventional measures of central tendency (e.g., mean and median) and dispersion (e.g., standard deviation, root-mean-square-error RMSE, inter-quartile range, min-max range) are applied to these large error data sets. Plots and other data visualizations are also used to make observations about the performance and behavior of the prediction function.

4.3. Test Plan

The simulated flight scenarios were specified with various assumptions and restrictions intended to bound the test space and ensure favorable conditions for post-flight analyses.

- For all the flights in CASPEr-1, the airplane is initially positioned on a selected STAR and the FMC is in control of lateral navigation.
- The normal initial values for the energy-related variables of altitude, airspeed, and weight are 15,000 ft, 280 kt, and 187,500 lbs, respectively.
- The airplane weight can vary from 150,000 to 225,000 lbs.
- The wind speed at ground level can vary from 0 to 25 knots. The wind gradient is linear and can vary from 0 to 5 kt per 1,000 ft. such that the maximum wind speed at 15,000 ft. is 100 kt. The

gusts can vary from 0 to 2 kt RMS at ground level with a gradient such that the maximum gusts are 6 kt RMS at 15,000 ft.

- The airplane always flies an initial level segment long enough such that the airplane flies at least 5 minutes before reaching the top-of-descent (TOD) point, whose precise location is computed by the FMC. This ensures that the predictions for the largest look-ahead time of 5 minutes cover the transition from level flight to descent starting at TOD.
- The initial along-track distance is not specified and instead the airplane is set back on the STAR to a position that accounts for the specified initial altitude and the initial level flight segment. For long STAR routes that guide the airplane down to around 3,000 ft. altitude, the initial airplane position was about 55 nautical miles from the end of the STAR.
- A typical flight lasted around 26 minutes from the initial position on a STAR with initial speed of 280 kt and continuing until reaching 400 ft. above ground level near the landing end of a runway.
- In all flights cases, the TP function is given the truth state of the airplane instead of the output of the on-board airplane sensors. The TP function has access to the flight plan entered in the FMC and it can also read the AFS modes and targets selected in the MCP.

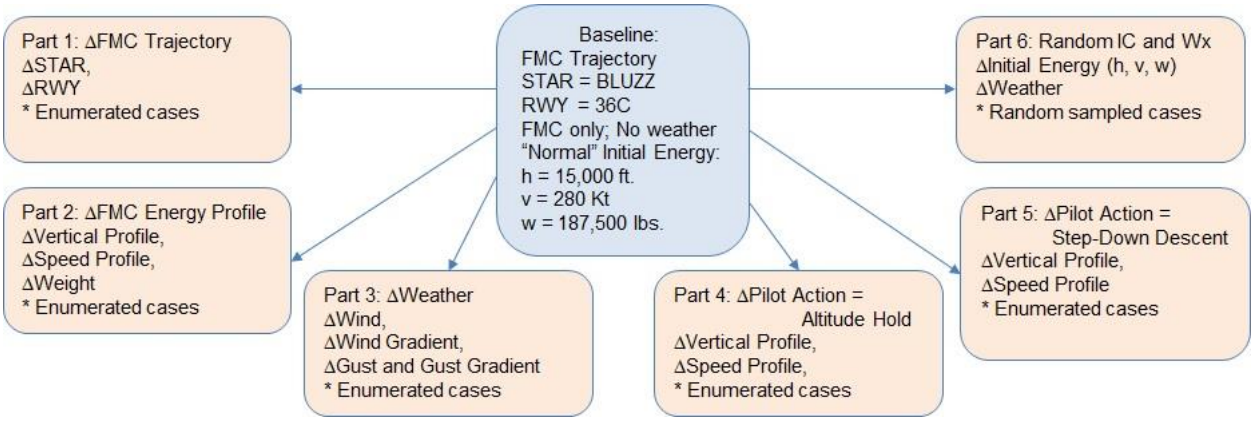

Figure 10: High-Level Breakdown of CASPEr-1 Test Plan

Figure 10 is a breakdown of the test plan for CASPEr-1. The test is designed to enable observation and measurement of the effect of changes in the flight operation factors on the performance of the prediction functions. Because there are no established standards that could be directly applied to assess prediction performance, the test was structured into six parts, each consisting of variations of one or more

factors relative to the conditions of a reference flight designated as the baseline. The chosen baseline flight was a descent on BLUZZ to runway 36C following the published trajectory restrictions for altitude and speed along the route, with normal initial airplane altitude, speed and weight, no wind, and with lateral and vertical navigation and speed controlled by the FMC.

As indicated in Figure 10, in Part 1 the controlled variables are the arrival route and the landing runway. In Part 2, the controlled variables are the airplane weight and the vertical and speed profiles. In Part 3, the wind speed, wind gradient, and gust intensity are varied. The FMC is always in control of the flights in Parts 1, 2, and 3. In Parts 4 and 5, there are pilot interventions in the operation of the automation to implement deviations from the programmed vertical and speed profiles. Specifically, Part 4 implements altitude holds of various durations at a specified altitude, and Part 5 implements a stepdown energy profile where the altitude and speed are reduced in a sequence of two or three steps of various durations. In Parts 1 to 5, the values of the flight operation factors are explicitly enumerated. In contrast, in Part 6, the values for the initial state (i.e., altitude, speed, and weight) and weather (i.e., wind speed, wind gradient, and gusts) are sampled from uniform random variable distributions with specified ranges.

The design of the test plan was influenced by the hypothesis (or conjecture) that the prediction accuracy depends on the look-ahead time and the flight operational condition. It is also expected that the prediction accuracy has an inverse relation with the magnitude, frequency, and complexity (i.e., variety) of flight operation variable changes during a flight. These expectations are motivated in part by the belief that these conditions can activate modelling errors in the prediction function due to approximations and unknown or underappreciated dynamics.

The full text of the CASPEr-1 test plan is given in Appendix A.

5. Baseline Flight: STAR BLUZZ to Runway 36C

The trajectory of arrival route BLUZZ landing north on runway 36C was chosen as the baseline (or reference) flight to simplify relative comparison of performance measures for different flights and conditions. The conditions for this baseline flight include following the published trajectory restrictions for altitude and speed along the waypoint-defined route starting from the normal initial altitude, speed, and weight (see Section 4.3), with no wind, and with the FMC in control of the lateral and vertical navigation and speed. This is a fully automated flight with no pilot intervention under benign weather conditions and a normal airplane energy management profile following the built-in programming of the FMC.

5.1. Specified and Flown Trajectory

Figure 11 shows the horizontal trajectory for arrival route BLUZZ landing north on runway 36C. At this scale, the flown (i.e., actual or observed) trajectory overlaps the planned (or specified) route except for the turn segment shown in the zoom-in inset where the two are clearly visible.

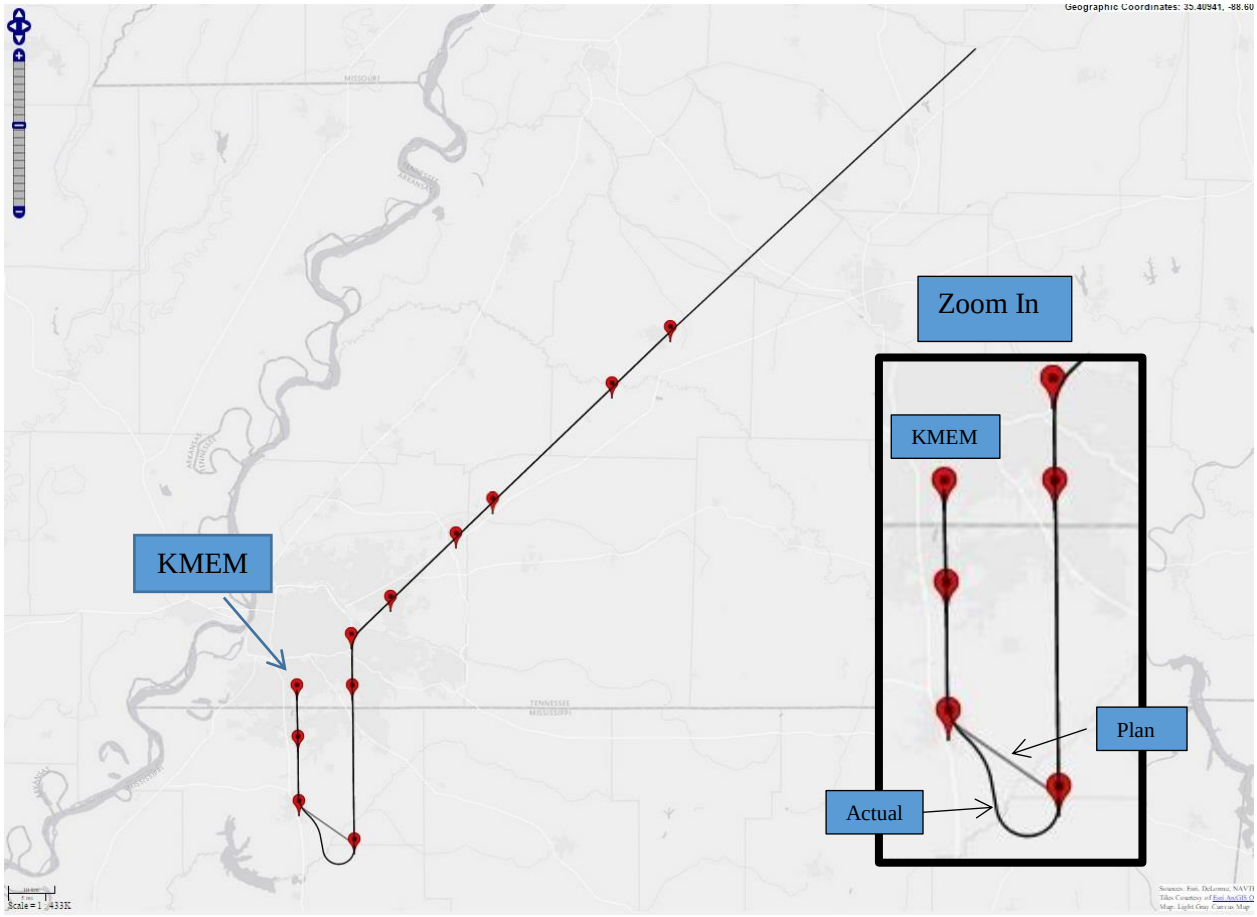

Figure 11: Plan View of Planned and Flown Trajectory for BLUZZ to Runway 36C (Red markers indicate waypoints)

Figure 12 shows the time histories for altitude and airspeed. The black vertical lines indicate the approximate location in time as the airplane flies by the waypoints. The last waypoint marking the location of the runway is not shown in the figure.

Figure 13 shows altitude and airspeed on a Cartesian plane. The black dots in this figure correspond to the approximate location of altitude and speed targets at the waypoints. The figure shows the initial airplane altitude is 15,000 ft. with airspeed of 280 kt. The energy management profile followed by the FMC is a function of the route constraints, airplane performance, and pilot selections such as Cost Index

[21]. All the altitude and speed transitions are related to the waypoints. The airplane reaches the first waypoint of the approach at NESBT at 3,000 ft. and 210 kt. The altitude and speed profile on approach are a function of the airplane weight, which was 187,500 lbs, the midpoint of the weight range. The final altitude and speed are 400 ft. and 130 kt. The simulation ends when the airplane reaches 400 ft. above the runway.

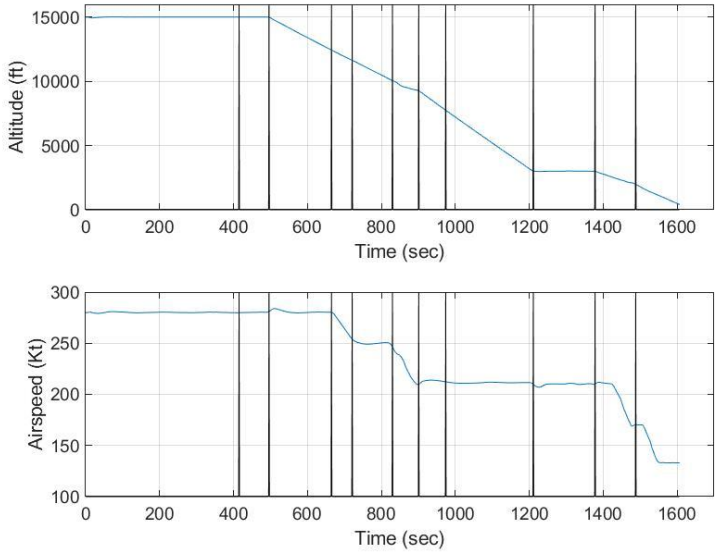

Figure 12: Time history of altitude and airspeed for Trajectory BLUZZ to Runway 36C

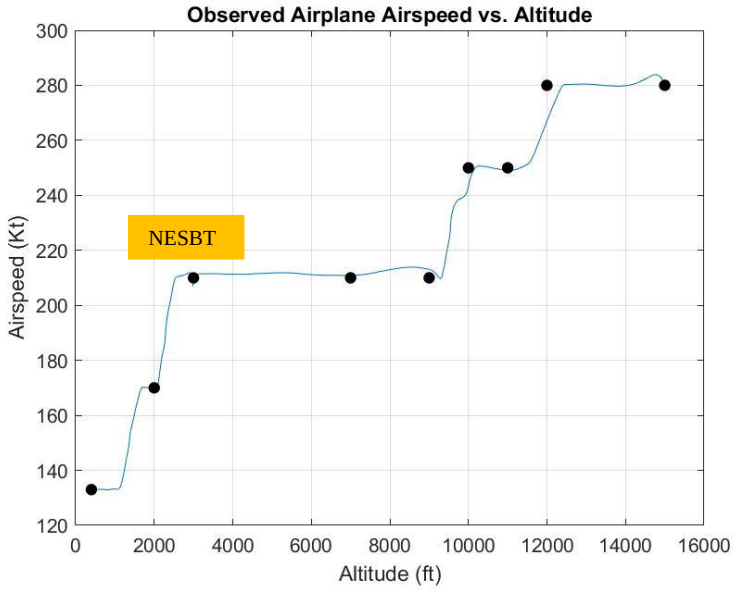

Figure 13: Altitude-vs-Airspeed Profile for Trajectory BLUZZ to Runway 36C

5.2. Predicted Trajectory

This section presents some of the prediction results for the trajectory on BLUZZ to runway 36C.

Figure 14 shows the plan view for the final part of the trajectory. The actual and predicted horizontal trajectories are indicated in the figure. The look-ahead times in seconds for the predictions shown here are $\tau = \{0, 59, 119, 179, 239, 299\}$. In this case, all the predictions are in close agreement, but in the transition segment connecting the end of the STAR at DINKE to the approach at NESBT there is clear discrepancy between the actual flown path and the predicted path.

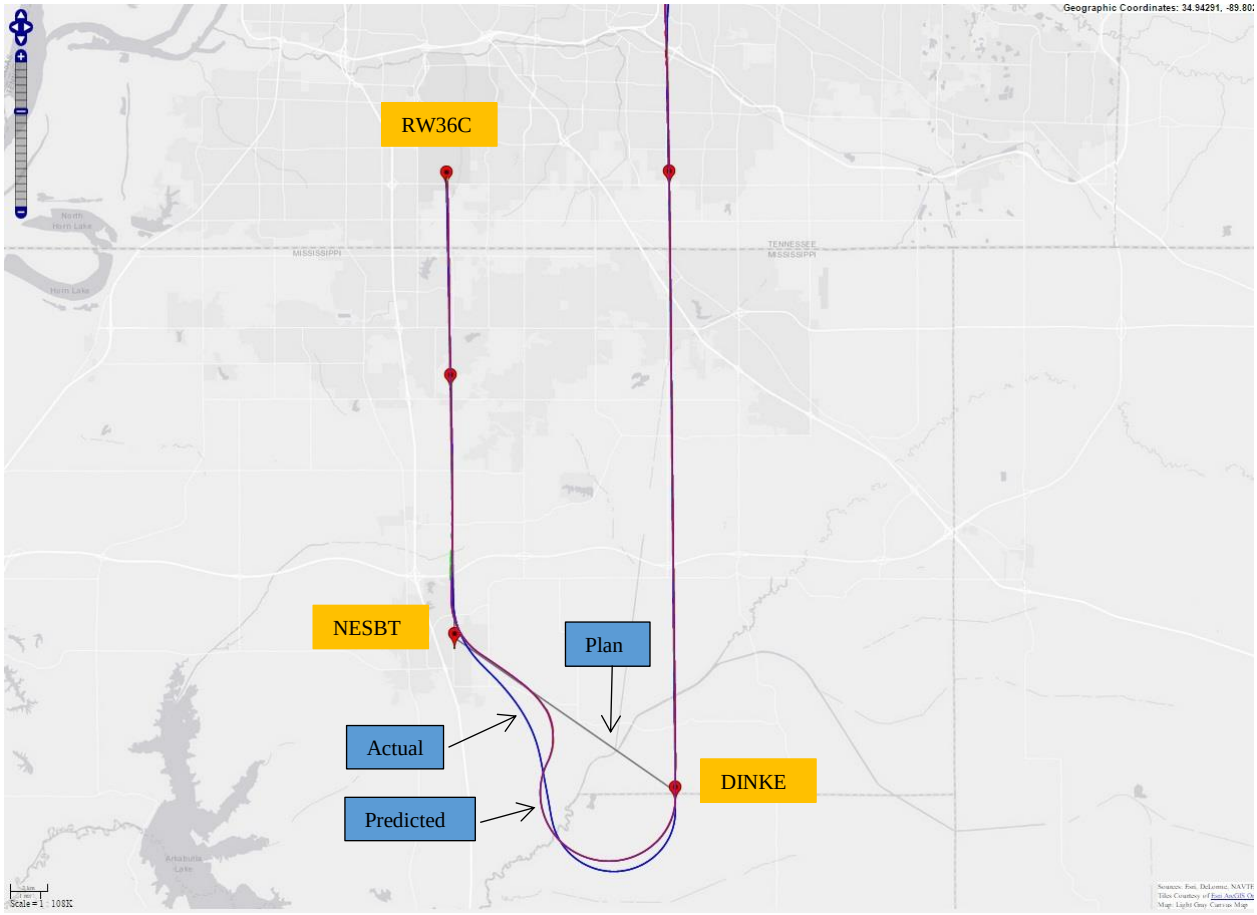

Figure 14: Plan View of Final Portion of Trajectory BLUZZ to Runway 36C

Figure 15, Figure 16, and Figure 17 show the flown trajectory for BLUZZ to runway 36C color coded for altitude, airspeed, and total energy relative prediction error for look-ahead of 299 seconds (i.e., predicting the airplane state almost 5 minutes into the future). The TP prediction function determines itself whether the airplane is in the descent phase, at which point it enables the generation of state

predictions. In the figures, this happens when the approximate location of the airplane is 35.7^0N, 89.2^0W where the path line transitions from gray to blue. The figures show that the relative predictions errors are largest mostly toward the end of the STAR, the transition to the approach, and during most of the approach. The predicted airspeed also has error of about 4% in a portion of the main arrival segment with a track angle of 225 degrees. The magnitude and location of the prediction errors are shown more clearly in Figure 18 and Figure 21.

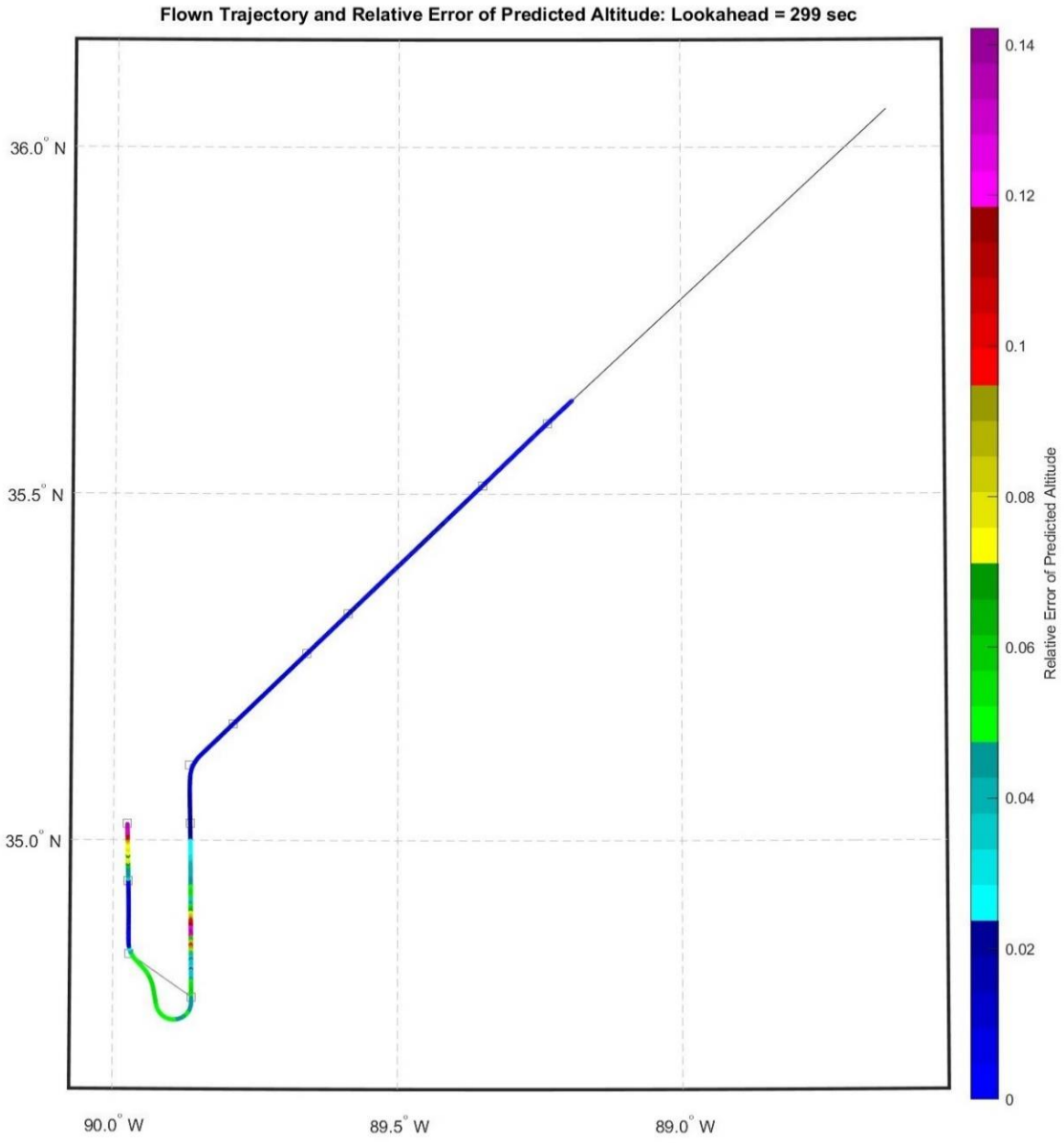

Figure 15: Plan View for BLUZZ to Runway 36C Color Coded for Relative Altitude Prediction Error for Look-ahead of 299 Seconds

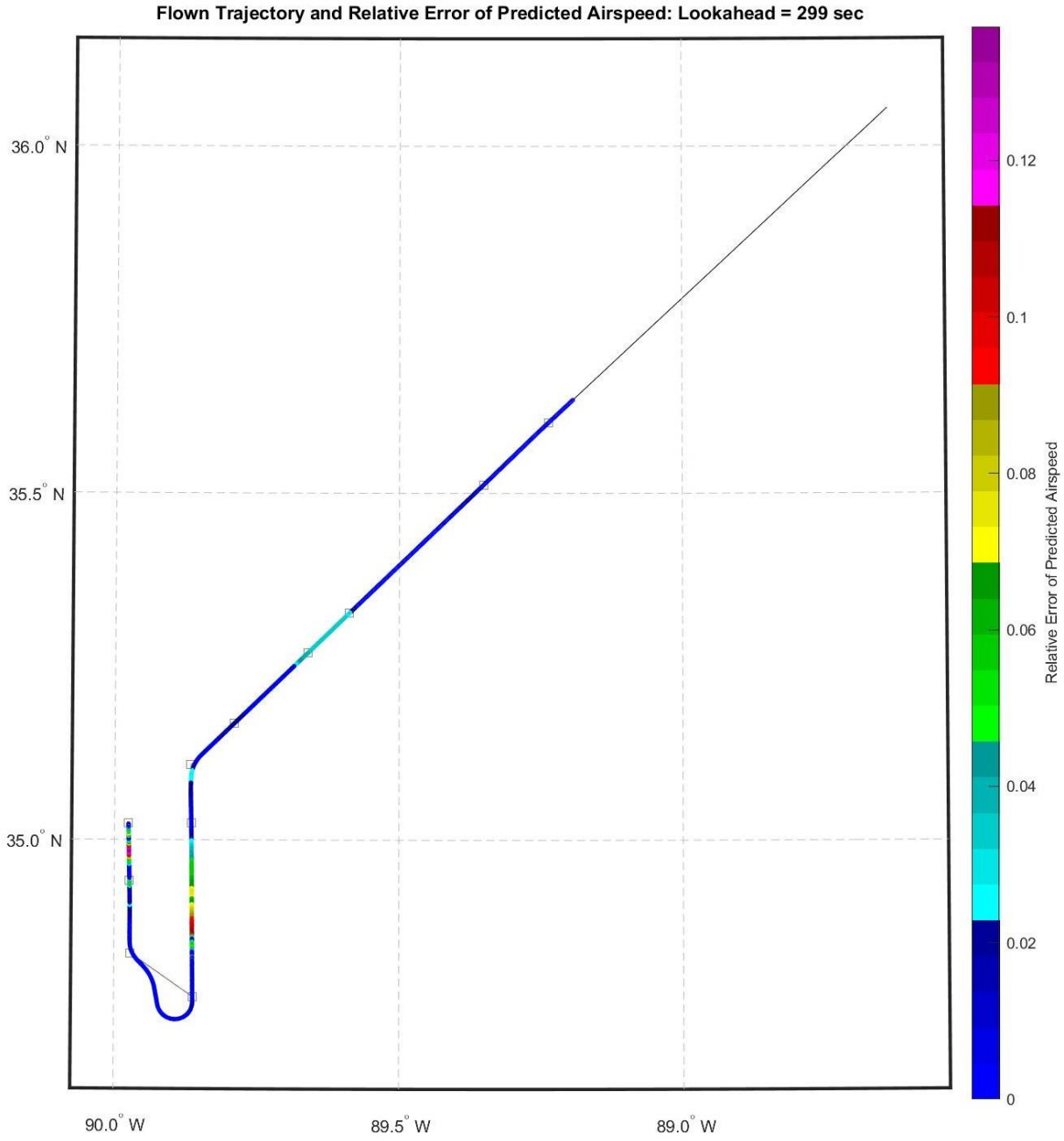

Figure 16: Plan View for BLUZZ to Runway 36C Color Coded for Relative Airspeed Prediction Error for Look-ahead of 299 seconds

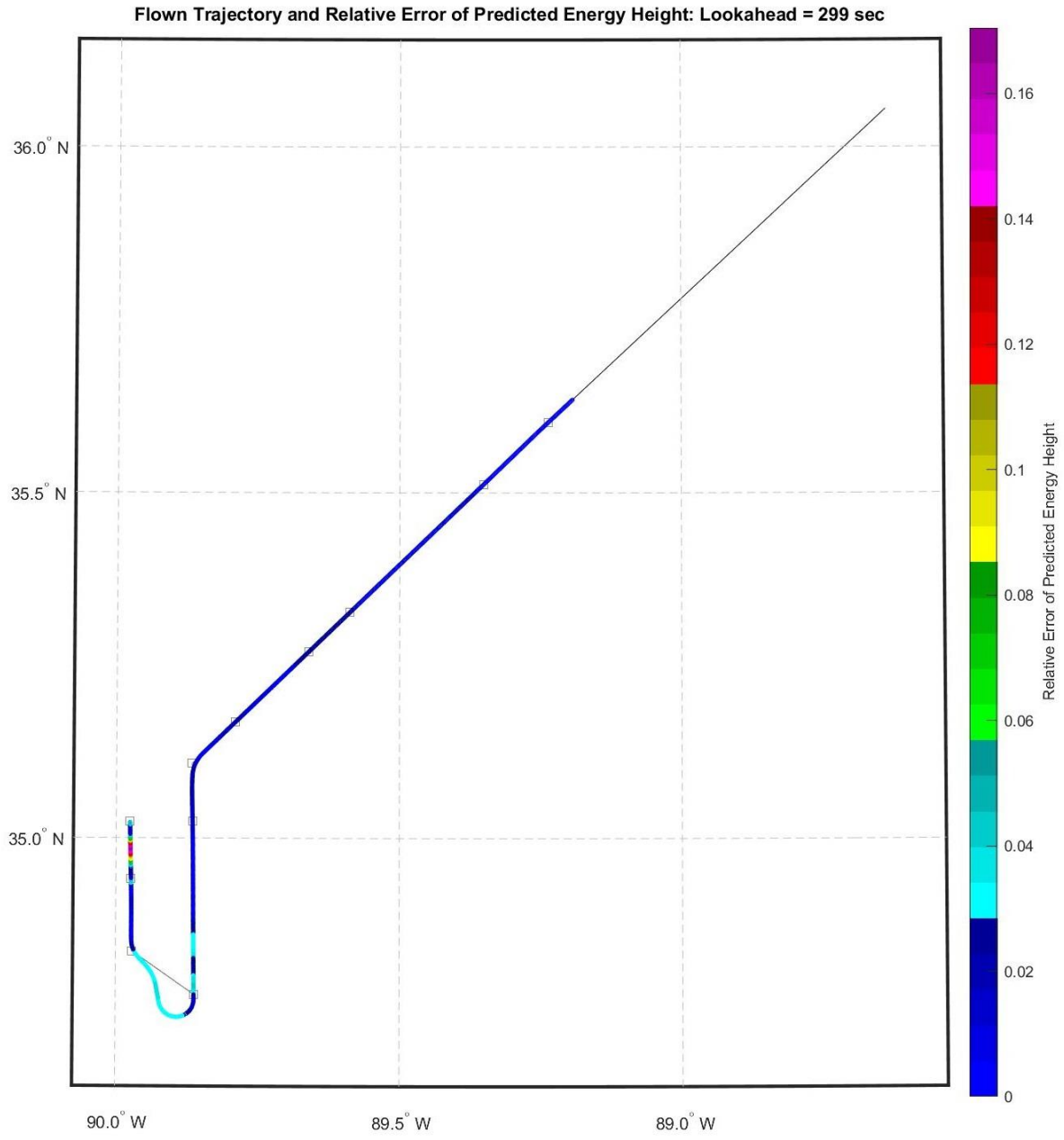

Figure 17: Plan View for BLUZZ to Runway 36C Color Coded for Relative Energy Prediction Error for Look-ahead of 299 Seconds

Figure 18 shows the time histories for predicted altitude, airspeed, and total energy for look-ahead times ranging from 0 to 299 seconds in steps of 60 seconds (i.e., 1 minute increments). From this perspective, the altitude and energy predictions look very accurate throughout the whole flight, but the airspeed prediction accuracy has a noticeable deterioration in several segments of the flight.

Figure 19 shows altitude vs. airspeed predictions for BLUZZ to runway 36C. The predictions deteriorate noticeably after 9,000 ft. altitude at 210 kt and then again during approach after 2,000 ft. at 170 kt. These altitude and airspeed prediction errors may be due to errors in the prediction of automation modes and targets. These prediction errors may also be due to errors in the models of airplane flight dynamics.

Figure 20 shows the time histories of the absolute errors in the predictions. The maximum altitude prediction error is around 600 ft. near time 1100 seconds, but the error is within ±200 ft. for most of the flight. The airspeed prediction error is approximately ±20 kt with two major error clusters: one is from the middle to the end of the STAR at DINKE where the error seems to increase with time followed by sharp corrections, and the other error cluster is during the approach phase starting at NESBT. The energy prediction error shows the combined effects of the altitude and airspeed prediction errors.

Figure 21 shows the time histories of relative prediction errors. For altitude, airspeed, and energy, the error is within approximately ±15%. The relative error gives more weight to errors at lower altitude and airspeed, and this is noticeable in the plots. The relative predicted energy error shows a trend of increasing relative error as the airplane advances on the STAR toward DINKE, then, after a correction between DINKE and NESBT, the relative error increases again toward the end of the approach phase.

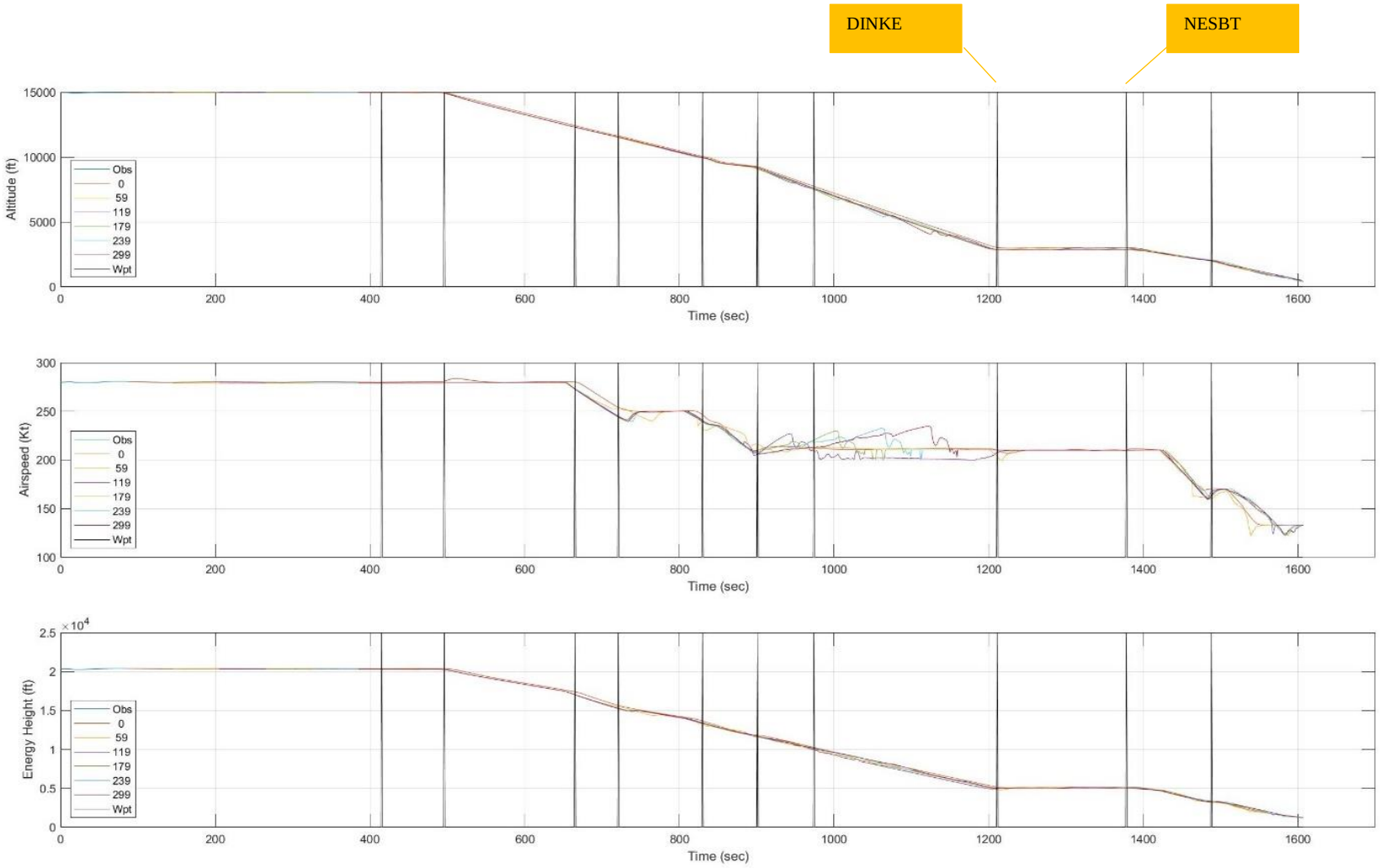

Figure 18: Time Histories of Predicted Altitude, Airspeed, and Energy for Trajectory BLUZZ to Runway 36C

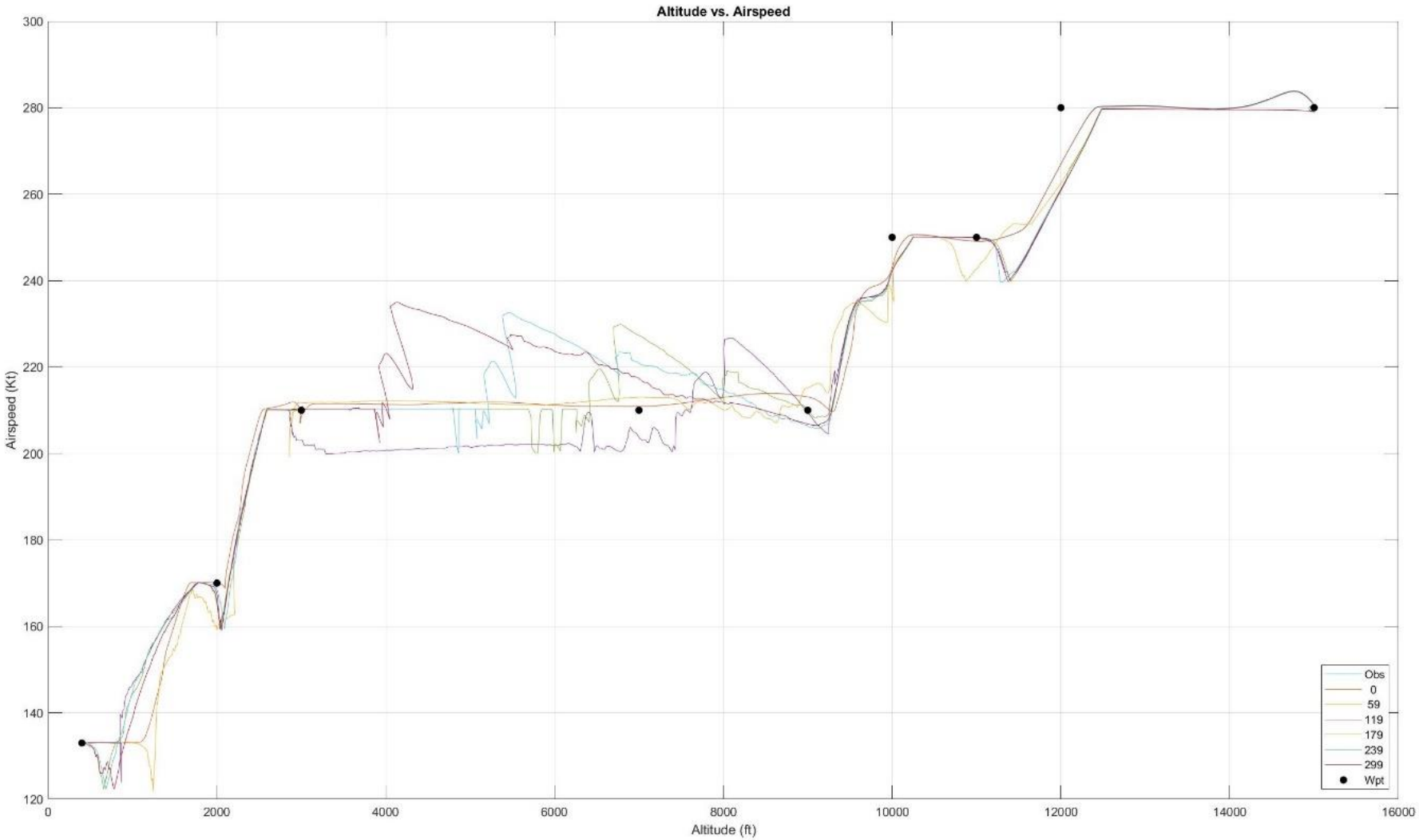

Figure 19: Altitude-vs-Airspeed Prediction Profiles for Trajectory BLUZZ to Runway 36C

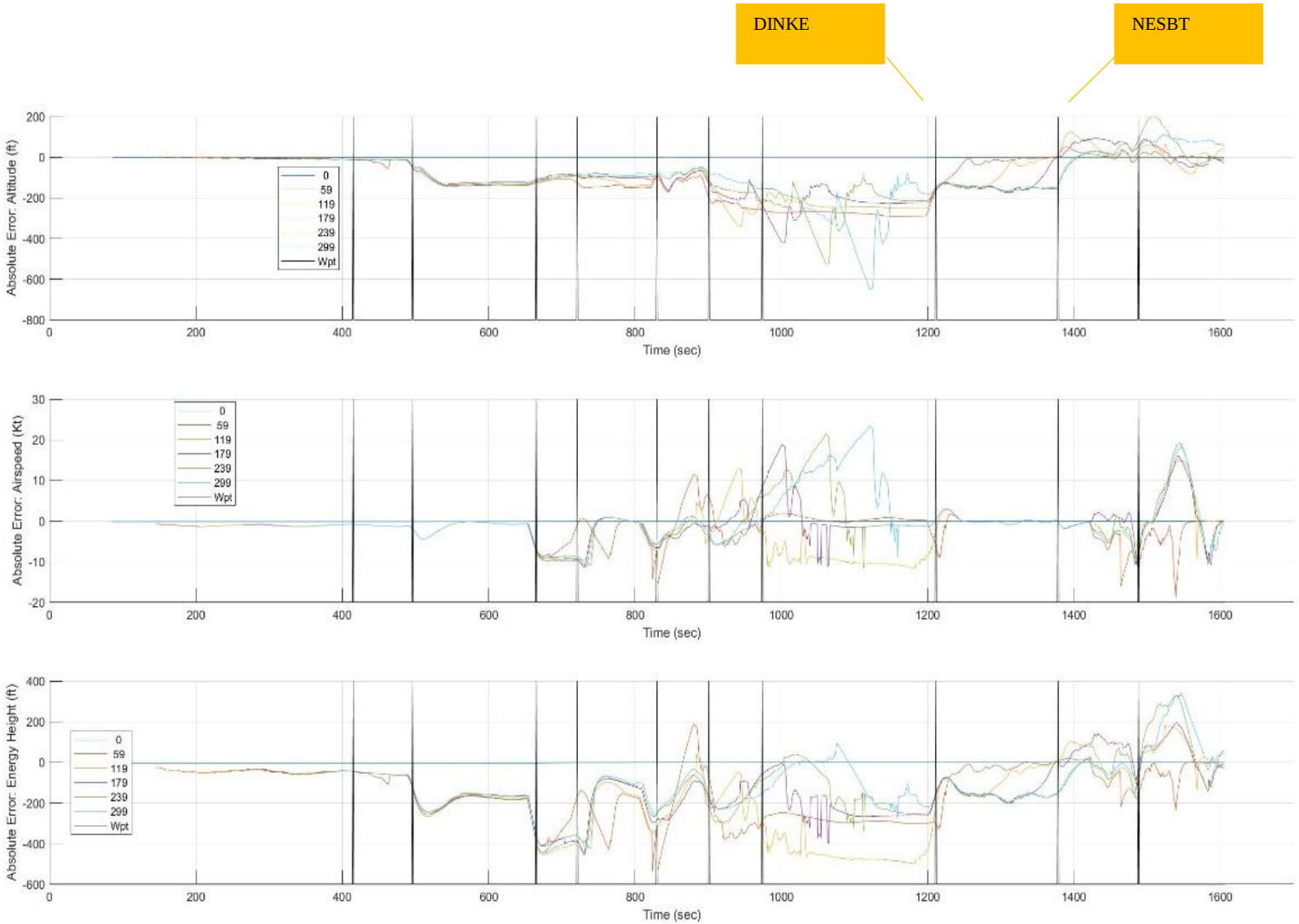

Figure 20: Time Histories of Absolute Error of Predicted Altitude, Airspeed, and Energy for Trajectory BLUZZ to Runway 36C

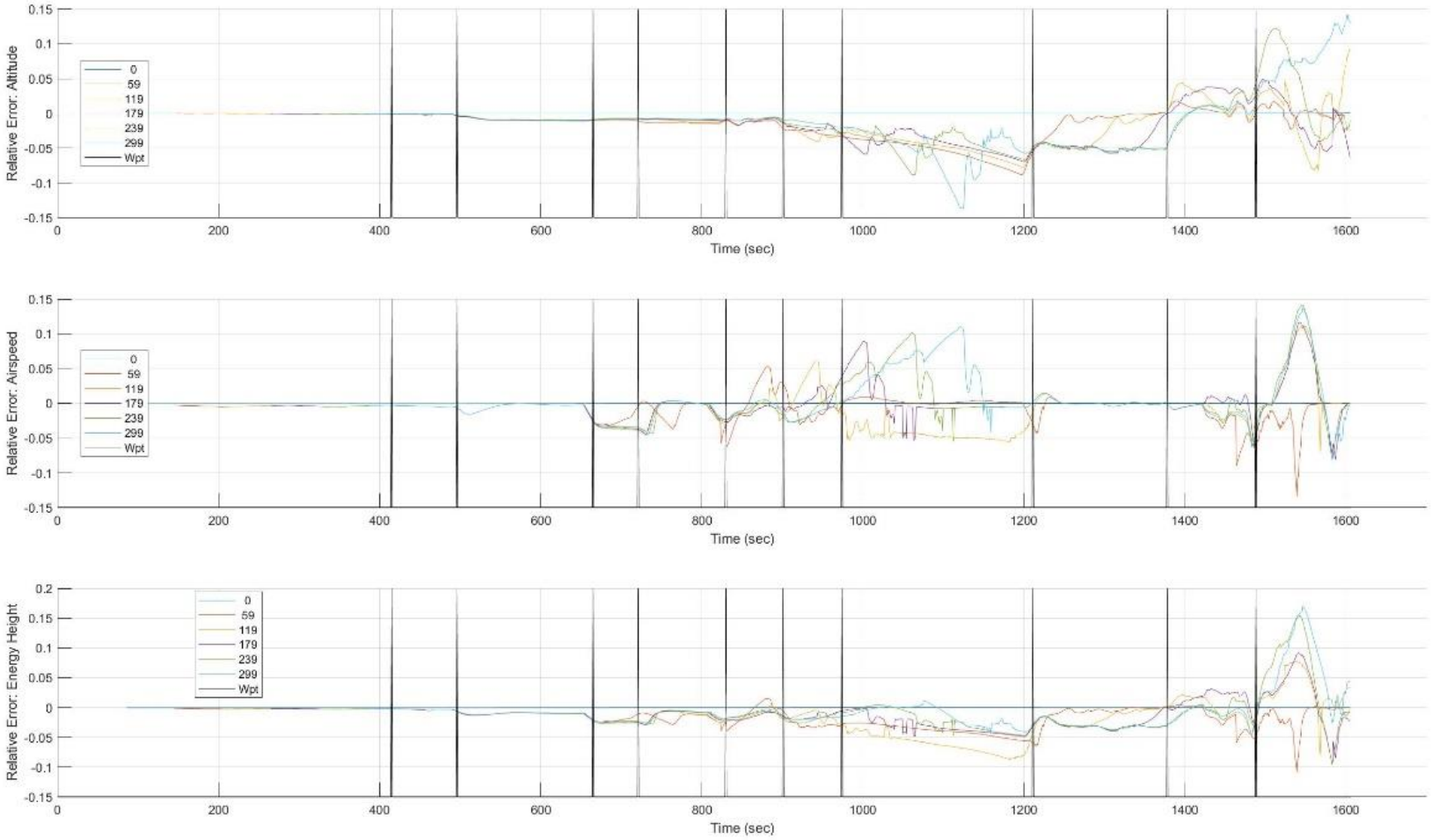

Figure 21: Time Histories of Relative Error of Predicted Altitude, Airspeed, and Energy for Trajectory BLUZZ to Runway 36C

Figure 22 is a heatmap of relative error for the predicted altitude for trajectory BLUZZ to runway 36C. Here the horizontal time axis corresponds to the "predicted time" $t + \tau$, and the vertical axis is the look-ahead time τ from 0 to 299 seconds. The relative error is color coded with the mapping from relative error to color as indicated by the colorbar on the right side of the figure. The waypoints are indicated by the black dots on the vertical axis and the black vertical lines. The heatmap shows that before time 900 seconds, the error is less than 2% (i.e., 0.02). In the time interval between 900 and 1200 seconds, the error tends to increase as time approaches 1200 seconds, where the marker for DINKE is located. The slanted band in this time interval reaching from 8% to 14% error for look-ahead larger than 150 seconds (indicated by red oval) is an interesting feature which is probably due to a combination of factors such as look-ahead time, time at which the predictions are generated (and hence, the state of the airplane at the time), and characteristics of the trajectory in the interval between time of prediction t and time predicted $t + \tau$. Features such as this one are examined further later in this report. For the time interval between 1200 and just before 1400 seconds, which corresponds to the segment between DINKE and NESBT, the altitude prediction error increases with look-ahead time but is smaller than 6%. The error pattern is much more complex after NESBT at about 1400 seconds when the airplane is in the approach phase.

Figure 23 shows the heatmap of relative error for predicted airspeed. The error patterns are clearly correlated with the locations of the waypoints. Two features of special interest are the slanted error band for look-ahead 0 to 299 seconds starting at around time 750 seconds, and the error pattern in the area between time 1000 and 1200 seconds and look-ahead 0 to 150 seconds. These features may offer additional clues about the factors which influence the prediction error. The error pattern during approach, starting around time 1400 seconds, is complex and highly detailed.

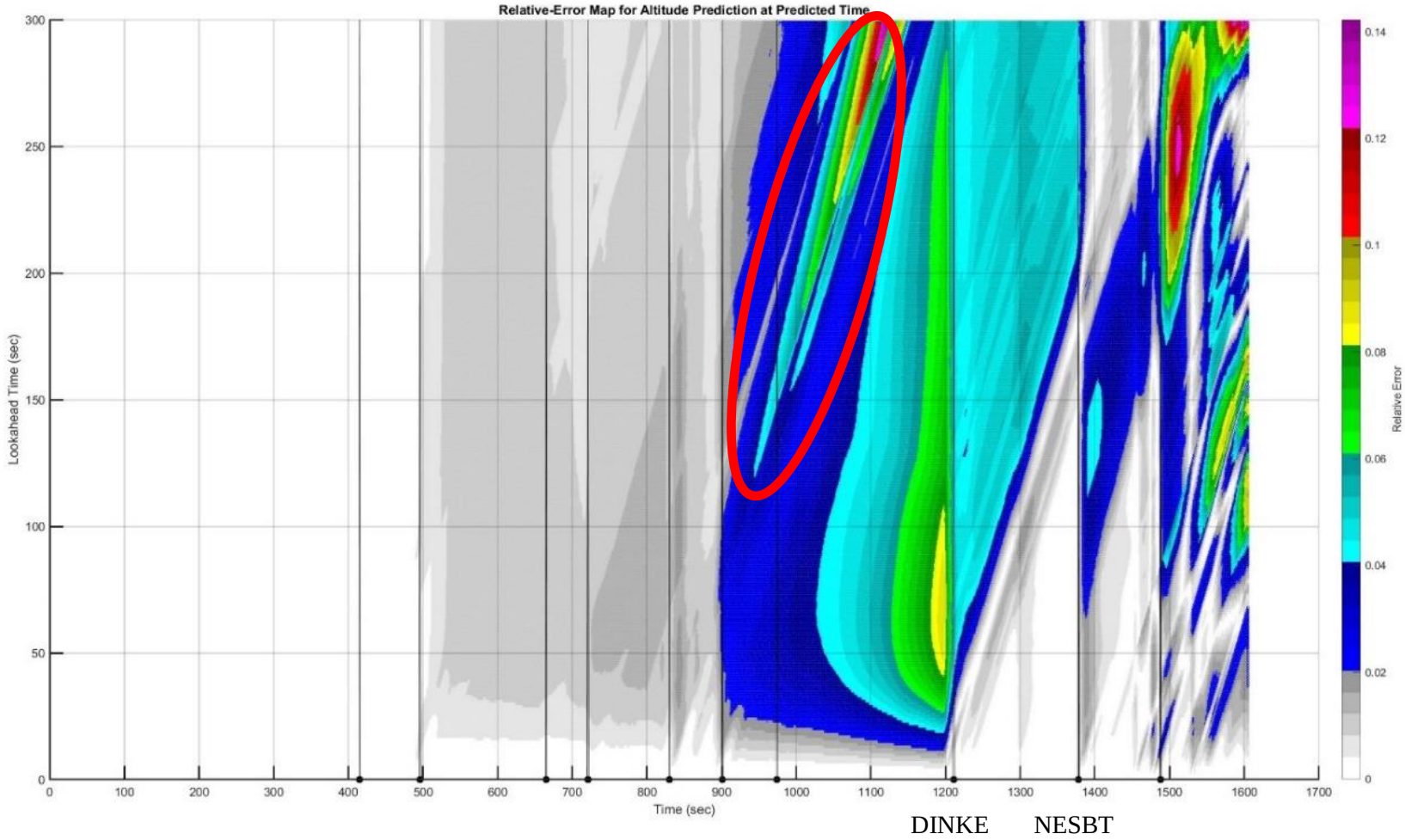

Figure 22: Heatmap for Relative Error of Predicted Altitude for Trajectory BLUZZ to Runway 36C (Time is $t + \tau$)

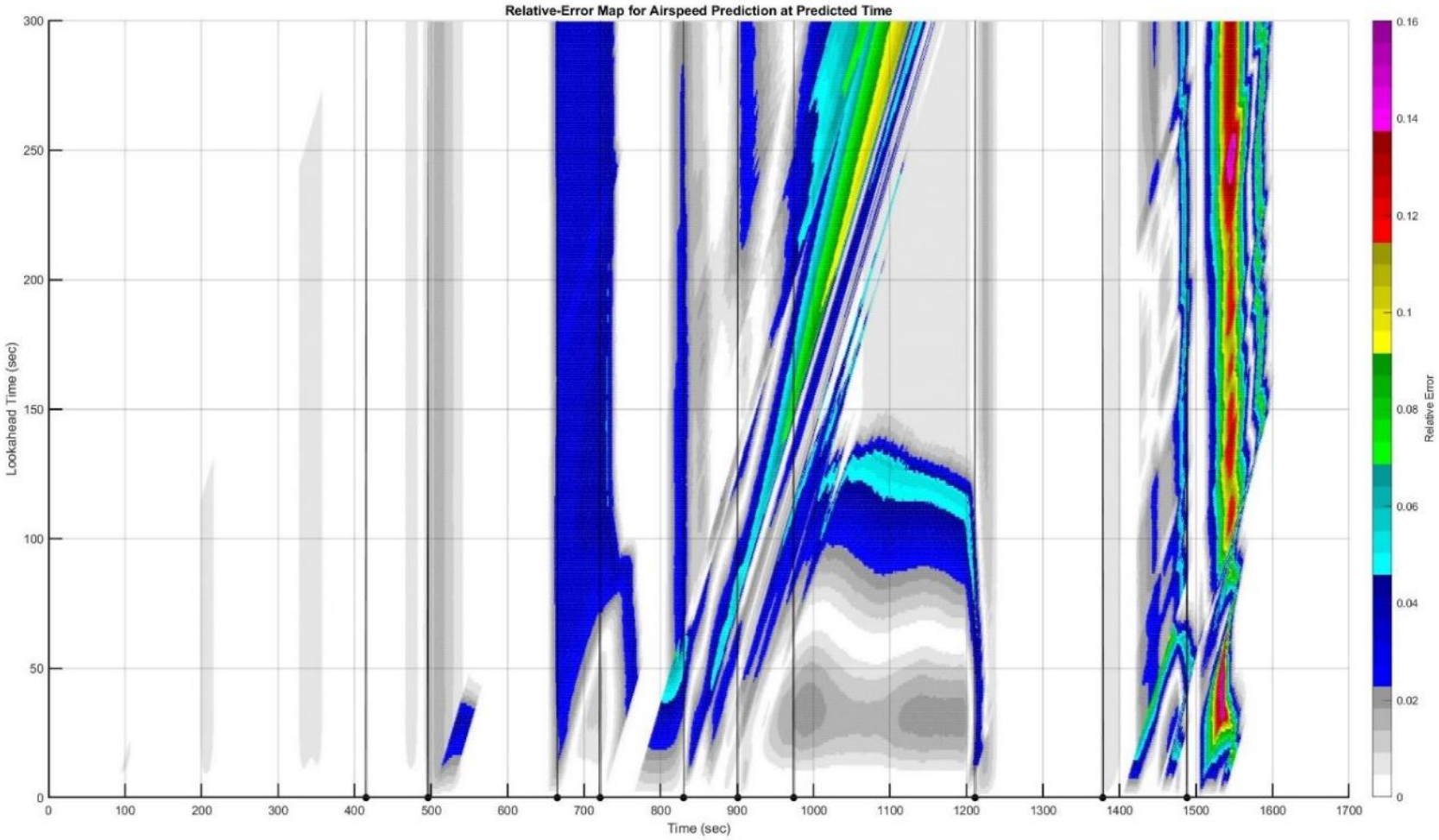

Figure 23: Heatmap of Relative Error of Predicted Airspeed for Trajectory BLUZZ to Runway 36C (Time is $t + \tau$)

Figure 24 and Figure 25 show statistics as a function of look-ahead for the distributions of relative error of altitude and speed prediction for the trajectory BLUZZ to runway 36C. The computed statistics include conventional measures of central tendency (mean and median) and dispersion (standard deviation, root-mean-square-error RMSE, inter-quartile range IQR, min, max, min-max range), and also quartiles of the absolute value of the relative error $|e_{Pred,Rel}(t, \tau)|$. The figures show that the error distributions are well centered, since the mean and the median are very small. Also, the RMS, the standard deviation, and the inter-quartile range are small compared to the range or maximum absolute value of the error, which are indications that the error distributions have long tails, which itself is an indication of the presence of outliers.

Figure 26 shows the percentile absolute error for altitude and airspeed prediction as a way to describe the tails of the error distributions. It can be observed that 90% of the prediction errors are smaller than about 5% and the remaining 10% of the errors are smaller than about 15%.

Considering the results shown above, the comparison of prediction performance based on error distributions should include statistical metrics for central tendency, average dispersion, and the tails of the distributions. The chosen metrics are the median as a measure of central tendency, the RMS for dispersion relative to the center, and the maximum absolute value of the error as a measure of the extreme values.

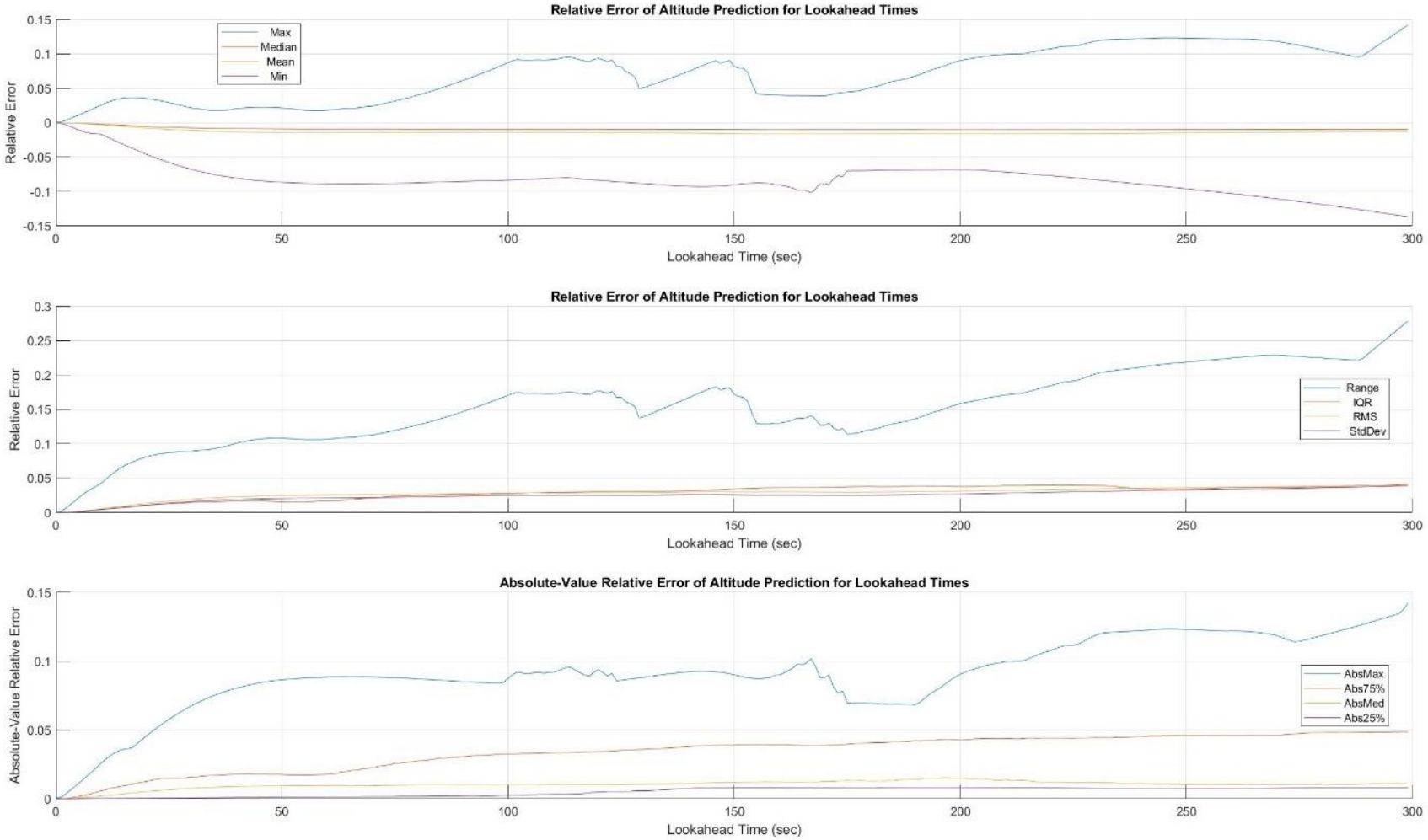

Figure 24: Statistics for Altitude Prediction Error for Trajectory BLUZZ to Runway 36C

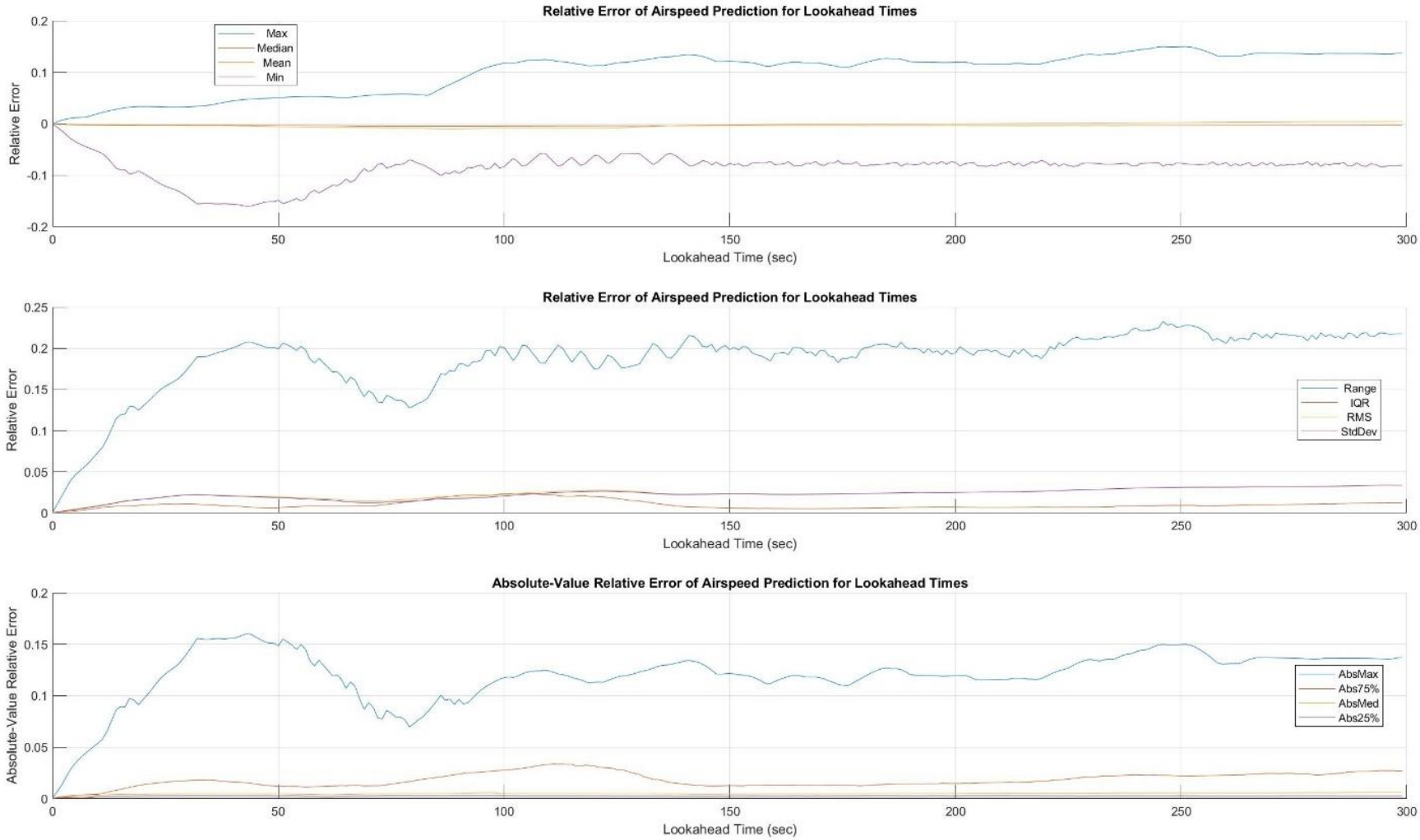

Figure 25: Statistics for Airspeed Prediction Error for Trajectory BLUZZ to Runway 36C

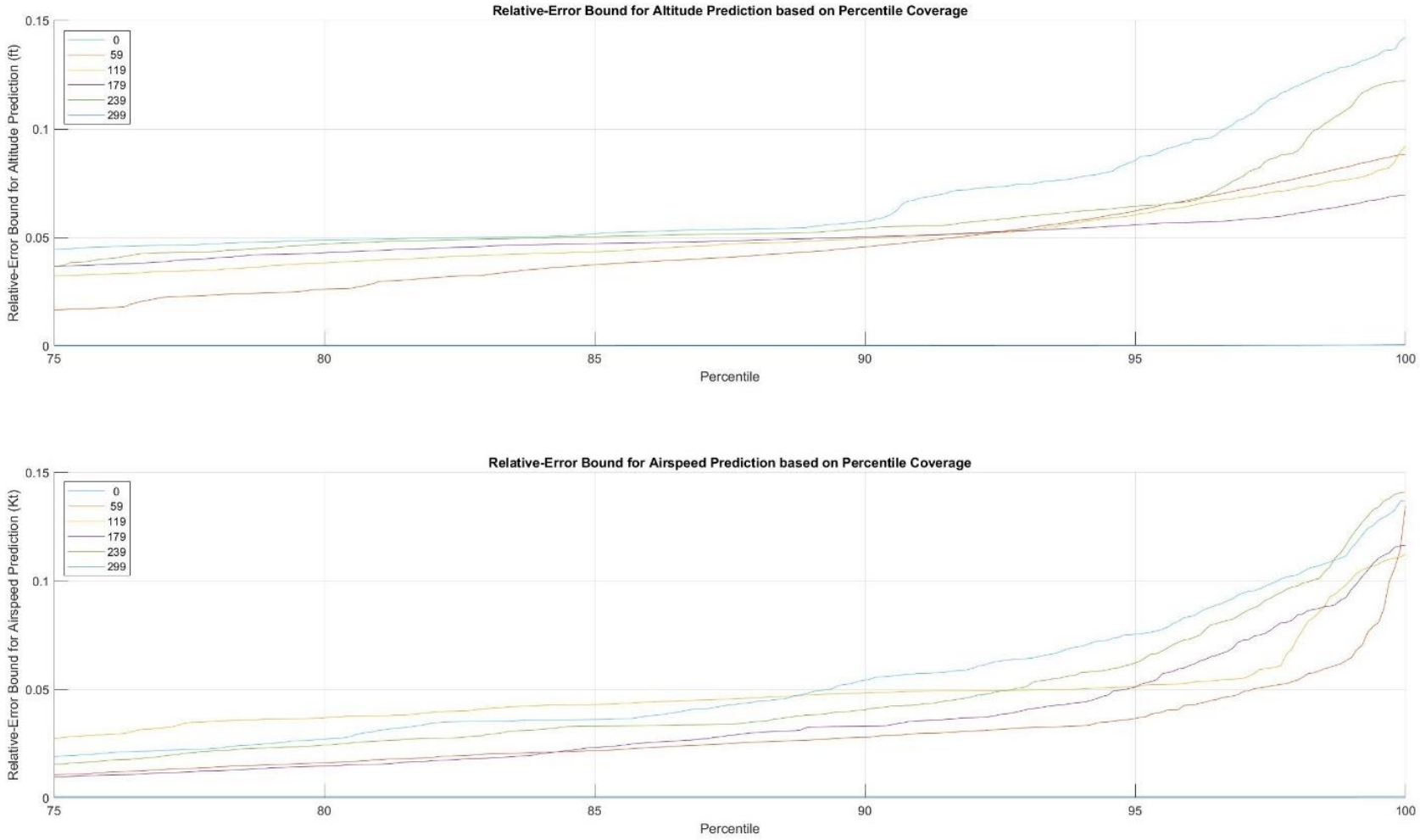

Figure 26: Percentile for Absolute Value of Altitude and Airspeed Prediction Error for Trajectory BLUZZ to Runway 36C

6. Part 1: FMC-Controlled Energy without Pilot Intervention: All Routes

This section presents the results and analysis for Part 1 of CASPEr-1. The results for Parts 2 to 6 will appear in future reports.

The goal here is to determine what the predictors did during the test flights with regard to prediction performance and behavior. Table 1 shows how the test flights in Part 1 were organized. The data is examined by grouping it four different ways:

- As a single set consisting of the aggregation of the error data for the twenty-eight flights (i.e., aggregation of all the flights);
- As seven sets, one for each STAR, consisting of the aggregation of the error data across four runways (i.e., aggregation across the runways for each STAR);
- As four sets, one for each runway, consisting of the aggregation of the error data across seven STARs (i.e., aggregation across the STARs for each runway); and
- As twenty-eight separate flights, each identified by its STAR and runway.

These patterns of aggregation enable examination of prediction performance for all the test flights together, for the STARs, for the Runways, and for individual flights.

Table 1: Organization of Test Flights in Part 1

Part 1			**Runway**			
			09	**18C**	**27**	**36C**
STAR	**Corner-Point STAR**	**BLUZZ**	BLUZZ-09	BLUZZ-18C	BLUZZ-27	BLUZZ-36C
		VANZE	VANZE-09	VANZE-18C	VANZE-27	VANZE-36C
		HOBRK	HOBRK-09	HOBRK-18C	HOBRK-27	HOBRK-36C
		BRBBQ	BRBBQ-09	BRBBQ-18C	BRBBQ-27	BRBBQ-36C
	Cardinal-Point STAR	**HYTHR**	HYTHR-09	HYTHR-18C	HYTHR-27	HYTHR-36C
		MONAA	MONAA-09	MONAA-18C	MONAA-27	MONAA-36C
		CONDR	CONDR-09	CONDR-18C	CONDR-27	CONDR-36C

Performance is measured in terms of central tendency and dispersion metrics (i.e., median, RMS, abs-Max) for the prediction errors over the full look-ahead range. The baseline flight, BLUZZ to runway 36C, is used as a reference to normalize performance measures and thus simplify understanding of the results in terms of relative performance. Prediction performance measurements are used to generate observations about anomalous predictor behavior. The error data is also examined to identify possible

factors that influence prediction performance. These observations could be the basis for more focused and detailed analyses.

6.1. Aggregation of All Flights

The simulation data from Part 1 was first examined by aggregating the prediction error data from all the flights into a single set. Figure 27 to Figure 30 summarize the results.

Figure 27 shows the absolute-error statistics for altitude prediction. The central tendency of the error, as measured by the mean and the median, is very close to zero across the look-ahead range. Dispersion measured by standard deviation, RMS, IQR, and 75% percentile are all smaller than about 250 ft. and exhibit an increasing trend as the look-ahead τ increases. Intuitively, this trend is expected as in general the uncertainty about the state of the airplane increases the farther ahead the function tries to predict. The error range measured by Min, Max, range, and absMax statistics show that the worst-case error is six to ten times larger than the RMS and, in general, the worst-case error increases with the look-ahead τ. More importantly, the figure shows that the worst-case error increases very quickly beginning at look-ahead τ = 0 with an inflection point at around τ = 25 second, and from then on the worst-case error settles into a variable undulation. Notice that the worst-case error is largest for τ between about 25 and 125 seconds, which is completely unexpected.

The results in Figure 28 for airspeed prediction error have similar characteristics. The central tendency is essentially zero, and the dispersion statistics such as RMS and IQR increase more or less linearly with look-ahead τ and are smaller than 10 kt. Here again the worst-case error increases quickly from τ = 0 with an inflection point at approximately τ = 25 seconds, followed by a variable undulation with a trend increasing with τ. The largest absMax value is at approximately τ = 190 seconds.

Figure 29 shows the primary statistics of median, RMS and absMax relative-error for altitude, airspeed, and energy prediction. The median error for altitude, airspeed, and energy are essentially 0 for the range of the look-ahead. The RMS increases roughly linearly with the look-ahead and is relatively small compared to the absMax statistic. The overall trend for the absMax statistic is closer to the expectation of it increasing with look-ahead for the three state variables. The most important aspect of these plots is the size of the absMax relative error. Notice that the peak absMax for altitude is around 400% and for airspeed is 55%, both at about τ = 200 seconds. These are very large errors that are indicative of weaknesses in the design of the prediction function.

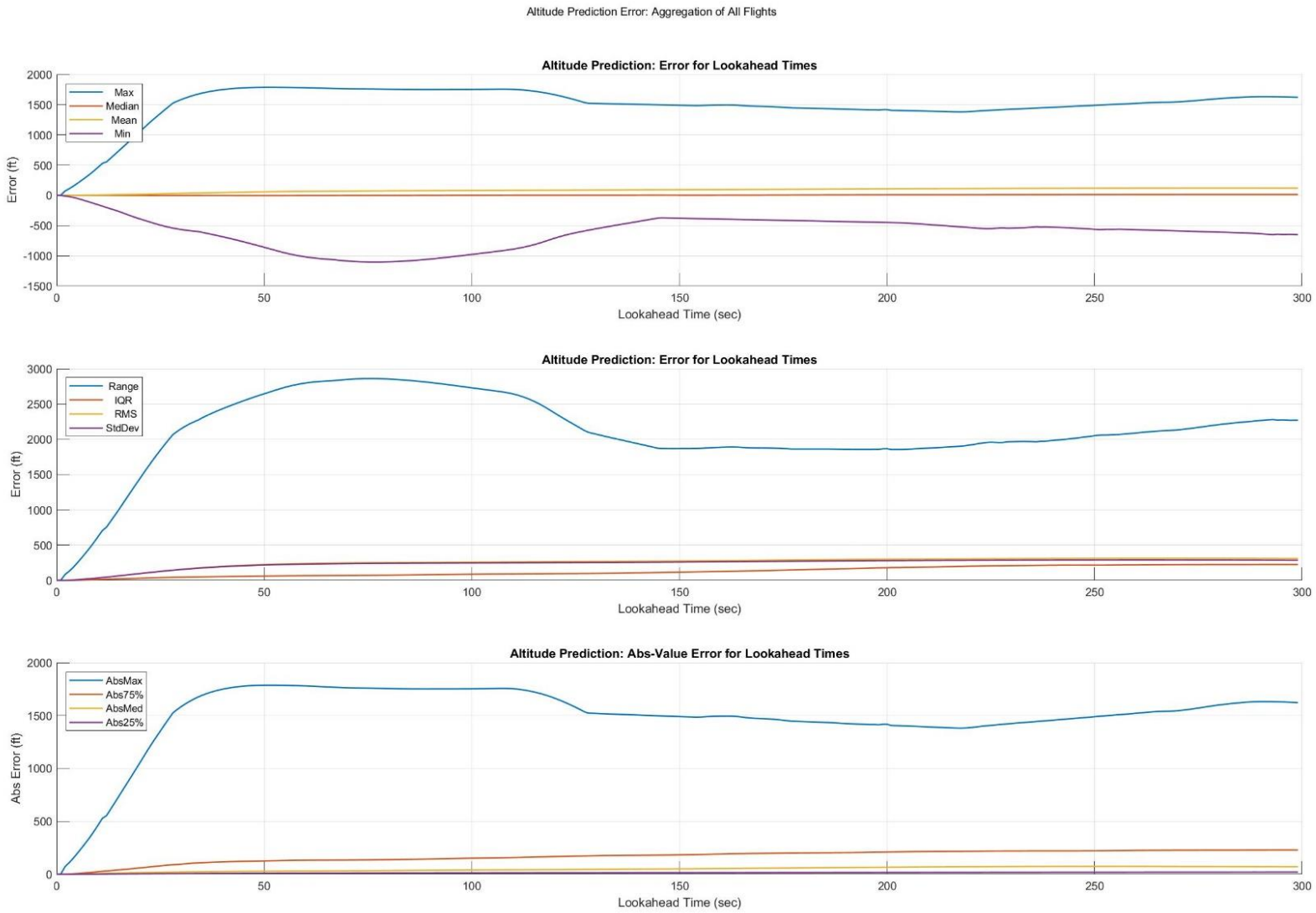

Figure 27: Aggregation of All the Flights: Absolute-Error Statistics for Altitude Prediction as a Function of Look-ahead τ

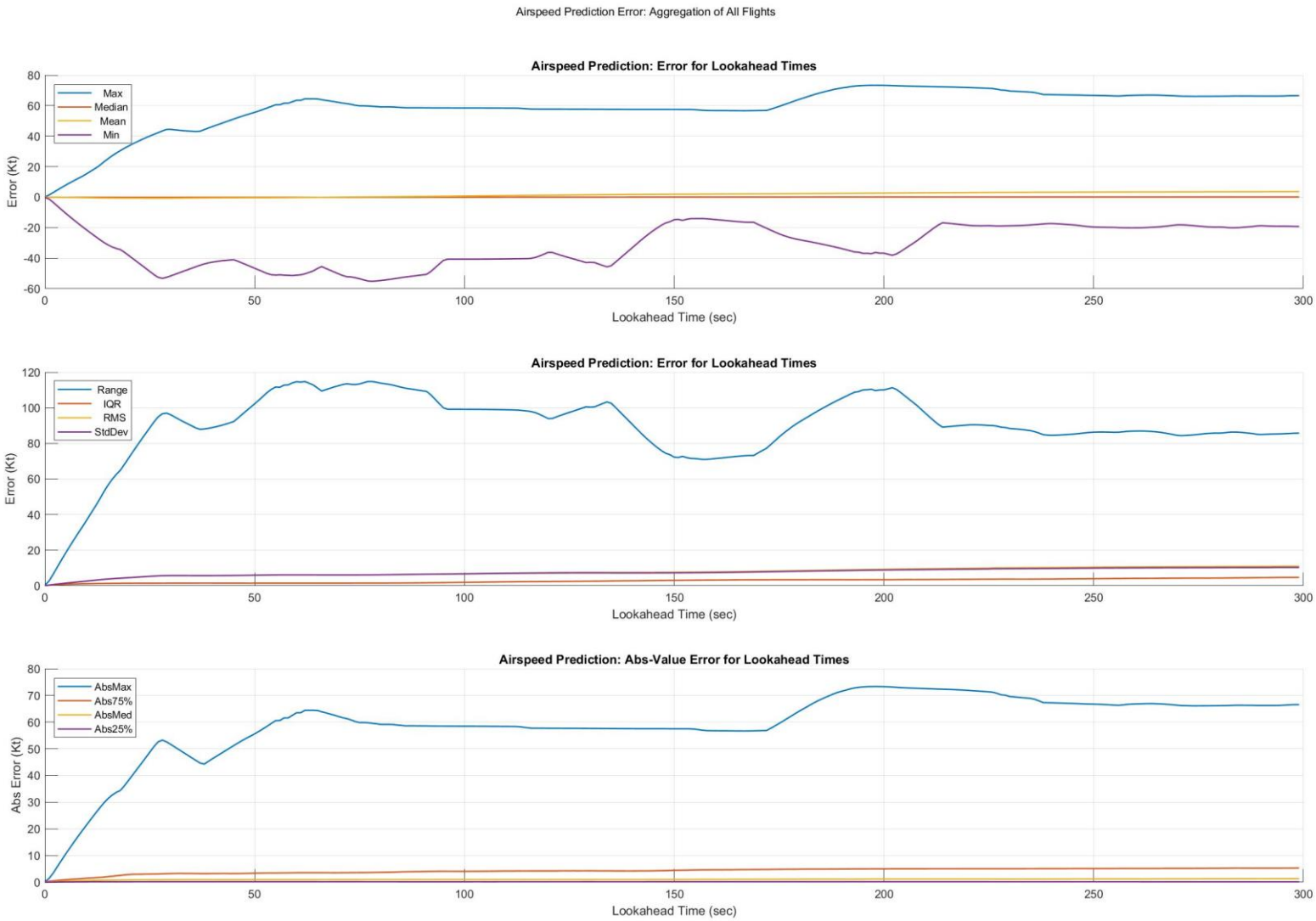

Figure 28: Aggregation of All the Flights: Absolute-Error Statistics for Airspeed Prediction as a Function of Look-ahead τ

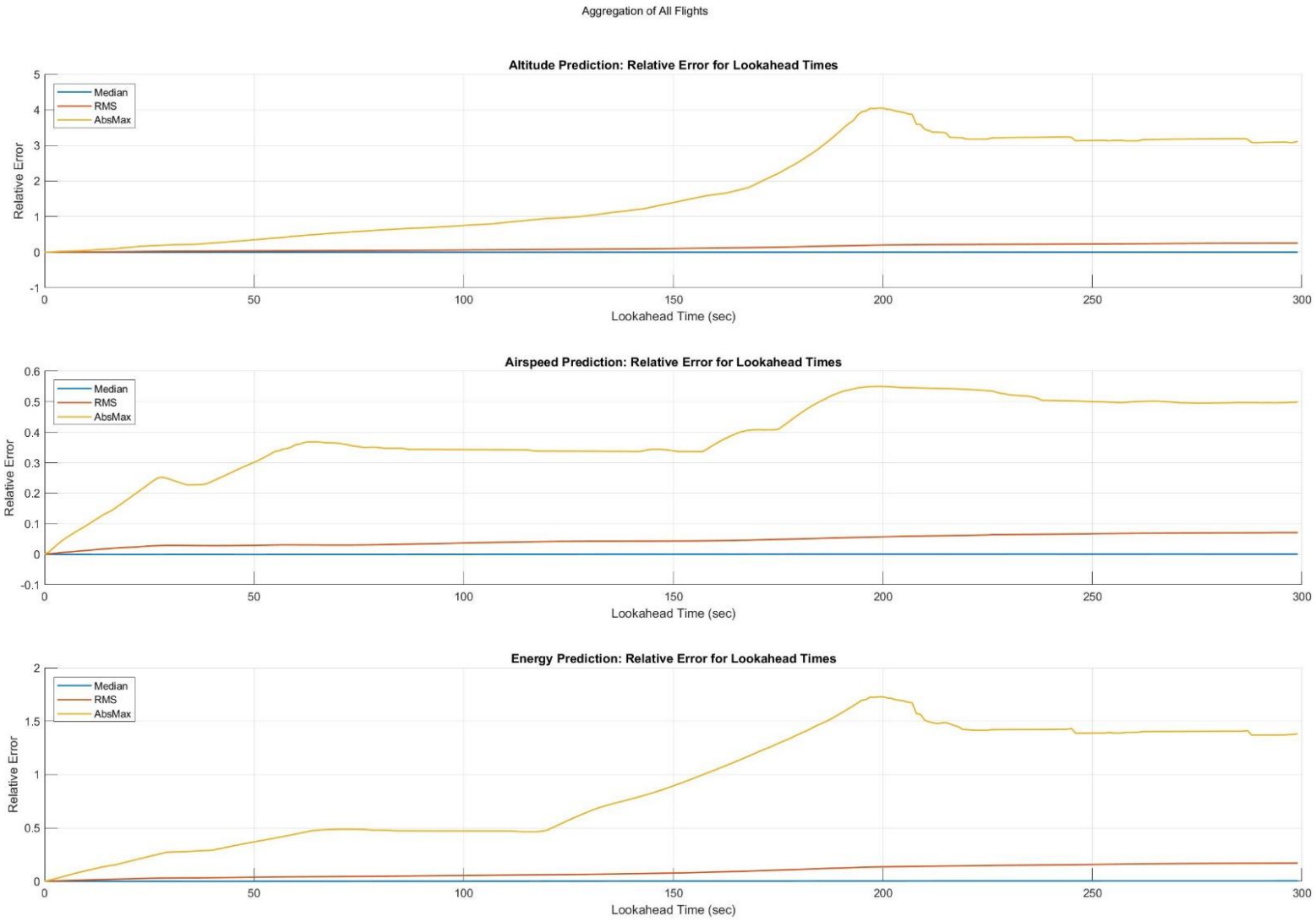

Figure 29: Aggregation of All the Flights: Relative-Error Statistics for Altitude, Airspeed, and Energy Prediction as a Function of Look-ahead τ

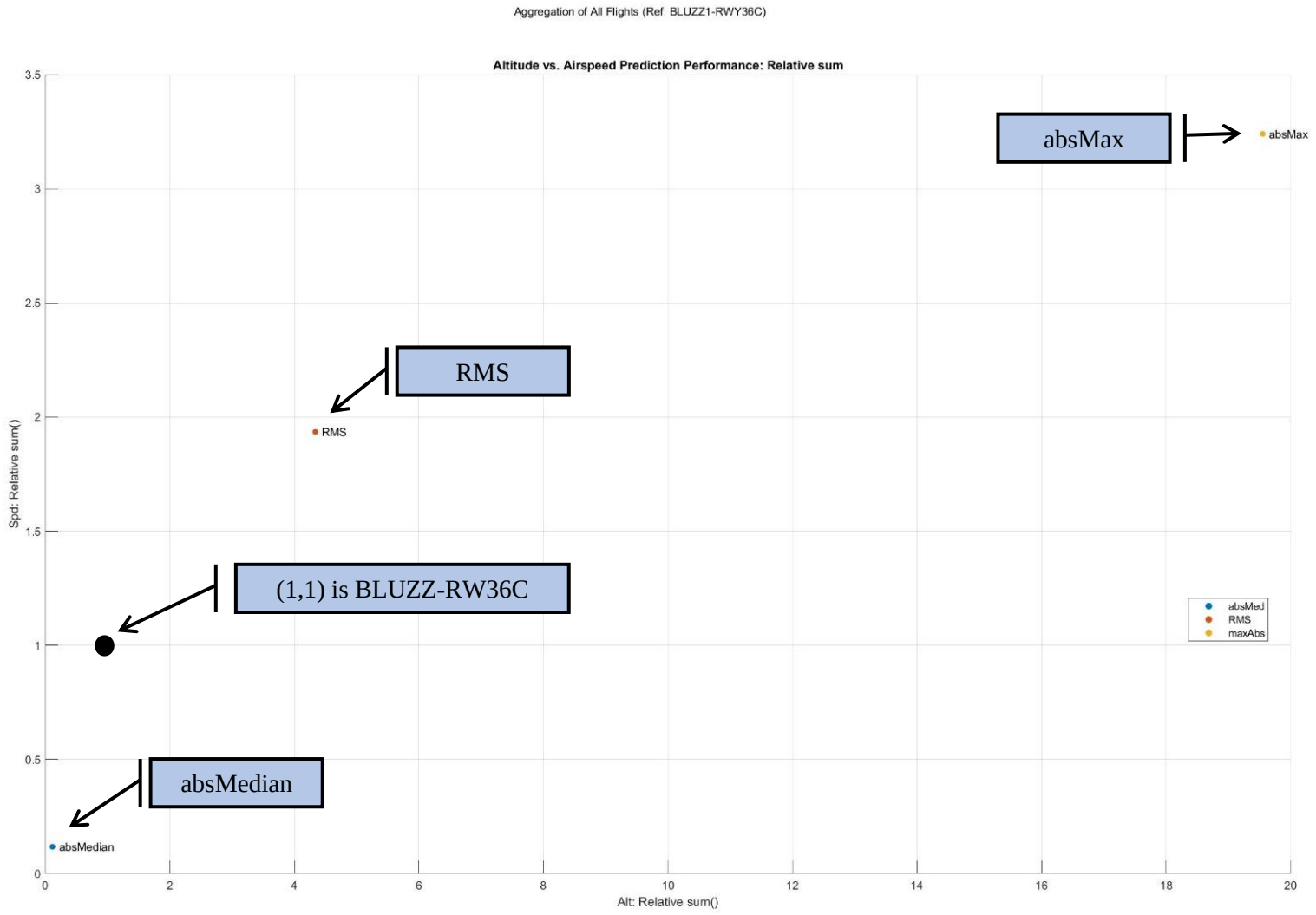

Figure 30: Aggregation of All Flights: Cumulative Relative- Error Statistics for Altitude and Airspeed Prediction Normalized With Respect to BLUZZ-RW36C

Figure 30 is a summary visualization of the prediction performance for all the test flights considered in aggregate. Let $S_{Agrg,Rel}(\tau)$ denote a summary statistic (i.e., median, RMS, or absMax) for the aggregate relative-error set for look-ahead τ. Also, let $C_{Agrg,Rel}$ denote the sum of $S_{Agrg,Rel}(\tau)$ for $\tau = 0 \ldots 299$; this is the cumulative sum (i.e., the integral) of one of the curves in Figure 29:

$$C_{Agrg,Rel} = \Sigma_{\tau=1 \,..\, 299} S_{Agrg,Rel}(\tau)$$

$S_{Ref,Rel}(\tau)$ and $C_{Ref,Rel}$ denote the same variables for the reference case BLUZZ to runway 36C:

$$C_{Ref,Rel} = \Sigma_{\tau=1 \,..\, 299} S_{Ref,Rel}(\tau)$$

The normalized cumulative statistics in Figure 30 are the ratios of the aggregate and the reference cumulative statistics for altitude and airspeed predictions:

$$c_{Agrg,Rel} = C_{Agrg,Rel} / C_{Ref,Rel}$$

In Figure 30 the large black dot at point (1,1) corresponds to the AbsMedian, RMS, and AbsMax statistics for the reference flight BLUZZ to runway 36C. The figure shows that the aggregate central tendency of the predictive function, as measured by the cumulative median, is closer to 0 than for the reference BLUZZ to 36C. The airspeed and altitude RMS relative-error RMS for the aggregate are, respectively, roughly 2 and 4 times larger than the reference. The cumulative worst-case relative error for altitude is about 20 time larger than the reference. Taken together, these results indicate that, in aggregate, the error dispersion of the prediction function was significantly worse than it did for the reference flight.

6.2. STARs: Aggregation of Runways

The relative effects of the STARs on prediction performance were examined by grouping the error data by the STARs and aggregating across the runways (i.e. aggregating along the rows in Table 1). Figure 31 to Figure 35 illustrate the results.

The RMS and absMax relative error for altitude, airspeed, and energy prediction for the STARs are given in Figure 31 and Figure 32. The median relative-error is not given as it is very small for all the energy-related variables. As expected, the relative error for altitude, airspeed, and energy increases with the look-ahead τ. The curves of RMS error of altitude prediction are clearly divided into two groups: the cardinal-point STARs (HYTHR, MONAA, and CONDR) have larger error than the corner-point STARs across the range of the look-ahead τ. The curves of RMS error of airspeed prediction overlap and vary with τ in all cases, though the error is clearly largest for HYTHR. The curves for RMS error of energy prediction reinforce the separation between cardinal-point and corner-point STARs. In Figure 32, the

altitude prediction error curves overlap until about $\tau = 150$ seconds, after which there are clearly two separate groups, again: cardinal-point STARs and corner-point STARs. The airspeed prediction error curves overlap until about $\tau = 200$ seconds and then separate into two group, however the groups here are not cardinal-point vs. corner-point STARs, as BLUZZ and BRBBQ have larger errors than the other corner-point STARs. Nevertheless, for the energy prediction error, the STARs form two clear groups: cardinal-point and corner-point.

Figure 33 and Figure 34 show the cumulative error statistics for airspeed and energy for all the STARs. With respect to cumulative RMS airspeed prediction error in Figure 33, CONDR, MONAA, BRBBQ, and BLUZZ are very similar, and HYTHR is almost twice as bad as HOBRK. With respect to the cumulative max-absolute airspeed prediction error, BRBBQ, BLUZZ, and HYTHR clearly perform worse than the rest, but the cumulative error curves in Figure 34 clearly show that, in terms of prediction performance, the corner-point STARs are on a different level than the cardinal-point STARs.

Figure 35 summarizes the prediction performance results for the STARs. In general, prediction performance is better for the corner-point STARs than for cardinal-point STARs, with altitude prediction performance being a clear discriminator between the two groups. Airspeed prediction performance on BLUZZ and BRBBQ, which are the northern arrival routes, is noticeably worse than on VANZE and HOBRK, which are the southern arrival routes. A cursory examination of the routes did not reveal any significant features that could explain the differences in airspeed prediction performance (see Figure 8 and Appendix B), but a detail analysis of the routes may identify factors that explain these observed differences. Such detailed analysis should be considered for future work.

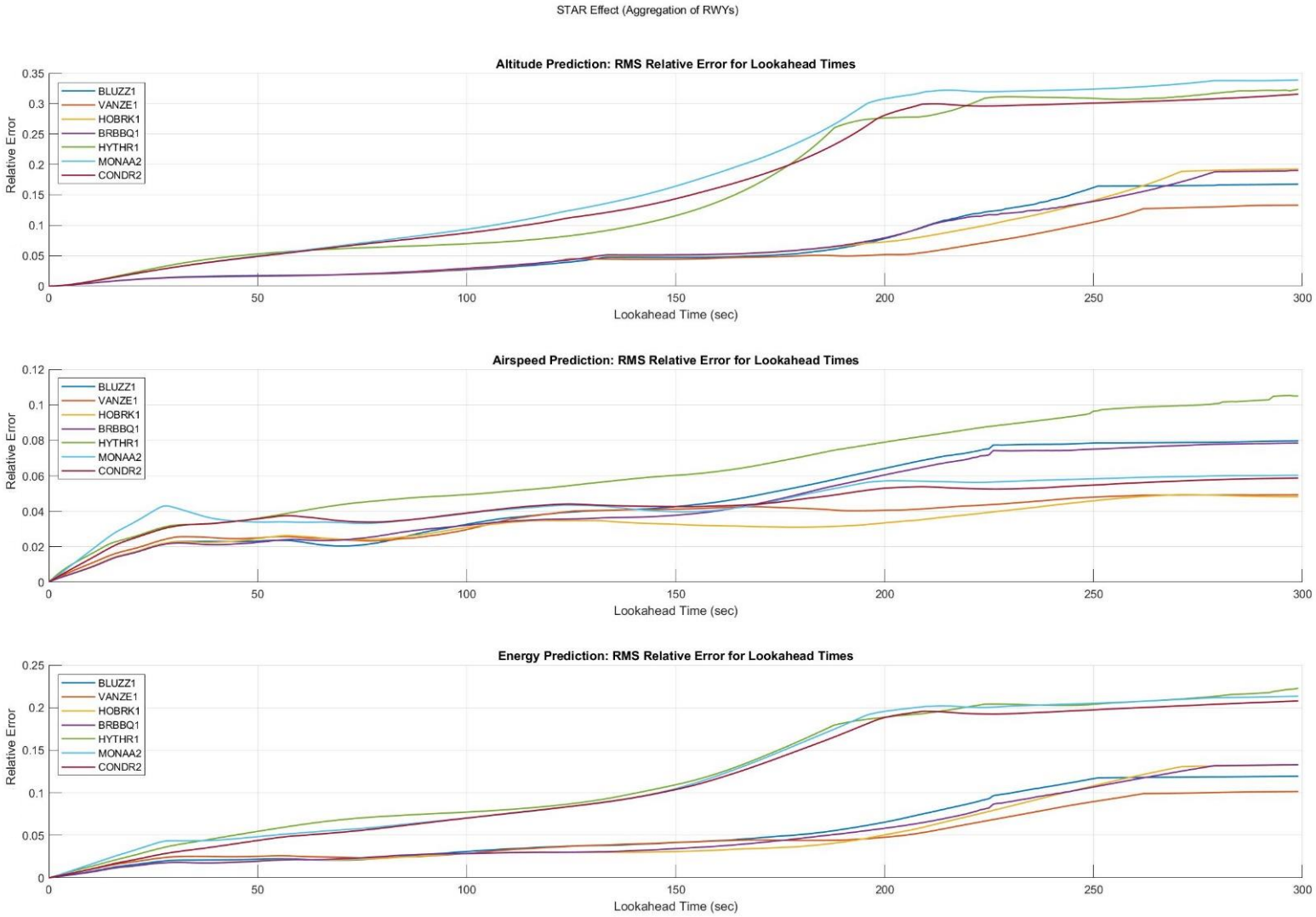

Figure 31: STARs (Aggregation of Runways): Relative-Error RMS Statistic for Altitude, Airspeed, and Energy Prediction as a Function of Look-ahead τ

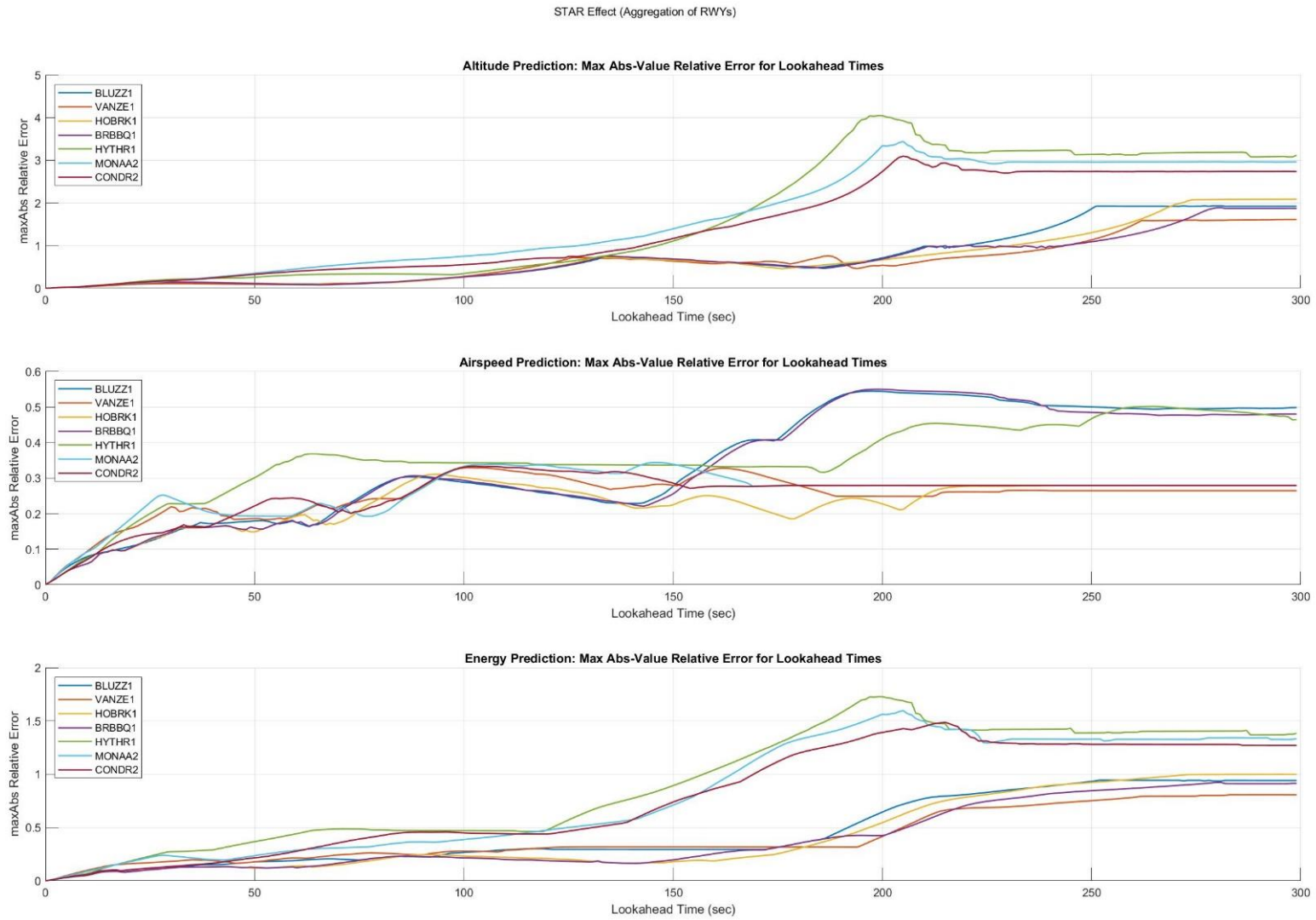

Figure 32: STARs (Aggregation of Runways): Relative-Error absMax Statistic for Altitude, Airspeed, and Energy Prediction as a Function of Look-ahead τ

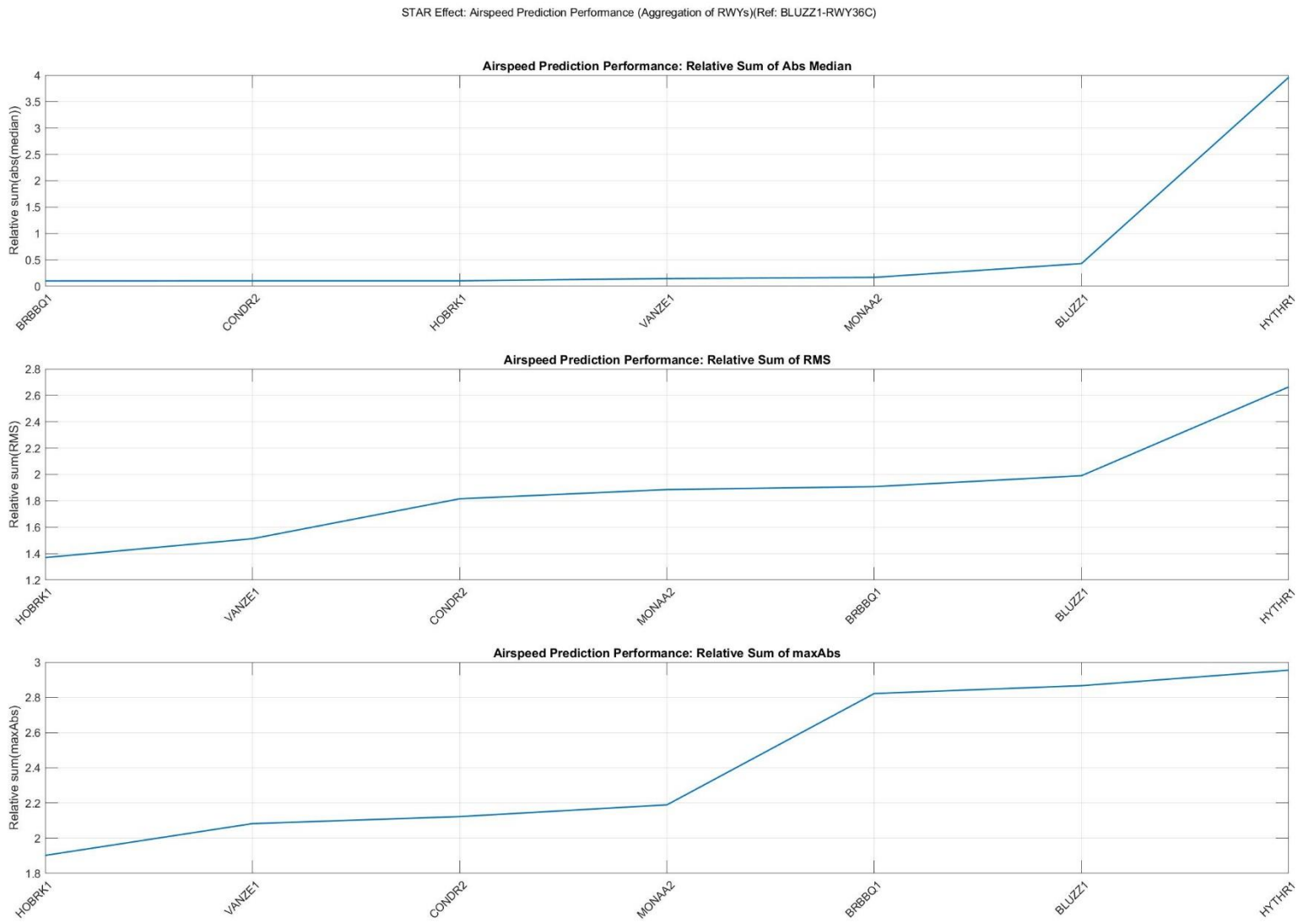

Figure 33: STARs (Aggregation of Runways): Ranked Cumulative Relative-Error Statistics for Airspeed Prediction Normalized With Respect to BLUZZ-RW36C

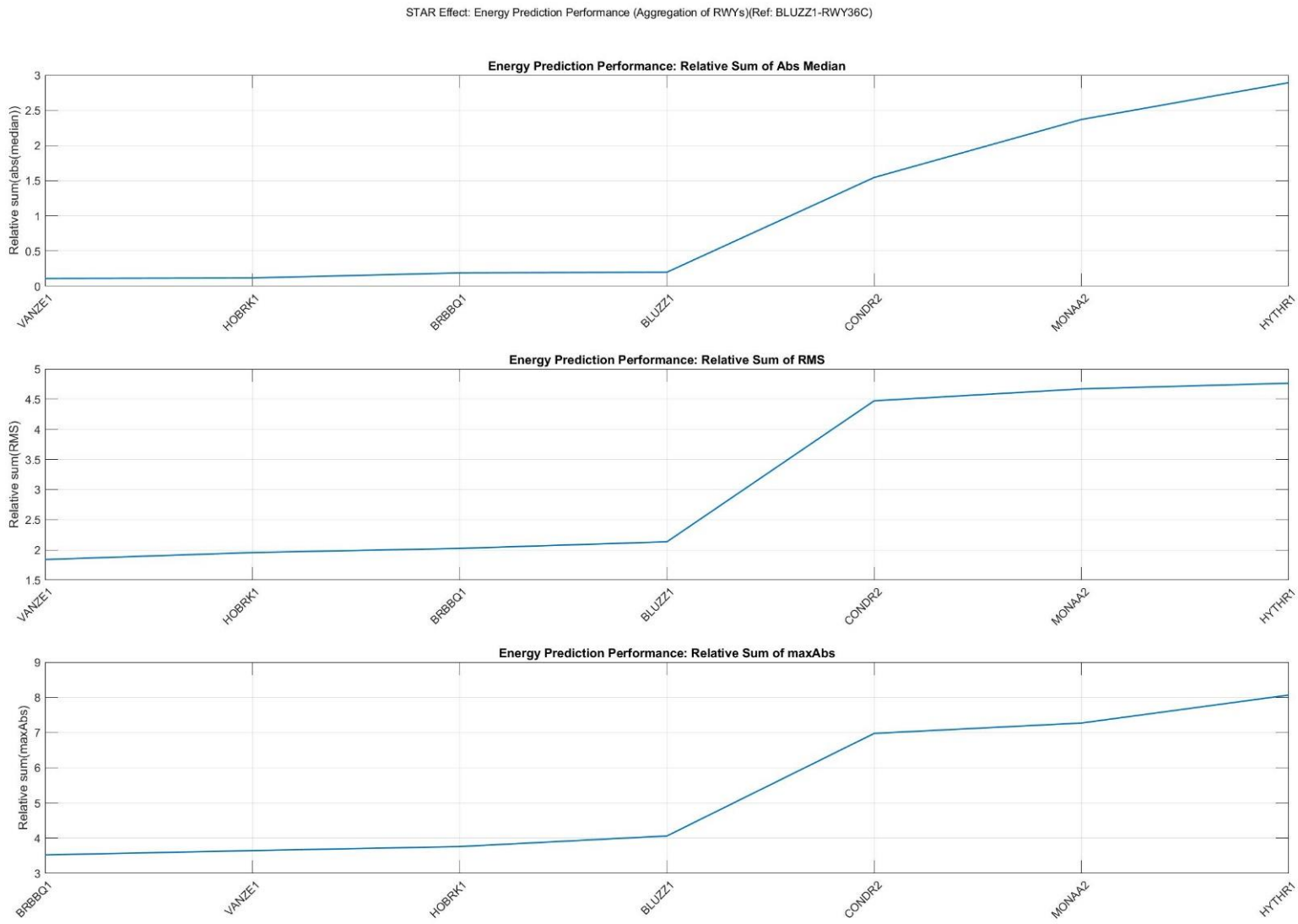

Figure 34: STARs (Aggregation of Runways): Ranked Cumulative Relative-Error Statistics for Energy Prediction Normalized With Respect to BLUZZ-RW36C

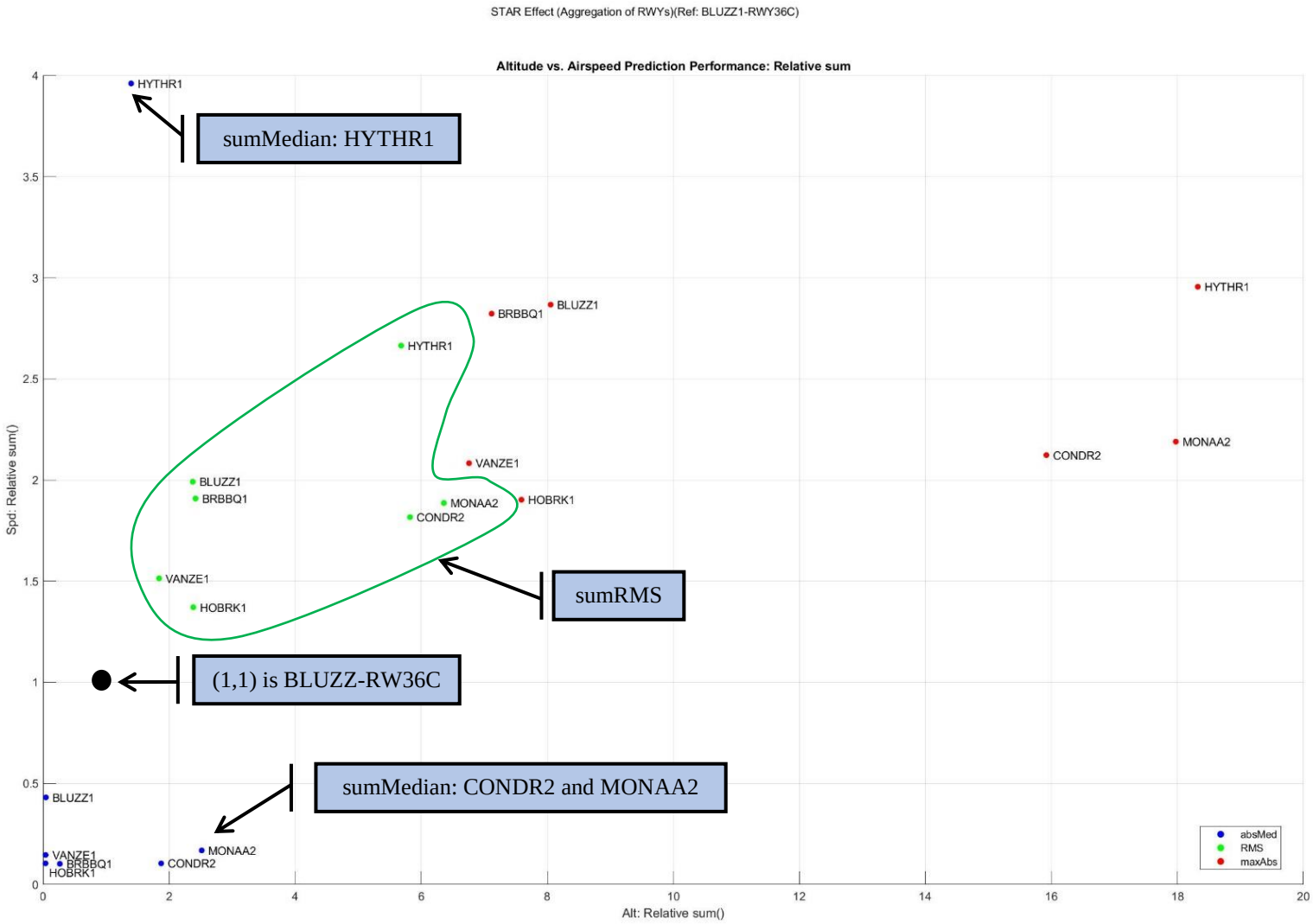

Figure 35: STARs (Aggregation of Runways): Cumulative Relative- Error Statistics for Altitude and Airspeed Prediction Normalized With Respect to BLUZZ-RW36C

6.3. Runways: Aggregation of STARs

The effect of the runways was examined by aggregating the flights from all the STARs for each runway (i.e., by aggregating along the columns in Table 1). The results are given in Figure 36 to Figure 40.

Figure 36 and Figure 37 show the RMS and maximum absolute values (absMax) for altitude, airspeed, and energy for the range of look-ahead τ. For the most part, the RMS increases monotonically with τ. Runway 18C has clearly the largest RMS errors for both altitude and airspeed, though the RMS error curves for energy are much closer together. All the altitude RMS error curves have inflection points and have the largest difference at around $\tau = 200$ seconds. Notice that the absMax error curves for altitude also have a similar characteristic. Furthermore, the airspeed absMax error for runway 18C peaks at around $\tau = 200$ seconds, too, and then settles at a value of 0.5, while all the others settle at around 0.3. These are interesting features that may be due to particular common characteristics of the approaches to the runways and should be examined more closely in future work to determine the likely causes, as this may offer insights into weaknesses of the prediction function.

Figure 38 and Figure 39 are the ranked cumulative error statistics for altitude and airspeed. These figures show that, in terms of aggregate RMS and absMax error statistics, prediction performance is significantly and consistently different for runways 27 and 18C. This is another feature that should be examined further in a future detailed study.

Figure 40 summarizes the prediction performance results. Aggregate prediction errors for all the runways have better central tendency and worse error dispersion than for the reference flight BLUZZ to runway 36C. With respect to RMS error for both altitude and airspeed, runways 09, 27, and 36C are closer to each other than any of them is closer to runway 18C. With respect to absMax error, runways 27 and 36C are on a separate cluster from runways 09 and 18C.

These differences in prediction performance may be related to the specific characteristics of the STARs, specifically their trajectory waypoint distributions and constraints. Notice that the STARs, seen as a single structure, as shown in Figure 8 and Figure 9, are not perfectly symmetric about east-west or north-south axes centered at KMEM. These asymmetries and characteristics of particular STARs and runways may be causally related to the differences in performance among the STARs (as described in the previous sub-section) and among the runways (as described here). The analysis of individual STAR-Runway combinations in the next subsection offers additional insights into the results given here.

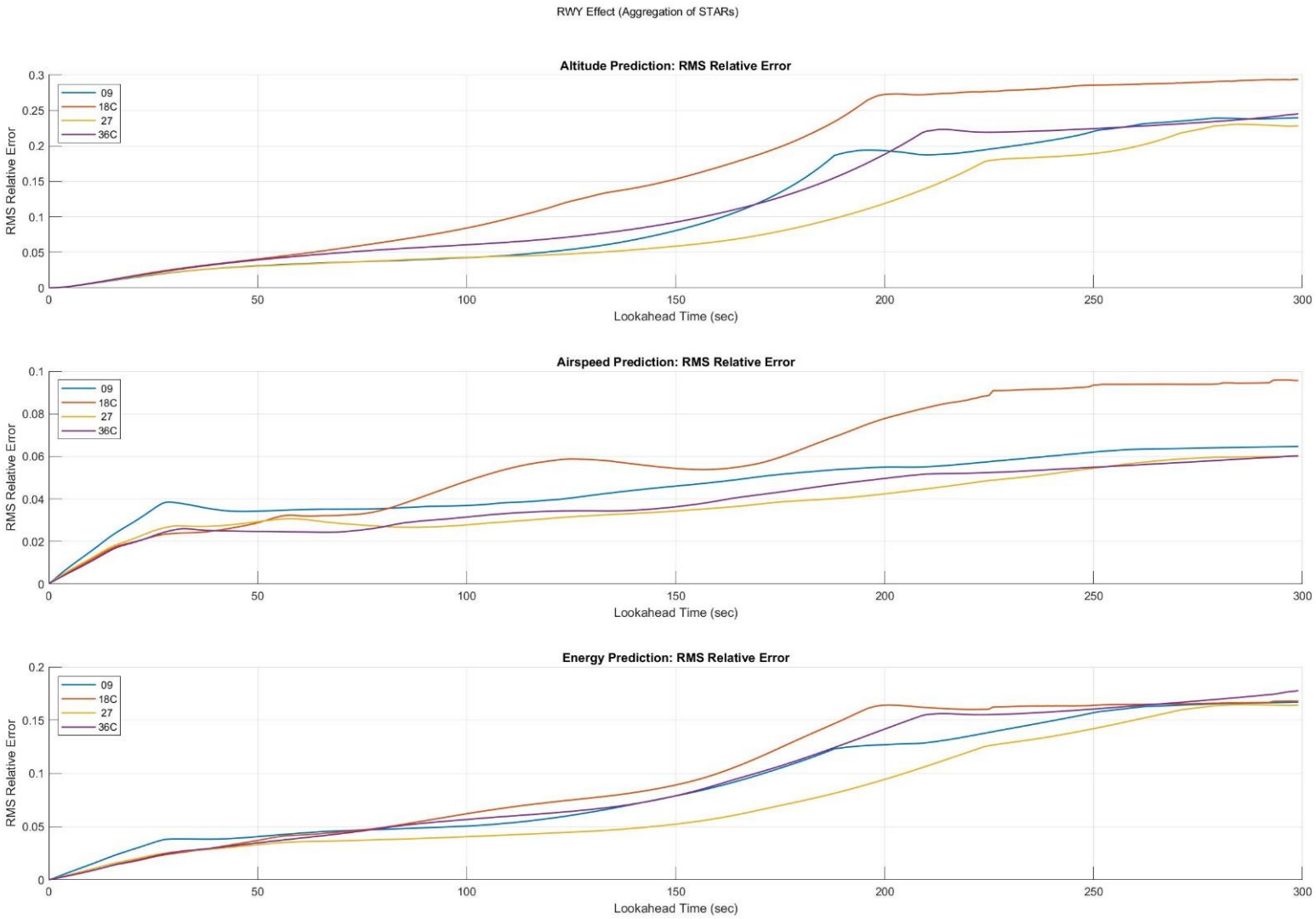

Figure 36: Runways (Aggregation of STARs): Relative-Error RMS Statistic for Altitude, Airspeed, and Energy Prediction as a Function of Look-ahead τ

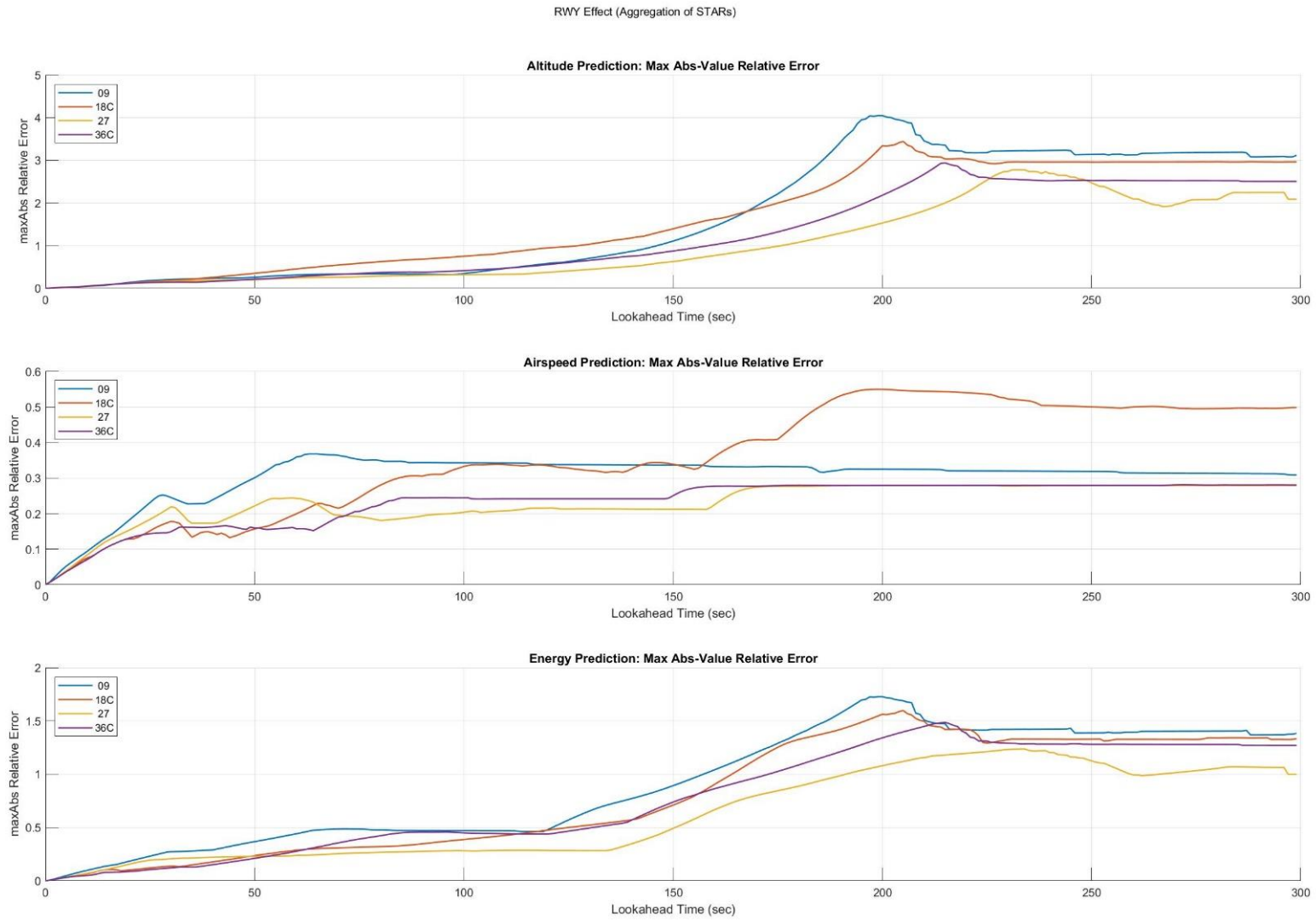

Figure 37: Runways (Aggregation of STARs): Relative-Error absMax Statistic for Altitude, Airspeed, and Energy Prediction as a Function of Look-ahead τ

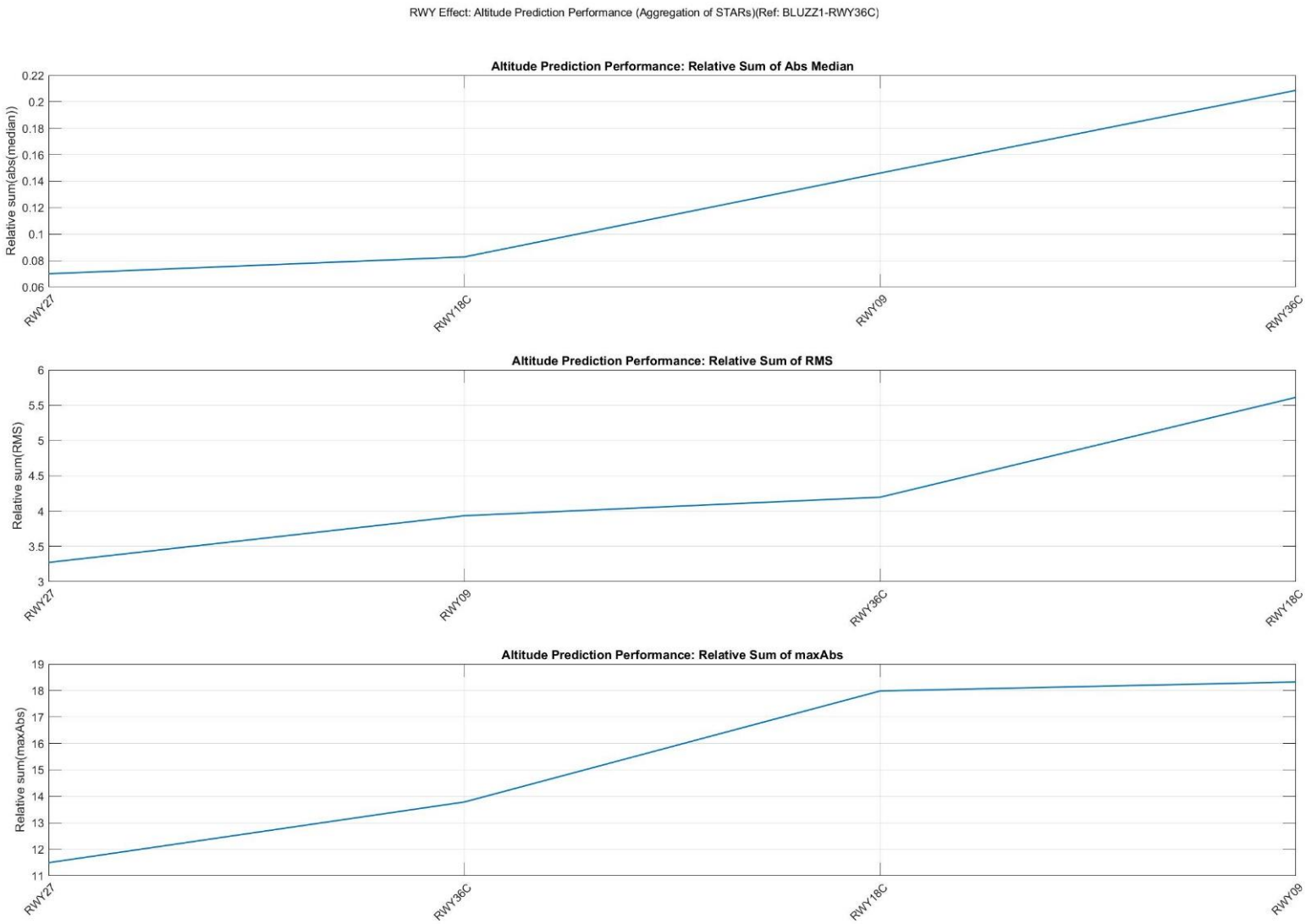

Figure 38: Runways (Aggregation of STARs): Ranked Cumulative Relative- Error Statistics for Altitude Prediction Normalized With Respect to BLUZZ-RW36C

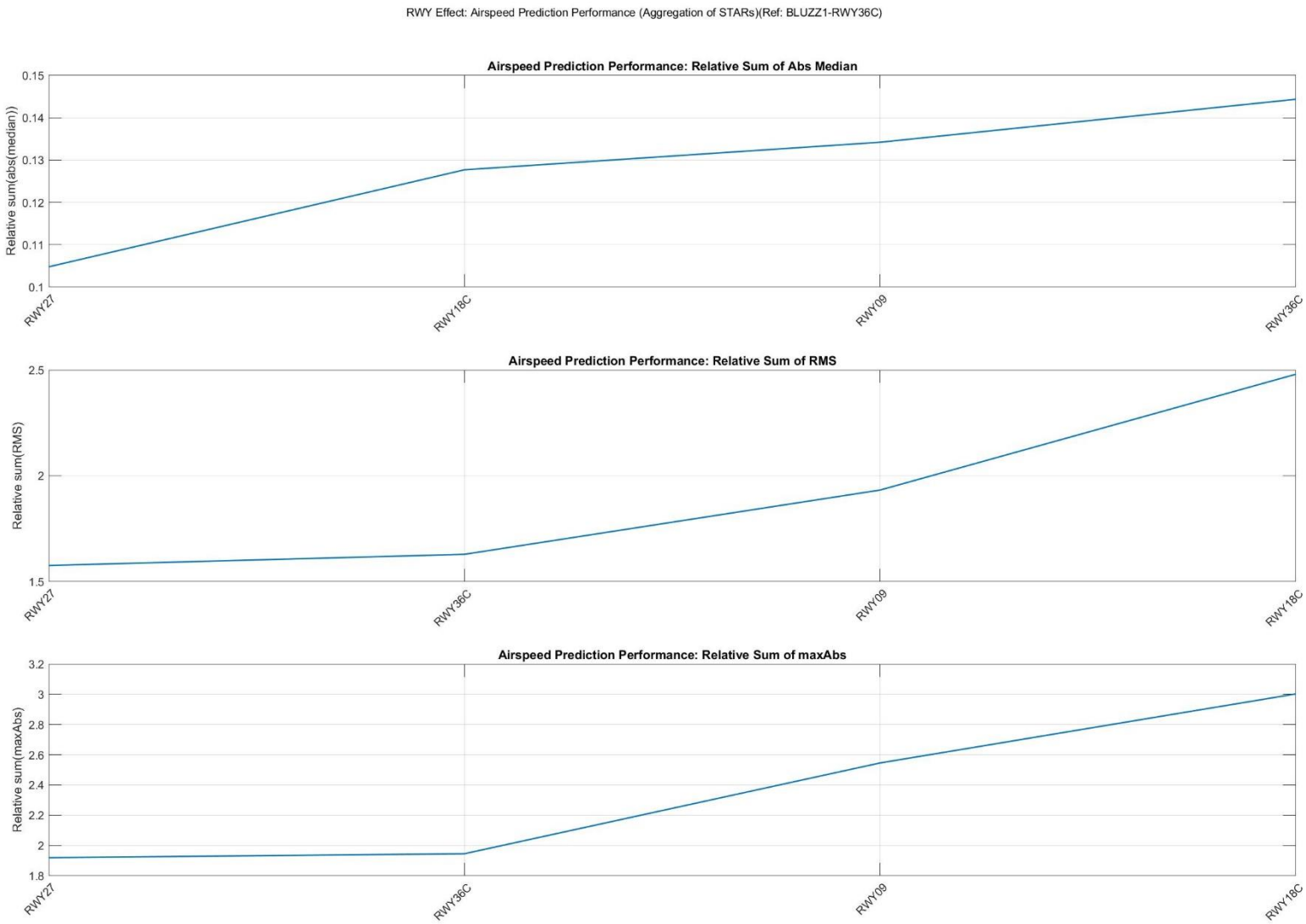

Figure 39: Runways (Aggregation of STARs): Ranked Cumulative Relative- Error Statistics for Airspeed Prediction Normalized With Respect to BLUZZ-RW36C

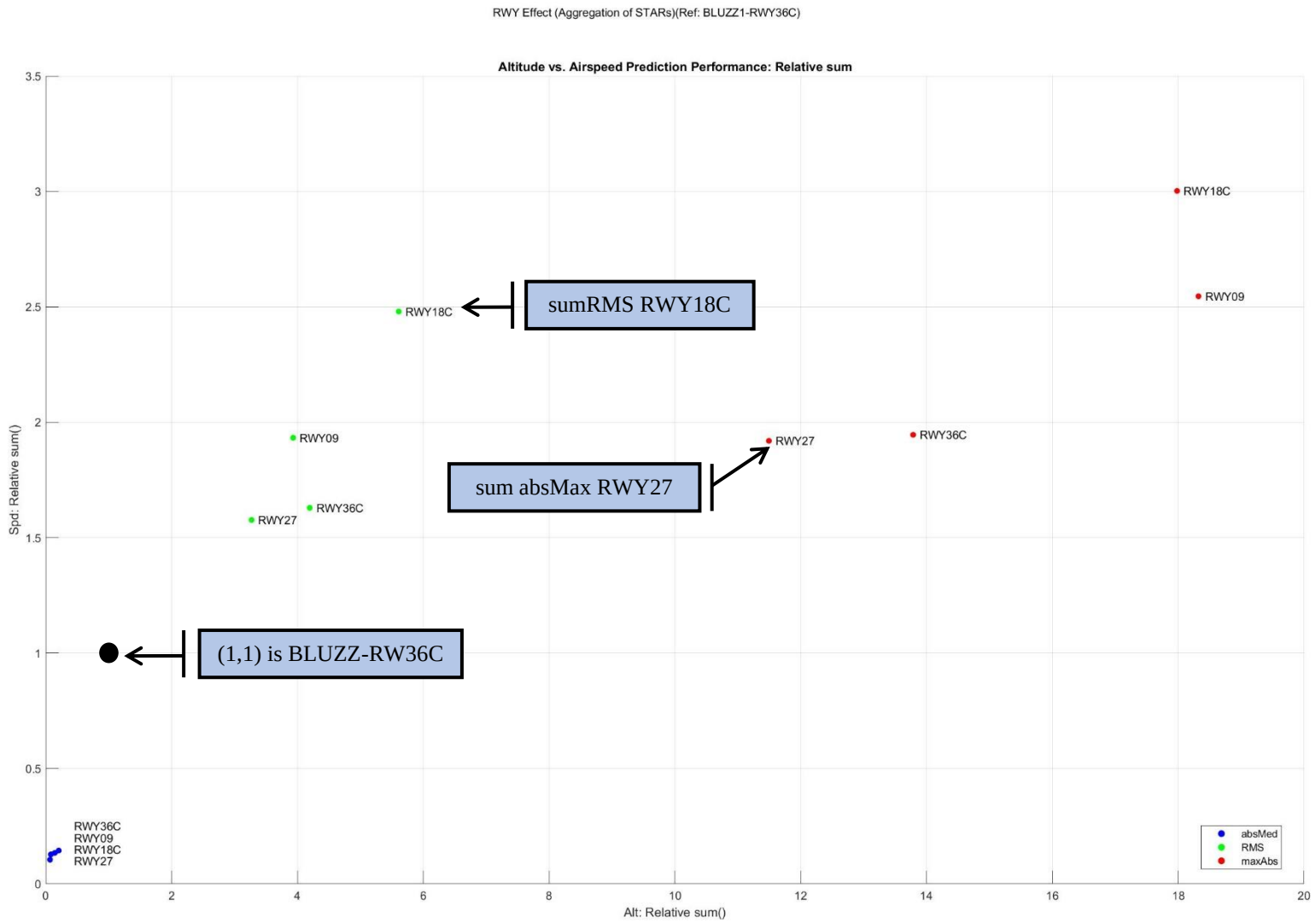

Figure 40: Runways (Aggregation of STARs): Cumulative Relative- Error Statistics for Altitude and Airspeed Prediction Normalized With Respect to BLUZZ-RW36C

6.4. Individual Flights

The prediction error results for individual STAR-Runway combinations are provided in Figure 41 to Figure 49, which show the relative error statistics as a function of look-ahead τ for altitude, airspeed, and energy prediction and the ranked cumulative relative-error statistics normalized with respect to BLUZZ-RW36C. Many of the plots in Figure 41 to Figure 46 are clearly similar. The numbers in Table 2 identify groups and subgroups of STAR-RWY combinations that have similar profiles in the plots in Figure 41 to Figure 46. These prediction performance similarities are likely related to symmetries and similarities in the location and structure of the STARs and the transitions from the STARs to the runways. Appendix C provides select additional data from each of the STAR-Runway flight combinations.

Table 2: STAR-RWY Combinations with Similar Profiles in Figure 41 to Figure 46 for Relative Error Statistics

Part 1			**Median Relative Error in Figure 41 and Figure 42**				**RMS Relative Error in Figure 43 and Figure 44**				**Max Absolute-Value Relative Error in Figure 45 and Figure 46**			
			Runway				**Runway**				**Runway**			
			09	**18C**	**27**	**36C**	**09**	**18C**	**27**	**36C**	**09**	**18C**	**27**	**36C**
STAR	**Corner-Point STAR**	**BLUZZ**			1	3	7	9	11	13	18	20	22	24
		VANZE		2	1		7	10	11	14	18	21	22	24
		HOBRK	1	3			8	10	12	14	19	21	23	24
		BRBBQ	1			2	8	9	12	13	19	20	23	24
	Cardinal-Point STAR	**HYTHR**	4		4		15a		15b		25a		25b	
		MONAA		5		6	16	15c	17	15d		25c	26	25d
		CONDR		5		6	17	15c	16	15d	26	25c		25d

The magnitudes of the curves in Figure 41 to Figure 46 are also interesting. Notice that the magnitude of the medians in Figure 41 for corner-point STARs is smaller than 3%, while median relative errors in Figure 42 for cardinal-point STARs are within 9% for altitude and 8% for airspeed predictions. Also the RMS and maximum absolute-value relative errors for corner-point STARs are in most cases much smaller than for cardinal-point STARs. These observations are consistent with the observations made in the preceding analysis for STARs with aggregation of the runways. Clearly, in most cases the locations, structures, and transitions to runway approaches of the corner-point STARs are more favorable to prediction performance than the structures of the cardinal-point STARs.

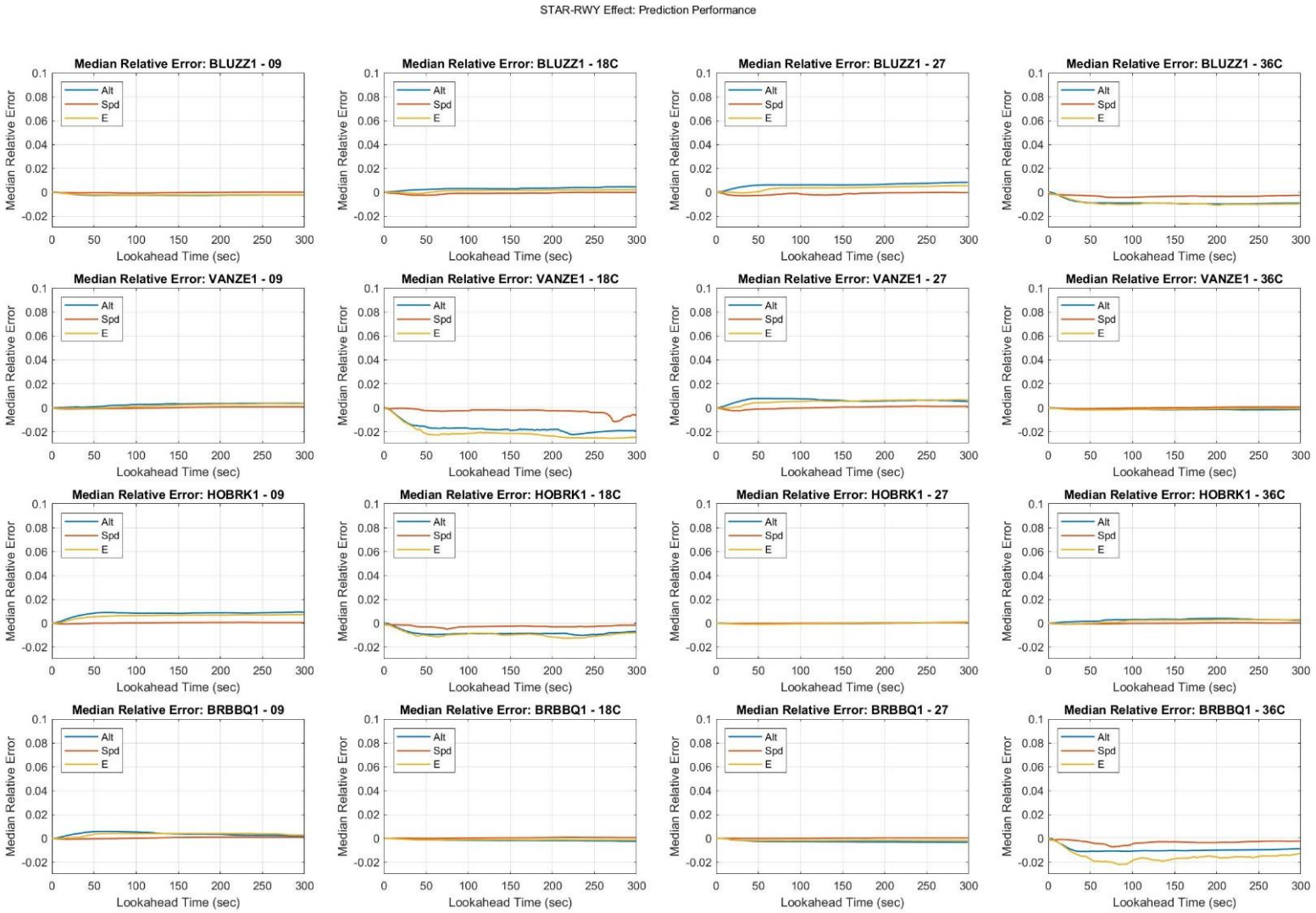

Figure 41: Corner-Point STARs to Every Runway: Median Relative Error for Altitude, Airspeed, and Energy Prediction as a Function of Look-ahead τ

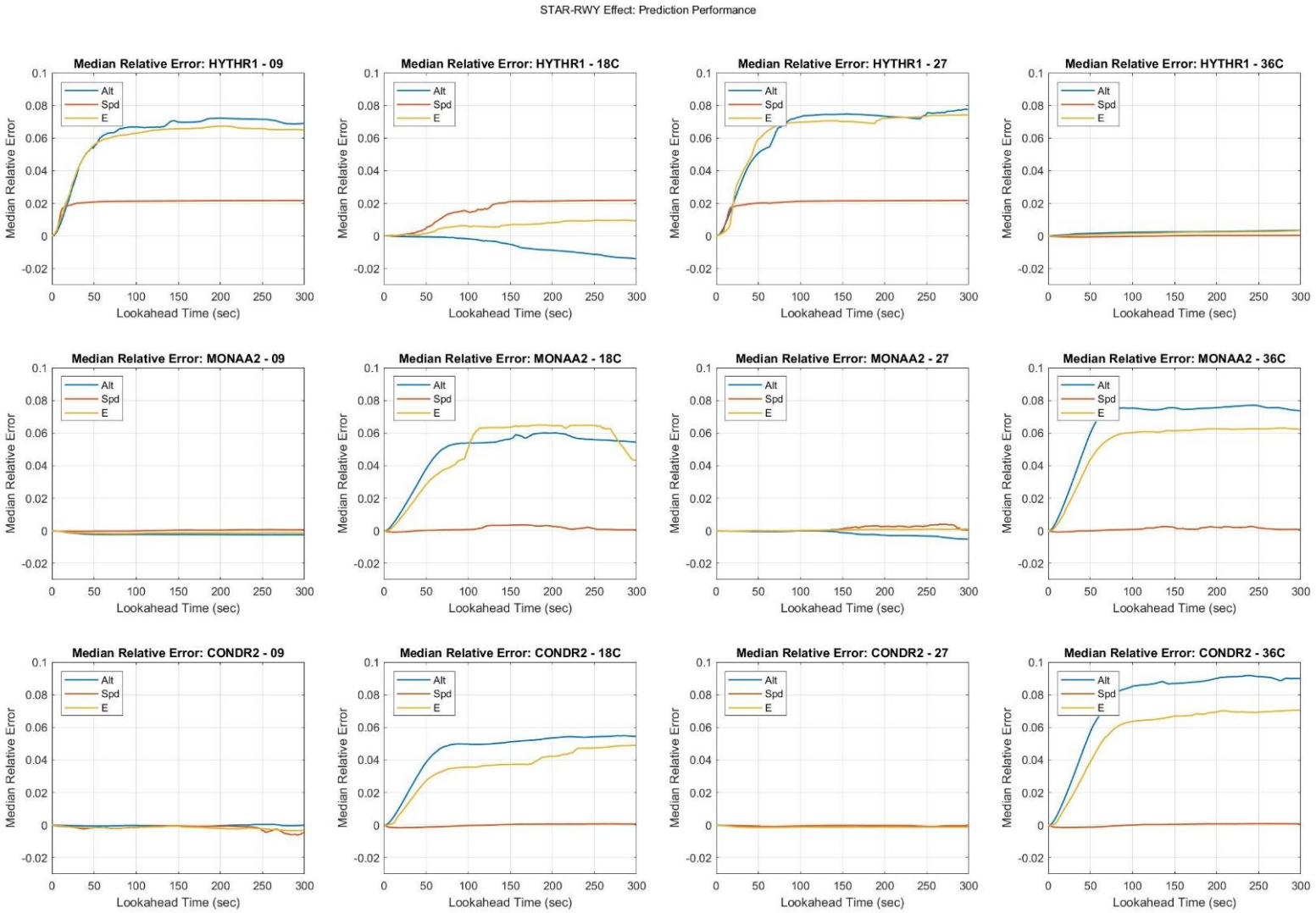

Figure 42: Cardinal-Point STARs to Every Runway: Median Relative Error for Altitude, Airspeed, and Energy Prediction as a Function of Look-ahead τ

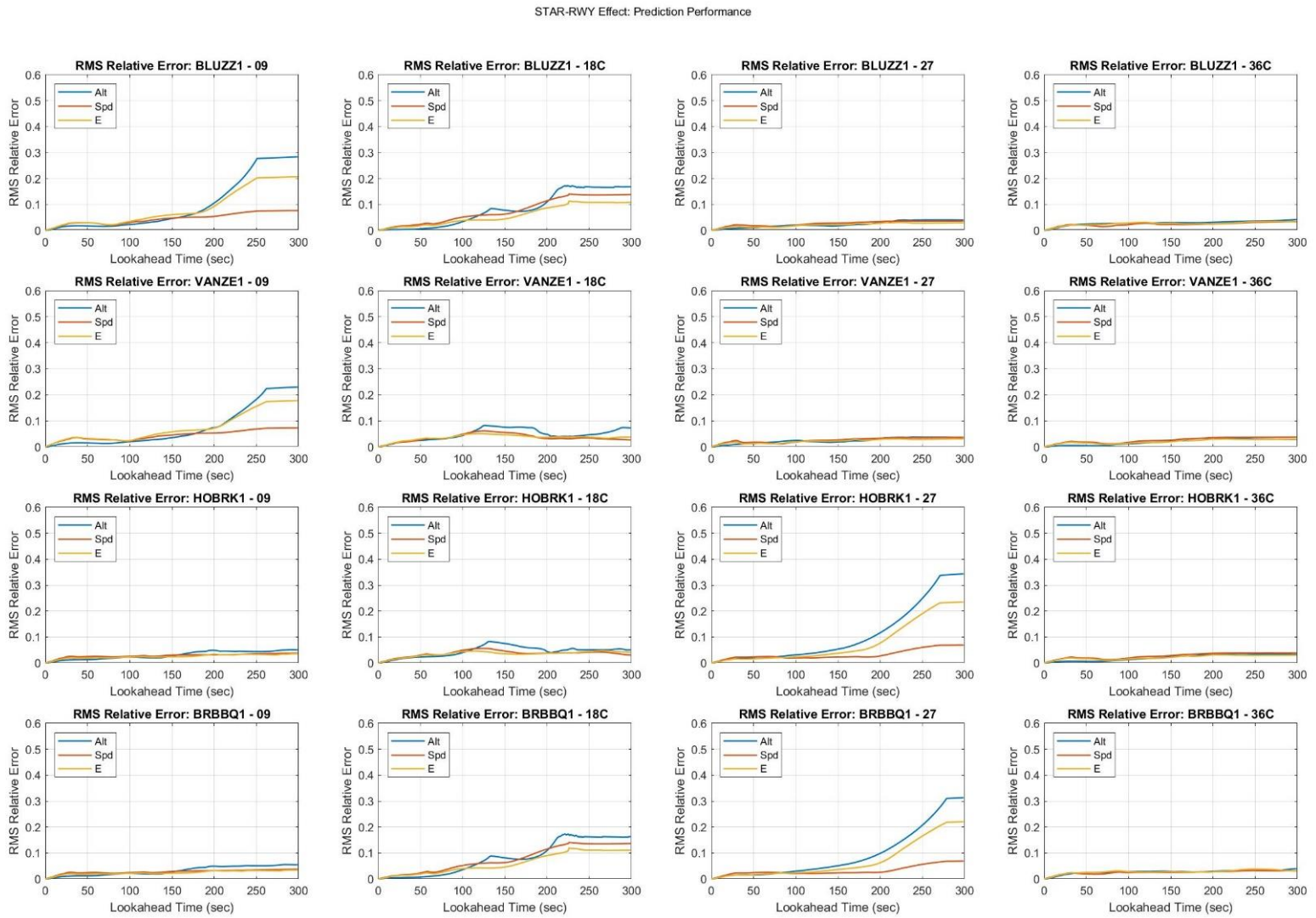

Figure 43: Corner-Point STARs to Every Runway: RMS Relative Error for Altitude, Airspeed, and Energy Prediction as a Function of Look-ahead τ

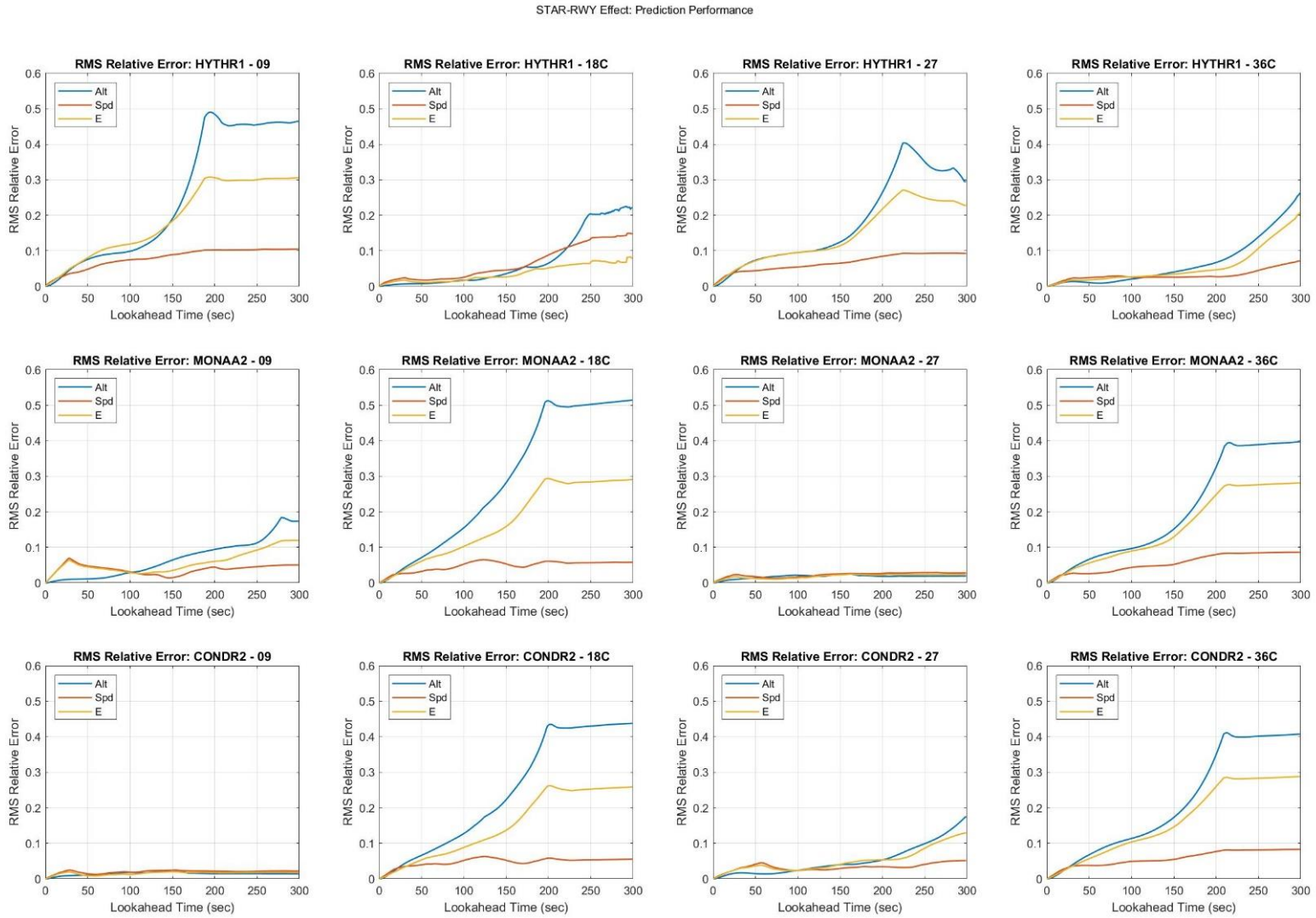

Figure 44: Cardinal-Point STARs to Every Runway: RMS Relative Error for Altitude, Airspeed, and Energy Prediction as a Function of Look-ahead τ

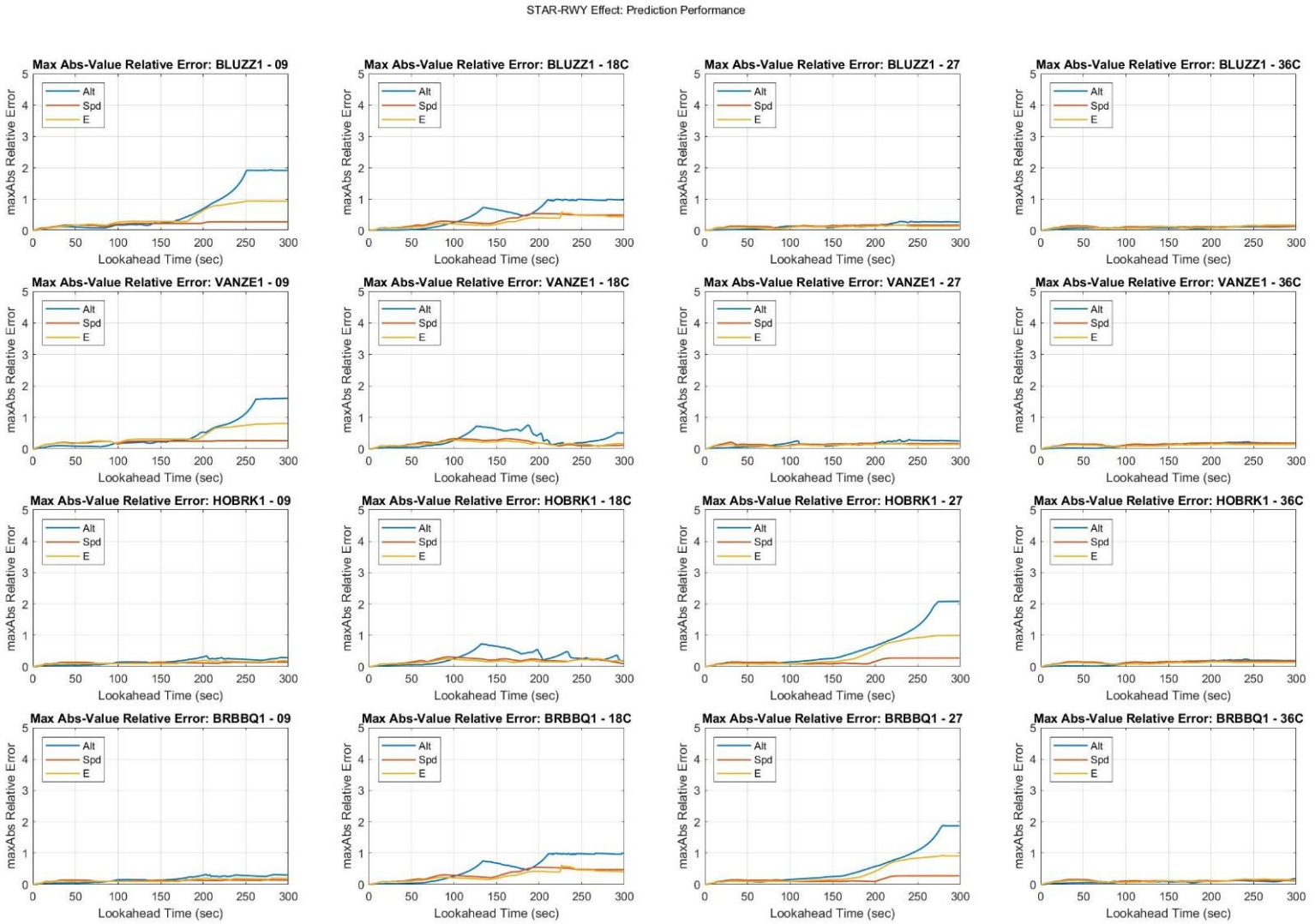

Figure 45: Corner-Point STARs to Every Runway: Maximum Absolute-Value Relative Error for Altitude, Airspeed, and Energy Prediction as a Function of Look-ahead τ

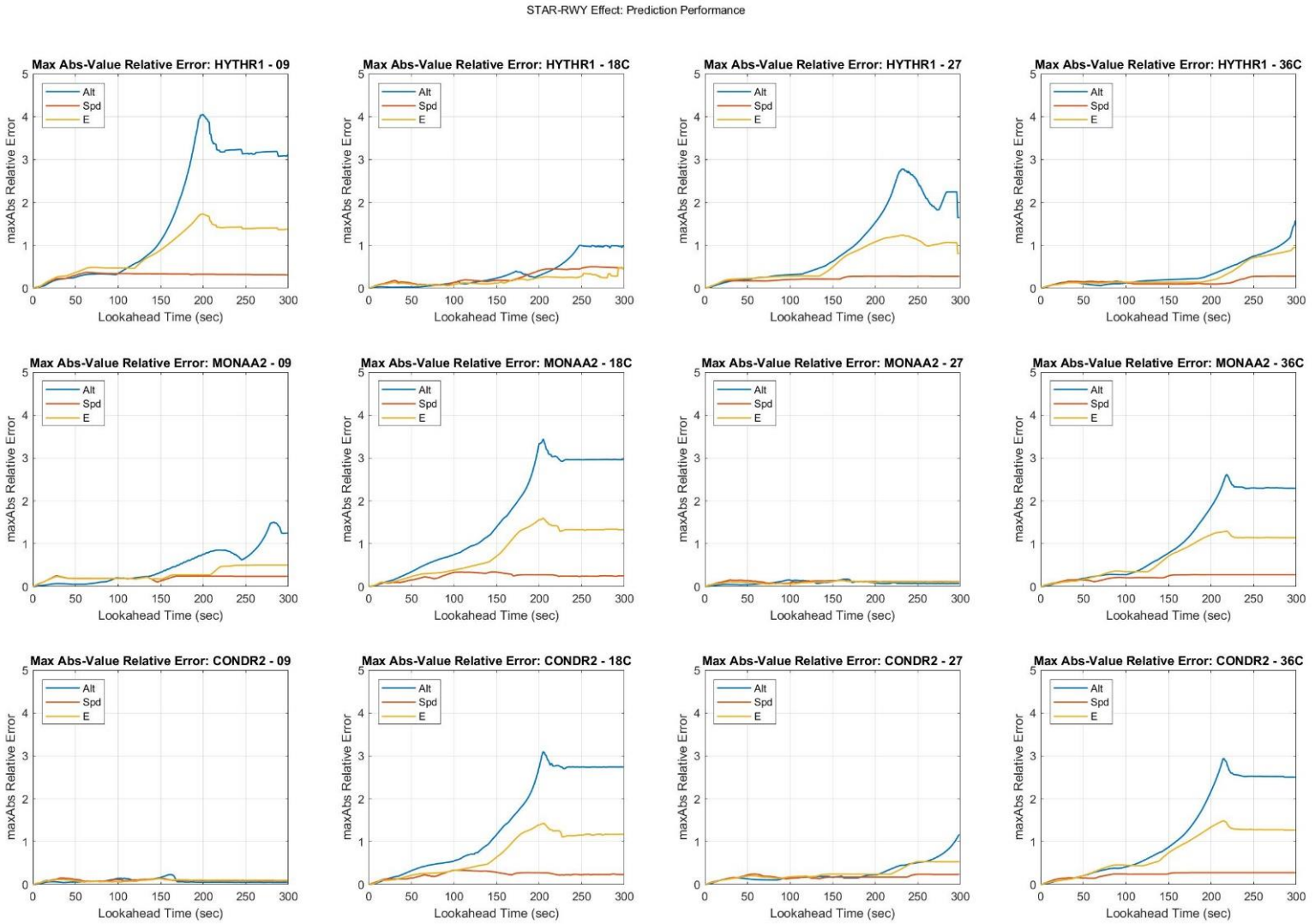

Figure 46: Cardinal-Point STARs to Every Runway: Maximum Absolute-Value Relative Error for Altitude, Airspeed, and Energy Prediction as a Function of Look-ahead τ

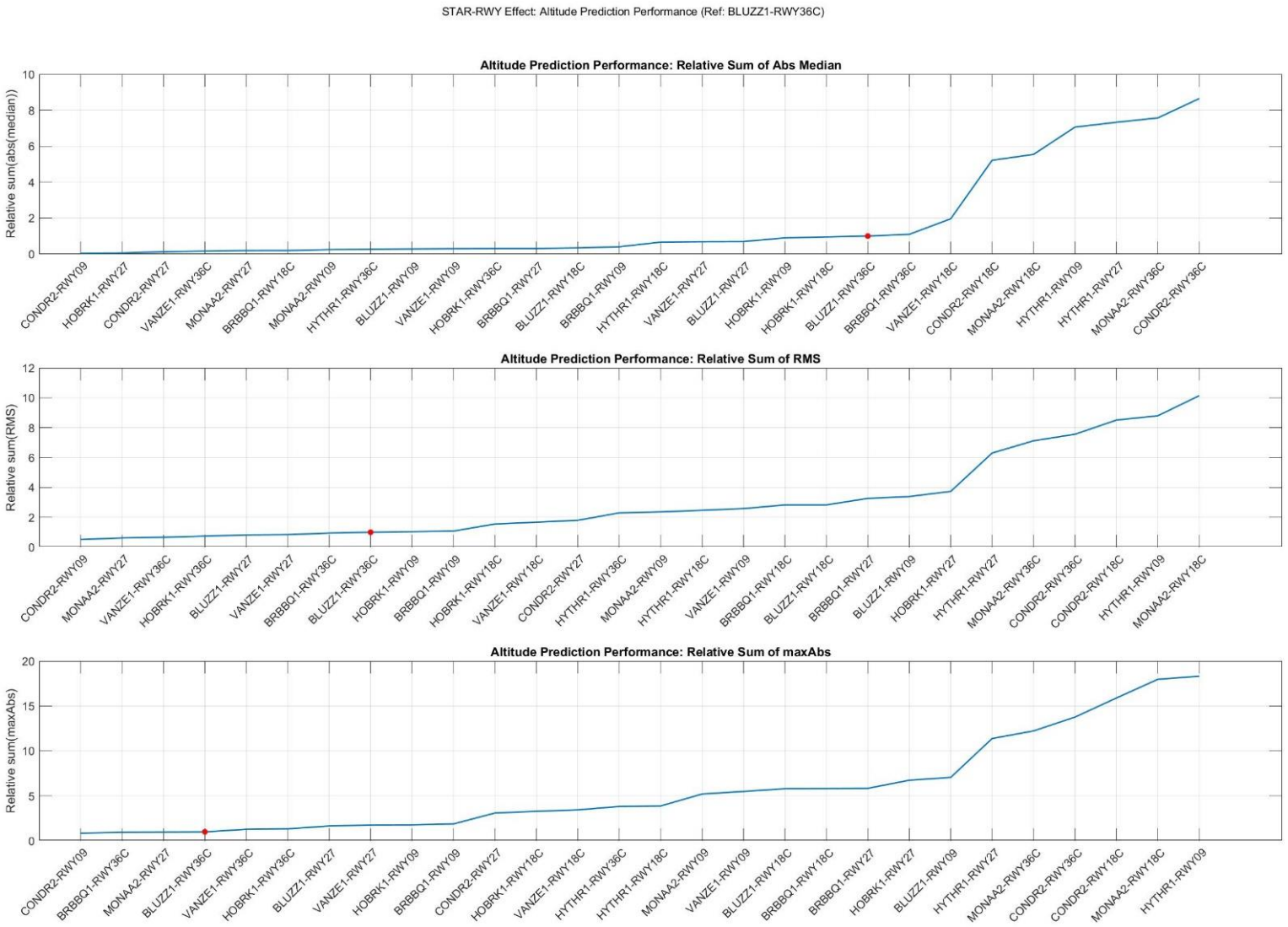

Figure 47: STAR-Runway Combinations: Ranked Cumulative Relative-Error Statistics for Altitude Prediction Normalized with Respect to BLUZZ-RW36C (red dot)

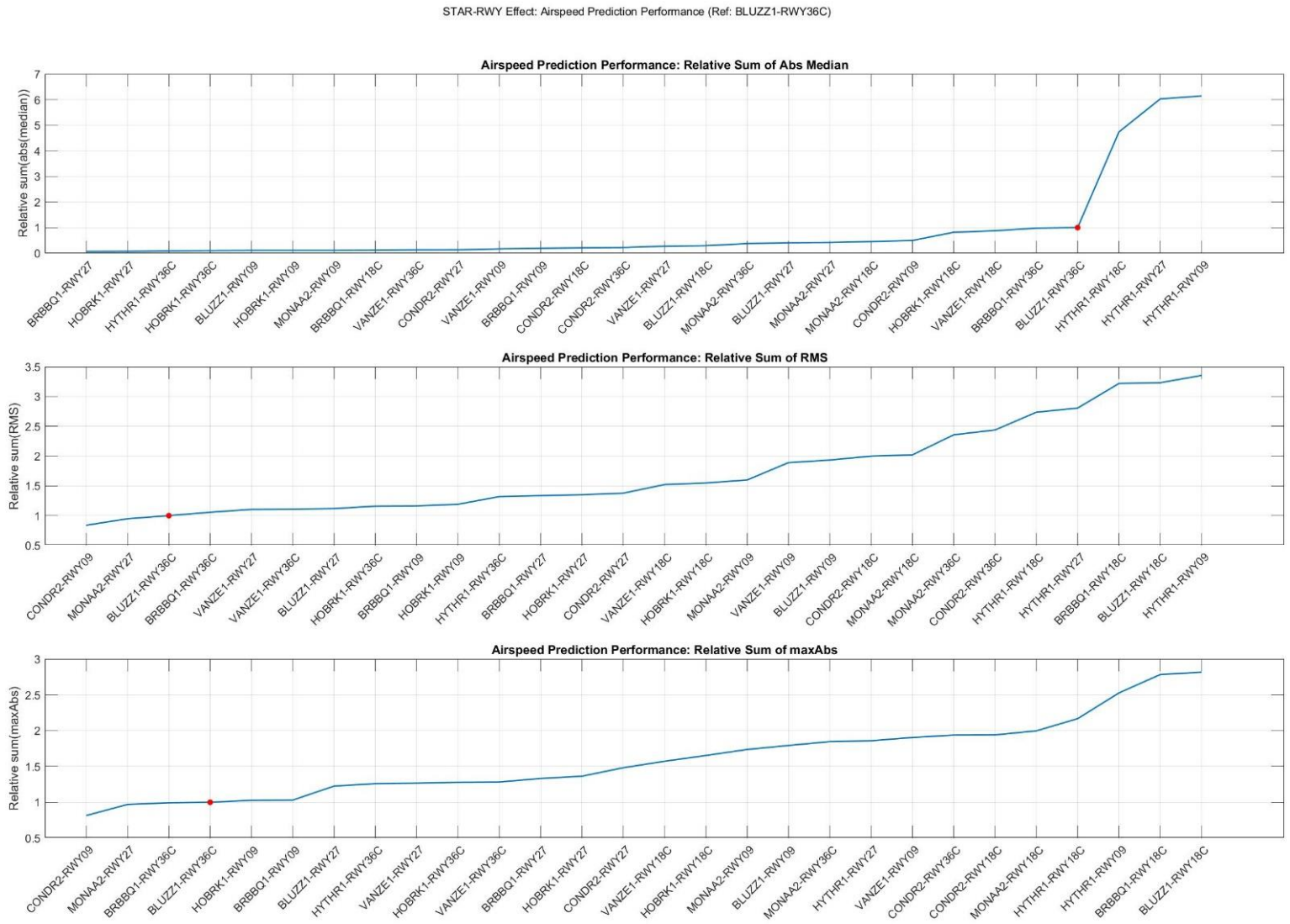

Figure 48: STAR-Runway Combinations: Ranked Cumulative Relative-Error Statistics for Airspeed Prediction Normalized with Respect to BLUZZ-RW36C (red dot)

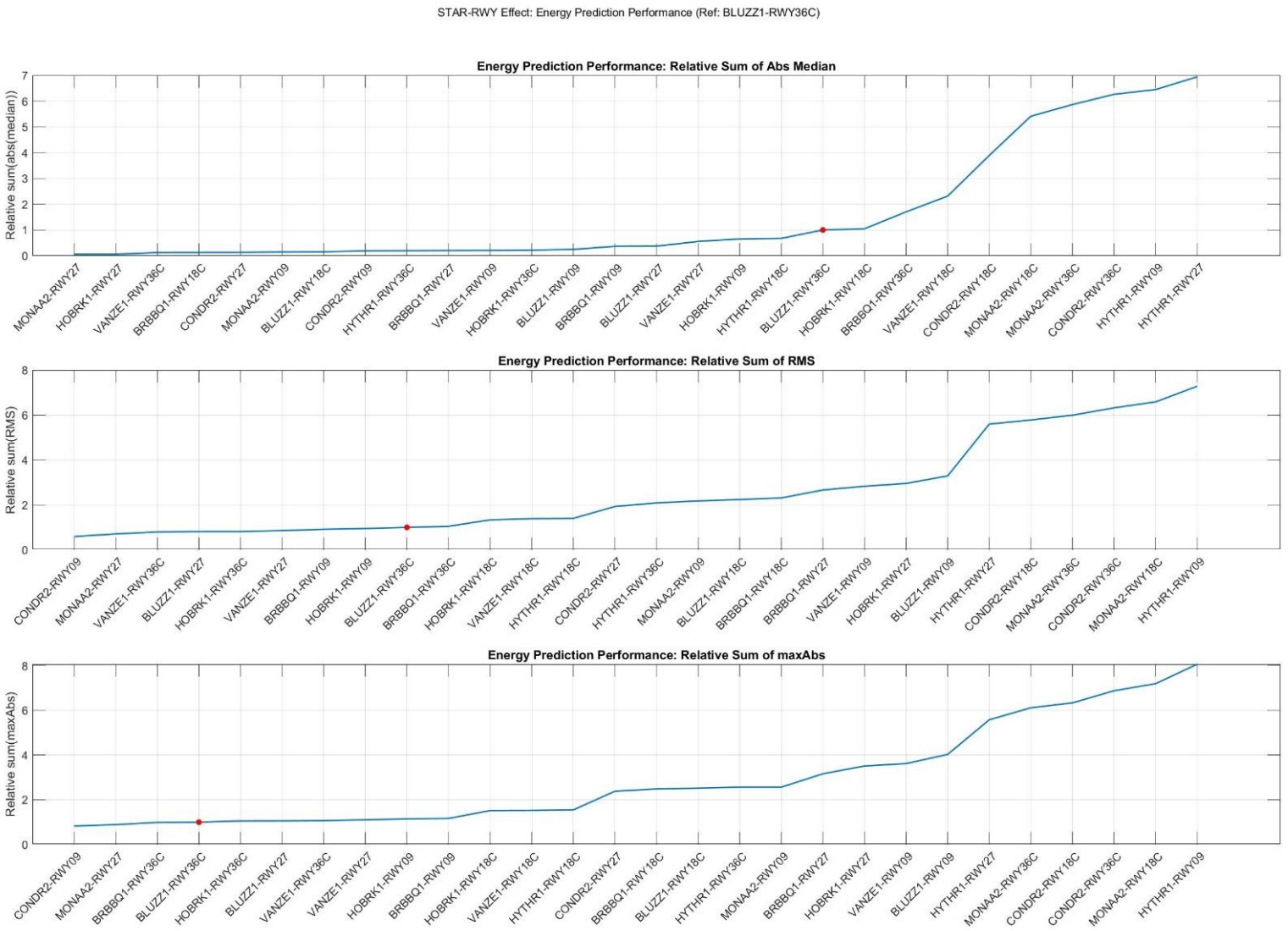

Figure 49: STAR-Runway Combinations: Ranked Cumulative Relative-Error Statistics for Energy Prediction Normalized with Respect to BLUZZ-RW36C (red dot)

The ranked normalized cumulative relative-error statistics in Figure 47 to Figure 49 allow additional observations about relative prediction performance, especially for the cardinal-point STARs. For altitude prediction, the following STAR-Runway combinations have the worst performance: CONDR-18C, MONAA-18C, HYTHR-09, HYTHR-27, MONAA-36C, and CONDR-36C. All of these have transitions to approach with lateral turns of around 90 degrees or larger. On the other hand, CONDR-09 and MONAA-27 transitions to approach essentially require no heading corrections, and these show much better altitude prediction performance. In general, it seems that altitude prediction performance is worse when the STAR has a small amount of structure (i.e., fewer waypoints and changes in trajectory) and the transition to approach is around 90 degrees, though it improves as the turns approach 180 degrees, as seen for HYTHR-36C, CONDR-27, and MONAA-09.

For airspeed prediction in Figure 48, HYTHR to runways 09, 18C, and 27 clearly have some of the worst prediction performance. Interestingly airspeed prediction performance is also poor for BLUZZ-09, BLUZZ-18C, BRBBQ-09, and BRBBQ-18C, all of which have structures similar to the worst-performing cardinal-point STAR-Runway combinations.

The energy prediction performance results in Figure 49 show that BRBBQ-27 and HOBRK-27 are among the worse-performing and these, too, have structural similarities to the worst-performing cardinal-point STAR-Runway combinations.

The examination of anomalies in the next section provides additional insights into the weaknesses of the prediction function.

6.5. Anomalies

The TP function exhibited multiple noteworthy behaviors that are designated here as anomalies according to the dictionary definition as “inconsistent with or deviating from what is usual, normal, or expected; marked by incongruity or contradiction; inappropriate” [22] [23]. Some anomalies seem to be related to software design, implementation, and execution problems, and other anomalies seem related to modeling problems.

The anomalies seemingly related to software design include random NaN (i.e., Not a Number) and 0 outputs. The NaN outputs are probably indications of internal calculation exceptions, such a divide-by-zero. Most of the twenty-eight flights in Part 1 of CASPEr-1 had hundreds of NaN values in the time histories of the airplane state prediction variables for many (and possibly) all look-ahead τ values. These NaN outputs may occur at random times scattered throughout the data, although a focused effort to characterize their arrival (i.e., locations in the data) has not been done.

Values of 0 in the data happened in some of the flights, but not all. These 0 values are clearly anomalous as none of the actual trajectory variables (i.e., altitude, airspeed, latitude, and longitude) for the airplane are near 0 at any point during the flights; the lowest altitude is around 400 feet above ground level. The 0 output values seem to appear in bursts over time for some look-ahead τ times, but here, too, no focused effort to characterize their arrival has been carried out. These anomalous outputs may have been due to irregular cyclic execution of the TP function, which could cause it to sporadically miss constraints in the execution delay. If this actually happened, it is possible that the simulation software detected the missing output update and recorded it with 0 values.

The NaN and 0 output values in the data were handled with a common policy that enabled the detailed processing of the data and evaluation of prediction performance. Specifically, each occurrence of a NaN or 0 value in a state prediction variable was replaced with the immediately preceding value in the time series. For a burst of anomalous outputs the effect of this policy is that the variable value is held constant during the burst until a valid value is reached. Visual inspection of the prediction data showed that these corrections to the data are rarely noticeable and their statistical effect is likely insignificant in comparison to the large prediction errors in the data.

Other anomalous behavior seems related to modeling errors and limitations. Figure 50 and Figure 51 show the approach to runway 09 for flights on STARs BLUZZ and HYTHR, respectively. Figure 52 shows the approach to runway 18C from STAR MONAA. The inset sections of the approach plates show that the initial approach fixes (IAF) for the approaches to these runways are fly-by waypoints. The actual flown trajectories are colored blue as indicated in the figures. The gray colored lines from IAF to the final approach fix (FAF) are the defined trajectories. All other trajectories are predicted. Notice that the predicted trajectories goes over the IAFs, which is an indication that the predictor modeled these as fly-over waypoints. In addition, the green and blue lines with sharp forward transitions are an indication that at some point the predictor detected the large errors in the predicted trajectories and computed corrections, though the updated trajectory predictions were still noticeably different from the actual flown trajectories.

Figure 53 shows the approach to runway 09 from STAR MONAA. This approach requires a 180-degree turn to line up with the runway. In the actual flown trajectory the airplane turned left as it approached (i.e., flew by) the IAF at BUDEE. However, all the predicted trajectories pass over BUDEE and turn right. The green and blue predicted trajectories show that at some point the predictor detected the errors and applied multiple corrections, but clearly it did not have a good model or adequate real-time information to generate a credible prediction of the trajectory of the airplane.

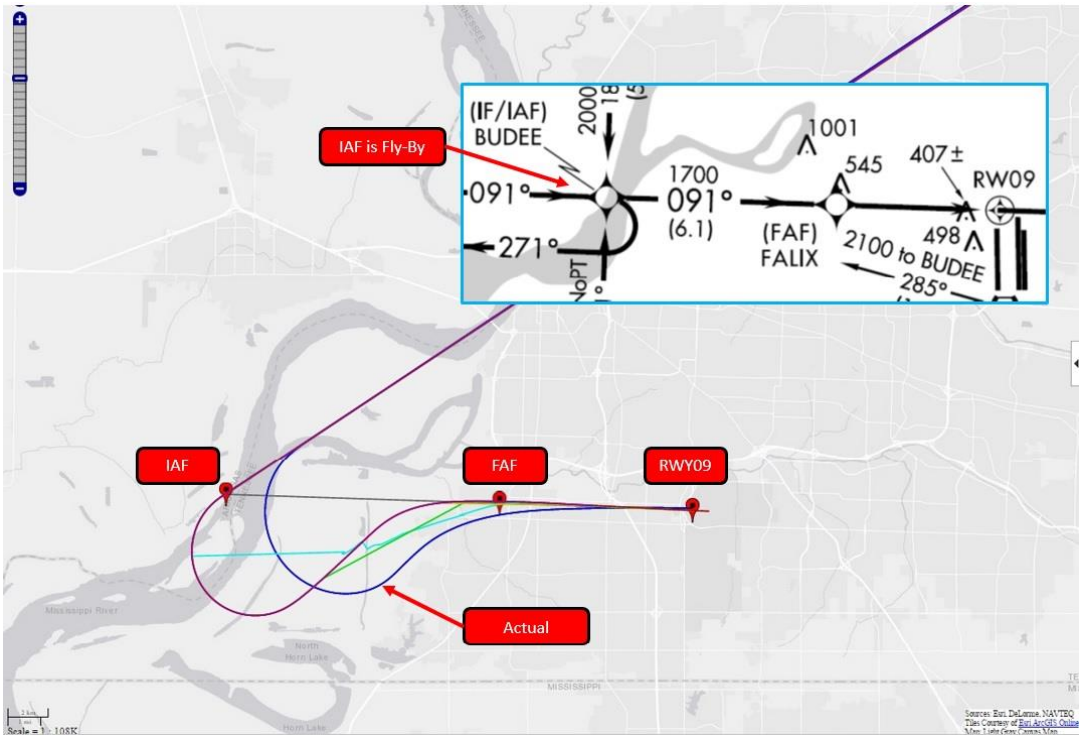

Figure 50: Approach to Runway 09 from Arrival Route BLUZZ

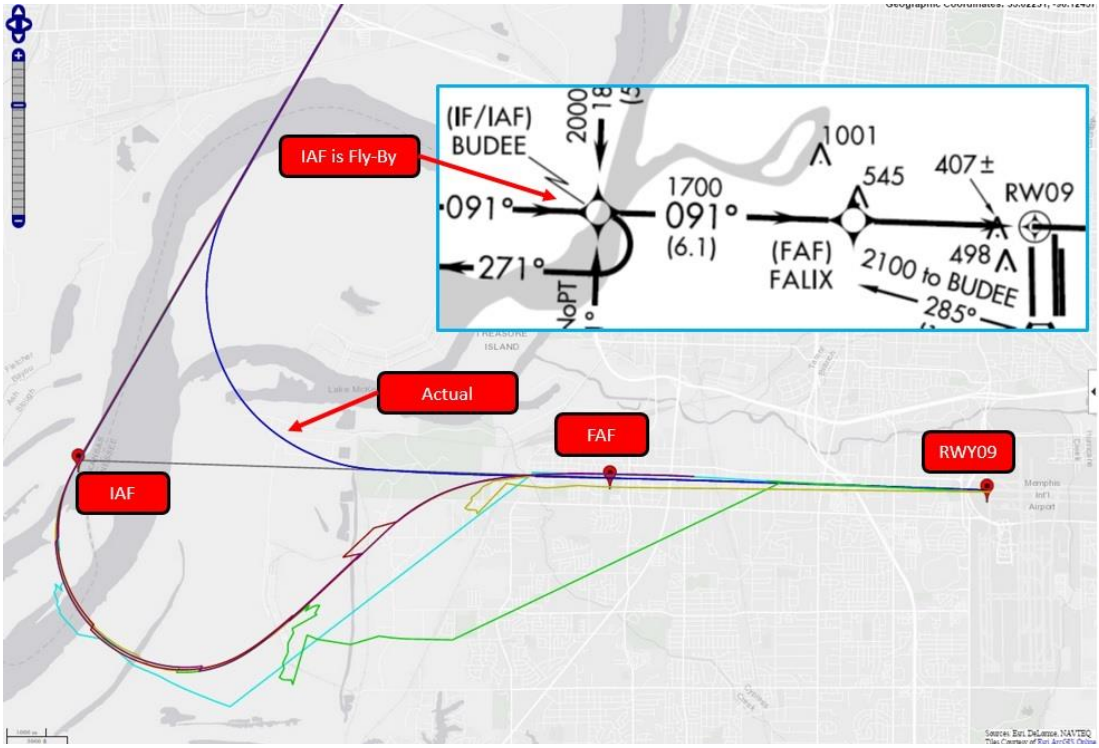

Figure 51: Approach to Runway 09 from Arrival Route HYTHR

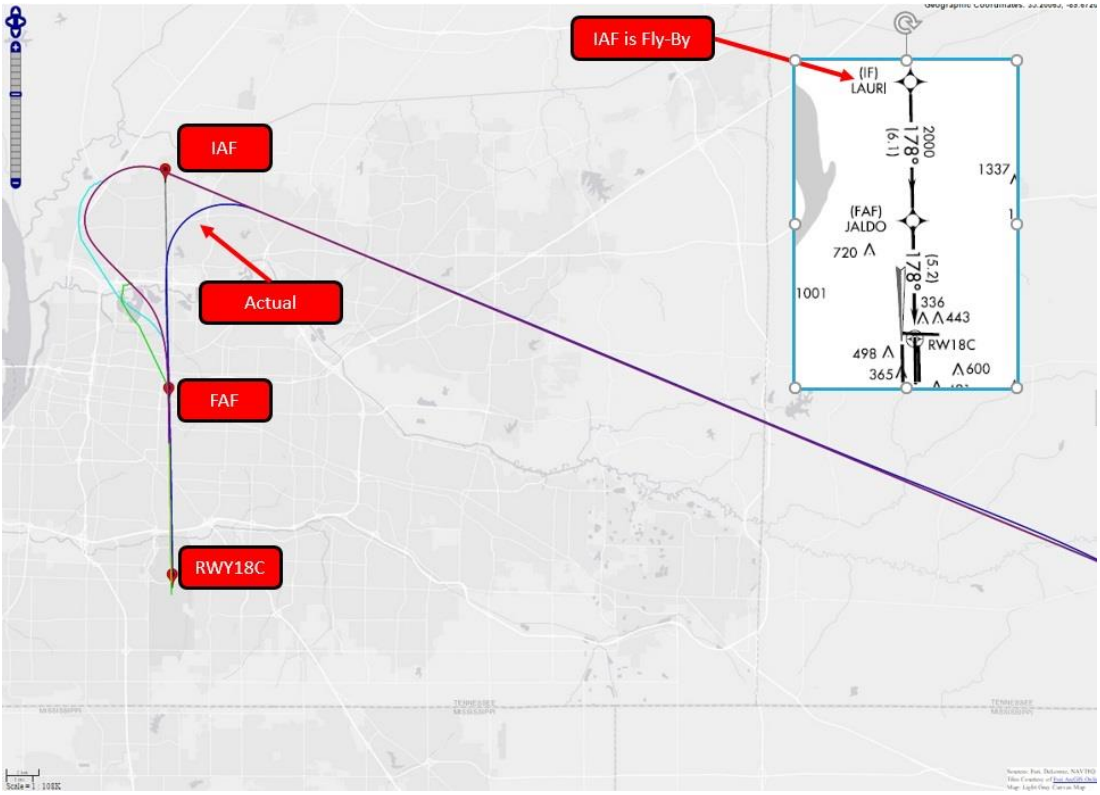

Figure 52: Approach to Runway 18C from Arrival Route MONAA

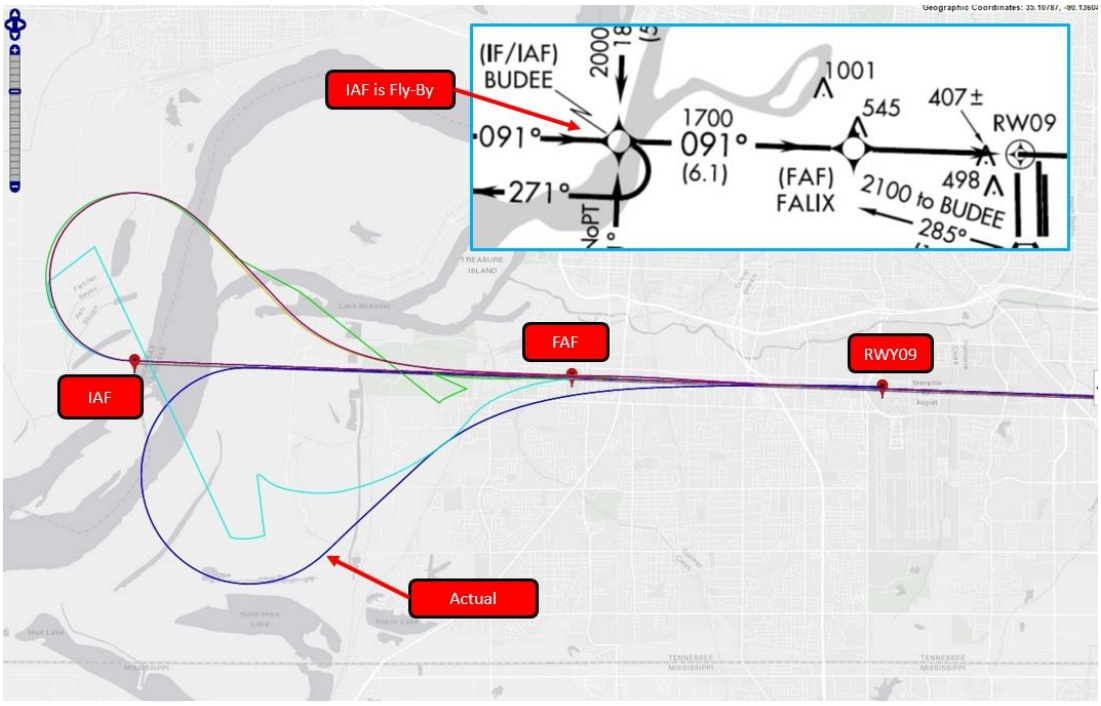

Figure 53: Approach to Runway 09 from Arrival Route MONAA

Figure 54 to Figure 57 show additional examples of anomalies that may be due to modeling errors.

- In Figure 54, both altitude and airspeed predictions have persistent bias from early in the flight until the end.
- Figure 55 and Figure 56 show widely varying altitude and speed predictions for the approach phase where the airplane transitions from 4,000 ft. at 210 kt to 400 ft. at 130 kt. The altitude and airspeed prediction pattern in Figure 55 for HYTHR to runway 18C appears to show that the predictor predicted for the look-ahead $\tau = 299$ seconds that the airplane was not going to decelerate to the normal landing speed of 130 kt, but instead was going to decelerate to about 190 kt while still continuing the descent to the runway. Predictions for smaller look-ahead τ initially followed this predicted trajectory but eventually made corrections that brought them closer to the actual trajectory.
- Figure 57 shows yet another pattern of anomalous behavior. In this case the airspeed is predicted to increase from 210 kt to approximately 230 kt after the altitude crosses 9,000 ft. This is followed by a correction back to 210 kt. at different points in time for different look-ahead τ. A similar pattern was observed in the baseline flight BLUZZ-36C (see Figure 19).

Some of these complex anomalies may be due to erroneous predictions of automation mode transitions. Future analysis should examine the relation between errors in trajectory predictions and errors in automation mode predictions.

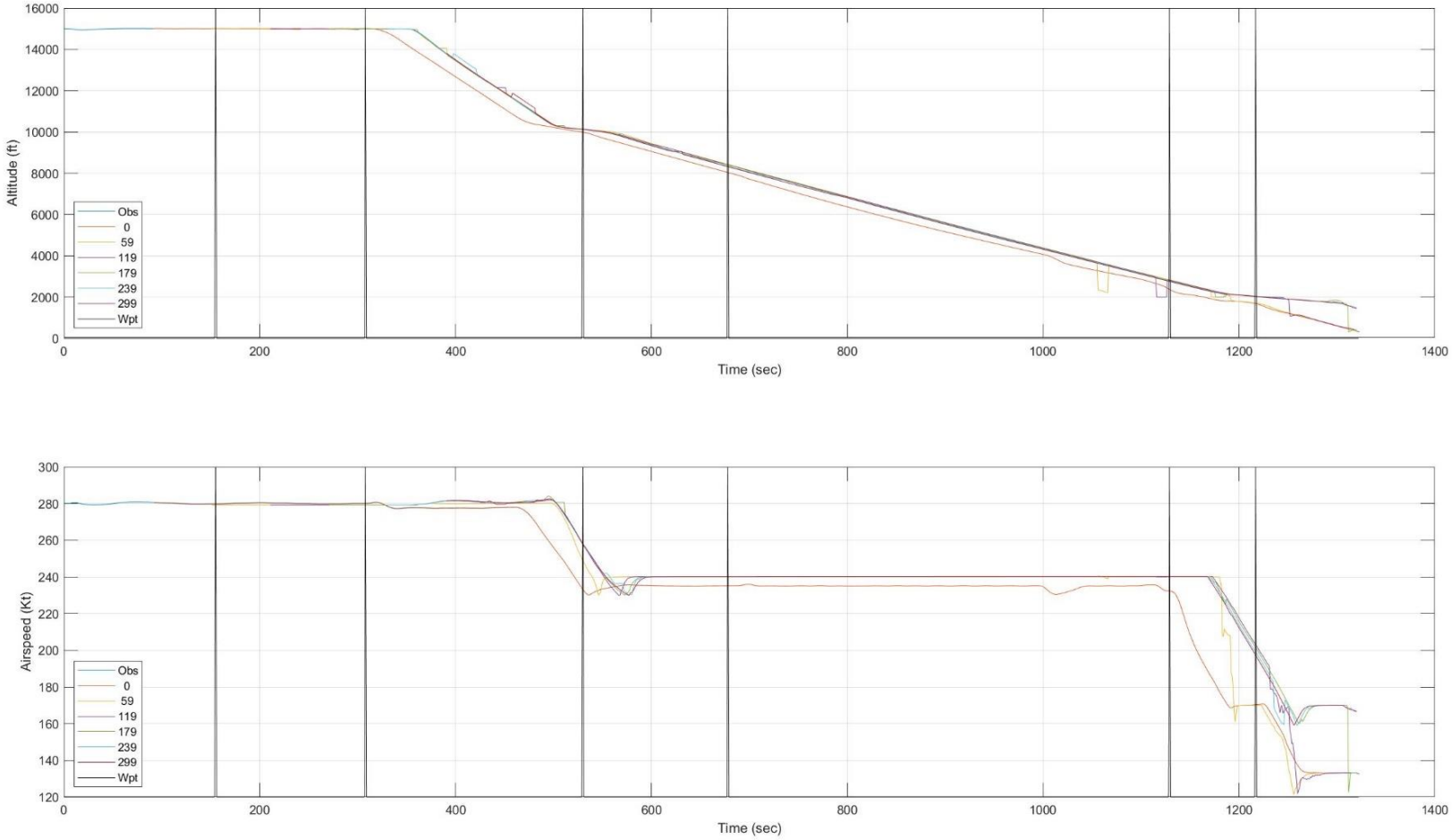

Figure 54: HYTHR to Runway 09: Time History of Predicted Altitude and Airspeed

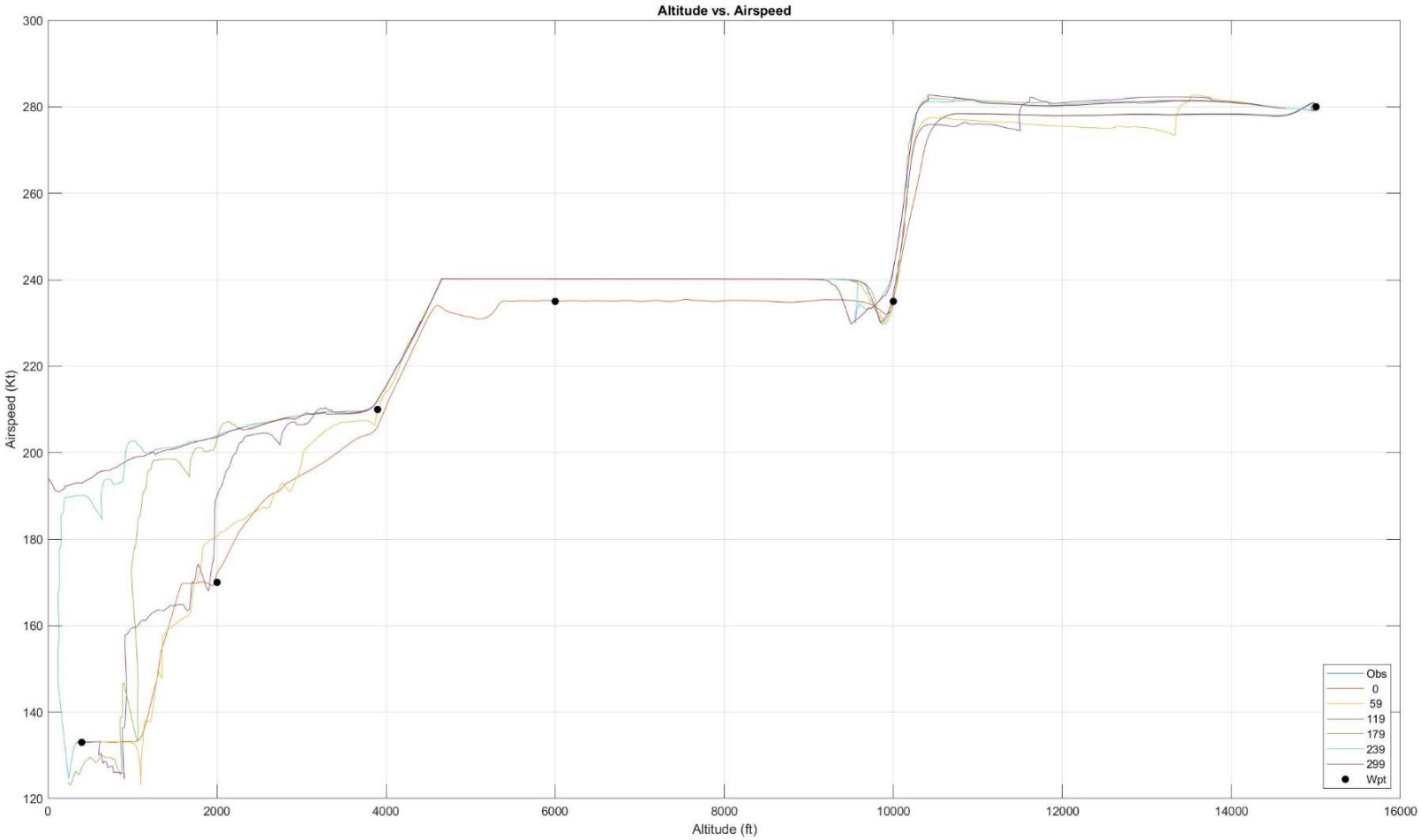

Figure 55: HYTHR to Runway 18C: Altitude vs. Airspeed Actual and Predictions

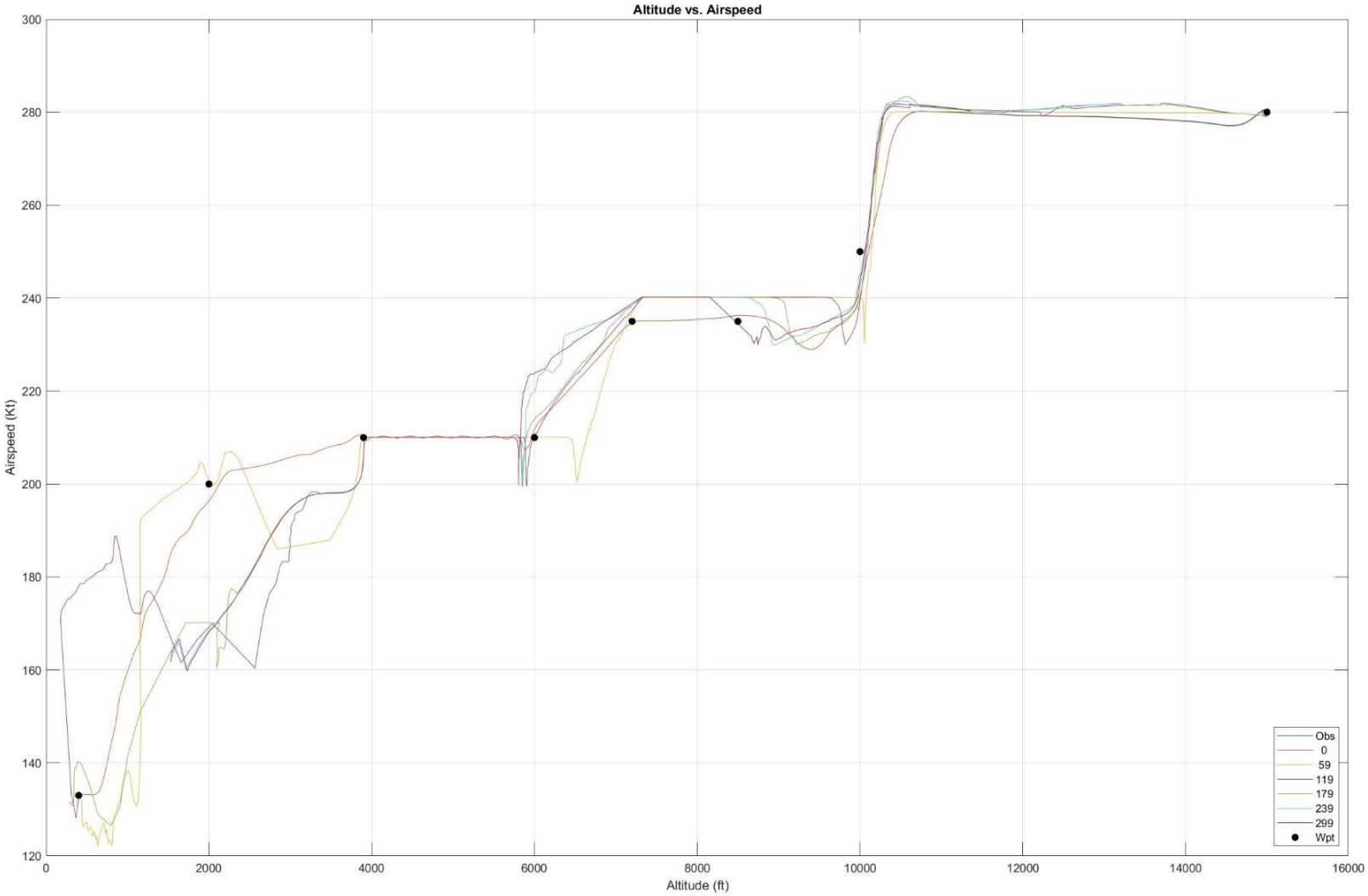

Figure 56: MONAA to Runway 18C: Altitude vs. Airspeed Actual and Predictions

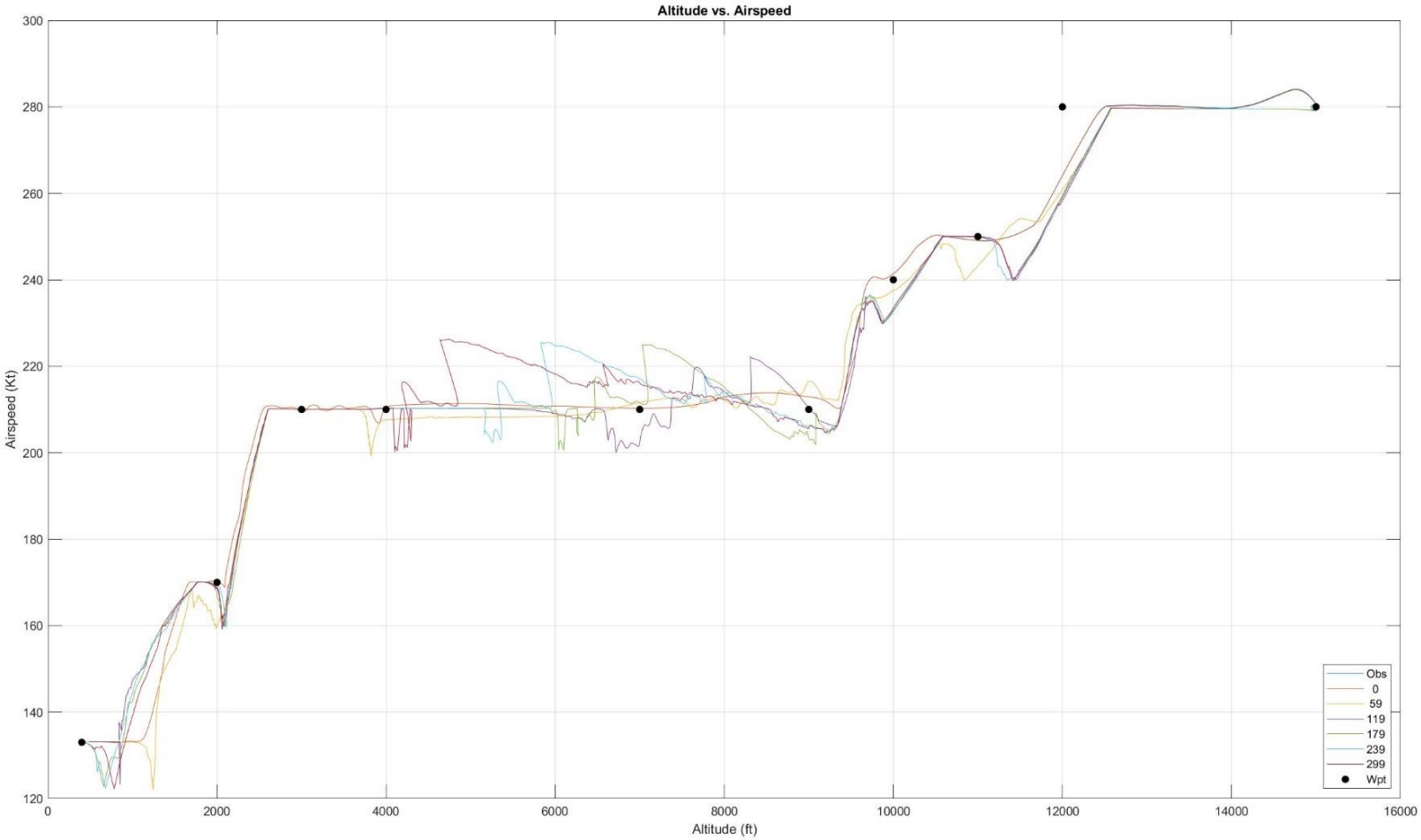

Figure 57: BRBBQ to Runway 36C: Altitude vs. Airspeed Actual and Predictions

7. Final Remarks

Analysis of the data for Part 1 of CASPEr-1 has shown interesting results. In general, the TP function had good altitude and airspeed prediction performance for most STARs, but the performance in terms of relative error deteriorates significantly in the approach phase. Prediction performance is sensitive to characteristics of the planned trajectory and varies over a wide range, being significantly worse for some trajectories. Similarities in performance results for trajectories with similar characteristics hint that more detailed analysis of the structure of the planned trajectories may offer insights into the degree of performance sensitivity to particular trajectory features. Also, observed anomalous behavior suggests that there may be important weaknesses in the prediction of automation mode. This should be investigated further to characterize automation mode prediction performance and its relation to trajectory prediction performance and anomalous behavior. The results also indicate that the software implementation of the TP function has critical shortcomings which should be corrected.

The data analysis results for Parts 2 to 6 of CASPEr-1 will appear in future reports. Part 1 examined the effect of the planned trajectory by varying the arrival route and the destination runway in the terminal area at KMEM. Part 2 tested the effect of airplane weight and also altitude and speed with varying energy profiles. Part 3 was about the effect of wind and gusts. Part 4 and 5 tested various pilot intervention patterns. Part 6 was intended to enable measurement of the prediction uncertainty with confidence intervals. Analyses of all these are in progress.

Furthermore, preliminary results and lessons learned from CASPEr-1 have informed the design of a second, more thorough round of performance characterization tests for the TP function called CASPEr-2. The results of CASPEr-2 will appear in future reports.

The final product from this work will be a report documenting a proposed approach to assess the goodness of onboard airplane energy state and automation mode prediction functions.

8. References

[1] Commercial Aviation Safety Team: Airplane State Awareness Joint Safety Analysis Team, "Final Report: Analysis and Results," 2014.

[2] Commercial Aviation Safety Team: Airplane State Awareness Joint Safety Analysis Team, "Final Report: Analysis and Recommendations," 2014.

[3] Commercial Airplane Safety Team, "Safety Enhancement SE 207.1 (R&D)," 2016.

[4] Commercial Airplane Safety Team, "Safety Enhancement SE 208.1 (R&D)," 2016.

[5] S. Young, T. Daniels, E. Evans, T. Etherington, K. Shish, M. Uijit de Haag, S. Schuet and D. Kiggins, "Evaluating Technologies for Improved Airplane State Awareness and Prediction," in *AIAA SciTech Forum*, San Diego, CA, January 4-8, 2016.

[6] K. Shish, J. Kaneshige, D. Acosta, S. Schuet, T. Lombaerts, L. Martin and A. N. Madavan, "Aircraft Mode and Energy-State Prediction, Assessment, and Alerting," *Journal of Guidance, Control, and Dynamics*, vol. 40, no. 4, April 2017.

[7] K. Shish, J. Kaneshige, D. Acosta, S. Schuet, T. Lombaerts, L. Martin and A. N. Madavan, "Trajectory Prediction and Alerting for Aircraft Mode and Energy State Awareness," in *AIAA SciTech Forum*, Kissimmee, Florida, 2015.

[8] P. P. Duan, M. Uijt de Haag, T. Etherington and L. Smith-Velazquez, "Energy state prediction methods for airplane state awareness," in *IEEE/AIAA 35th Digital Avionics Systems Conference (DASC)*, 2016.

[9] M. R. Endsley, "Toward a Theory of Situation Awareness in Dynamic Systems," *Human Factors Journal*, vol. 37, no. 1, pp. 32 - 64, March 1995.

[10] RTCA, "DO-200B: Standards for Processing Aeronautical Data (Revision B)," 2015.

[11] Federal Aviation Administration (FAA), *Advisory Circular AC-25.1309-1A: System Design and Analysis*, 1988.

[12] SAE International, *Aerospace Recommended Practice ARP4754A: Guidelines for the Development of Civil Aircraft and Systems, Revision A*, 2010.

[13] RTCA, "DO-178C: Software Considerations in Airborne Systems and Equipment Certification," December 13, 2011.

[14] A. Avizienis, J.-C. Laprie, B. Randell and C. Landwehr, "Basic Concepts and Taxonomy of Dependable and Secure Computing," *IEEE Transactions on Dependable and Secure Computing*, vol. 1, no. 1, pp. 11 - 33, January - March 2004.

[15] J. C. Helton, "Conceptual and Computational Basis for Quantification of Margins and Uncertainty," Sandia National Laboratories, 2009.

[16] D. C. Montgomery, Design and Analysis of Experiments, 8th ed., Wiley, 2012.

[17] Federal Aviation Administration (FAA), "Instrument Flight Procedures Information Gateway," [Online]. Available: https://www.faa.gov/air_traffic/flight_info/aeronav/procedures/. [Accessed 24 October 2018].

[18] Federal Aviation Administration (FAA), "Pilot/Control Glossary," 2017. [Online]. Available: https://www.faa.gov/Air_traffic/Publications/media/PCG_10-12-17.pdf. [Accessed 25 October 2018].

[19] Eurocontrol Experimental Centre, "User Manual for the Base of Aircraft Data (BADA), Revision 3.12," Eurocontrol, 2014.

[20] H. Kopetz, Real-Time Systems: Design Principles for Distributed Embedded Applications, 2nd ed., Springer Science + Business Media, 2011.

[21] Airbus, "Getting to Grips with the Cost Index," Airbus Flight Operations Support & Line Assistance, 1998.

[22] Merriam-Webster, "Dictionary by Merriam-Webster," Merriam-Webster, Incorporated, 2018. [Online]. Available: https://www.merriam-webster.com/. [Accessed 3 December 2018].

[23] Oxford, "English Dictionary, Thesaurus, & Grammar Help," Oxford University Press, 2018. [Online]. Available: https://en.oxforddictionaries.com/. [Accessed 3 December 2018].

Appendix A. CASPEr-1 Test Plan

CASPEr: Characterization of Airplane State Prediction Error

Notes:

1. Airport: KMEM
2. The FMC always controls lateral navigation.
3. Normal initial altitude is 15,000 ft.
4. Normal initial speed is 280 kt.
5. Normal initial weight is 187,500 lbs. This is the mid-point of the initial weight range.
6. Range for the initial weight is 150,000 – 225,000 lbs.
7. Approach is always on an existing STAR at KMEM set back on the route at a distance corresponding to initial altitude. On BLUZZ ONE landing north, this is near the LTOWN waypoint.

Summary:

Part	**Title**	**Purpose**	**Number of Runs**
1	FMC-Controlled Energy Without Pilot Intervention: All Routes	Test arrival routes and landing directions. No weather.	28
2	FMC-Controlled Energy Without Pilot Intervention: Energy Cube Extremes	Test at end-points of energy cube defined by ranges of airplane altitude, speed, and weight. No weather.	8
3	FMC-Controlled Energy Without Pilot Intervention: Weather	Test for effects of weather conditions, including wind direction, gusts, and wind gradient. Maximum wind speed only.	29
4	FMC-Controlled Energy with Altitude Hold Intervention	Test for single altitude-hold intervention. No weather.	12
5	Stepdown Energy Management	Test descent with multiple step-downs in altitude and speed. No weather.	18
6	Uncertainty Quantification with Monte Carlo Simulations	Random sampling of controlled variables	100
		Total Number of Runs	195

Part 1: FMC-Controlled Energy without Pilot Intervention: All Routes

Description: The purpose is to exercise all the arrival routes and approach directions. The FMC controls lateral, vertical, and speed profiles. In effect, the FMC manages the energy of the airplane. No pilot inputs, except where and when required to complement FMC controls. Normal initial conditions and energy factors (altitude, speed, and weight). No weather.

Variable	**Values**	**Number of Values**
STAR	BLUZZ ONE, HYTHR ONE, BRBBQ TWO, CONDR TWO, HOBRK TWO, VANZE ONE, MONAA TWO	7
Runway	9, 18C, 27, 36C	4
Weather:		
Wind Speed	0	1
Initial Energy Factors		
Altitude	Normal	1
Speed	Normal	1
Weight	Normal	1
Descent Energy Factors		
Altitude	Per published STAR and Approach routes; Managed by FMC	1
Speed	Per published STAR and Approach routes; Managed by FMC	1
Weight	Normal for the airplane	1
Pilot Inputs	As needed	
	Number of Runs	28 See Note 1

Notes:

1. Number of runs: 7 STARs x 4 Runway Approaches = 28

Part 2: FMC-Controlled Energy without Pilot Intervention: Energy Cube End-Points

Description: The purpose is to observe the effects of extremes in the energy cube defined by the ranges of altitude, speed, and weight. No weather. No pilot inputs, except where and when required to complement FMC controls.

- This is implemented by changing the altitude and speed constraints of the waypoints.
- Horizontal locations of the waypoints remain as on published on STAR and approach charts.
- TOD is at the same horizontal along-track distance to DINKE as LTOWN on the published STAR, i.e., 55 NM.
- Altitude:
  - Initial: Min = 11,000 ft.; Max = 19,000 ft.
  - Descent: Approximately constant angle along track from TOD to DINKE
- Speed:
  - Initial: Min = 210 kt ; Max = 290 kt
  - Descent: Constant to DINKE
- Must ensure that the procedure for required pilot inputs (e.g., flap setting, landing gear) is adequate in all cases.

Variable	**Values**	**Number of Values**
STAR	BLUZZ ONE	1
Runway	36C	1
Weather:		
Wind Speed	0	1
Initial Energy Factors		
Altitude	Min, Max	2
Speed	Min, Max	2
Weight	Min, Max	2
Descent Energy Factors		
Altitude	Min and Max for STAR and Approach route; Managed by FMC	Match (min ➔ min, max ➔ max) with Initial Energy Factor: Altitude
Speed	Min and Max for STAR and Approach route; Managed by FMC	Match (min ➔ min, max ➔ max) with Initial Energy Factor: Speed
Weight	Min and Max for airplane	Match (min ➔ min, max ➔ max) with Initial Energy factor: Weight
Pilot Inputs	As needed	
	Number of Runs	8 See Note 1

Notes:

1. Number of runs: 2 altitudes x 2 speeds x 2 weights = 8

Part 3: FMC-Controlled Energy without Pilot Intervention: Weather

Description: The purpose is to observe the effects of weather variables, including wind speed, wind direction, wind gradient, gust speed, and gust gradient. No pilot inputs, except where and when required to complement FMC controls.

Variable	Values	Number of Values
STAR	BLUZZ ONE	1
Runway	36C	1
Weather:		
Wind Direction ("from")	North-East, South-West, North, South	4
Wind Speed	Max	7 See Notes 1 - 5 below
Gusts	Mid, Max	
Wind Gradient	Mid, Max	
Initial Energy Factors		
Altitude	Normal	1
Speed	Normal	1
Weight	Normal	1
Descent Energy Factors		
Altitude	Normal for STAR and Approach route; Controlled by FMC	1
Speed	Normal for STAR and Approach route; Controlled by FMC	1
Weight	Normal for airplane	1
Pilot Inputs	As needed	
	Number of Runs	28 + 1 = 29 See Notes 6 and 7

Notes:

1. Test sequence for wind speed, gusts, and gradients:

Index	Speed	Gusts	Wind Gradient
1	Max	0	0
2	Max	Mid	0
3	Max	Max	0
4	Max	0	Mid
5	Max	0	Max
6	Max	Mid	Mid
7	Max	Max	Max

2. Max wind speed at ground level is 25 knots for headwind and crosswind components, and 10 knots for tailwind component. Maximum wind speeds <u>at ground level</u> for each wind direction is as specified in the following table.

Wind Direction	Maximum Wind Speed at ground level (Kt)
North	25
North-East	25
South-East	14
South	10

3. Note that to maintain approach simplicity we are not including gust speed/strength in the wind constraint. We are assuming that this is valid since we are not simulating the final landing part of the approach.
4. Max wind gradient is 5 knots per 1,000 ft. altitude.
5. Max gusts is 6 knots RMS at 15,000 ft. and 2 knots RMS at ground level. Note that gusts always have a gradient.
6. Number of runs: 4 wind directions x 7 wind speed/gust/gradient combos = 28
7. Add one run: Max Wind, Max Gradient, No gusts (i.e., Index 5 in table of Note 1), North-East wind direction. All previously defined runs include wind forecast given to the FMC. For this extra run, wind forecast is not given to the FMC. Intended as a sample run to measure the effect on FMC and TFMS/TPS of not having a wind forecast.

Part 4: FMC-Controlled Energy with Altitude Hold Intervention

Description: The purpose is to observe the effects of simple tactical interventions. No weather.

Variable	Values	Number of Values
STAR	BLUZZ ONE	1
Runway	36C	1
Weather:		
Wind Speed	0	1
Initial Energy Factors		
Altitude	Normal	1
Speed	Normal	1
Weight	Normal	1
Descent Energy Factors		
Altitude	Normal for STAR and Approach route; Controlled by FMC, except during pilot interventions	1
Speed	Normal for STAR and Approach route; Controlled by FMC	1
Weight	Normal for airplane	1
Pilot Inputs		
Altitude Hold	11,000 ft. 9,000 ft. 7,000 ft.	3 See Note 1 below
Hold Duration	3.0, 4.0, 5.0 min at 11,000 ft. 1.0, 2.0, 3.0 min at 9,000 ft. 1.0, 1.5, 2.0 min at 7,000 ft.	3 See Note 2 below
Input Event Subsequences	{1} (No return to normal profile. Permanent hold.) {1, 2}	2 See Notes 3 and 4 below
	Number of Runs	12 See Note 5

Notes:

1. At most one hold per descent. Holding at one of the listed altitudes.
2. Hold duration options are dependent on the hold altitude. There should be one simulation run for each of these hold durations.
3. It is assumed that Pilot Input is a random variable from the point of view of the predictors. It is expected that every Pilot Input event may cause a relatively abrupt change in the predicted state of the airplane and the automation. The only way to measure the accuracy of a predictions is to allow the airplane state to evolve without additional Pilot Input events and to reach the time of the predicted state in order to make a prediction error measurement.
4. Conceptually, a full Pilot Input event sequence for an altitude hold has two events: (1) Select hold altitude, (2) Select return to normal descent. In order to measure the state prediction error, there should be one simulation run for each Pilot Input event. (See Note 3). For example, for an altitude-hold scenario there should be one run with only the first Pilot Input event (event 1) and another run with two Pilot Input events (events 1 and 2).

5. Number of runs: 3 + 9 = 12
    a. Runs with one Pilot Input event: 3 altitudes (each with indefinite hold time) = 3
    b. Runs with two Pilot Input events: 3 altitudes x 3 hold times for each altitude = 9

Part 5: Step-down Energy Management

Description: The purpose is to observe the effects of more complex Pilot Input sequences. The FMC manages the altitude and speed, except during pilot interventions. No weather.

Variable	Values	Number of Values
STAR	BLUZZ ONE	1
Runway	36C	1
Weather:		
Wind Speed	0	1
Initial Energy Factors		
Altitude	Normal	1
Speed	Normal	1
Weight	Normal	1
Descent Energy Factors		
Altitude	Managed by FMC for normal for STAR and Approach trajectory , except during pilot interventions	1
Speed	Stepped down with following speed targets: • 250 KT for altitude step at 11,000 ft. • 230 KT for altitude step at 9,000 ft. • 210 KT for altitude step at 7,000 ft.	1
Weight	Normal for airplane	1
Pilot Inputs		
Altitude Steps	Two steps = {11,000 ft.; 9,000 ft.} Three steps = {11,000 ft.; 9,000 ft.; 7,000 ft.}	2 See Note 1 below
Speed	Stepped-down	1 See Descent Energy Factors: Speed above; See Note 2 below
Vertical Descent Speed	2,000 fpm 3,000 fpm	2 See Note 3
Distance-to-reference-waypoint for stepdown transitions	Early stepdown transitions = • 30 NM for altitude step at 11,000 ft. • 20 NM for altitude step at 9,000 ft. • 10 NM for altitude step at 7,000 ft. Late stepdown transitions = • 25 NM for altitude step at 11,000 ft. • 15 NM for altitude step at 9,000 ft. • 5 NM for altitude step at 7,000 ft. Reference waypoint is DINKE	2 See Note 4 below
Input Event Subsequences	For two steps of altitude and speed: • {1}	3 for two steps, 4 for three steps

	○ Airplane remains at first step of altitude and speed • {1, 2} ○ Airplane remains at second step of altitude and speed. • {1, 2, 3} ○ Airplane returns to normal altitude and speed at the end of the second step. For three steps of altitude and speed: • {1} ○ Airplane remains at first step of altitude and speed • {1,2} ○ Airplane remains at second step of altitude and speed • {1, 2, 3} ○ Airplane remains at third step of altitude and speed • {1, 2, 3, 4} ○ Airplane returns to normal altitude and speed at the end of the third step	See Notes 5 and 6 below.
	Number of Runs : Two steps	10 See Note 7
	Number of Runs : Three steps	8 See Note 8
	Total Number of Runs	18

Notes:

1. Stepdown sequence begins with Pilot Input applied at 14,000 ft. to descend to the first altitude step. Additional Pilot Inputs are applied to descend to the next level at one of the distance-to-reference-waypoint options listed in the table.
2. Pilot Inputs for speed targets are made at the same time as Pilot Inputs for altitude transitions.
3. For a particular run, all stepdown transitions are made with the same target vertical speed.
4. For a particular run, the stepdown transitions are either all early (i.e., at the farthest listed distance to DINKE) or all late (i.e., at the closest listed distance to DINKE).
5. A two-step descent requires three Pilot Input events: (1) Select descent to first level, (2) Select descent to second level, and (3) Select descent back to normal altitude
6. A three-step descent requires four Pilot Input events: (1) Select descent to first level, (2) Select descent to second level, (3) Select descent to third level, and (3) Select descent back to normal altitude.
7. Number of runs for two stepdown levels for altitude and speed:

Number of Pilot Input events	Number of Vertical Descent Speeds for Transitions (2000 or 3000 fpm)	Number of Timings for Stepdown Transitions (Early or Late)	Total Number of Runs	Comment
1	2	Not applicable	2	Initial transition is from 14,000 ft. to the first step; Airplane remains at first step of altitude and speed; There is no stepdown transition from this level.
2	2	2	4	Airplane remains at second step of altitude and speed; Stepdown transitions are at the end of each step.
3	2	2	4	Airplane returns to normal altitude and speed at the end of the second step; Stepdown transitions are at the end of each step.
		Total	10	

8. Number of runs for three stepdown levels for altitude and speed:

Number of Pilot Input events	Number of Vertical Descent Speeds for Transitions (2000 or 3000 fpm)	Number of Timings for Stepdown Transitions (Early or Late)	Total Number of Runs	Comments
1	2	Not applicable	2	Transition is from 14,000 ft. to the first step; Airplane remains at first step of altitude and speed; There is no stepdown transition from this level. These runs are the same as the runs in the first row of the table in Note 7 for two stepdown levels. It is not necessary to re-redo these runs.

2	2	2	4	Airplane remains at second step of altitude and speed; Stepdown transitions are at the end of each step. These runs are the same as the runs in the second row of the table in Note 7 for two stepdown levels. It is not necessary to re-redo these runs.
3	2	2	4	Airplane remains at third step of altitude and speed; Stepdown transitions are at the end of each step.
4	2	2	4	Airplane returns to normal altitude and speed at the end of the third step; Stepdown transitions are at the end of each step.
		Total	14 – 6 = 8	

Part 6: Uncertainty Quantification with Monte Carlo Simulation

Description: The purpose is to quantify the state prediction uncertainty. This is a Monte Carlo simulation experiment for low confidence estimation of uncertainty in state prediction error. No Pilot Inputs.

- Altitude:
  - Initial: Min = 14,000 ft.; Max = 16,000 ft.
  - Descent: Normal
- Speed:
  - Initial: Min = 250 kt; Max = 310 kt.
  - Descent: Normal

Variable	**Values**	**Number of Values**
STAR	BLUZZ ONE	1
Runway	36C	1
Weather:		
Wind Speed	0 to Max, Uniform Distribution	Sampled See Note 1
Wind Direction ("from")	0 to 360 degrees, Uniform Distribution	Sampled
Gusts	0 to Max, Uniform Distribution	Sampled
Wind Gradient	0 to Max, Uniform Distribution	Sampled
Initial Energy Factors		
Altitude	Min to Max, Uniform Distribution	Sampled
Speed	Min to Max, Uniform Distribution	Sampled
Weight	Min to Max, Uniform Distribution	Sampled
Descent Energy Factors		
Altitude	Normal for STAR and Approach route; Managed by FMC	1
Speed	Normal for STAR and Approach route; Managed by FMC	1
Weight	Normal for airplane	Sampled
	Number of Runs	100

Notes:

1. To satisfy the wind speed limitations for landing, the range of wind speed at ground level must depend on wind direction. The Max wind speed is set as follows:
   a. For wind direction within ±66 degrees of the landing direction (i.e., North for runway 36C): Max = 10 / cos(θ) knots, where θ is the angle between the landing direction and the wind direction.
   b. Otherwise: Max wind speed = 25 knots

Appendix B. KMEM Terminal Procedures

This appendix has the STAR and approach procedures at KMEM used in CASPEr-1. This information is provided here for easy reference.

B.1. Standard Terminal Arrival Routes (STAR)

B.1.1. BLUZZ

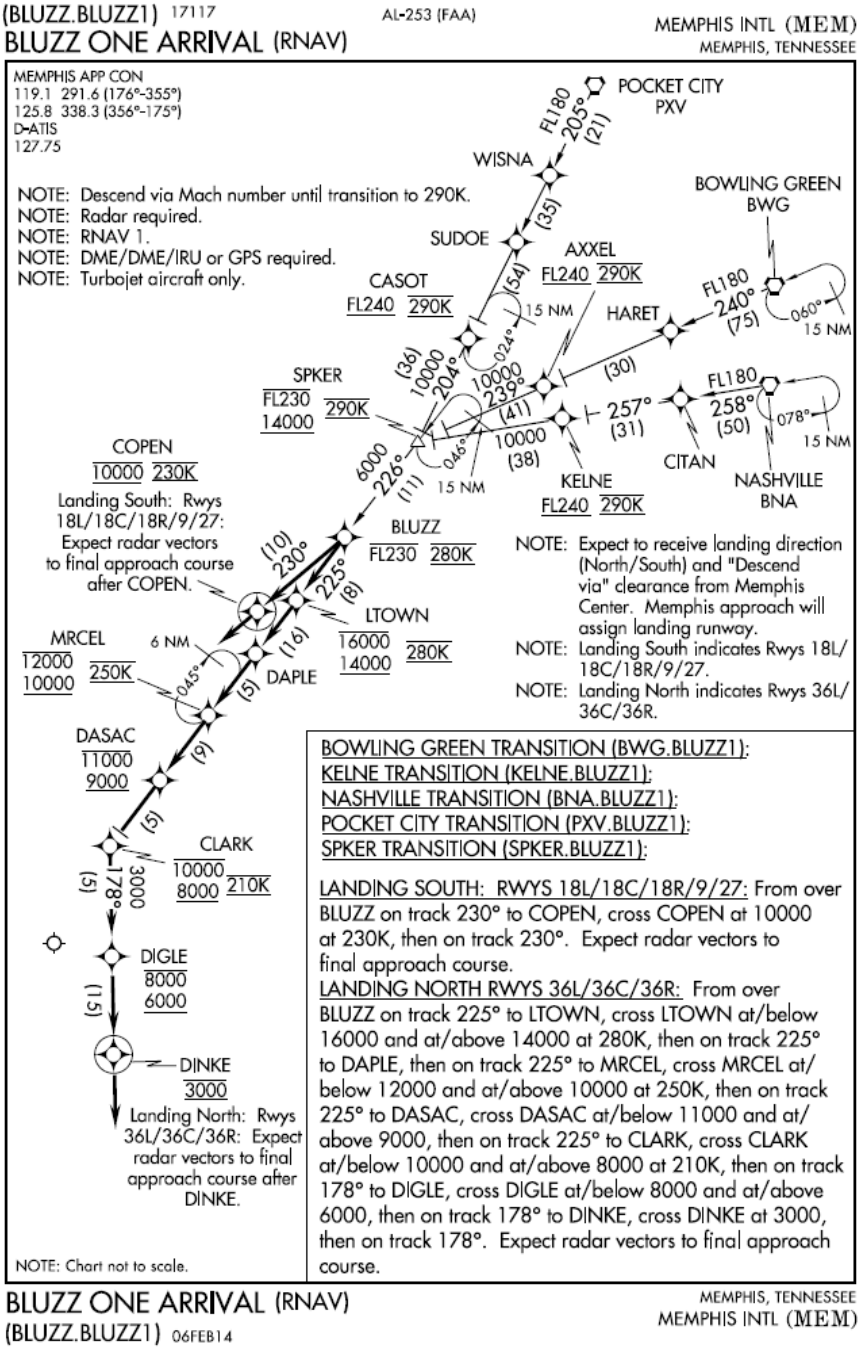

B.1.2. VANZE

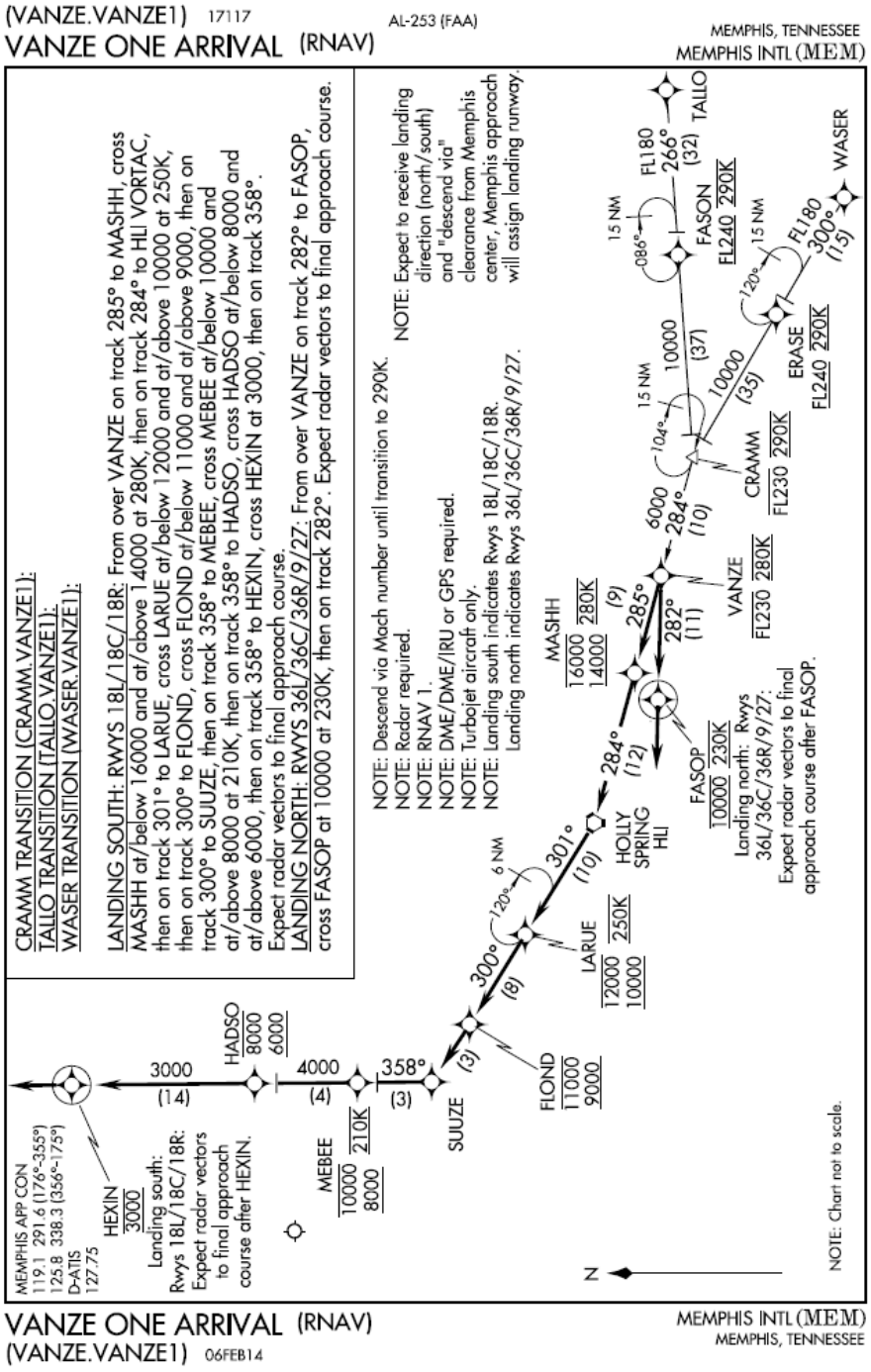
(VANZE.VANZE1) 17117
AL-253 (FAA)
VANZE ONE ARRIVAL (RNAV)
MEMPHIS, TENNESSEE
MEMPHIS INTL (MEM)
CRAMM TRANSITION (CRAMM.VANZE1):
TALLO TRANSITION (TALLO.VANZE1):
WASER TRANSITION (WASER.VANZE1):
LANDING SOUTH: RWYS 18L/18C/18R: From over VANZE on track 285° to MASHH, cross MASHH at/below 16000 and at/above 14000 at 280K, then on track 284° to HLI VORTAC, then on track 301° to LARUE, cross LARUE at/below 12000 and at/above 10000 at 250K, then on track 300° to FLOND, cross FLOND at/below 11000 and at/above 9000, then on track 300° to SUUZE, then on track 358° to MEBEE, cross MEBEE at/below 10000 and at/above 8000 at 210K, then on track 358° to HADSO, cross HADSO at/below 8000 and at/above 6000, then on track 358° to HEXIN, cross HEXIN at 3000, then on track 358°. Expect radar vectors to final approach course.
LANDING NORTH: RWYS 36L/36C/36R/9/27: From over VANZE on track 282° to FASOP, cross FASOP at 10000 at 230K, then on track 282°. Expect radar vectors to final approach course.
NOTE: Descend via Mach number until transition to 290K.
NOTE: Radar required.
NOTE: RNAV 1.
NOTE: DME/DME/IRU or GPS required.
NOTE: Turbojet aircraft only.
NOTE: Landing south indicates Rwys 18L/18C/18R. Landing north indicates Rwys 36L/36C/36R/9/27.
NOTE: Expect to receive landing direction (north/south) and "descend via" clearance from Memphis center, Memphis approach will assign landing runway.
MEMPHIS APP CON
119.1 291.6 (176°-355°)
125.8 338.3 (356°-175°)
D-ATIS
127.75
HEXIN
3000
Landing south: Rwys 18L/18C/18R: Expect radar vectors to final approach course after HEXIN.
3000
(14)
HADSO
8000
6000
4000
(4)
MEBEE
10000
8000
210K
358°
(3)
SUUZE
(3)
300°
(8)
FLOND
11000
9000
120°
6 NM
LARUE
12000
10000
250K
301°
(10)
HOLLY SPRING HLI
284°
(12)
MASHH
16000
14000
280K
285°
(9)
282°
(11)
FASOP
10000
230K
Landing north: Rwys 36L/36C/36R/9/27: Expect radar vectors to final approach course after FASOP.
6000
284°
(10)
VANZE
FL230
280K
104°
15 NM
CRAMM
FL230
290K
10000
(35)
086°
15 NM
10000
(37)
FASON
FL240
290K
120°
15 NM
ERASE
FL240
290K
FL180
300°
(15)
FL180
266°
(32)
TALLO
WASER
N
NOTE: Chart not to scale.
VANZE ONE ARRIVAL (RNAV)
(VANZE.VANZE1) 06FEB14
MEMPHIS INTL (MEM)
MEMPHIS, TENNESSEE

B.1.3. HOBRK

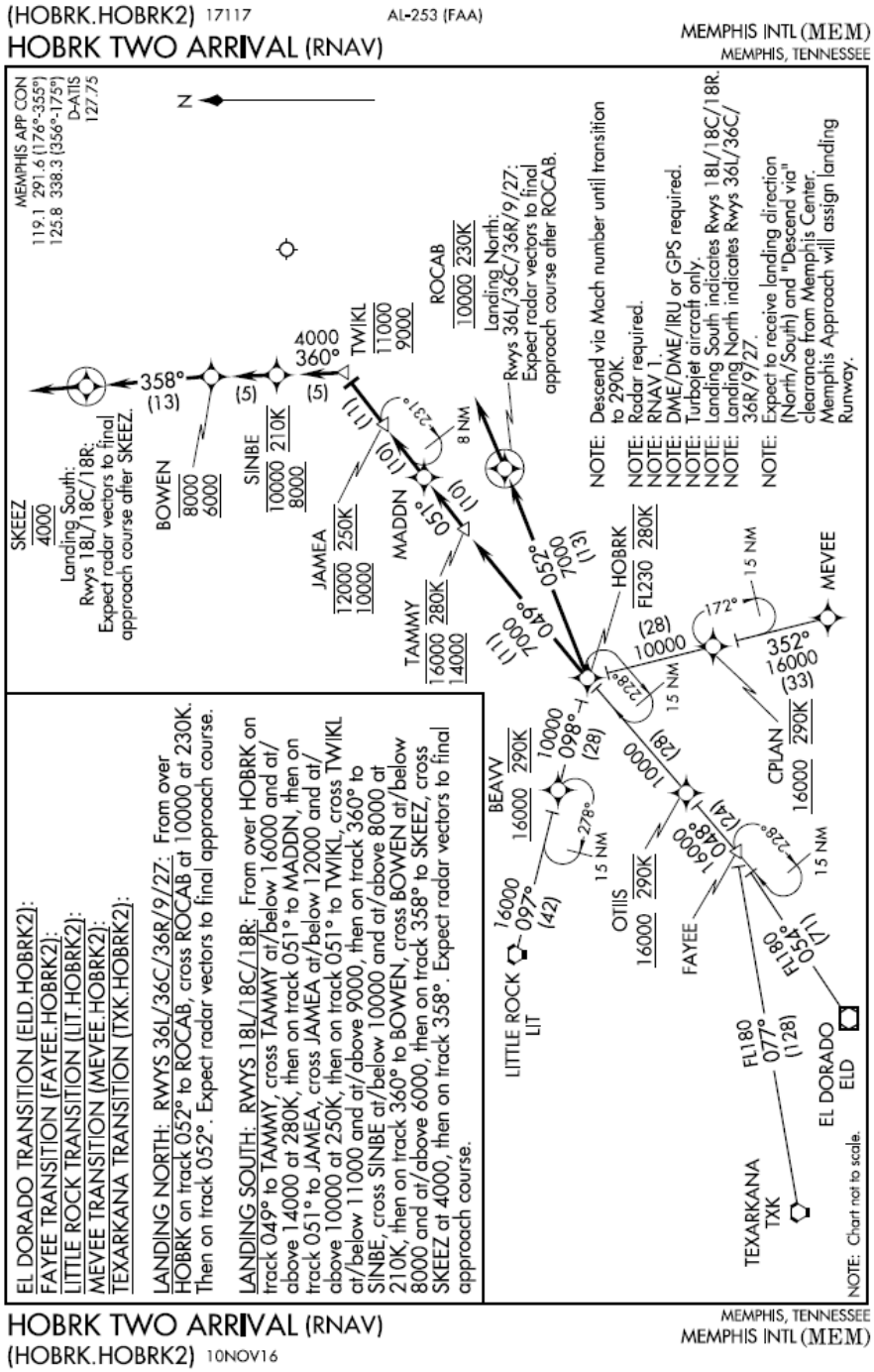
(HOBRK.HOBRK2) 17117
AL-253 (FAA)
HOBRK TWO ARRIVAL (RNAV)
MEMPHIS INTL (MEM)
MEMPHIS, TENNESSEE
MEMPHIS APP CON
119.1 291.6 (176°-355°)
125.8 338.3 (356°-175°)
D-ATIS
127.75
N
SKEEZ
4000
Landing South:
Rwys 18L/18C/18R:
Expect radar vectors to final approach course after SKEEZ.
BOWEN
8000
6000
358°
(13)
(5)
SINBE
10000
8000
4000
360°
(5)
TWIKL
11000
9000
(11)
231°
8 NM
ROCAB
10000 230K
Landing North:
Rwys 36L/36C/36R/9/27:
Expect radar vectors to final approach course after ROCAB.
JAMEA
12000 250K
10000
(10)
MADDN
051°
(10)
TAMMY
16000 280K
14000
049°
7000
(11)
052°
7000
(13)
HOBRK
FL230 280K
NOTE: Descend via Mach number until transition to 290K.
NOTE: Radar required.
NOTE: RNAV 1.
NOTE: DME/DME/IRU or GPS required.
NOTE: Turbojet aircraft only.
NOTE: Landing South indicates Rwys 18L/18C/18R.
NOTE: Landing North indicates Rwys 36L/36C/36R/9/27.
NOTE: Expect to receive landing direction (North/South) and "Descend via" clearance from Memphis Center. Memphis Approach will assign landing Runway.
EL DORADO TRANSITION (ELD.HOBRK2):
FAYEE TRANSITION (FAYEE.HOBRK2):
LITTLE ROCK TRANSITION (LIT.HOBRK2):
MEVEE TRANSITION (MEVEE.HOBRK2):
TEXARKANA TRANSITION (TXK.HOBRK2):
LANDING NORTH: RWYS 36L/36C/36R/9/27: From over HOBRK on track 052° to ROCAB, cross ROCAB at 10000 at 230K. Then on track 052°. Expect radar vectors to final approach course.
LANDING SOUTH: RWYS 18L/18C/18R: From over HOBRK on track 049° to TAMMY, cross TAMMY at/below 16000 and at/above 14000 at 280K, then on track 051° to MADDN, then on track 051° to JAMEA, cross JAMEA at/below 12000 and at/above 10000 at 250K, then on track 051° to TWIKL, cross TWIKL at/below 11000 and at/above 9000, then on track 360° to SINBE, cross SINBE at/below 10000 and at/above 8000 at 210K, then on track 360° to BOWEN, cross BOWEN at/below 8000 and at/above 6000, then on track 358° to SKEEZ, cross SKEEZ at 4000, then on track 358°. Expect radar vectors to final approach course.
LITTLE ROCK
LIT
16000
097°
(42)
BEAVV
16000 290K
10000
098°
(28)
278°
15 NM
OTIIS
16000 290K
10000
(28)
228°
15 NM
(28)
10000
172°
15 NM
CPLAN
16000 290K
352°
16000
(33)
MEVEE
FAYEE
16000
048°
(24)
228°
15 NM
FL180
077°
(128)
FL180
054°
(11)
TEXARKANA
TXK
EL DORADO
ELD
NOTE: Chart not to scale.
HOBRK TWO ARRIVAL (RNAV)
(HOBRK.HOBRK2) 10NOV16
MEMPHIS, TENNESSEE
MEMPHIS INTL (MEM)

B.1.4. BRBBQ

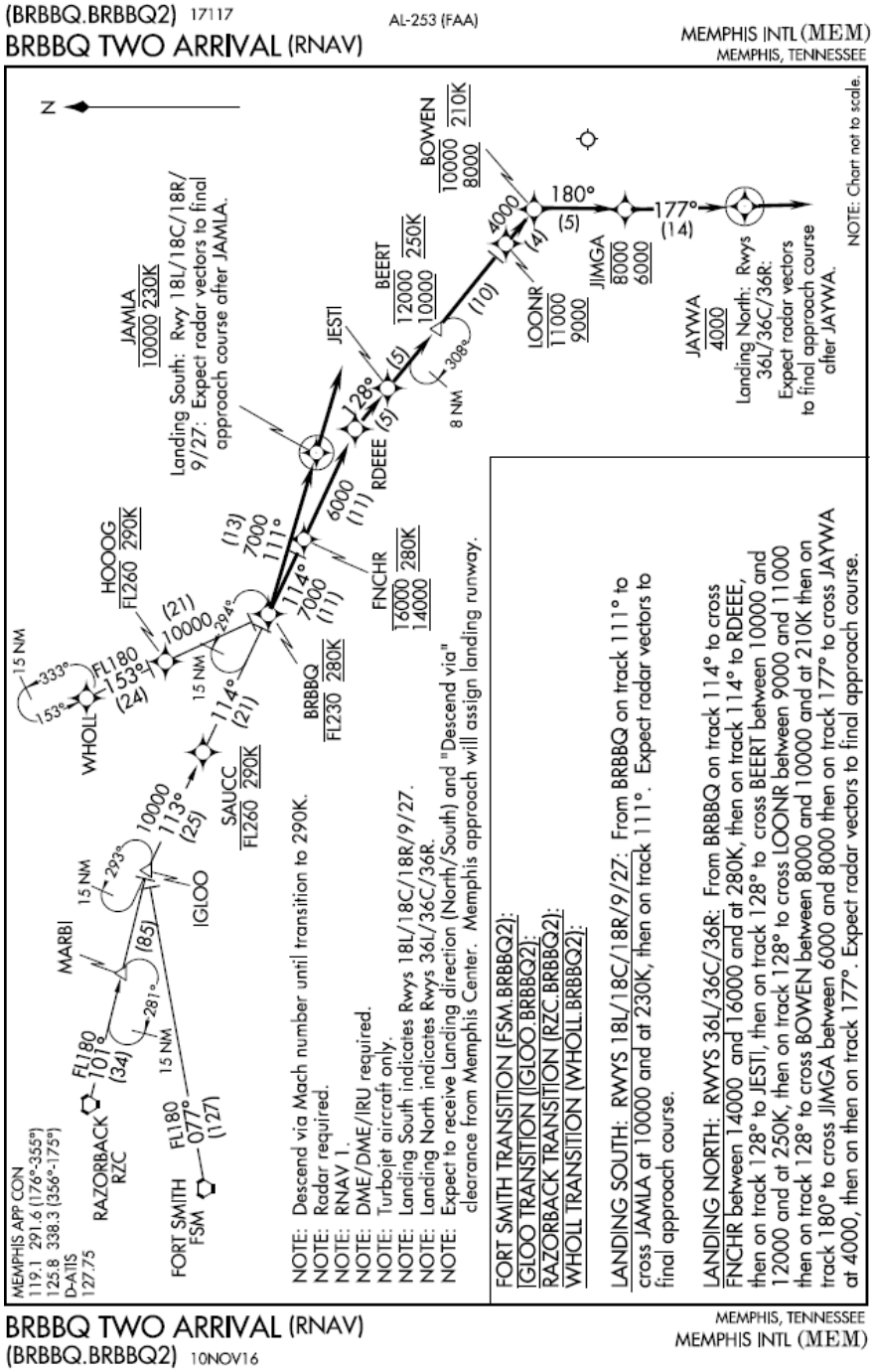
(BRBBQ.BRBBQ2) 17117
AL-253 (FAA)
BRBBQ TWO ARRIVAL (RNAV)
MEMPHIS INTL (MEM)
MEMPHIS, TENNESSEE
N
JAMLA
10000 230K
Landing South: Rwy 18L/18C/18R/
9/27: Expect radar vectors to final
approach course after JAMLA.
HOOOG
FL260 290K
JESTI
BEERT
12000 250K
10000
BOWEN
10000 210K
8000
LOONR
11000
9000
JIMGA
8000
6000
JAYWA
4000
Landing North: Rwys
36L/36C/36R:
Expect radar vectors
to final approach course
after JAYWA.
NOTE: Chart not to scale.
WHOLL
FL180
FNCHR
16000 280K
14000
RDEEE
BRBBQ
FL230 280K
SAUCC
FL260 290K
IGLOO
MARBI
RAZORBACK
RZC
FORT SMITH
FSM
MEMPHIS APP CON
119.1 291.6 (176°-355°)
125.8 338.3 (356°-175°)
D-ATIS
127.75
NOTE: Descend via Mach number until transition to 290K.
NOTE: Radar required.
NOTE: RNAV 1.
NOTE: DME/DME/IRU required.
NOTE: Turbojet aircraft only.
NOTE: Landing South indicates Rwys 18L/18C/18R/9/27.
NOTE: Landing North indicates Rwys 36L/36C/36R.
NOTE: Expect to receive Landing direction (North/South) and "Descend via" clearance from Memphis Center. Memphis approach will assign landing runway.
FORT SMITH TRANSITION (FSM.BRBBQ2):
IGLOO TRANSITION (IGLOO.BRBBQ2):
RAZORBACK TRANSITION (RZC.BRBBQ2):
WHOLL TRANSITION (WHOLL.BRBBQ2):
LANDING SOUTH: RWYS 18L/18C/18R/9/27: From BRBBQ on track 111° to cross JAMLA at 10000 and at 230K, then on track 111°. Expect radar vectors to final approach course.
LANDING NORTH: RWYS 36L/36C/36R: From BRBBQ on track 114° to cross FNCHR between 14000 and 16000 and at 280K, then on track 114° to RDEEE, then on track 128° to JESTI, then on track 128° to cross BEERT between 10000 and 12000 and at 250K, then on track 128° to cross LOONR between 9000 and 11000 then on track 128° to cross BOWEN between 8000 and 10000 and at 210K then on track 180° to cross JIMGA between 6000 and 8000 then on track 177° to cross JAYWA at 4000, then on then on track 177°. Expect radar vectors to final approach course.
BRBBQ TWO ARRIVAL (RNAV)
(BRBBQ.BRBBQ2) 10NOV16
MEMPHIS, TENNESSEE
MEMPHIS INTL (MEM)

B.1.5. HYTHR

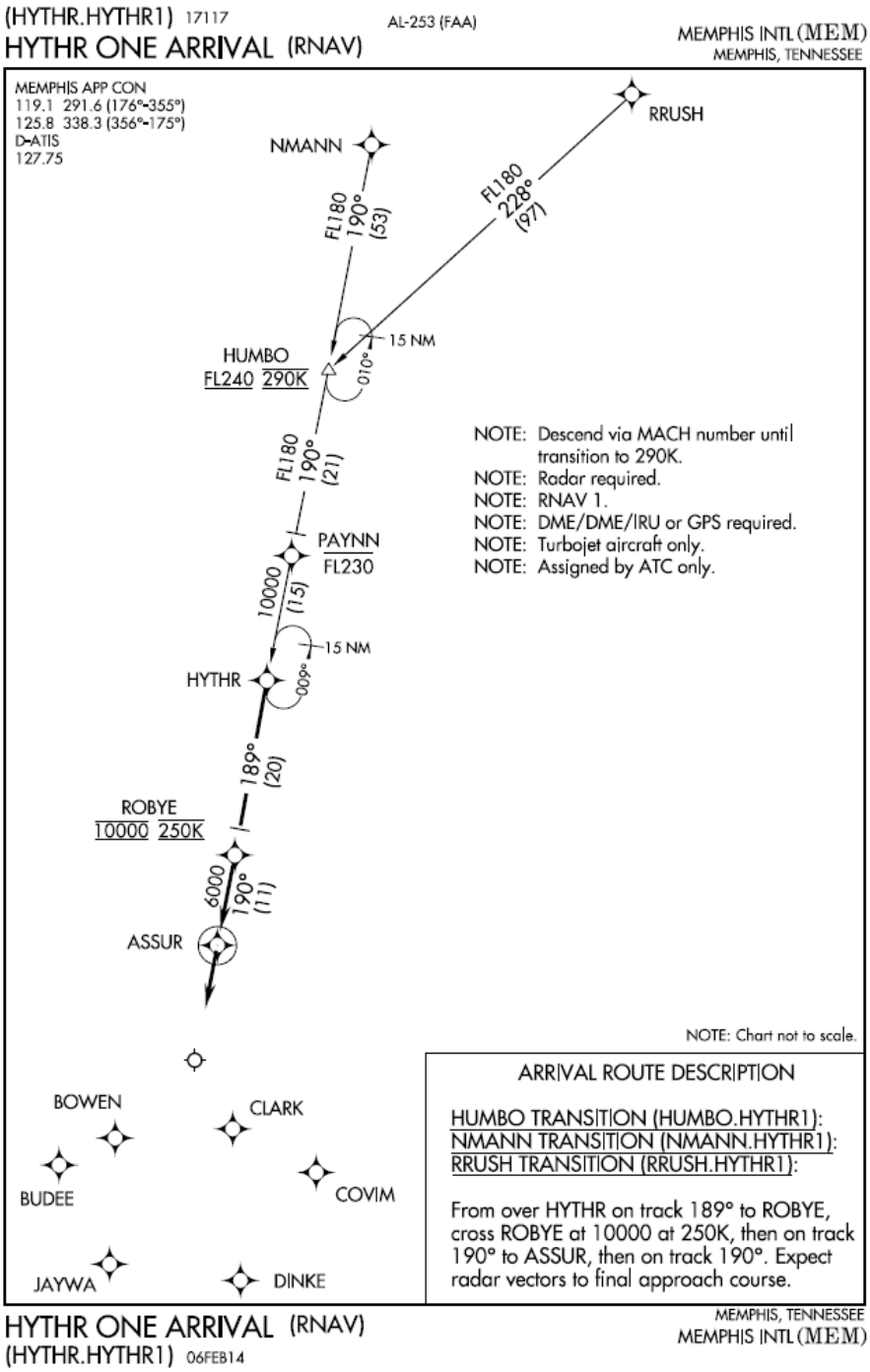
(HYTHR.HYTHR1) 17117
AL-253 (FAA)
HYTHR ONE ARRIVAL (RNAV)
MEMPHIS INTL (MEM)
MEMPHIS, TENNESSEE
MEMPHIS APP CON
119.1 291.6 (176°-355°)
125.8 338.3 (356°-175°)
D-ATIS
127.75
RRUSH
NMANN
FL180 190° (53)
FL180 228° (97)
15 NM
010°
HUMBO
FL240 290K
FL180 190° (21)
PAYNN
FL230
10000 (15)
15 NM
009°
HYTHR
189° (20)
ROBYE
10000 250K
6000 190° (11)
ASSUR
NOTE: Descend via MACH number until transition to 290K.
NOTE: Radar required.
NOTE: RNAV 1.
NOTE: DME/DME/IRU or GPS required.
NOTE: Turbojet aircraft only.
NOTE: Assigned by ATC only.
NOTE: Chart not to scale.
BOWEN
CLARK
BUDEE
COVIM
JAYWA
DINKE
ARRIVAL ROUTE DESCRIPTION
HUMBO TRANSITION (HUMBO.HYTHR1):
NMANN TRANSITION (NMANN.HYTHR1):
RRUSH TRANSITION (RRUSH.HYTHR1):
From over HYTHR on track 189° to ROBYE, cross ROBYE at 10000 at 250K, then on track 190° to ASSUR, then on track 190°. Expect radar vectors to final approach course.
HYTHR ONE ARRIVAL (RNAV)
(HYTHR.HYTHR1) 06FEB14
MEMPHIS, TENNESSEE
MEMPHIS INTL (MEM)

B.1.6. MONAA

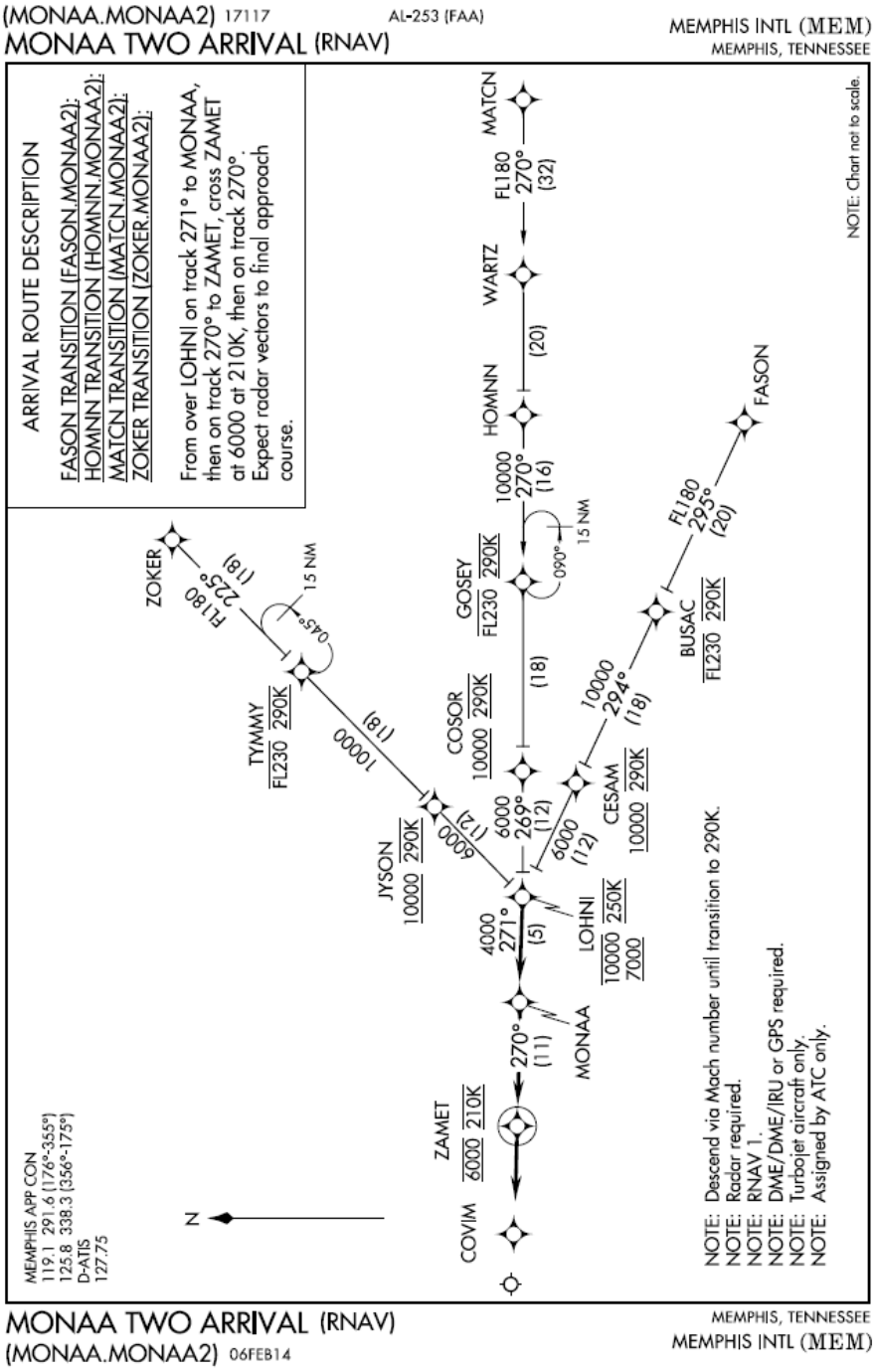
(MONAA.MONAA2) 17117
AL-253 (FAA)
MONAA TWO ARRIVAL (RNAV)
MEMPHIS INTL (MEM)
MEMPHIS, TENNESSEE
ARRIVAL ROUTE DESCRIPTION
FASON TRANSITION (FASON.MONAA2):
HOMNN TRANSITION (HOMNN.MONAA2):
MATCN TRANSITION (MATCN.MONAA2):
ZOKER TRANSITION (ZOKER.MONAA2):
From over LOHNI on track 271° to MONAA, then on track 270° to ZAMET, cross ZAMET at 6000 at 210K, then on track 270°. Expect radar vectors to final approach course.
NOTE: Chart not to scale.
ZOKER
FL180
225°
(18)
15 NM
045°
TYMMY
FL230 290K
10000
(18)
JYSON
10000 290K
8000
(12)
COSOR
10000 290K
6000
269°
(12)
GOSEY
FL230 290K
090°
15 NM
HOMNN
10000
270°
(16)
WARTZ
(20)
FL180
270°
(32)
MATCN
CESAM
10000 290K
6000
(12)
10000
294°
(18)
BUSAC
FL230 290K
FL180
295°
(20)
FASON
4000
271°
(5)
LOHNI
10000 250K
7000
MONAA
270°
(11)
ZAMET
6000 210K
COVIM
N
MEMPHIS APP CON
119.1 291.6 (176°-355°)
125.8 338.3 (356°-175°)
D-ATIS
127.75
NOTE: Descend via Mach number until transition to 290K.
NOTE: Radar required.
NOTE: RNAV 1.
NOTE: DME/DME/IRU or GPS required.
NOTE: Turbojet aircraft only.
NOTE: Assigned by ATC only.
MONAA TWO ARRIVAL (RNAV)
(MONAA.MONAA2) 06FEB14
MEMPHIS, TENNESSEE
MEMPHIS INTL (MEM)

B.1.7. CONDR

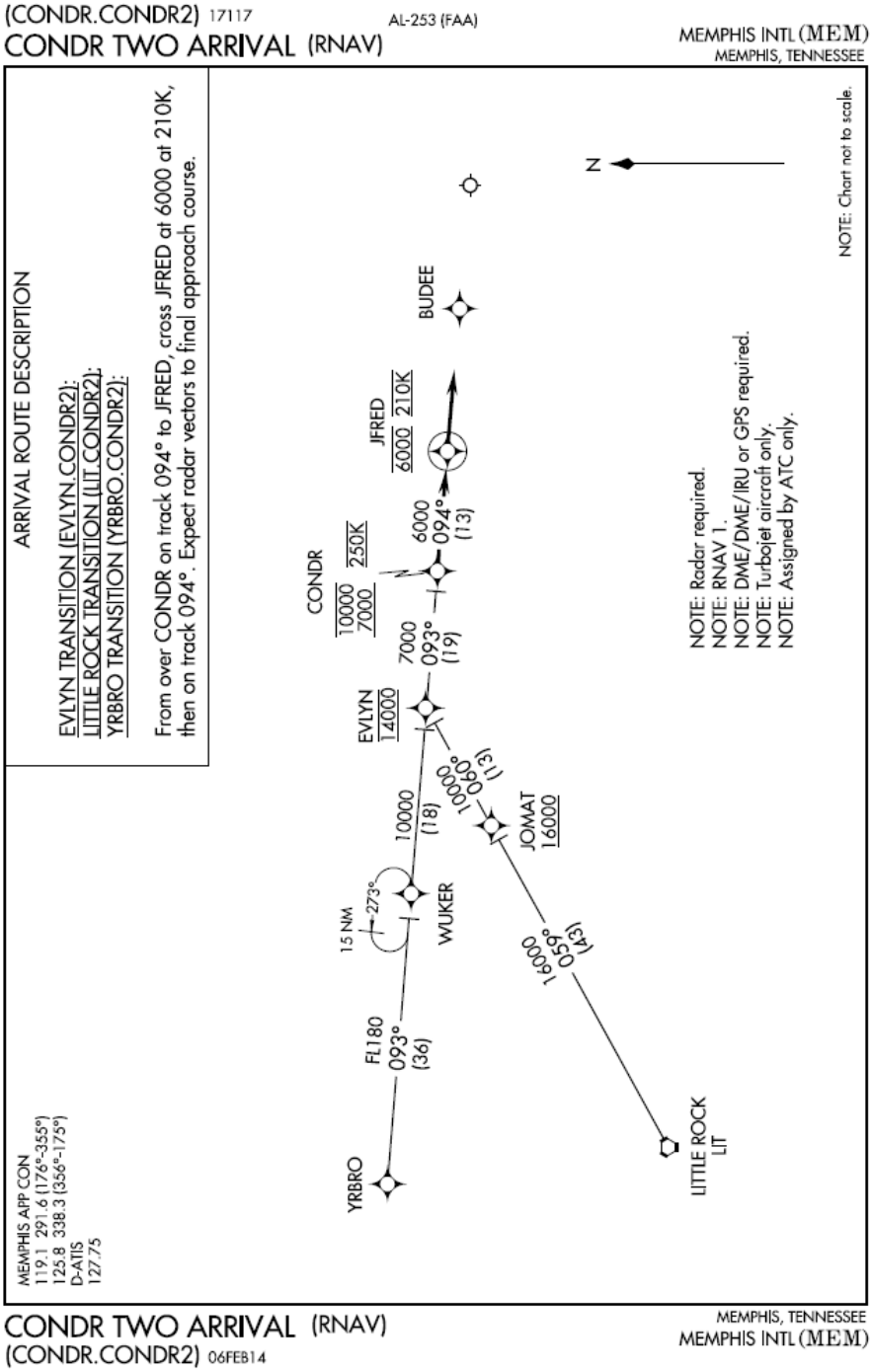
(CONDR.CONDR2) 17117
AL-253 (FAA)
CONDR TWO ARRIVAL (RNAV)
MEMPHIS INTL (MEM)
MEMPHIS, TENNESSEE
ARRIVAL ROUTE DESCRIPTION
EVLYN TRANSITION (EVLYN.CONDR2):
LITTLE ROCK TRANSITION (LIT.CONDR2):
YRBRO TRANSITION (YRBRO.CONDR2):
From over CONDR on track 094° to JFRED, cross JFRED at 6000 at 210K, then on track 094°. Expect radar vectors to final approach course.
MEMPHIS APP CON
119.1 291.6 (176°-355°)
125.8 338.3 (356°-175°)
D-ATIS
127.75
YRBRO
FL180
093°
(36)
15 NM
273°
WUKER
10000
(18)
EVLYN
14000
CONDR
10000
7000
250K
7000
093°
(19)
6000
094°
(13)
JFRED
6000
210K
BUDEE
10000
090°
(13)
JOMAT
16000
6000
059°
(43)
LITTLE ROCK
LIT
N
NOTE: Chart not to scale.
NOTE: Radar required.
NOTE: RNAV 1.
NOTE: DME/DME/IRU or GPS required.
NOTE: Turbojet aircraft only.
NOTE: Assigned by ATC only.
CONDR TWO ARRIVAL (RNAV)
(CONDR.CONDR2) 06FEB14
MEMPHIS, TENNESSEE
MEMPHIS INTL (MEM)

B.2. Runway Approaches

B.2.1. Runway 09

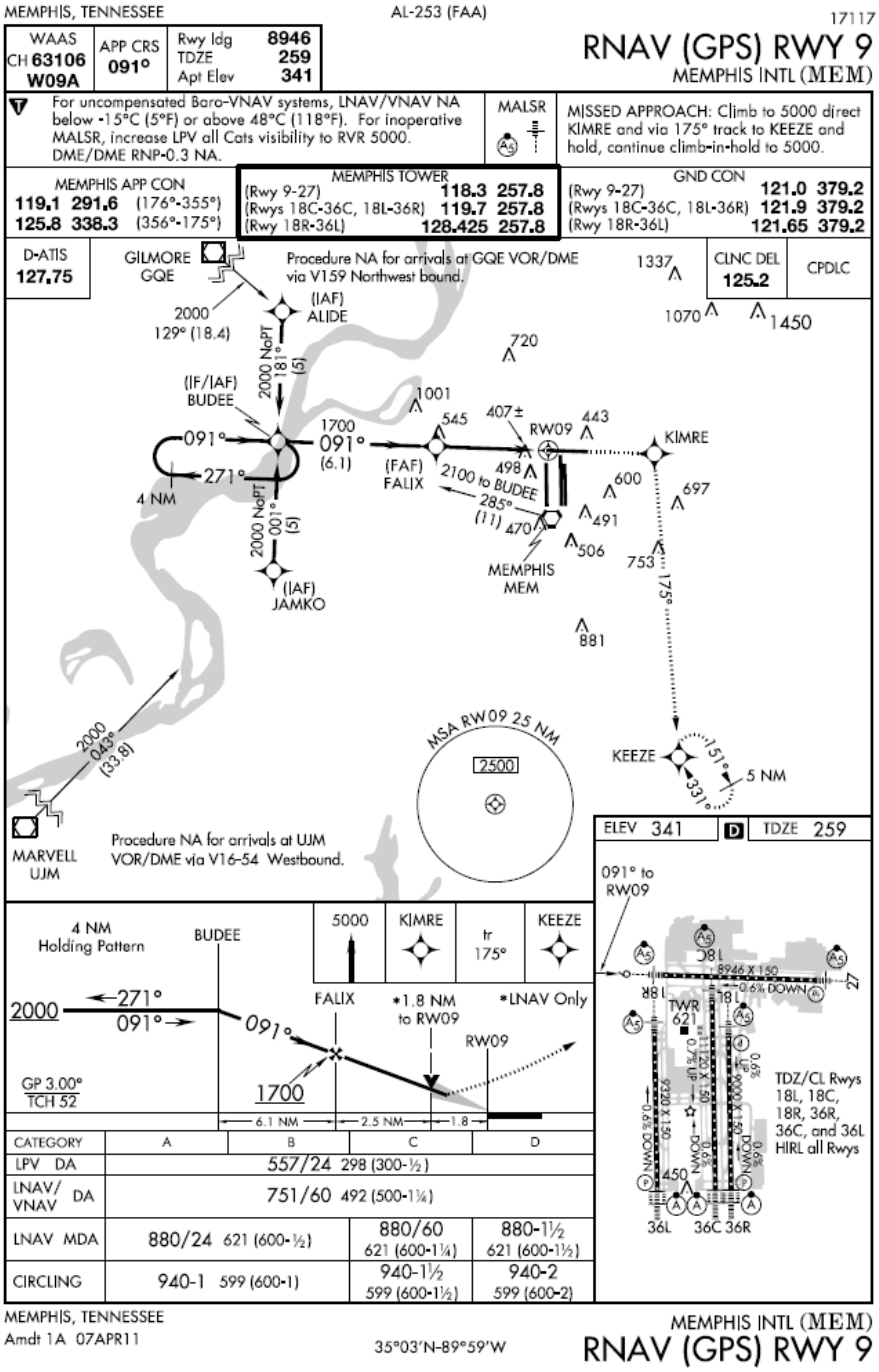

B.2.2. Runway 18C

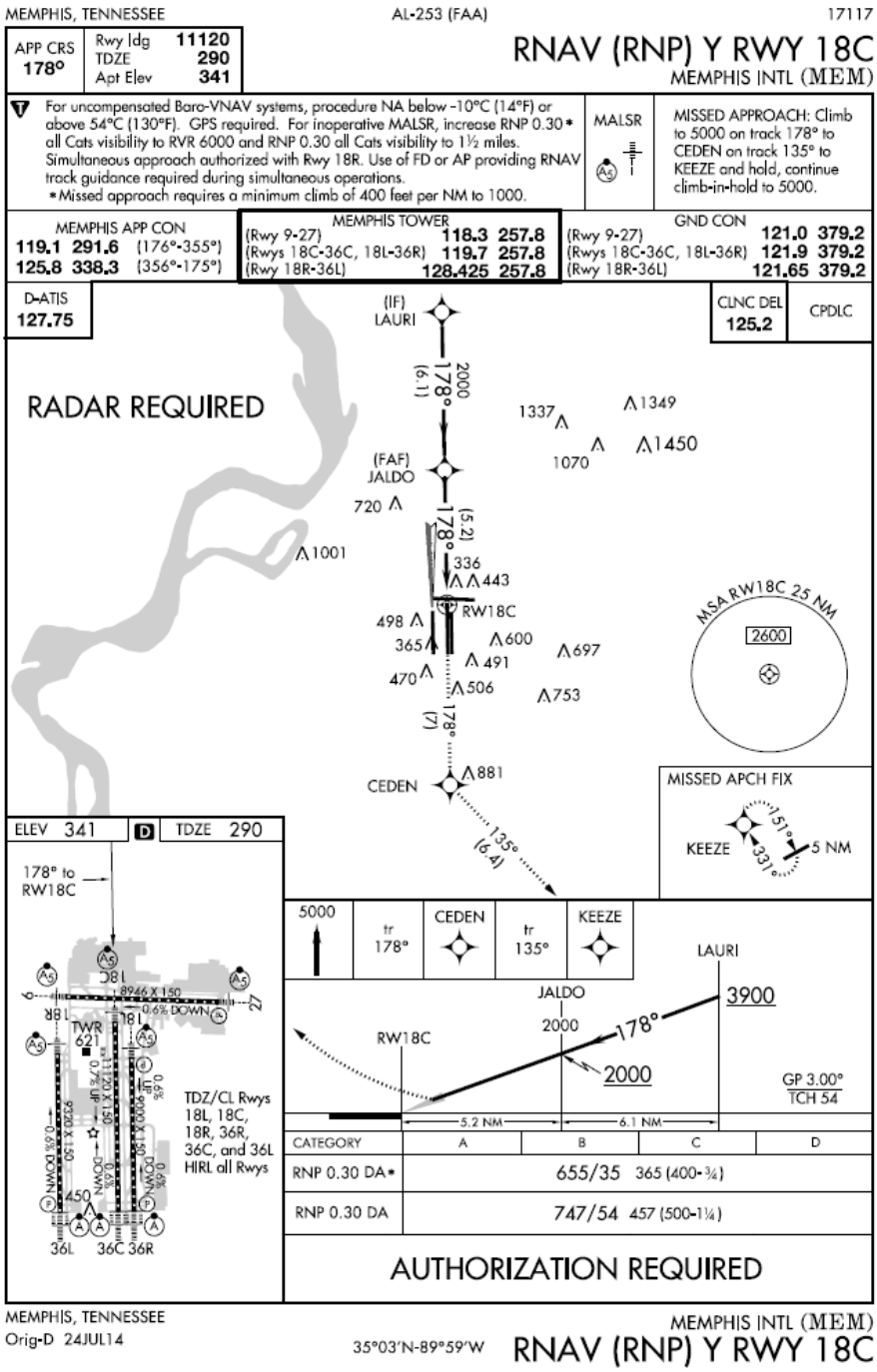

B.2.3. Runway 27

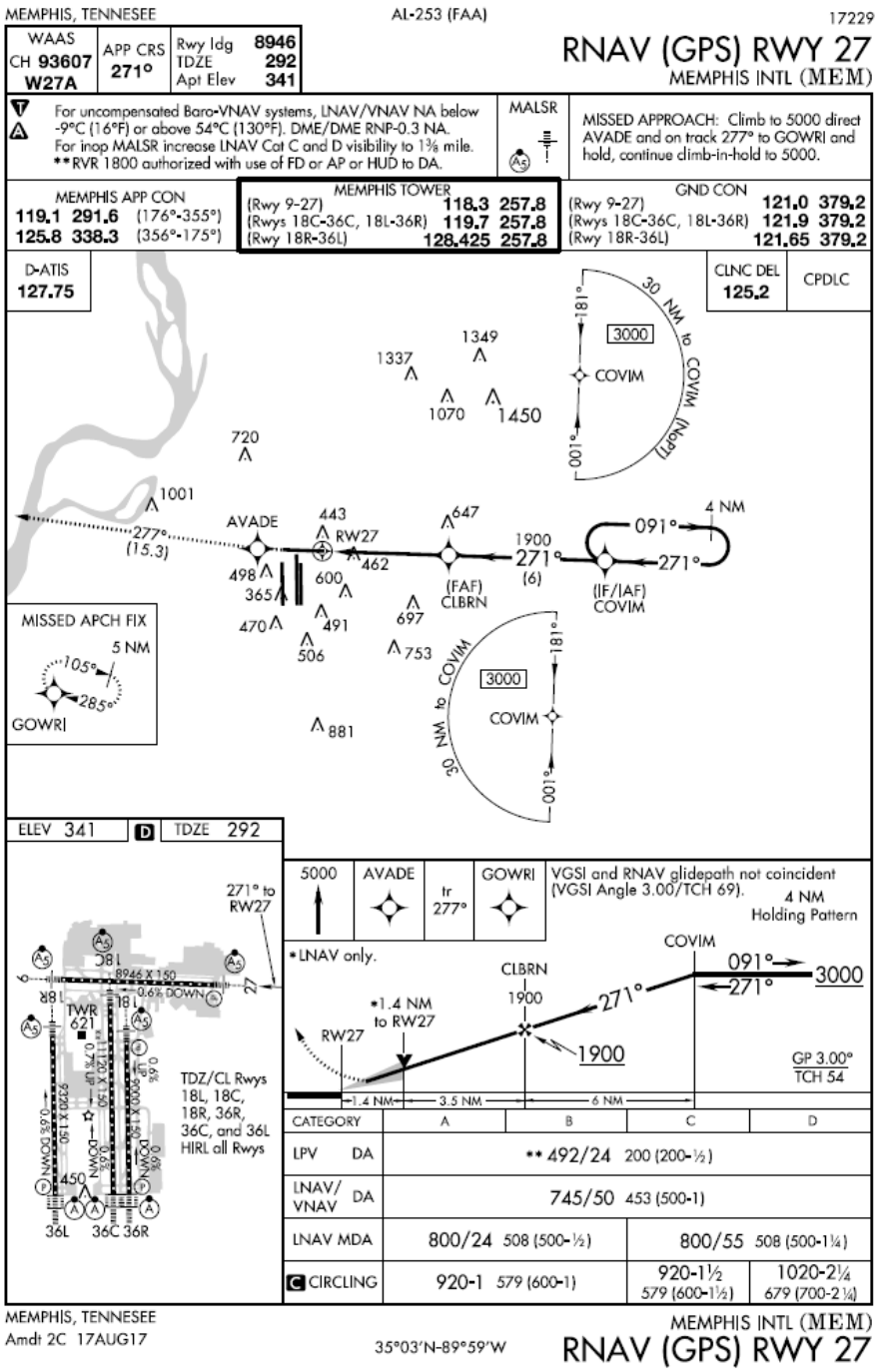

B.2.4. Runway 36C

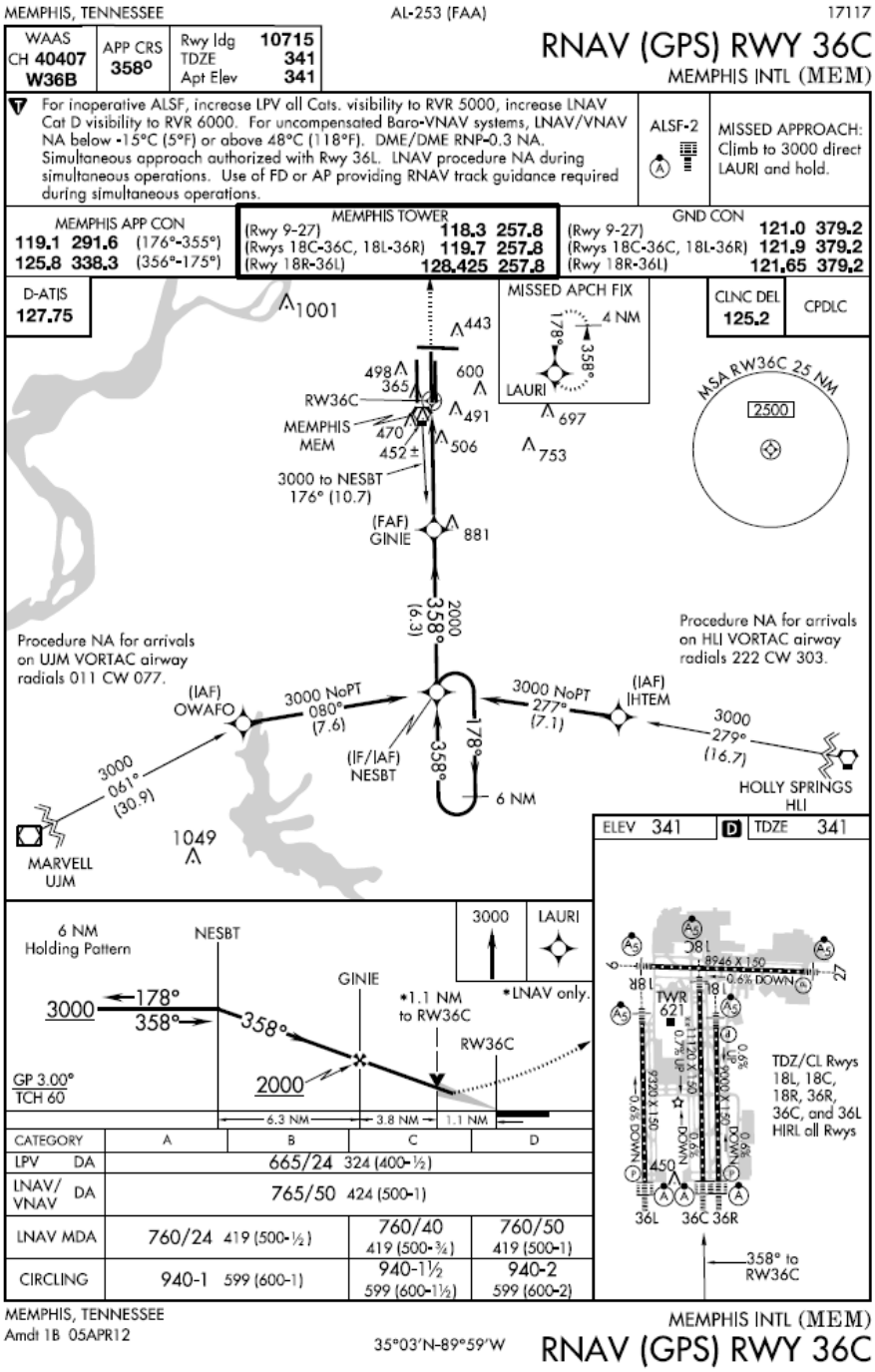

Appendix C. CASPEr-1, Part 1: Select Data for Individual Flights

This appendix includes plots with selected data from the twenty-eight simulated flights at KMEM in Part 1 of CASPEr 1.

C.1. Trajectory: BLUZZ to 09

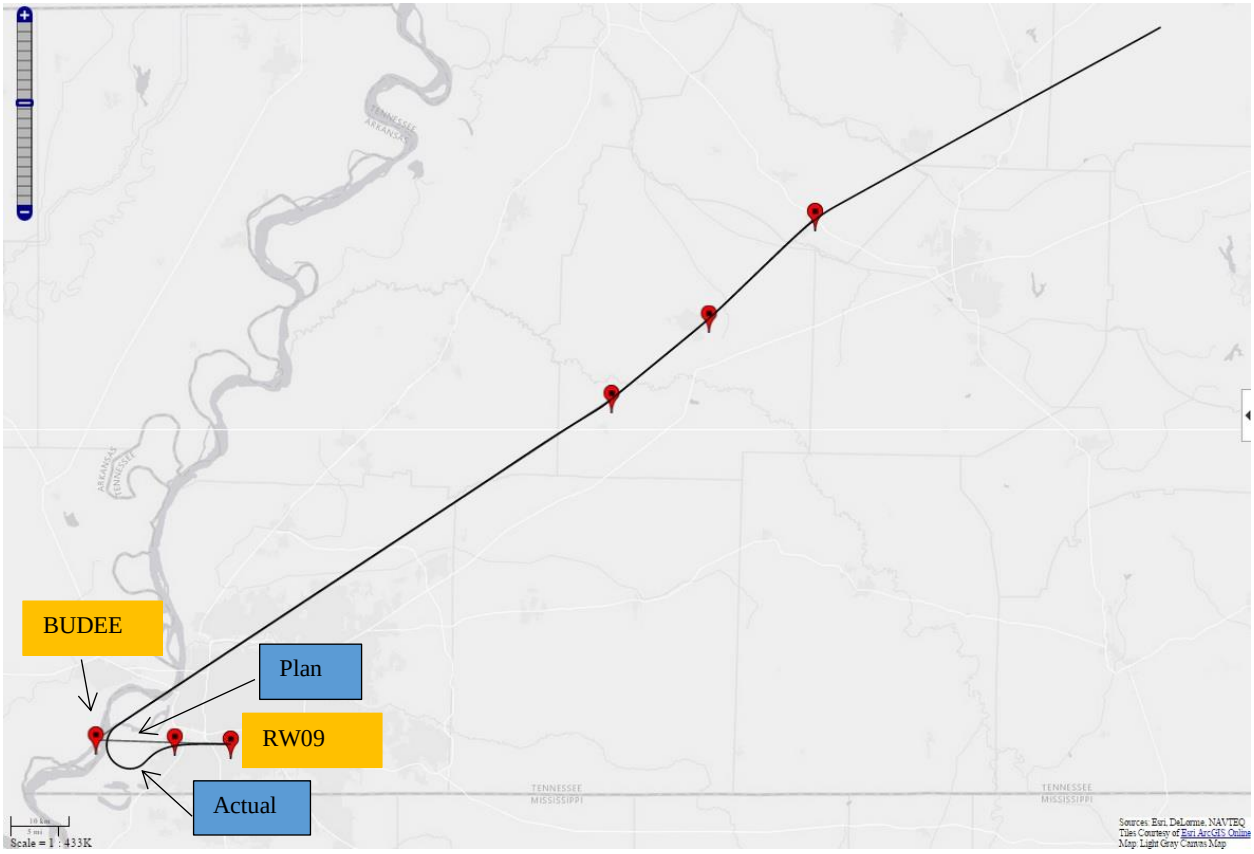

Figure C. 1: BLUZZ to Runway 09: Planned and Actual Trajectories (Red markers indicate waypoints)

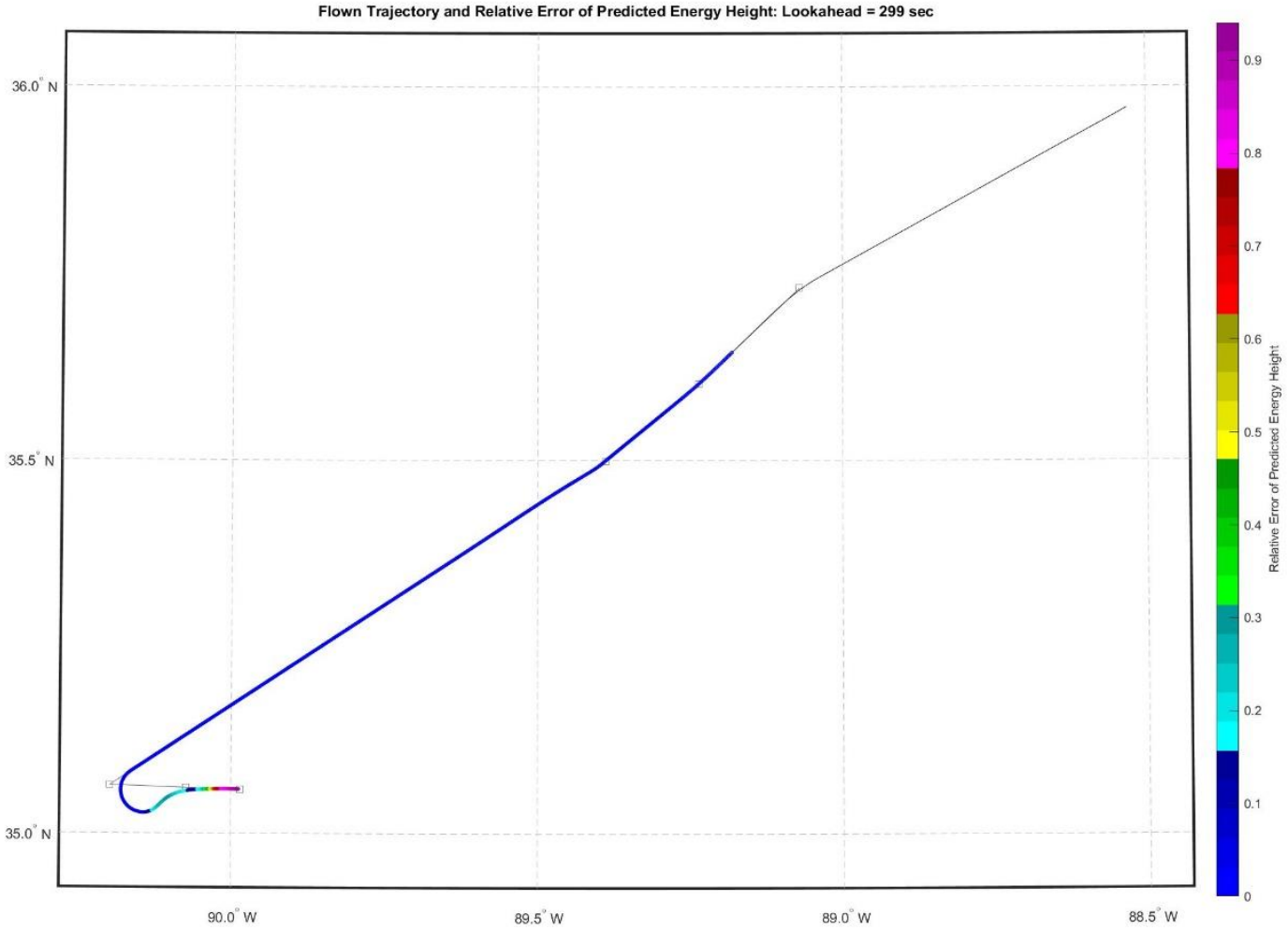

Figure C. 2: BLUZZ to Runway 09: Lateral Path Color-Coded for Energy Prediction Error for Look-Ahead of 299 Seconds

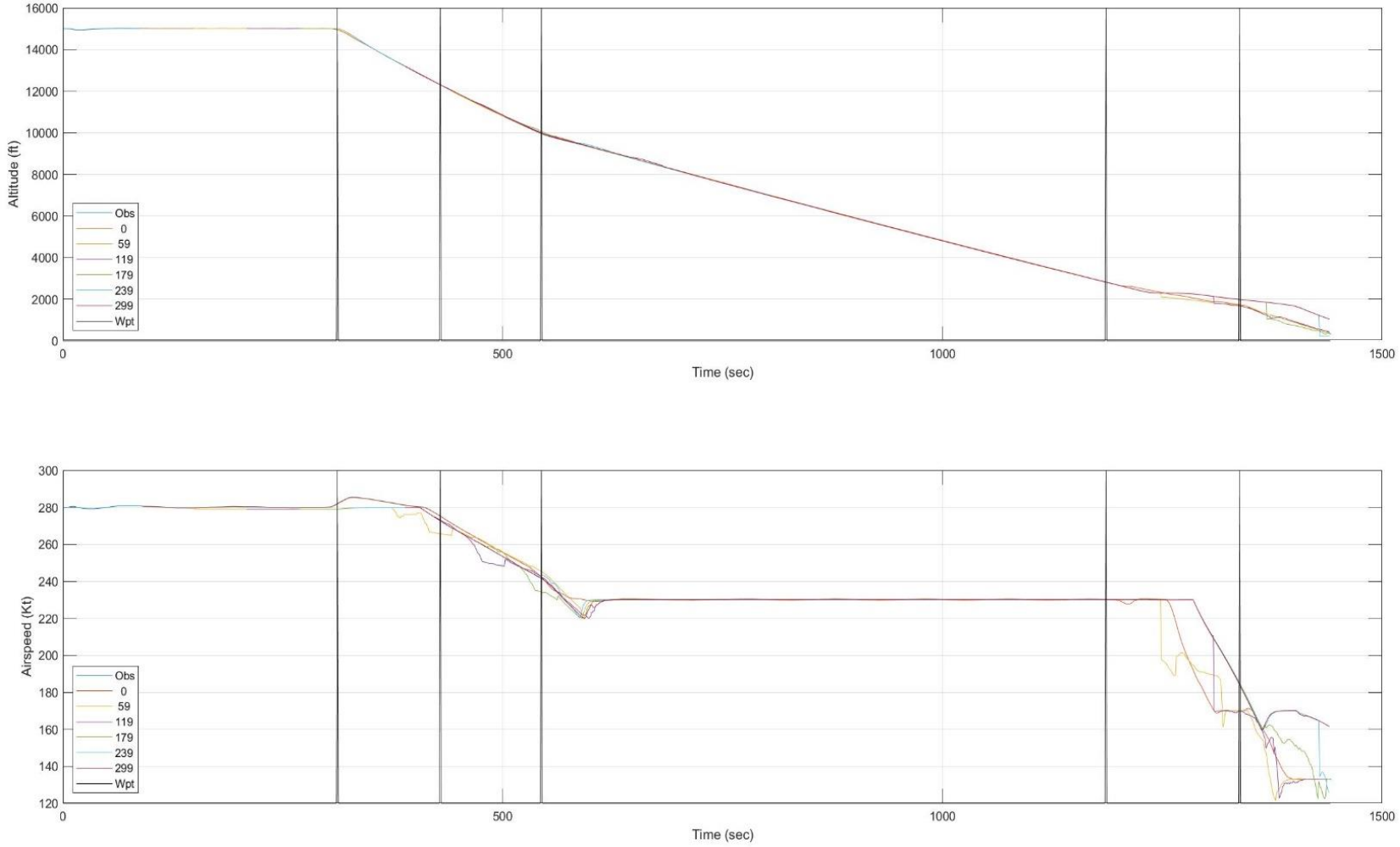

Figure C. 3: BLUZZ to Runway 09: Time History of Predicted Altitude and Airspeed

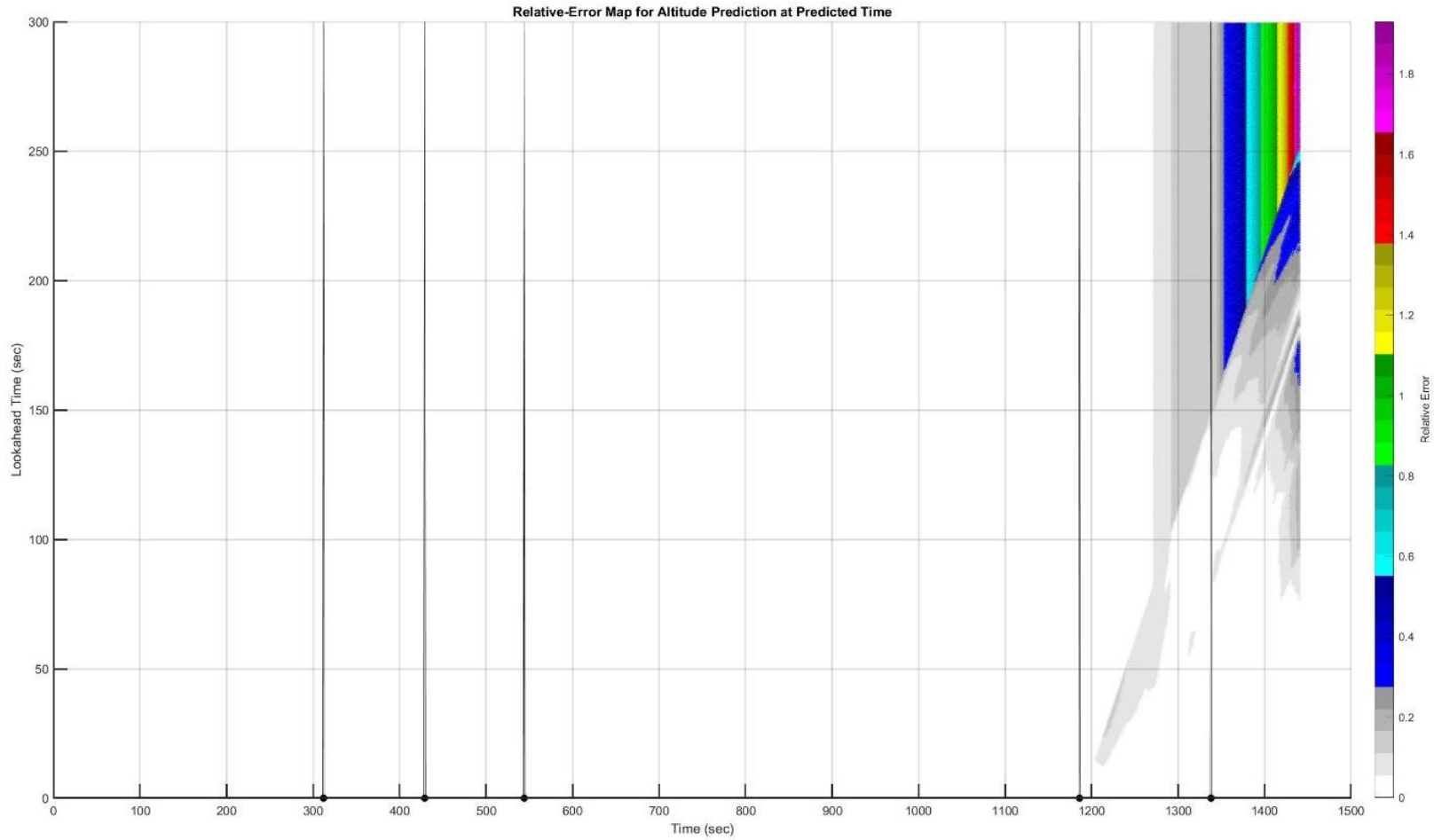

Figure C. 4: BLUZZ to Runway 09: Heatmap of Altitude Prediction Error (Time is $t + \tau$)

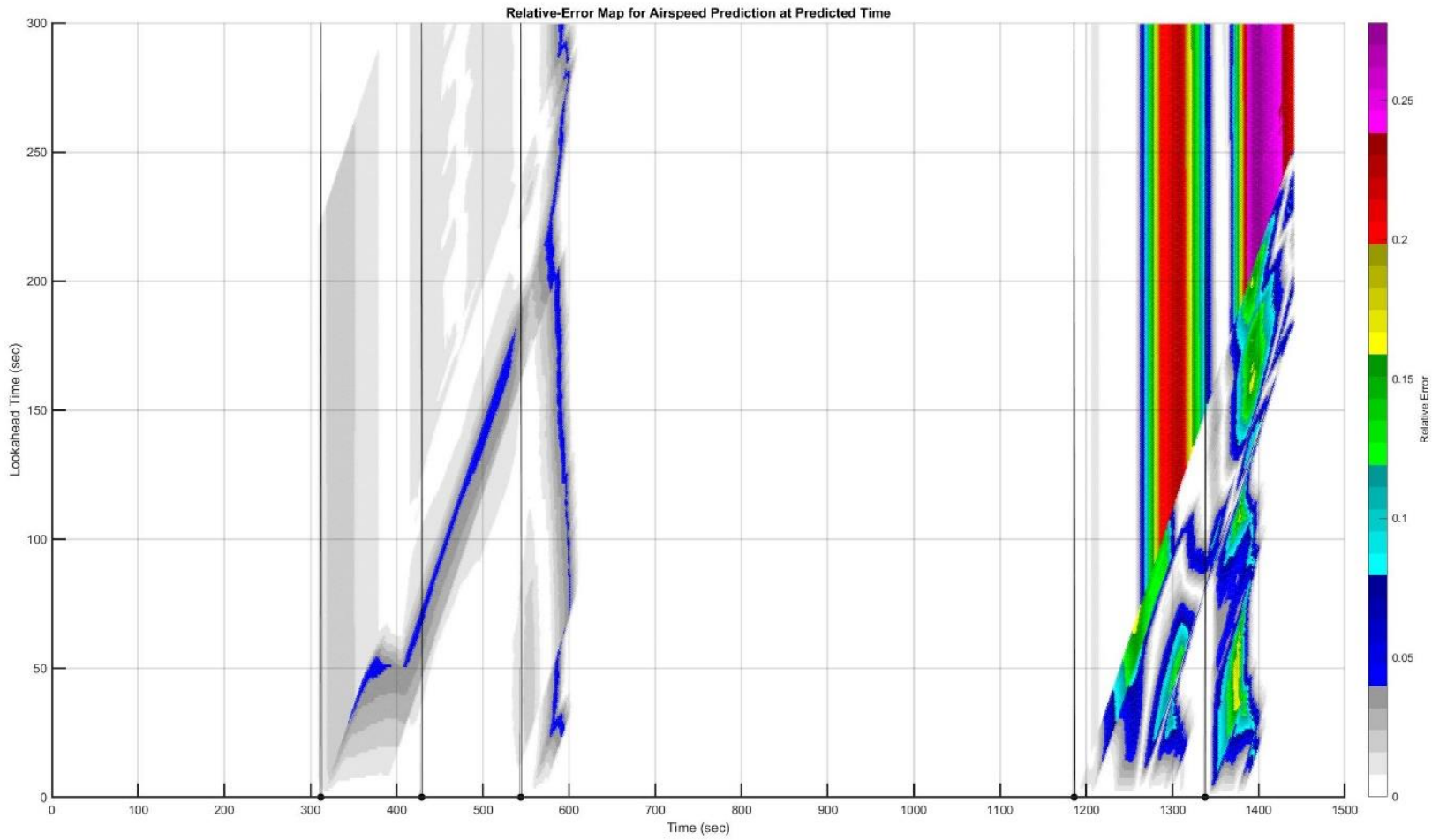

Figure C. 5: BLUZZ to Runway 09: Heatmap of Airspeed Prediction Error (Time is $t + \tau$)

C.2. Trajectory: BLUZZ to 18C

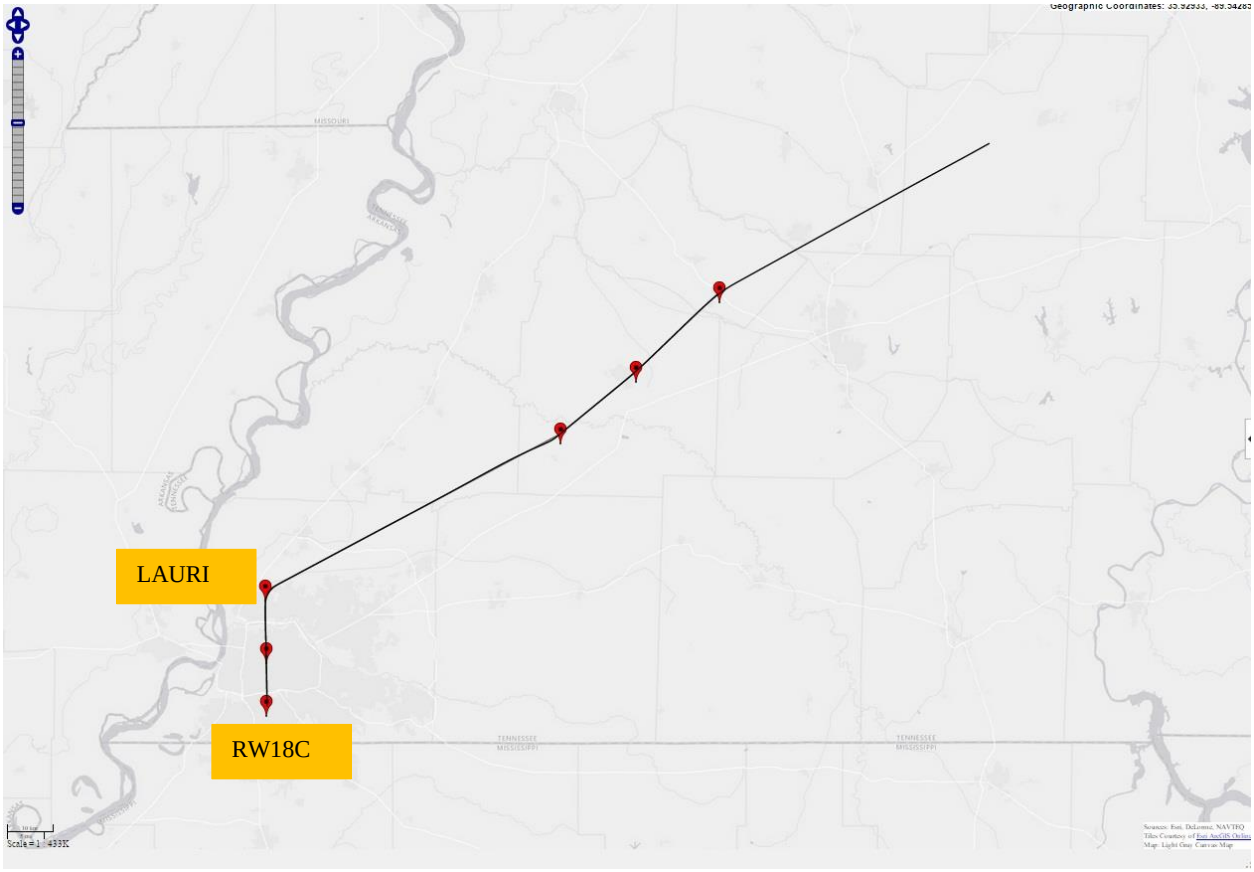

Figure C. 6: BLUZZ to Runway 18C: Planned and Actual Trajectories (Red markers indicate waypoints)

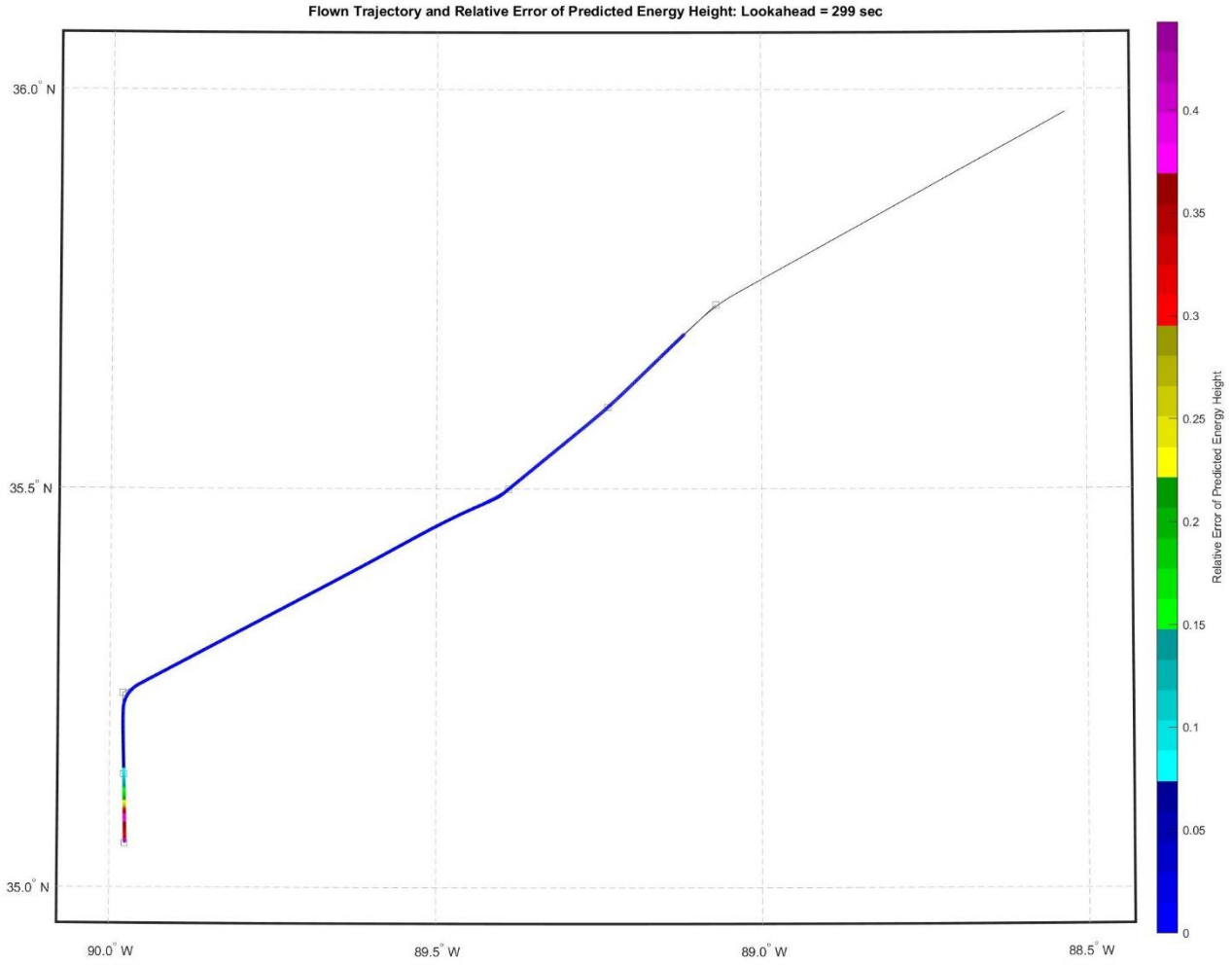

Figure C. 7: BLUZZ to Runway 18C: Lateral Path Color-Coded for Energy Prediction Error for Look-Ahead of 299 Seconds

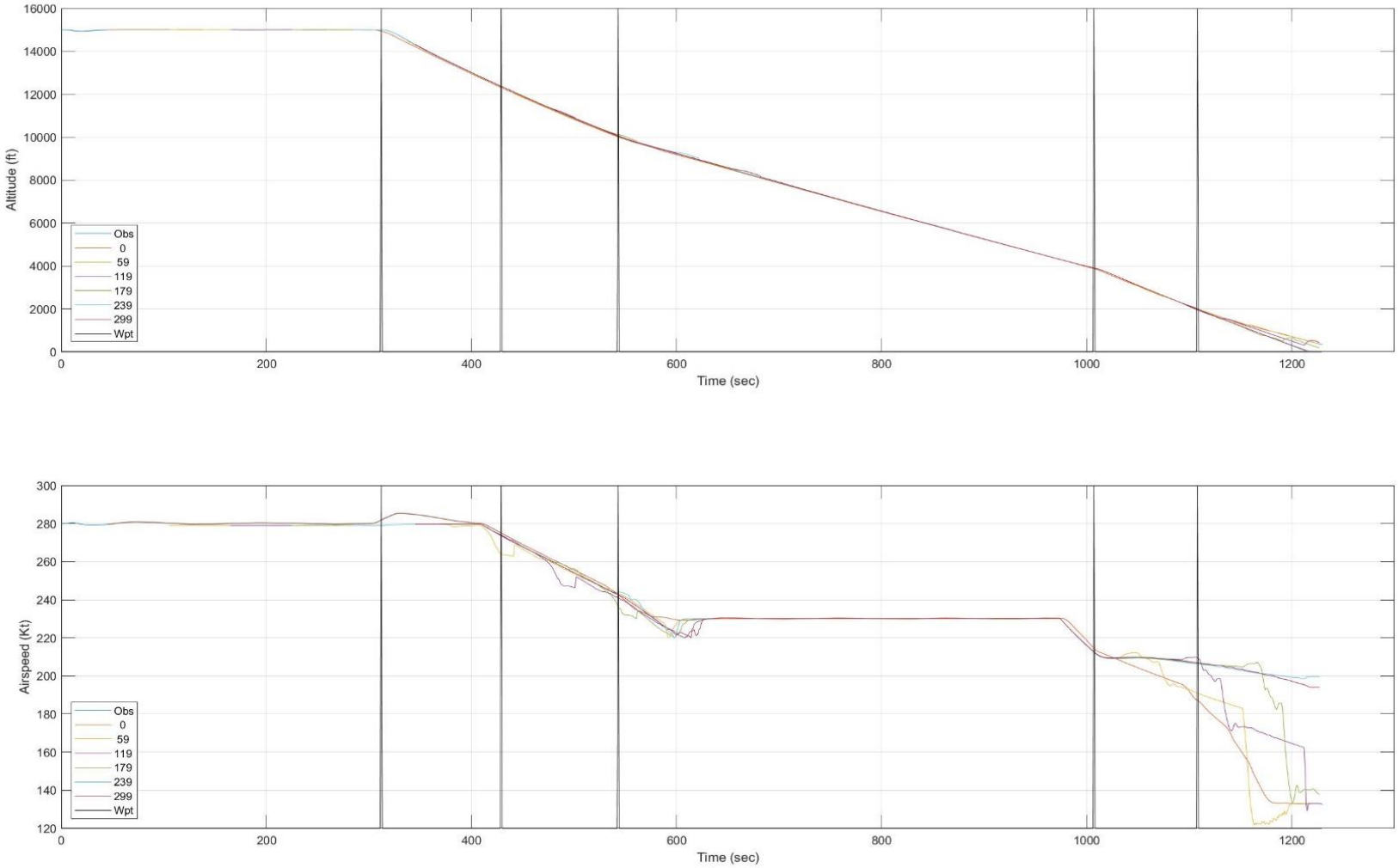

Figure C. 8: BLUZZ to Runway 18C: Time History of Predicted Altitude and Airspeed

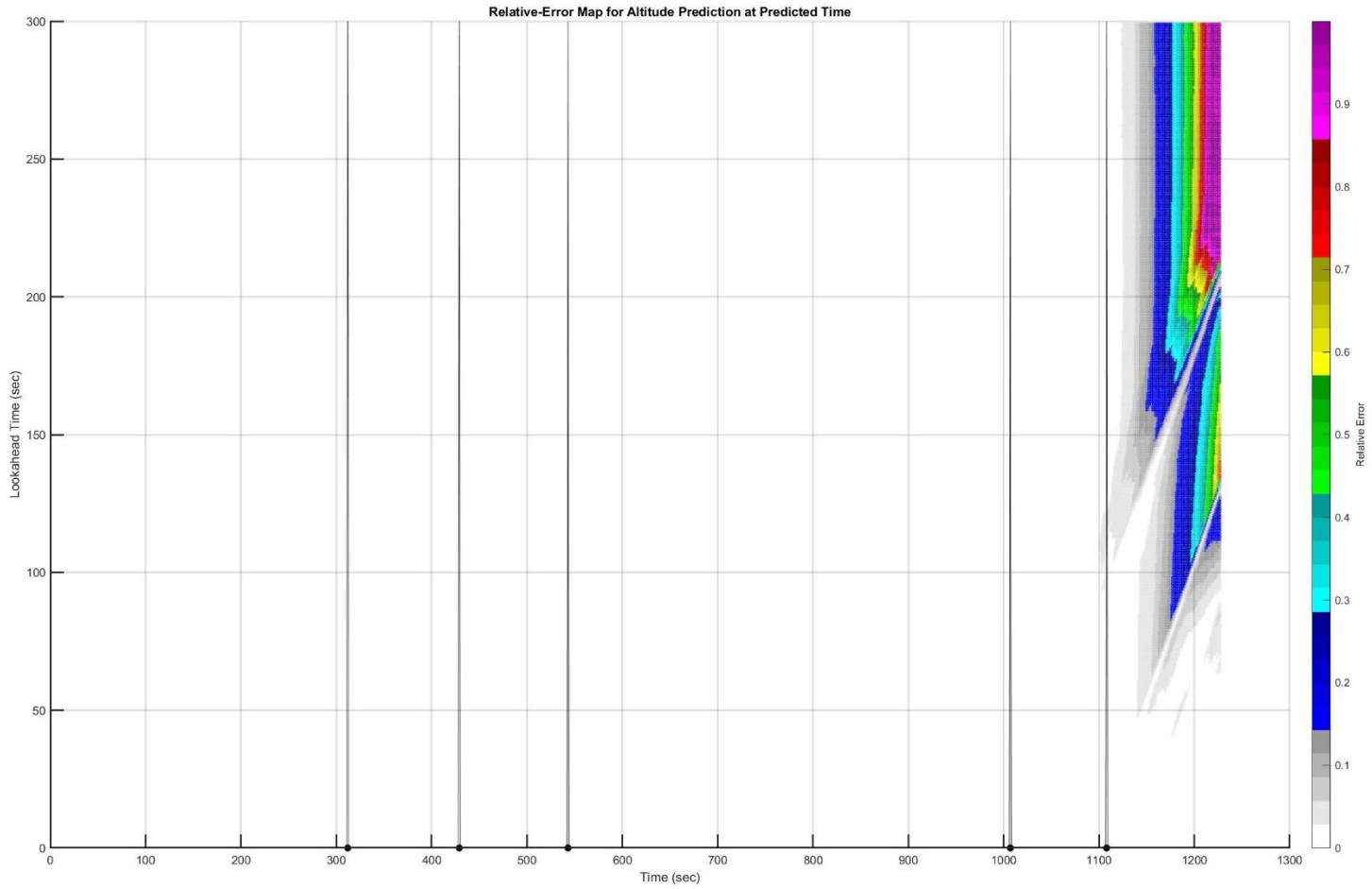

Figure C. 9: BLUZZ to Runway 18C: Heatmap of Altitude Prediction Error (Time is $t + \tau$)

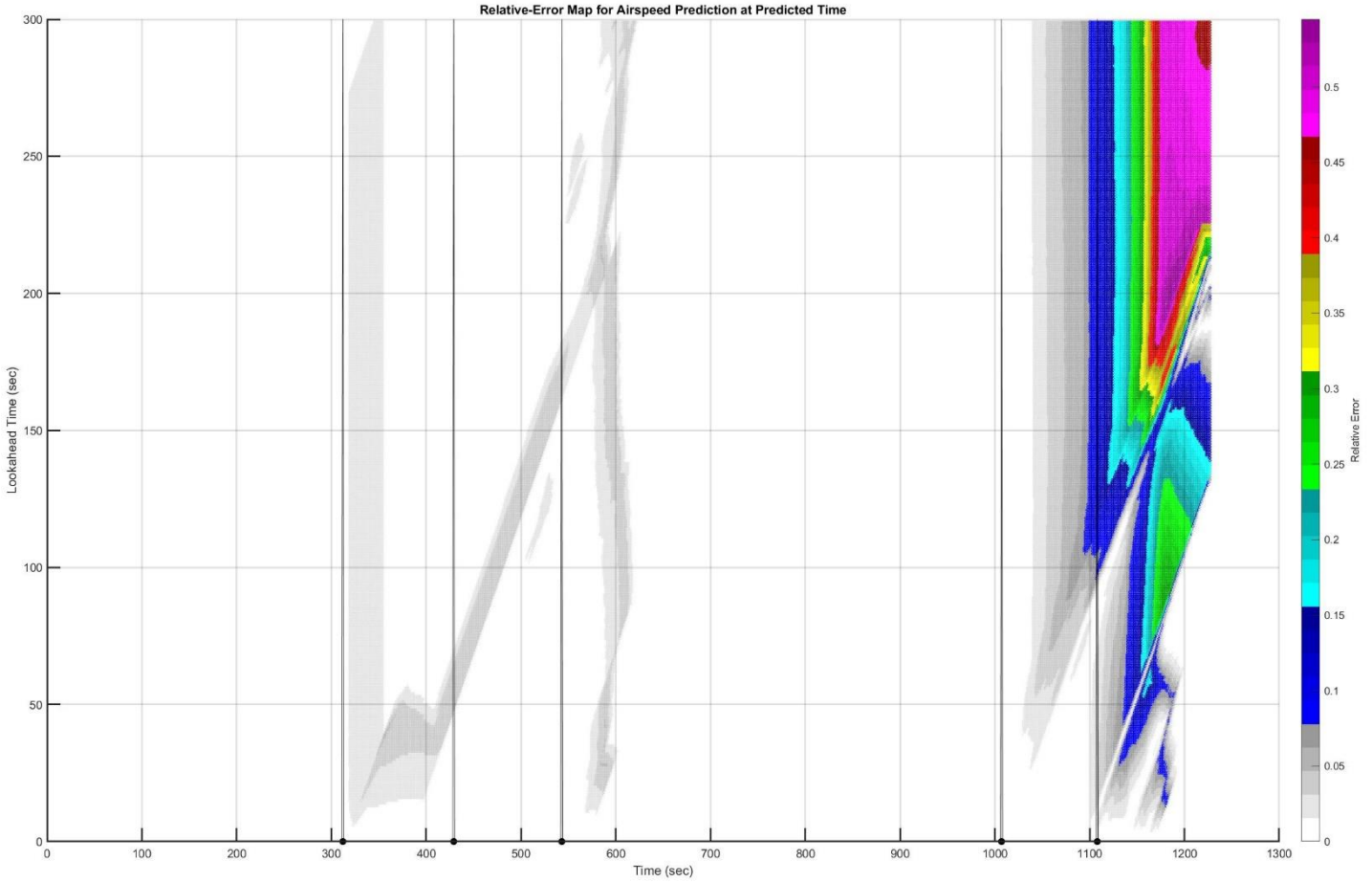

Figure C. 10: BLUZZ to Runway 18C: Heatmap of Airspeed Prediction Error (Time is $t + \tau$)

C.3. Trajectory: BLUZZ to 27

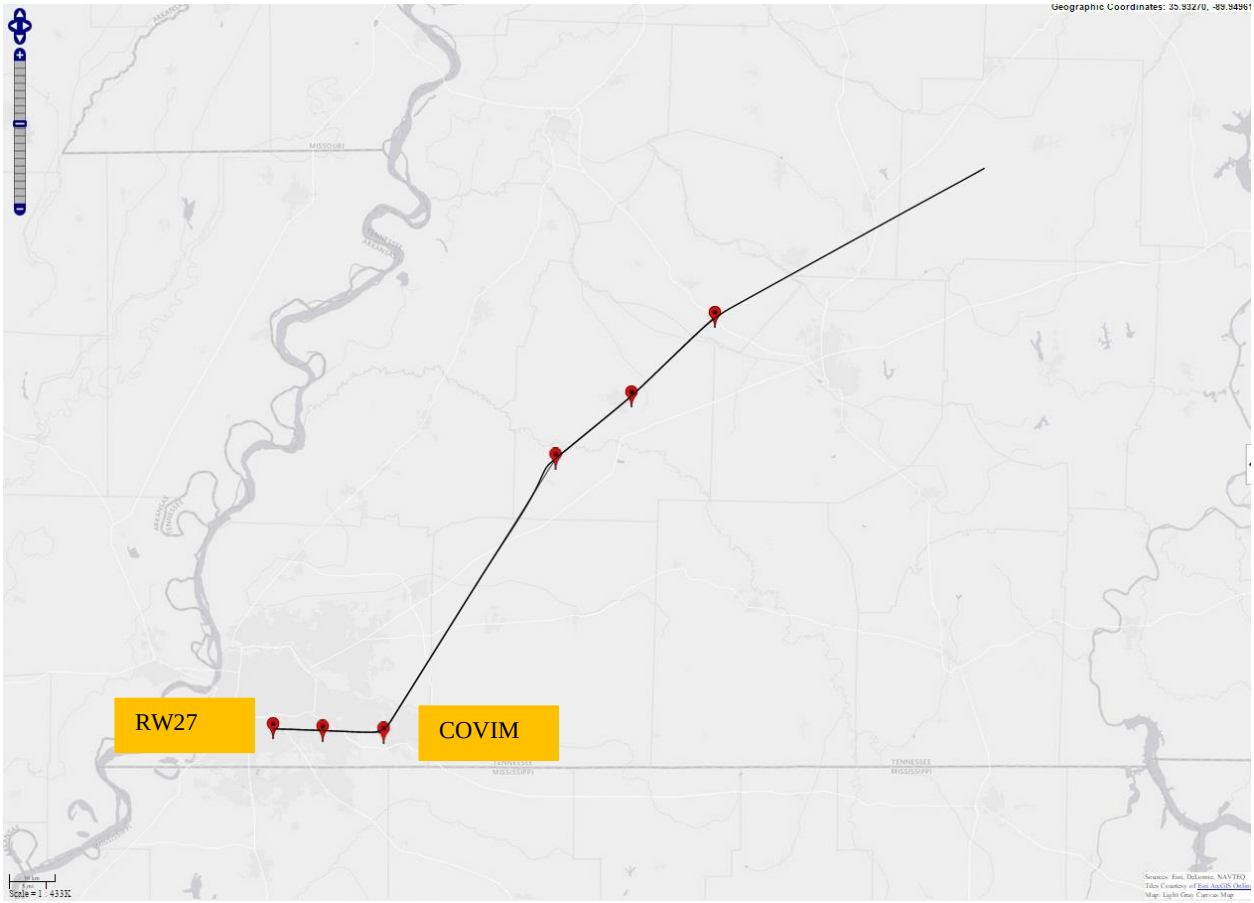

Figure C. 11: BLUZZ to Runway 27: Planned and Actual Trajectories (Red markers indicate waypoints)

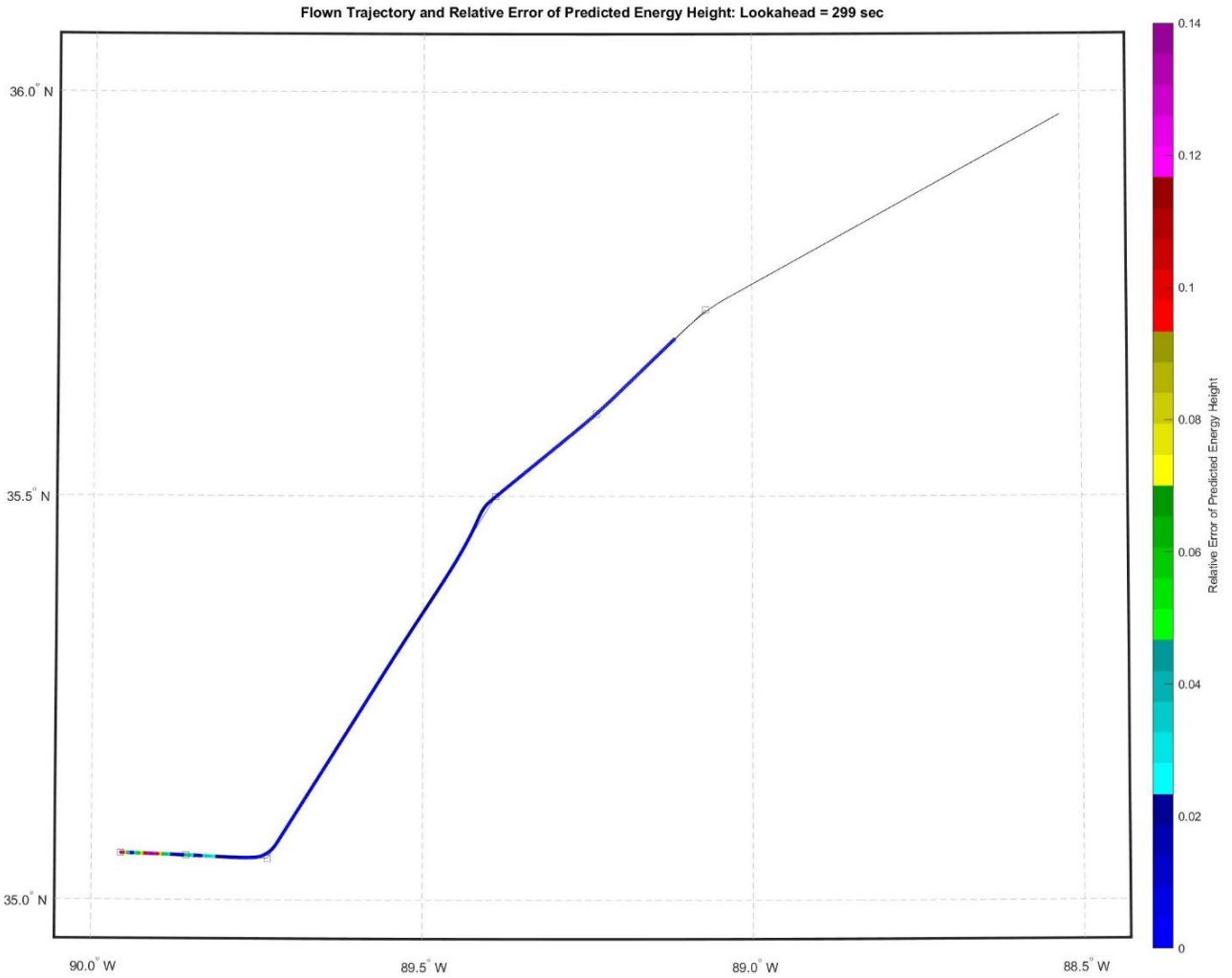

Figure C. 12: BLUZZ to Runway 27: Lateral Path Color-Coded for Energy Prediction Error for Look-Ahead of 299 Seconds

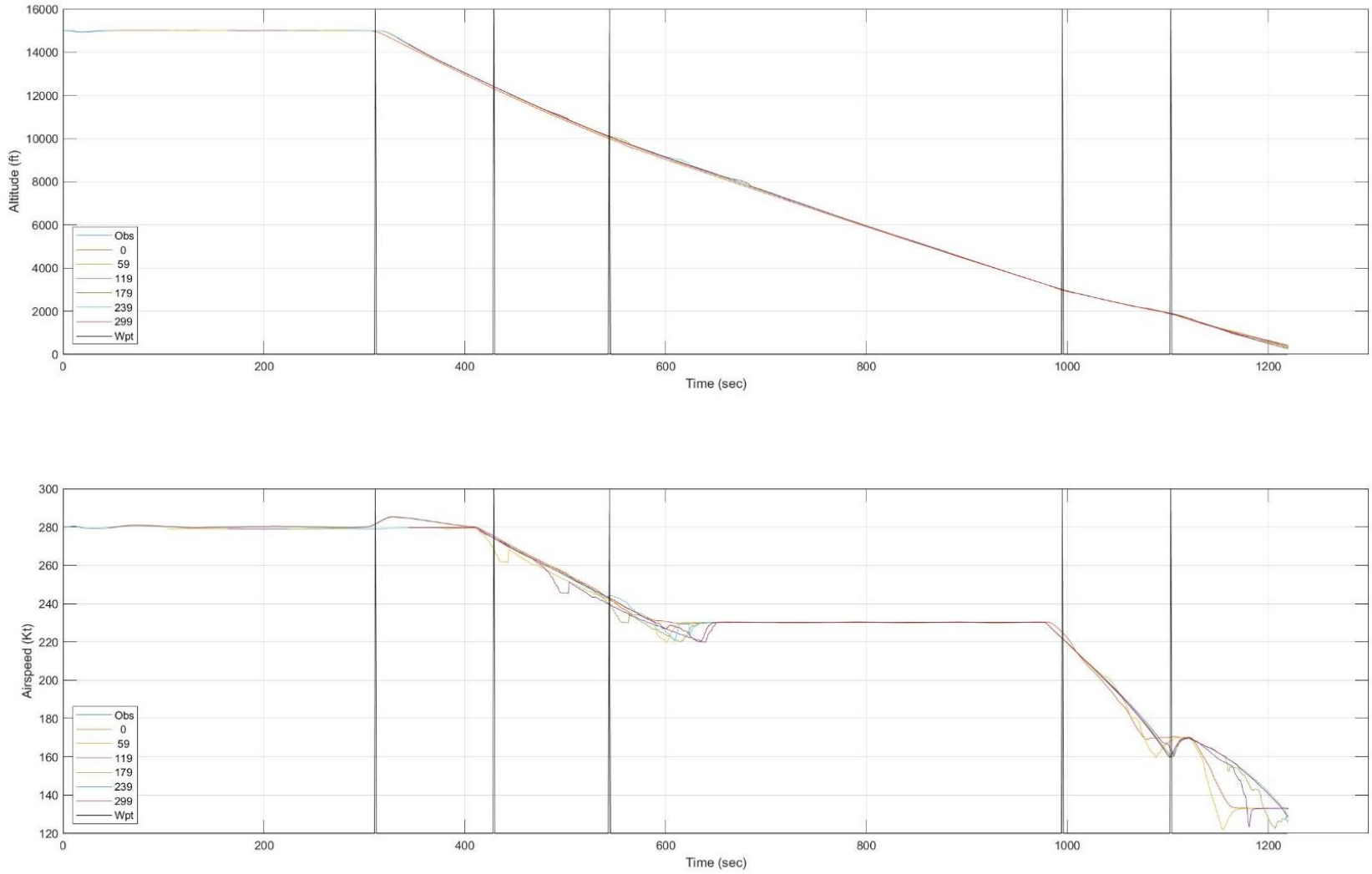

Figure C. 13: BLUZZ to Runway 27: Time History of Predicted Altitude and Airspeed

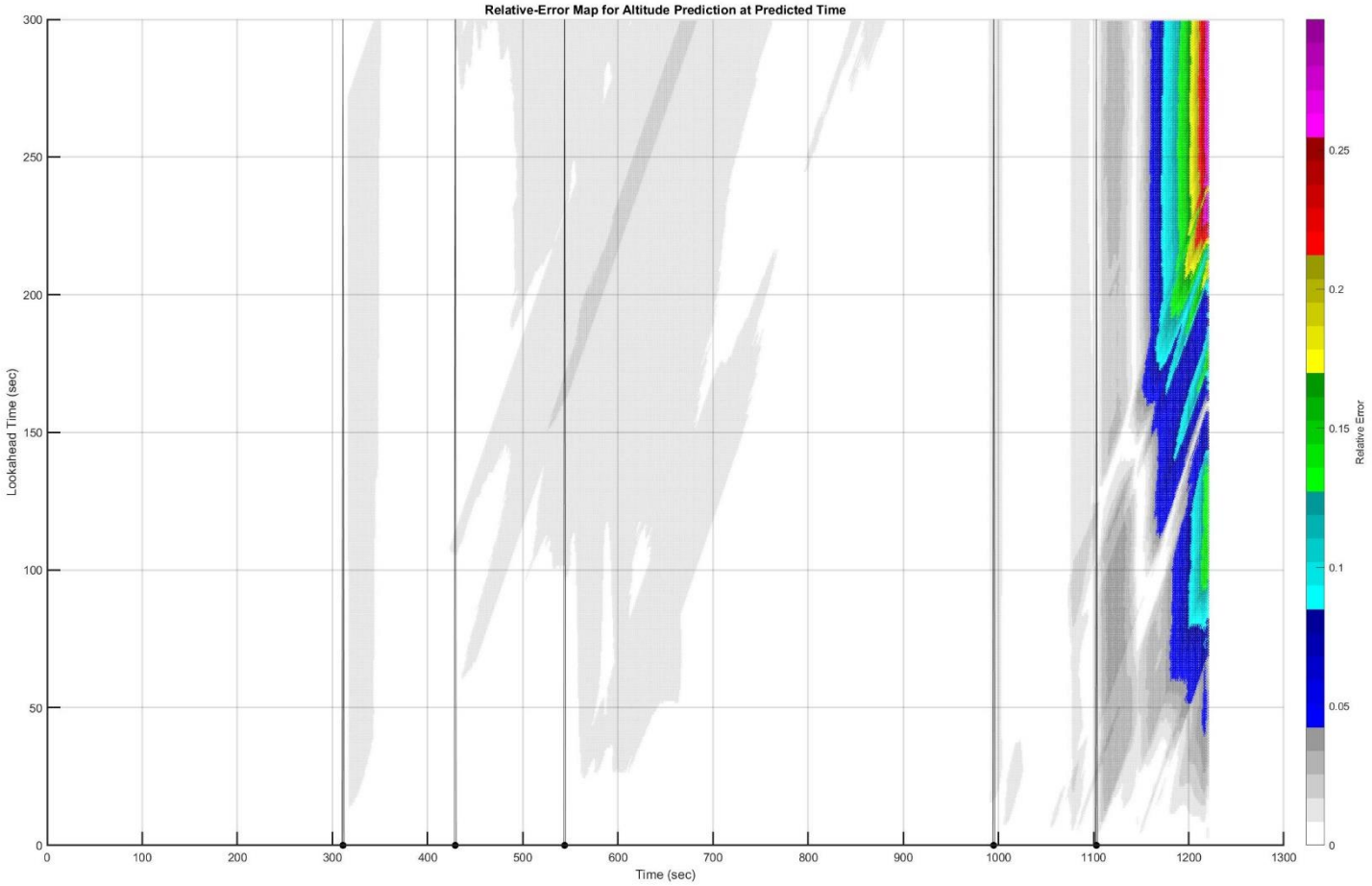

Figure C. 14: BLUZZ to Runway 27: Heatmap of Altitude Prediction Error (Time is $t + \tau$)

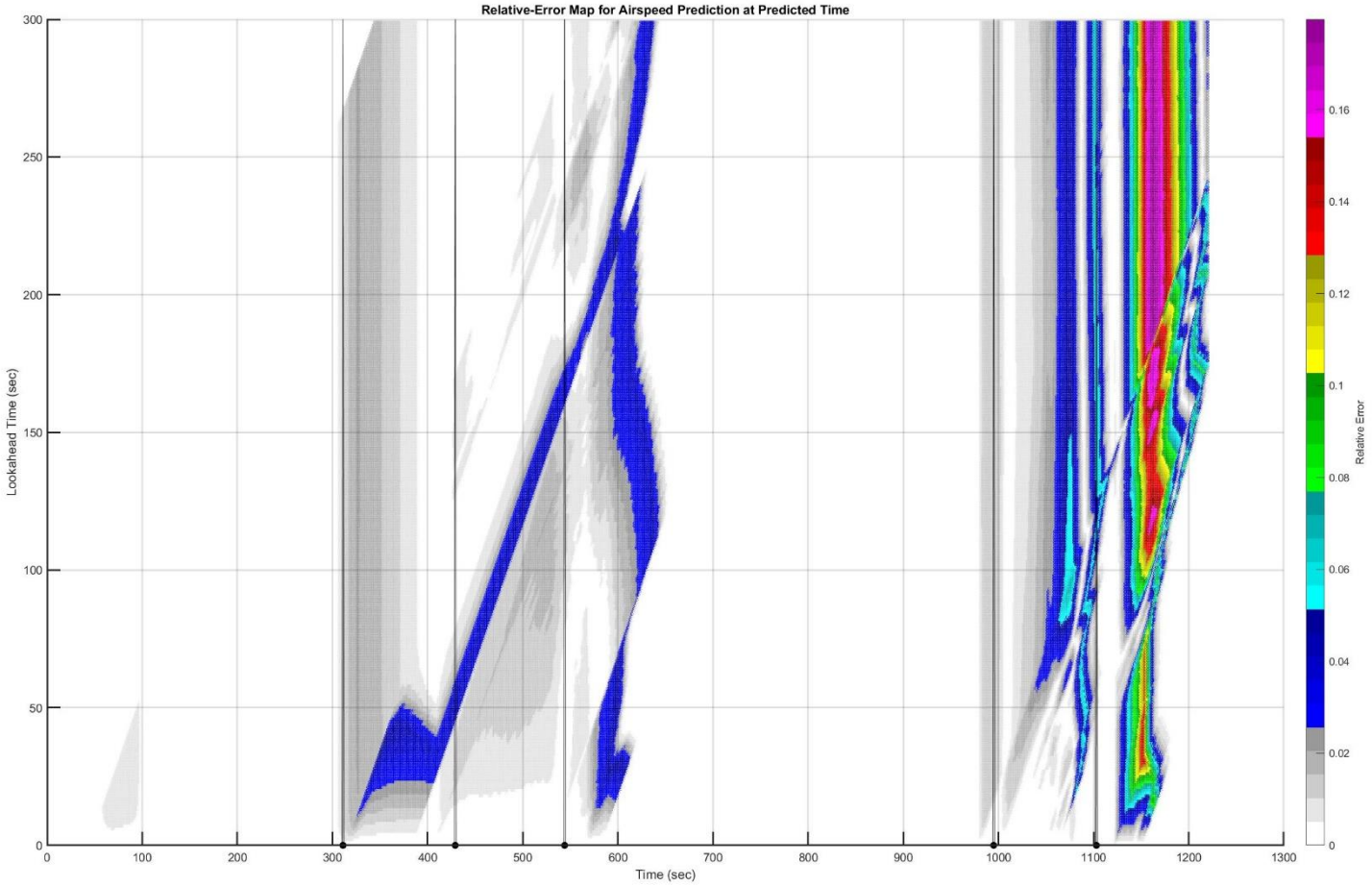

Figure C. 15: BLUZZ to Runway 27: Heatmap of Airspeed Prediction Error (Time is $t + \tau$)

C.4. Trajectory: BLUZZ to 36C

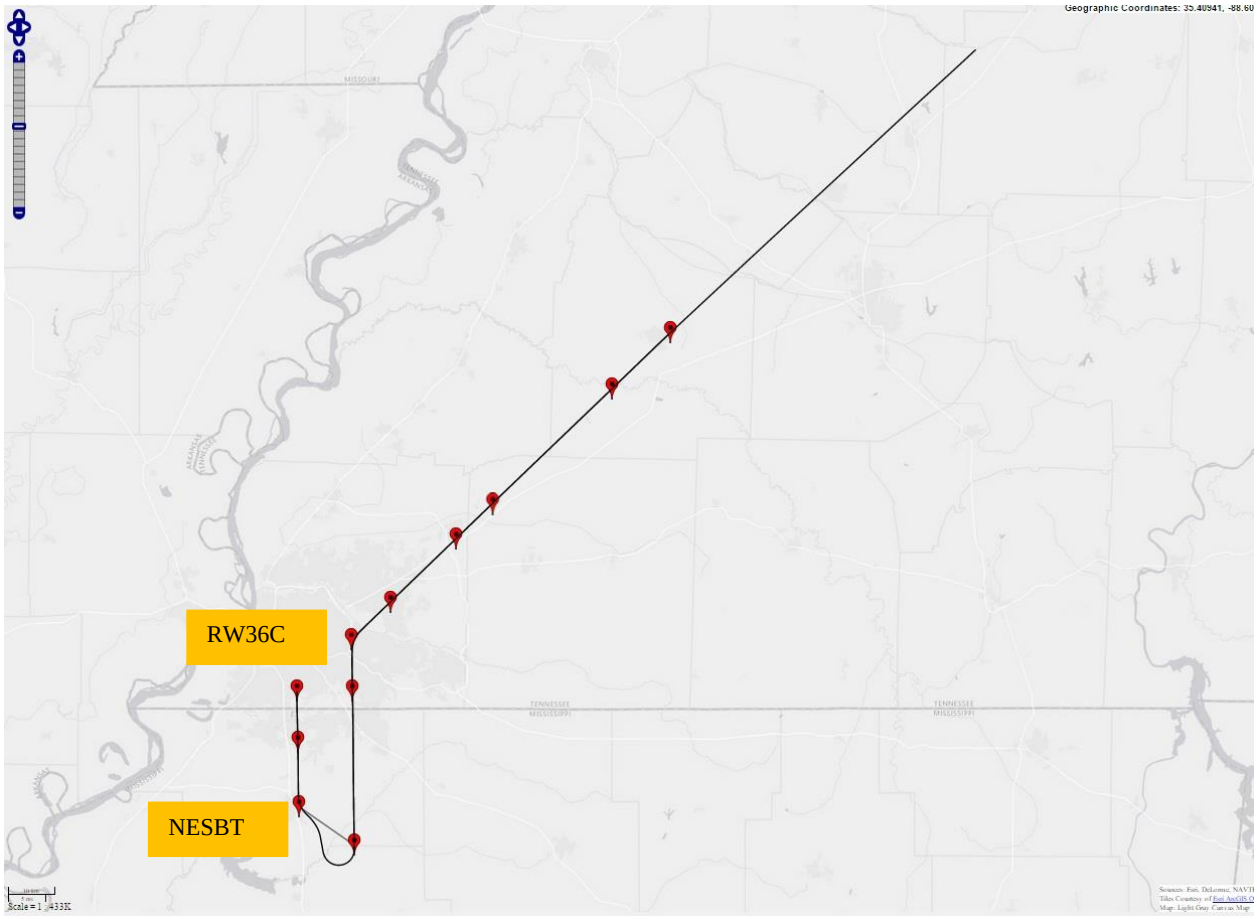

Figure C. 16: BLUZZ to Runway 36C: Planned and Actual Trajectories (Red markers indicate waypoints)

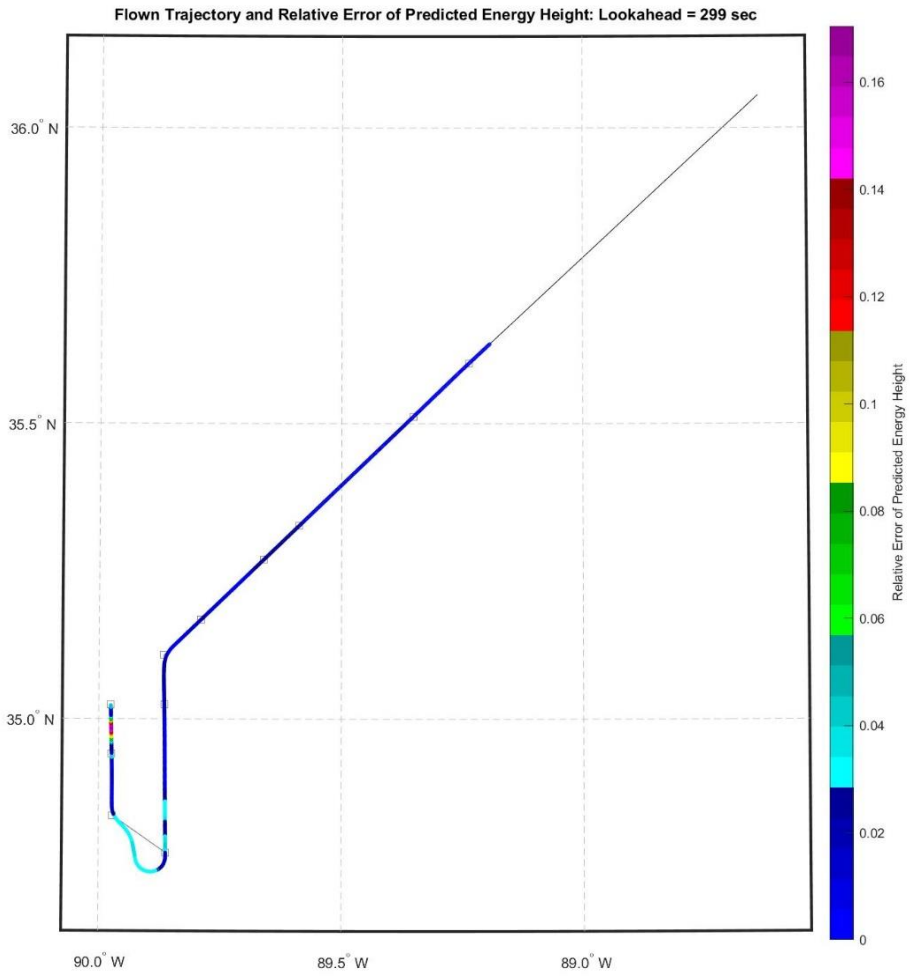

Figure C. 17: BLUZZ to Runway 36C: Lateral Path Color-Coded for Energy Prediction Error for Look-Ahead of 299 Seconds

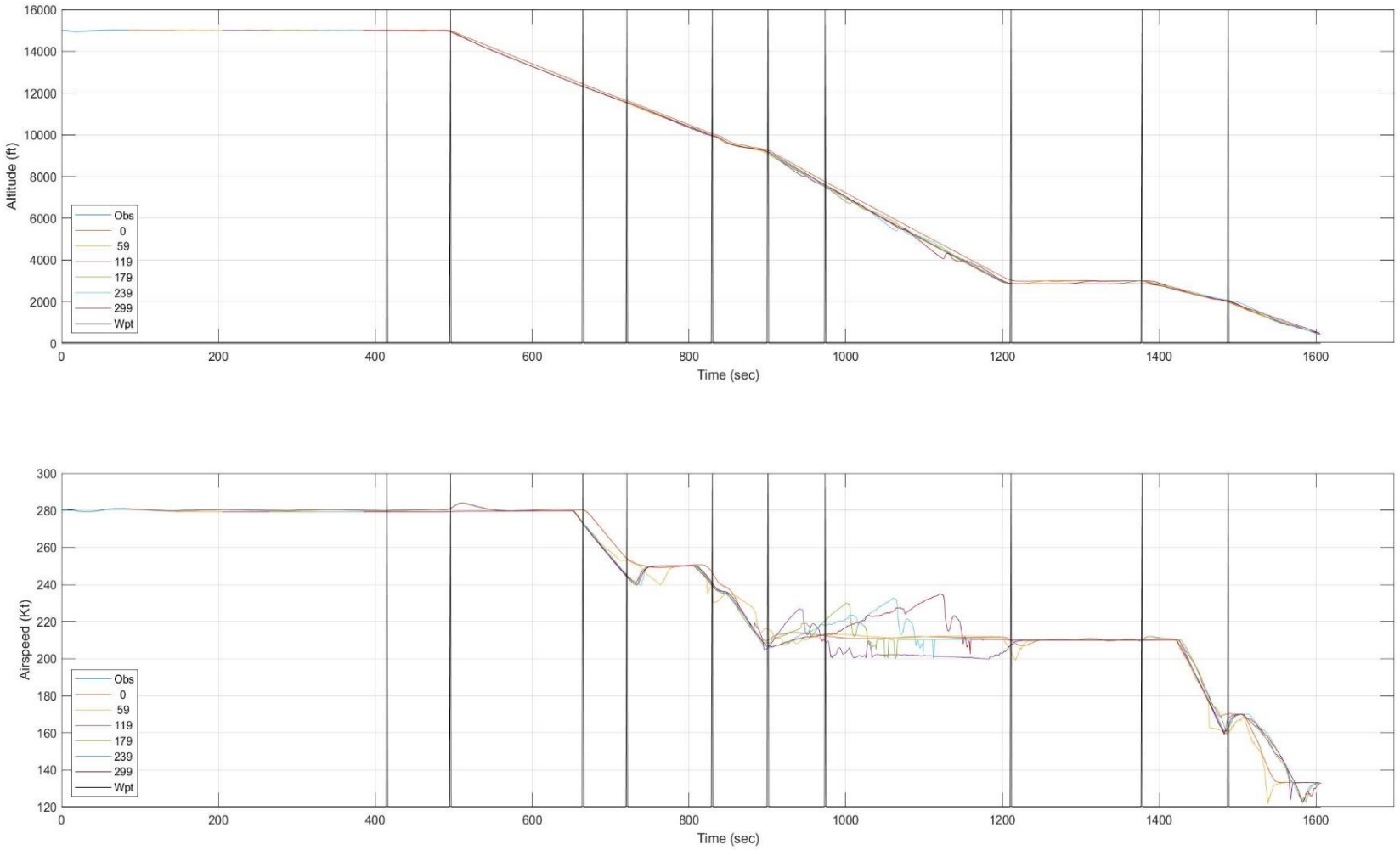

Figure C. 18: BLUZZ to Runway 36C: Time History of Predicted Altitude and Airspeed

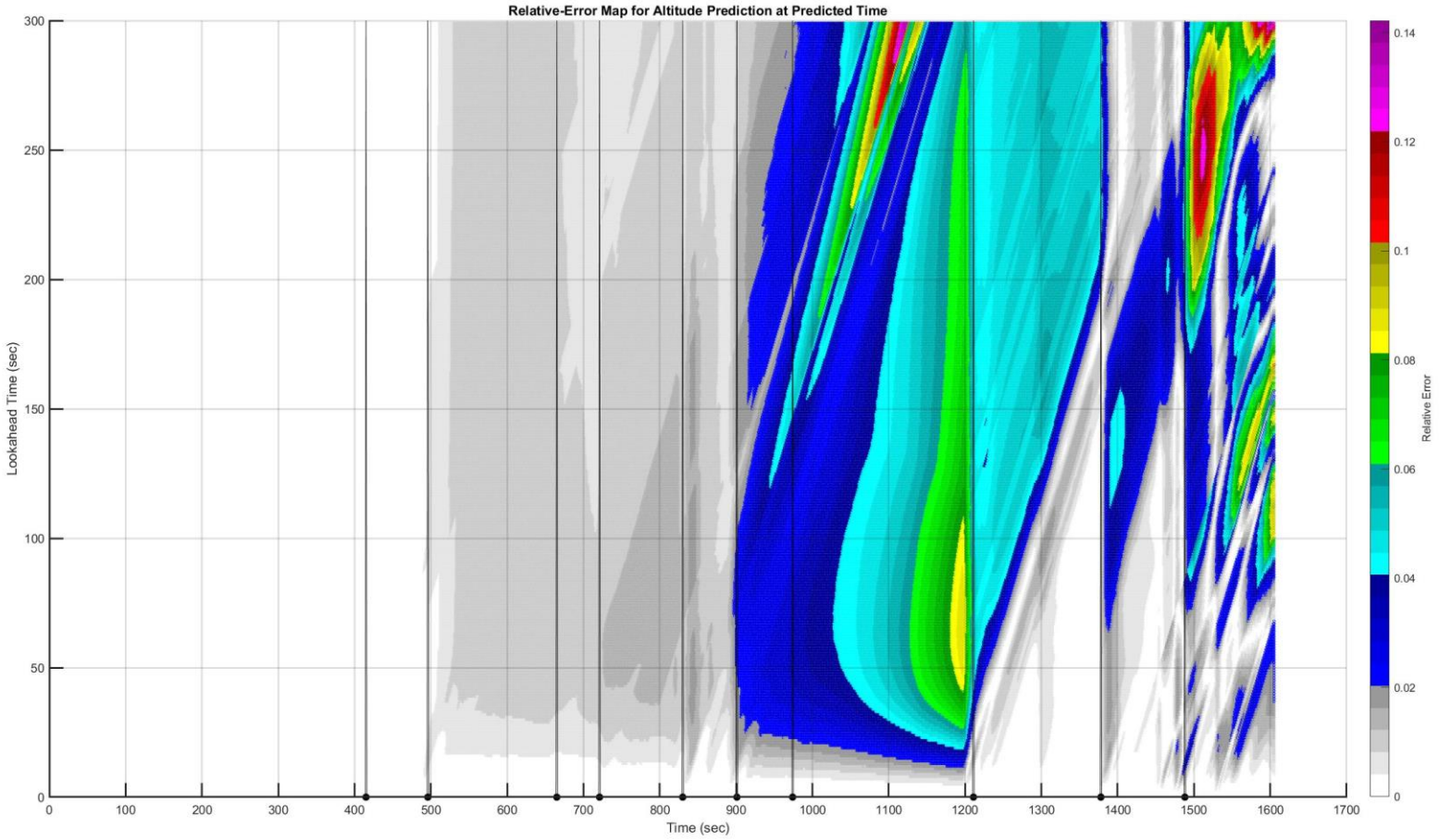

Figure C. 19: BLUZZ to Runway 36C: Heatmap of Altitude Prediction Error (Time is $t + \tau$)

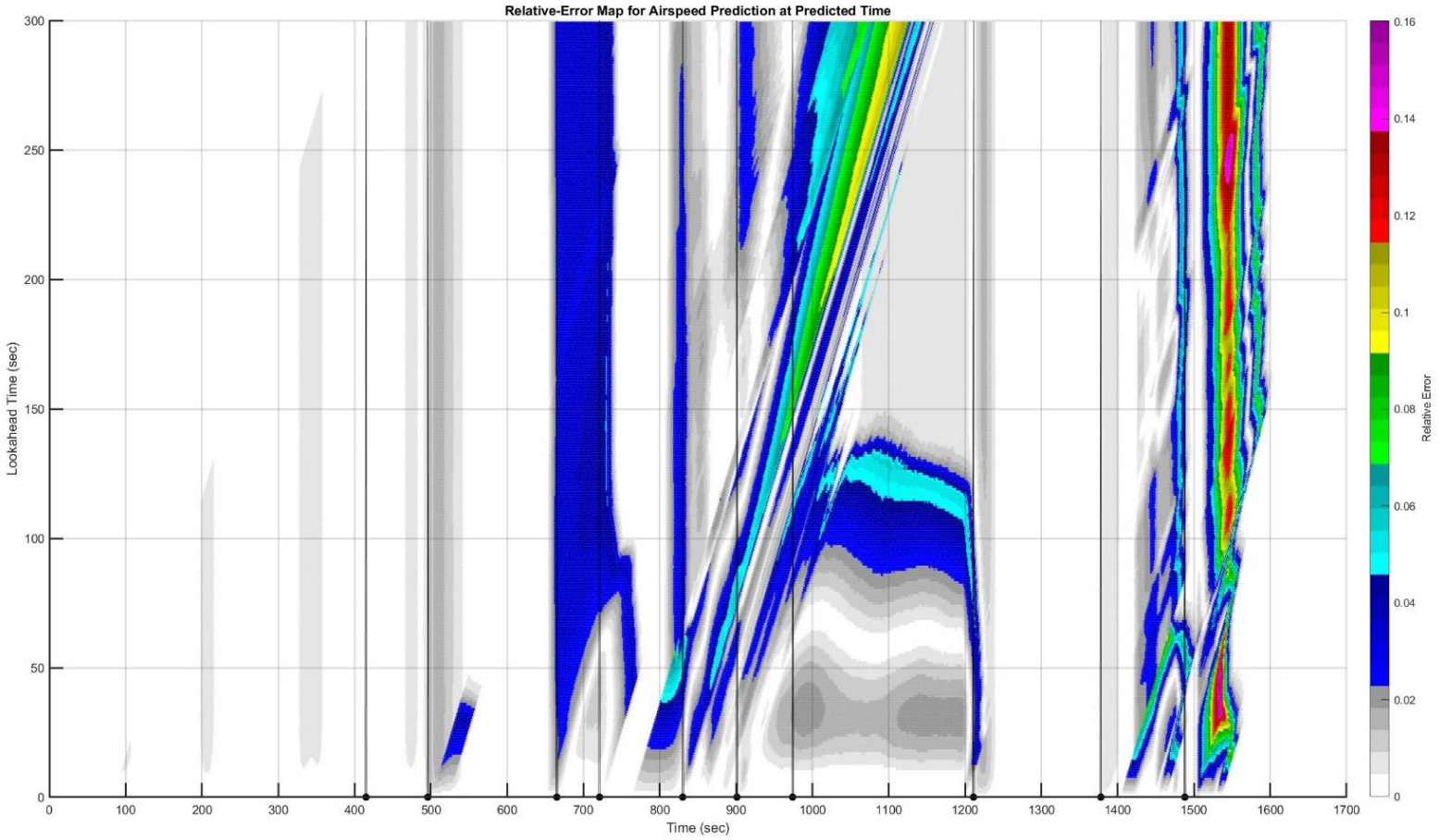

Figure C. 20: BLUZZ to Runway 36C: Heatmap of Airspeed Prediction Error (Time is $t + \tau$)

C.5. Trajectory: VANZE to 09

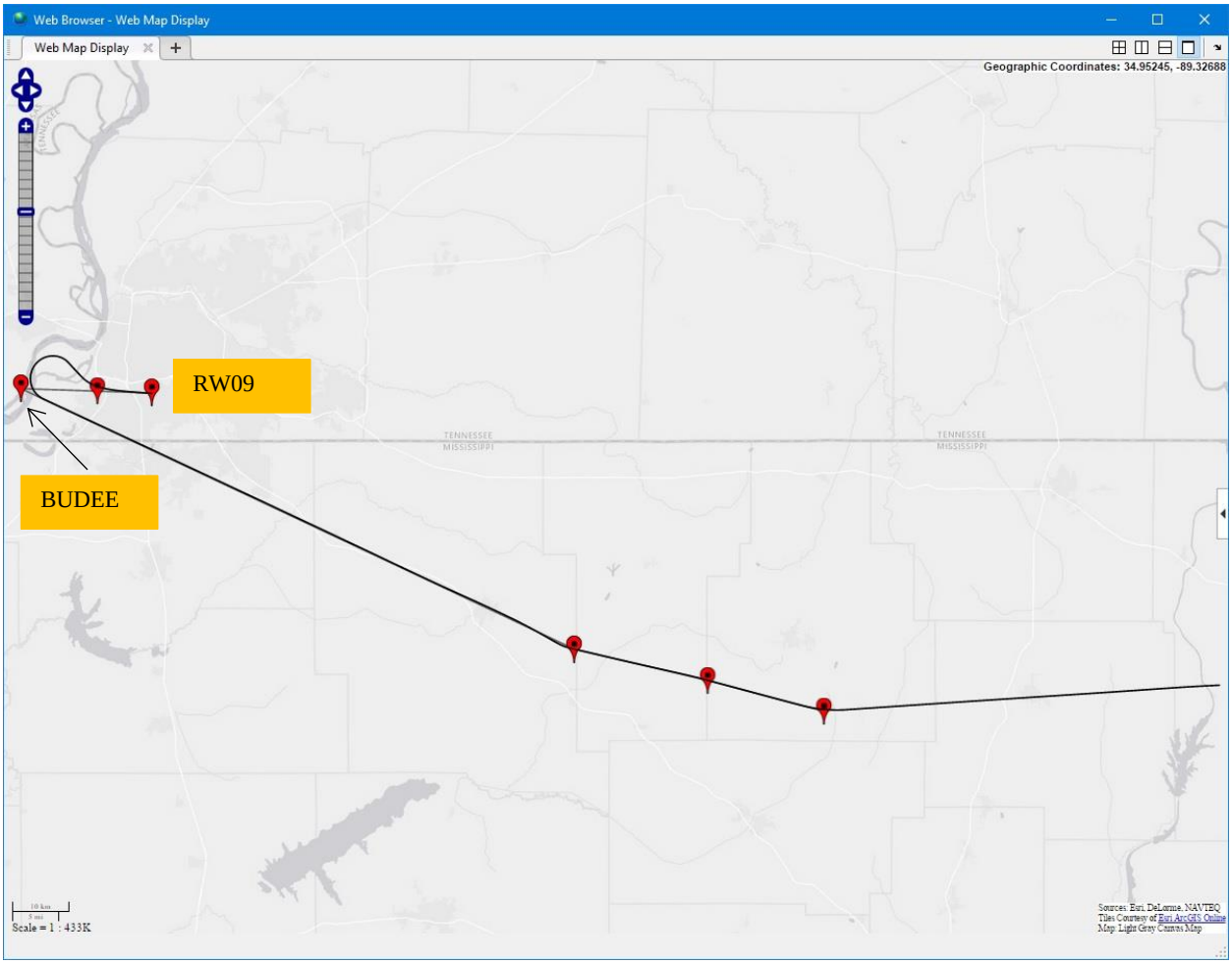

Figure C. 21: VANZE to Runway 09: Planned and Actual Trajectories (Red markers indicate waypoints)

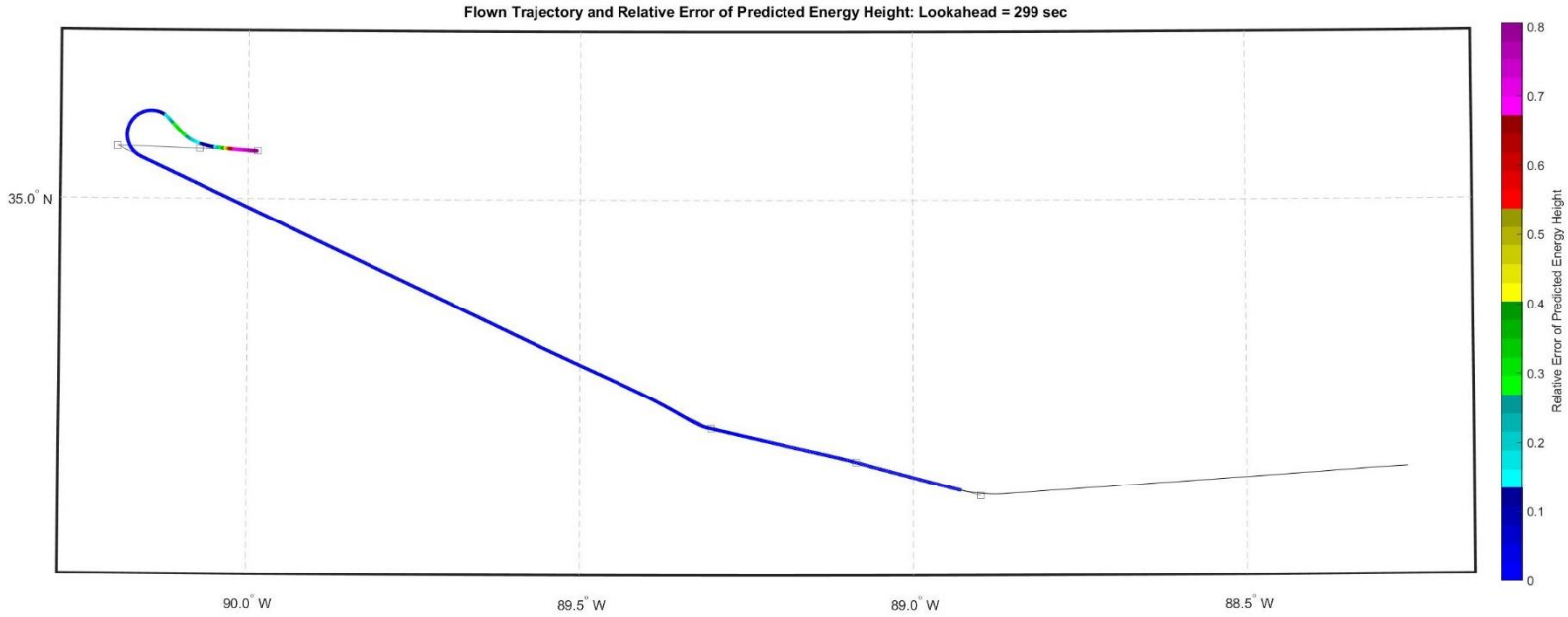

Figure C. 22: VANZE to Runway 09: Lateral Path Color-Coded for Energy Prediction Error for Look-Ahead of 299 Seconds

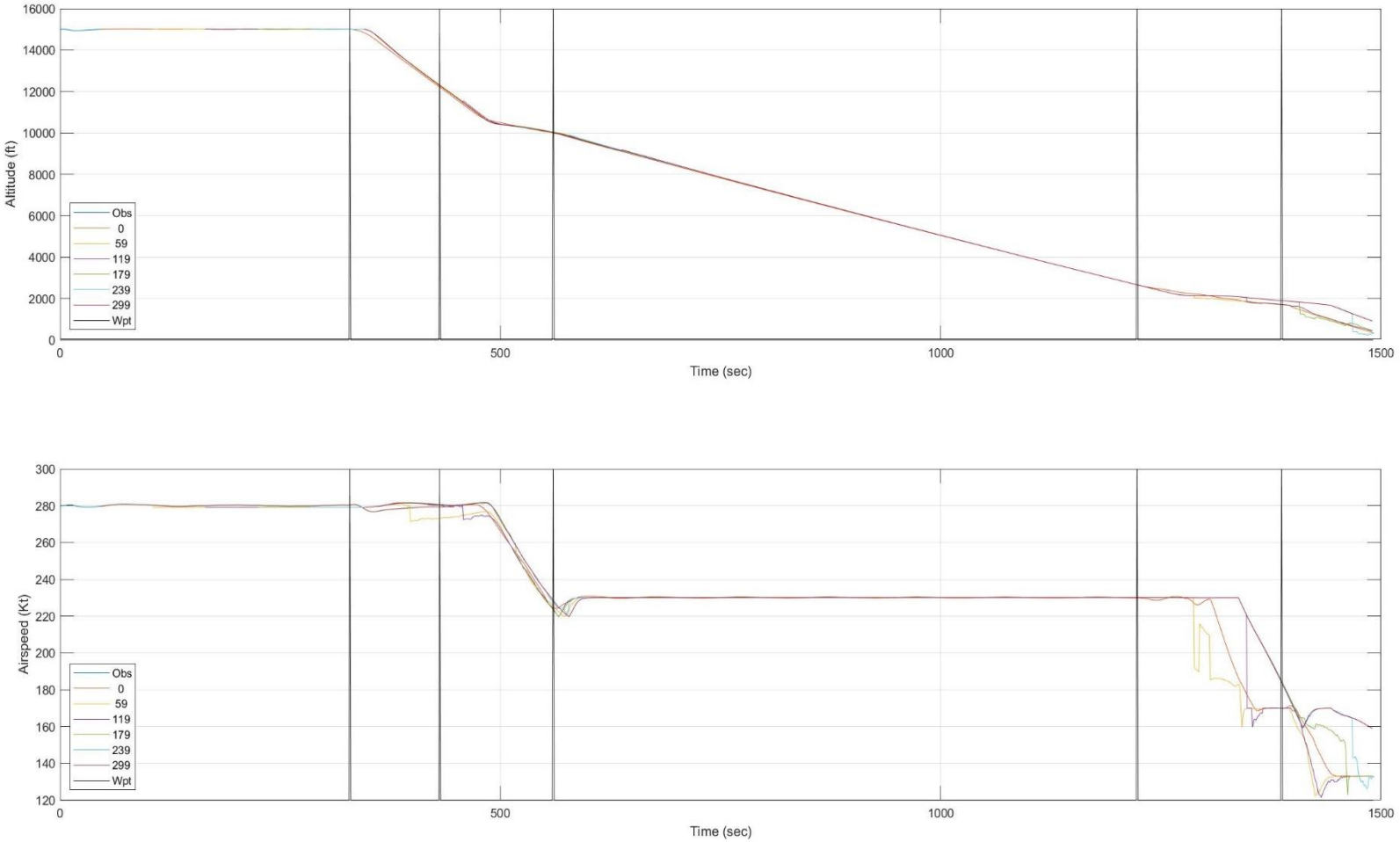

Figure C. 23: VANZE to Runway 09: Time History of Predicted Altitude and Airspeed

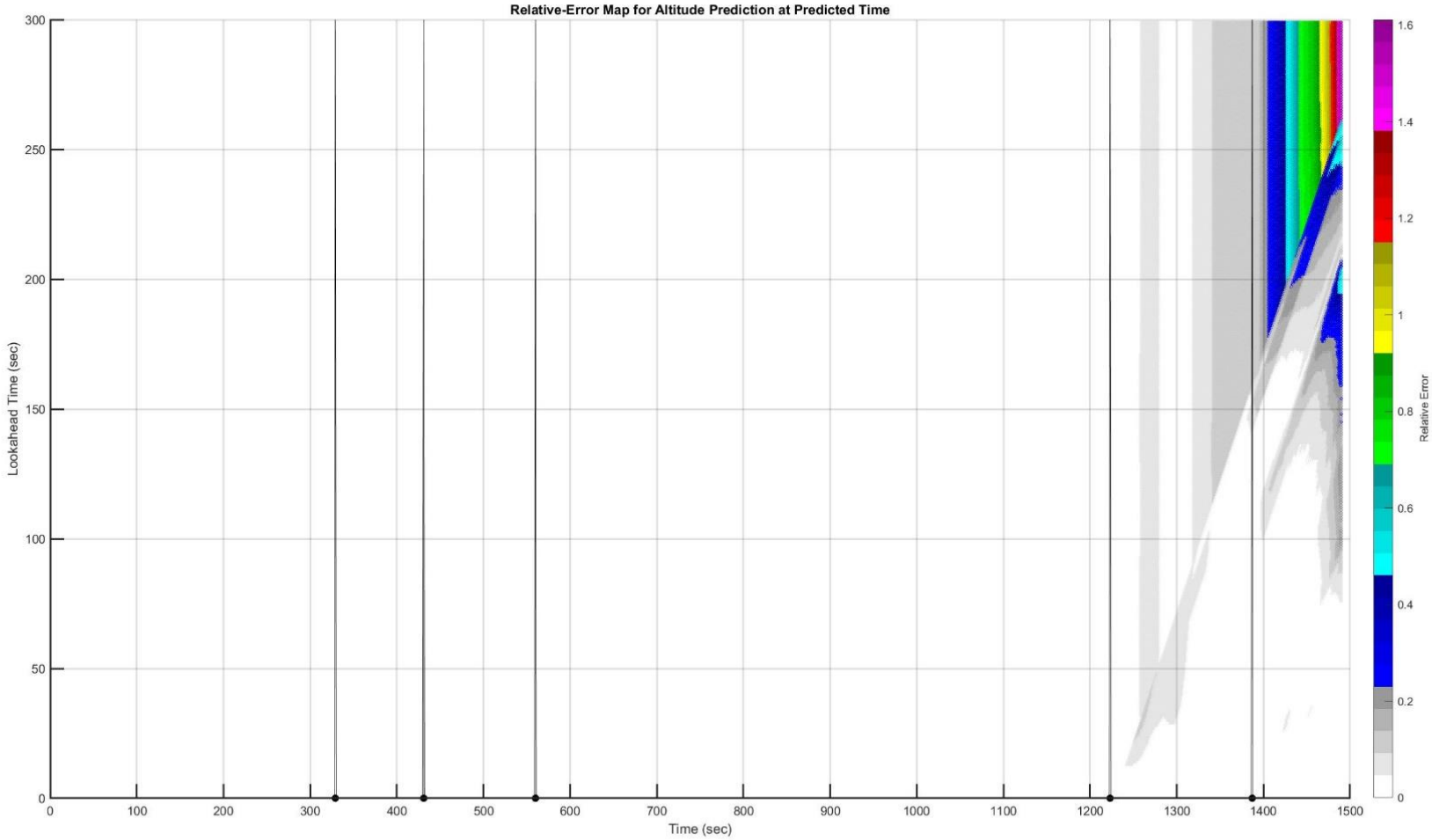

Figure C. 24: VANZE to Runway 09: Heatmap of Altitude Prediction Error (Time is $t + \tau$)

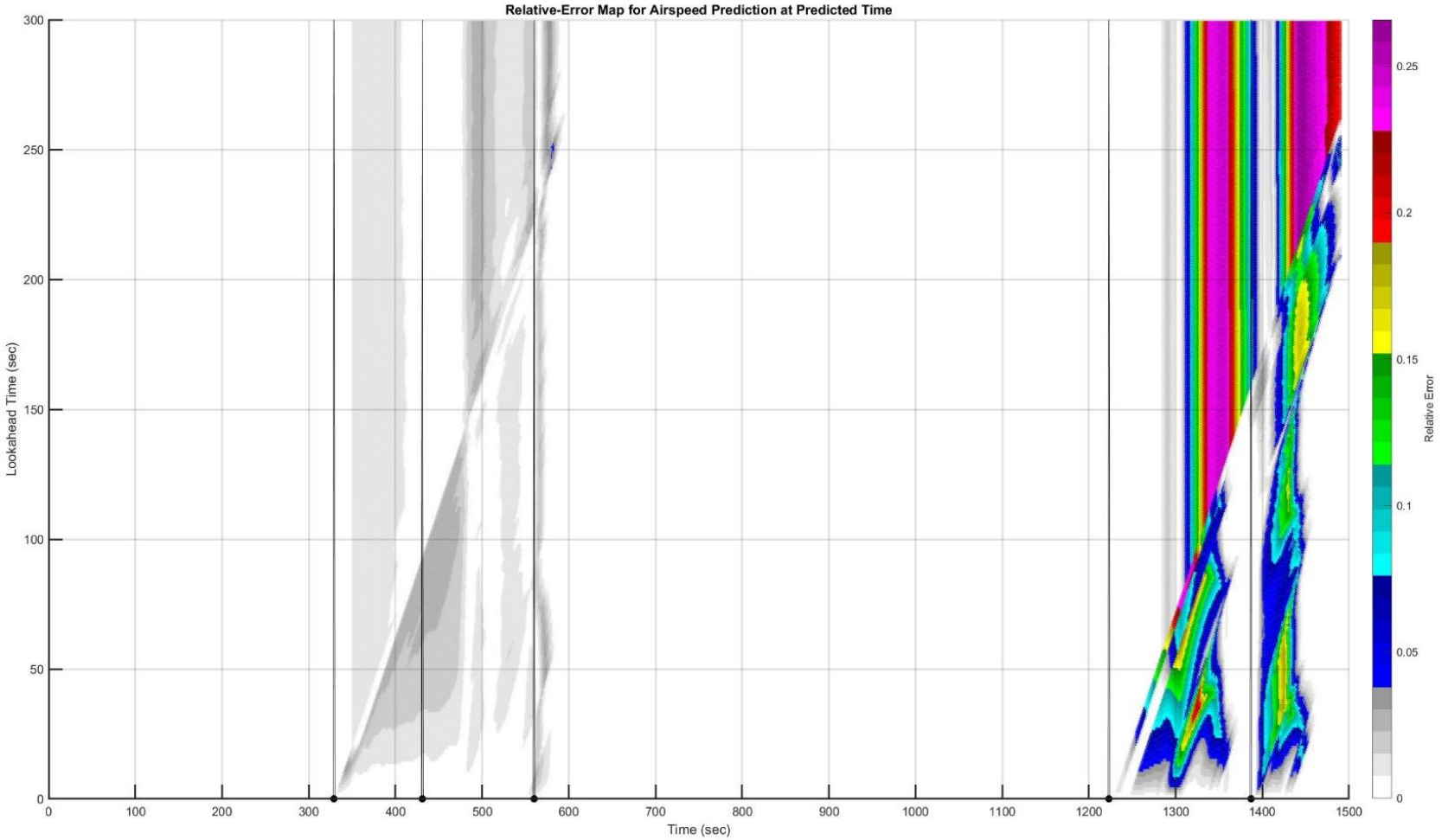

Figure C. 25: VANZE to Runway 09: Heatmap of Airspeed Prediction Error (Time is $t + \tau$)

C.6. Trajectory: VANZE to 18C

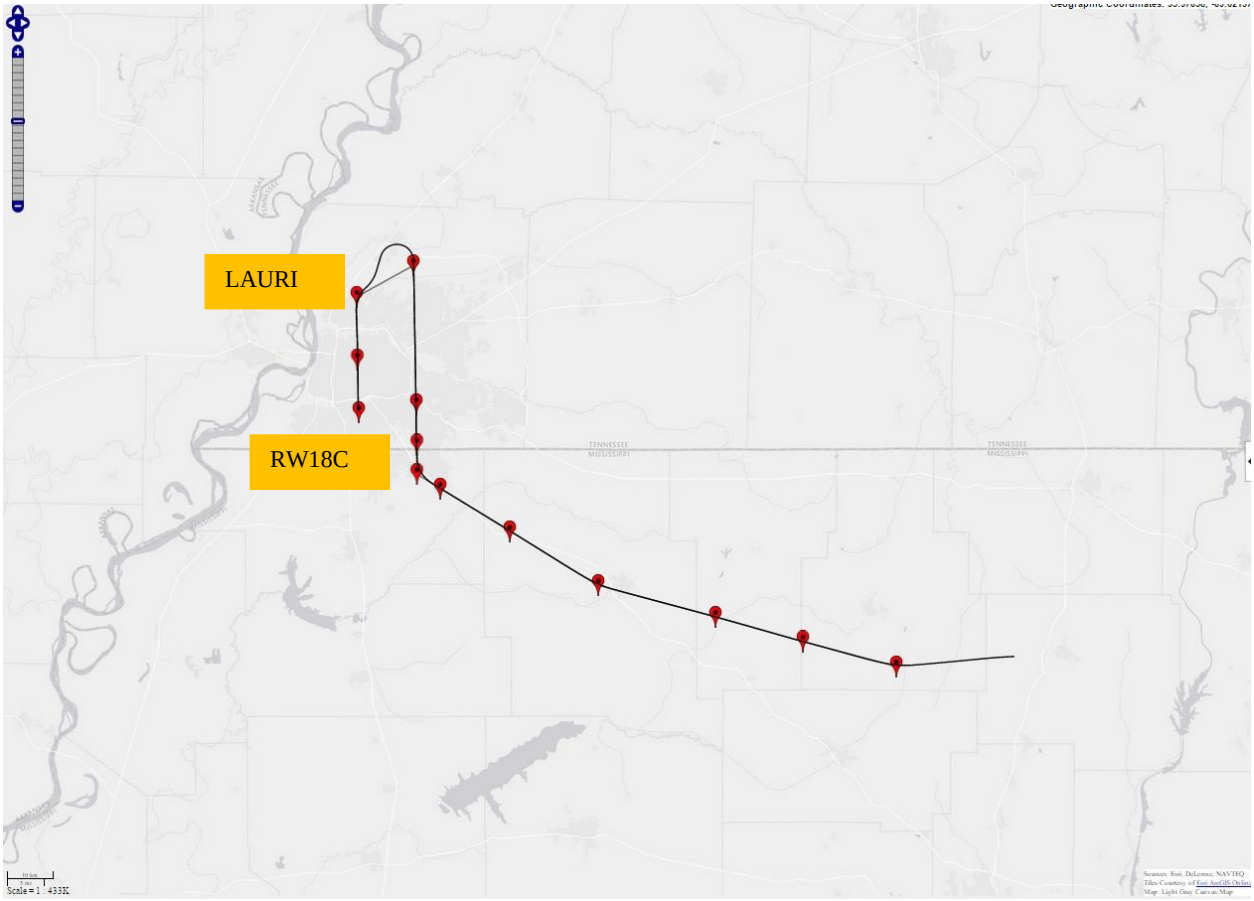

Figure C. 26: VANZE to Runway 18C: Planned and Actual Trajectories (Red markers indicate waypoints)

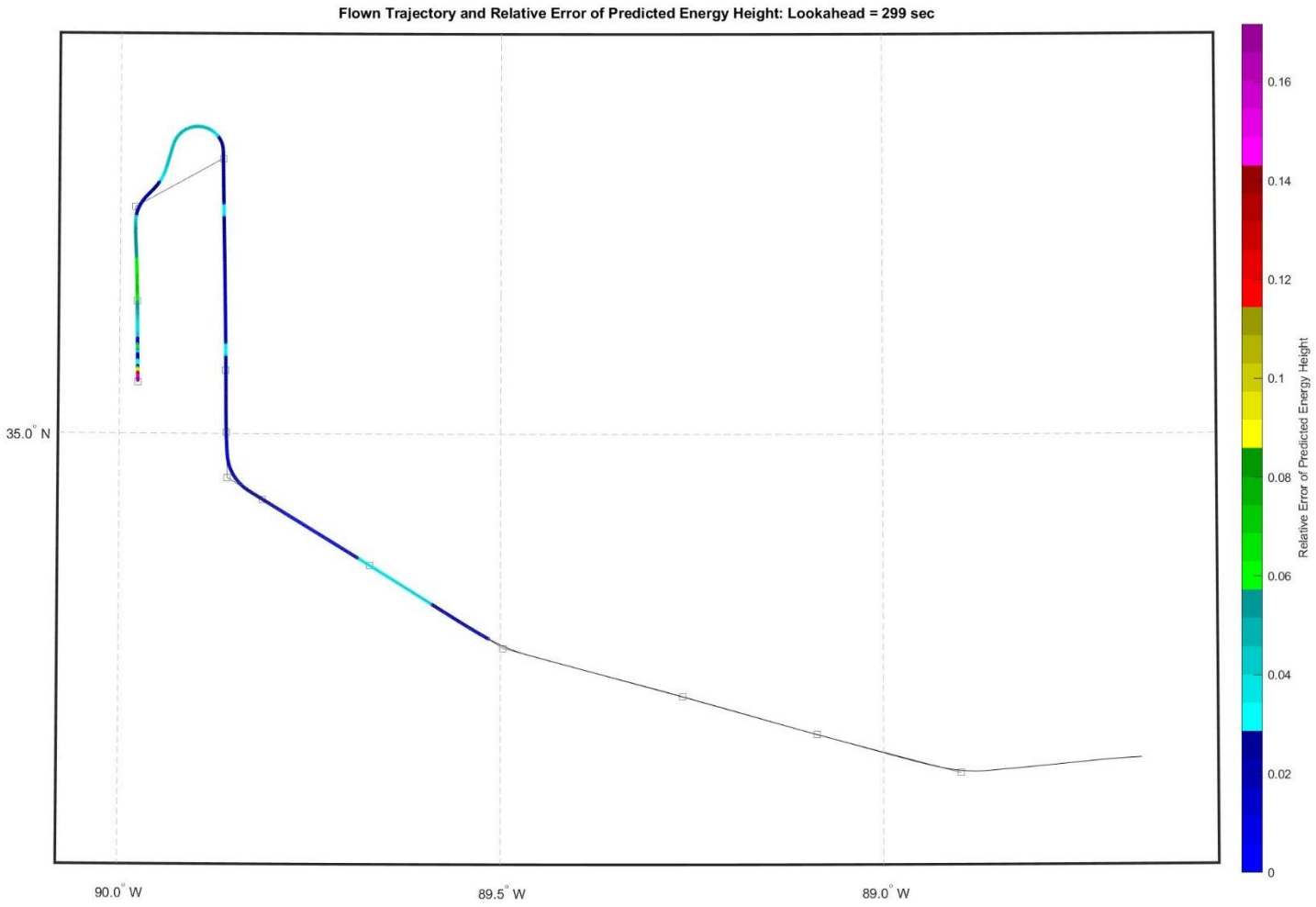

Figure C. 27: VANZE to Runway 18C: Lateral Path Color-Coded for Energy Prediction Error for Look-Ahead of 299 Seconds

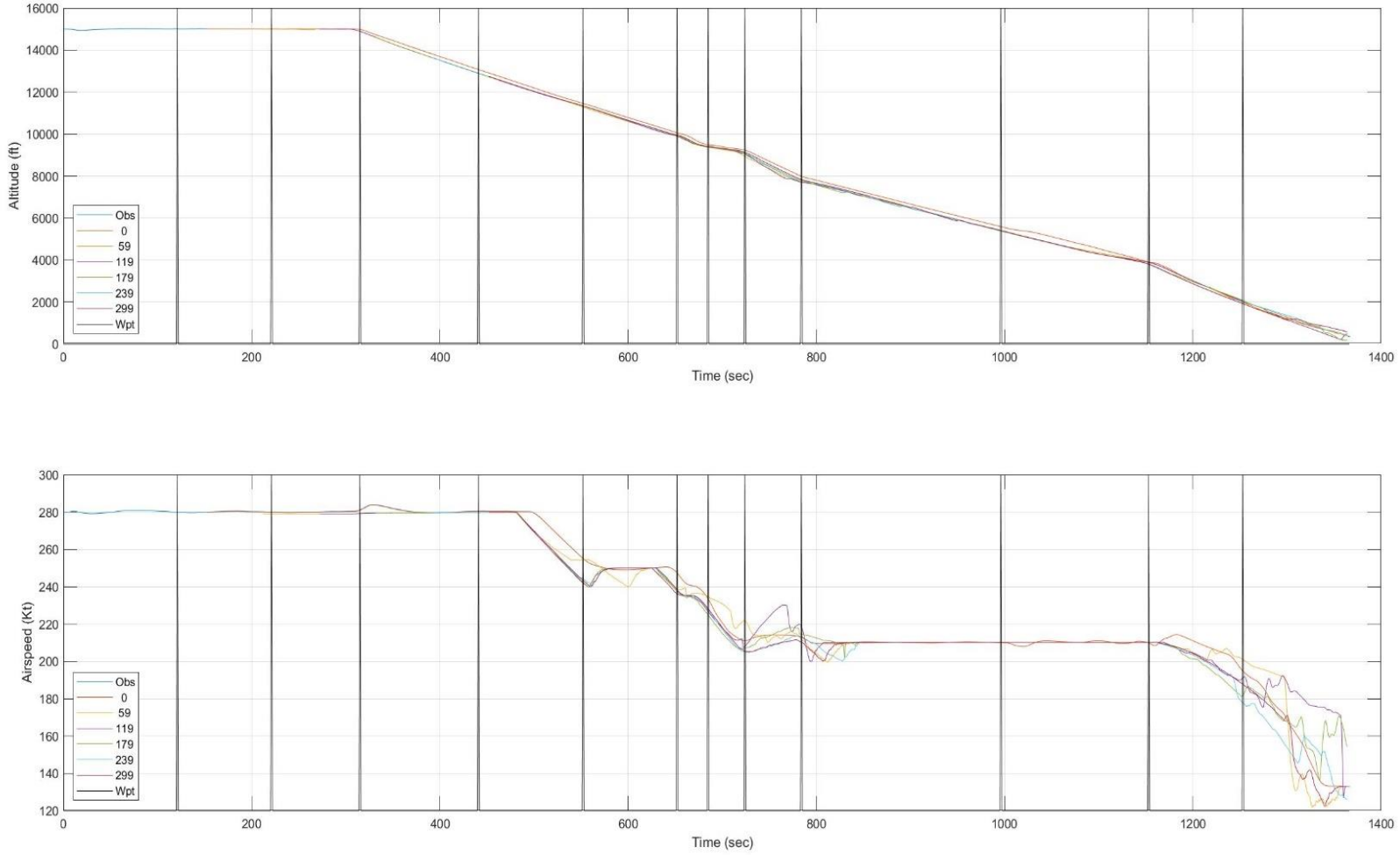

Figure C. 28: VANZE to Runway 18C: Time History of Predicted Altitude and Airspeed

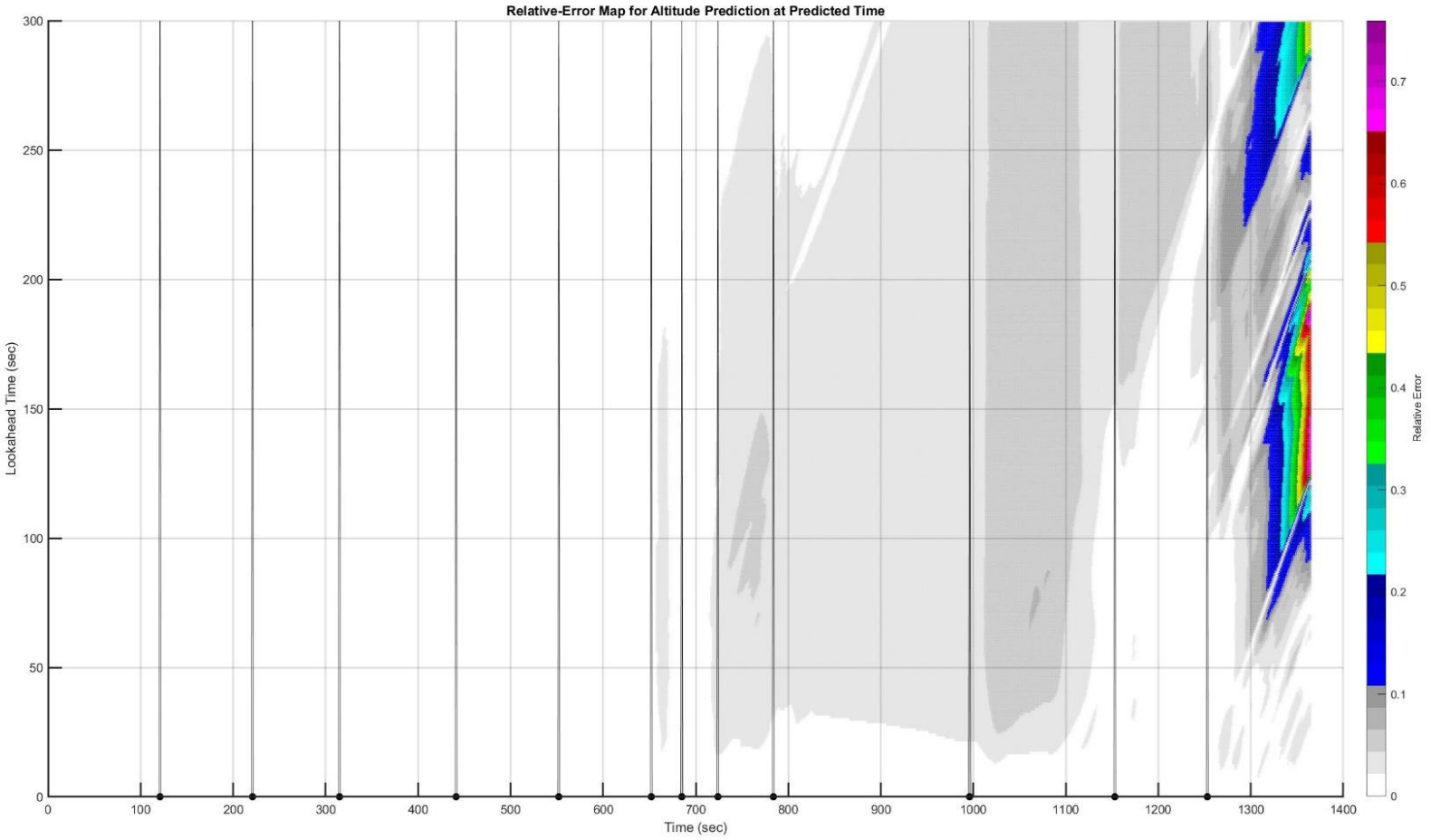

Figure C. 29: VANZE to Runway 18C: Heatmap of Altitude Prediction Error (Time is $t + \tau$)

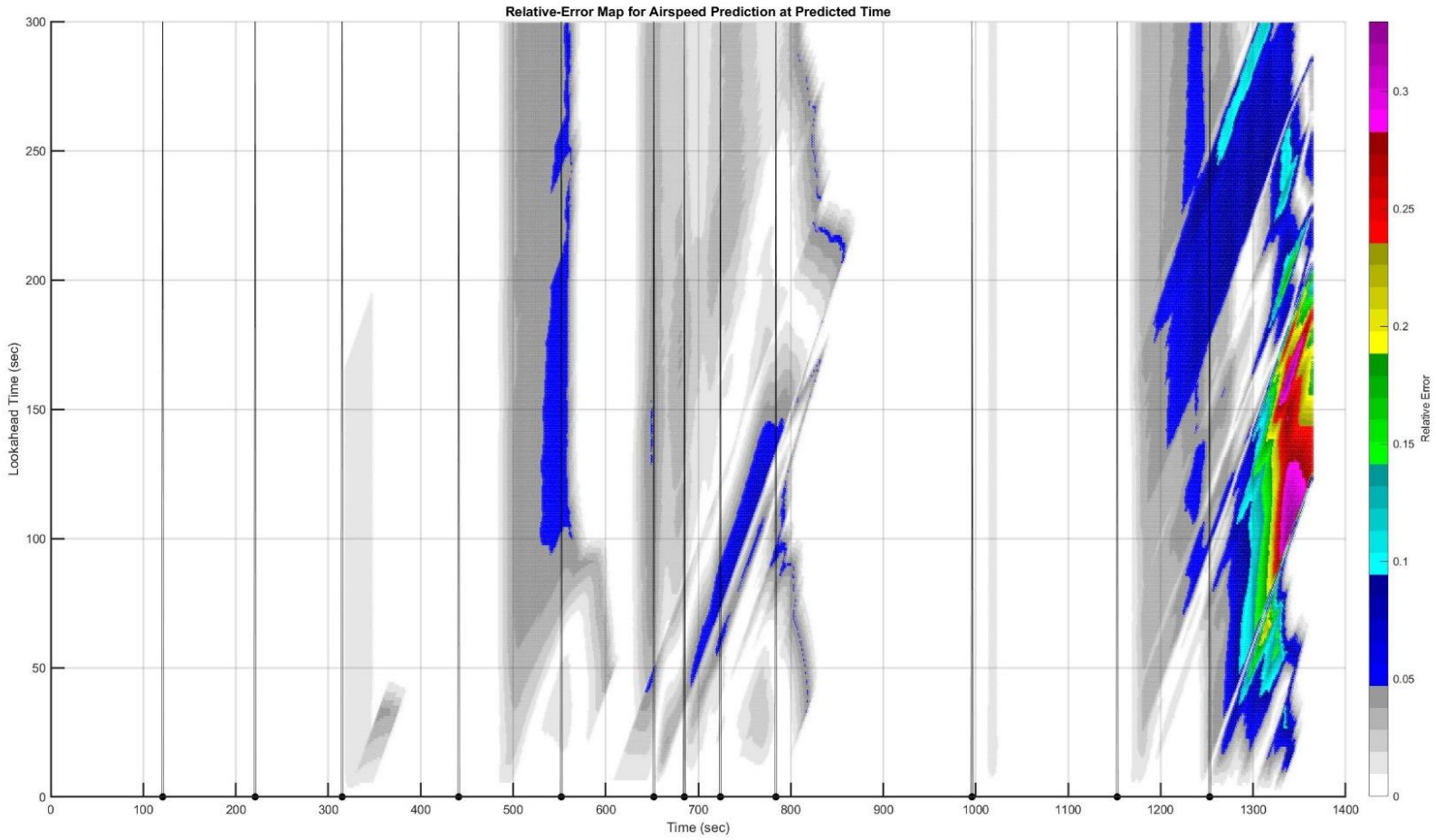

Figure C. 30: VANZE to Runway 18C: Heatmap of Airspeed Prediction Error (Time is $t + \tau$)

C.7. Trajectory: VANZE to 27

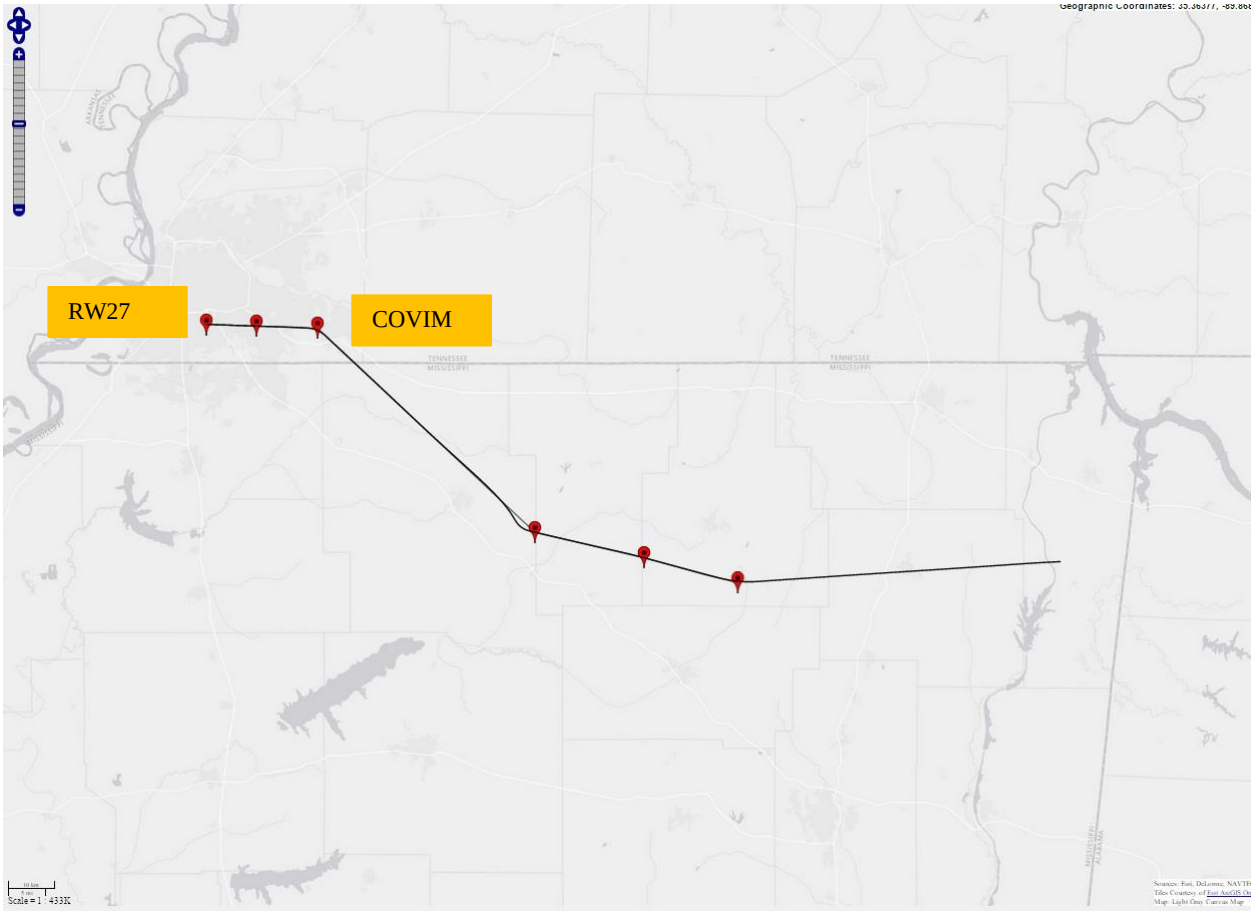

Figure C. 31: VANZE to Runway 27: Planned and Actual Trajectories (Red markers indicate waypoints)

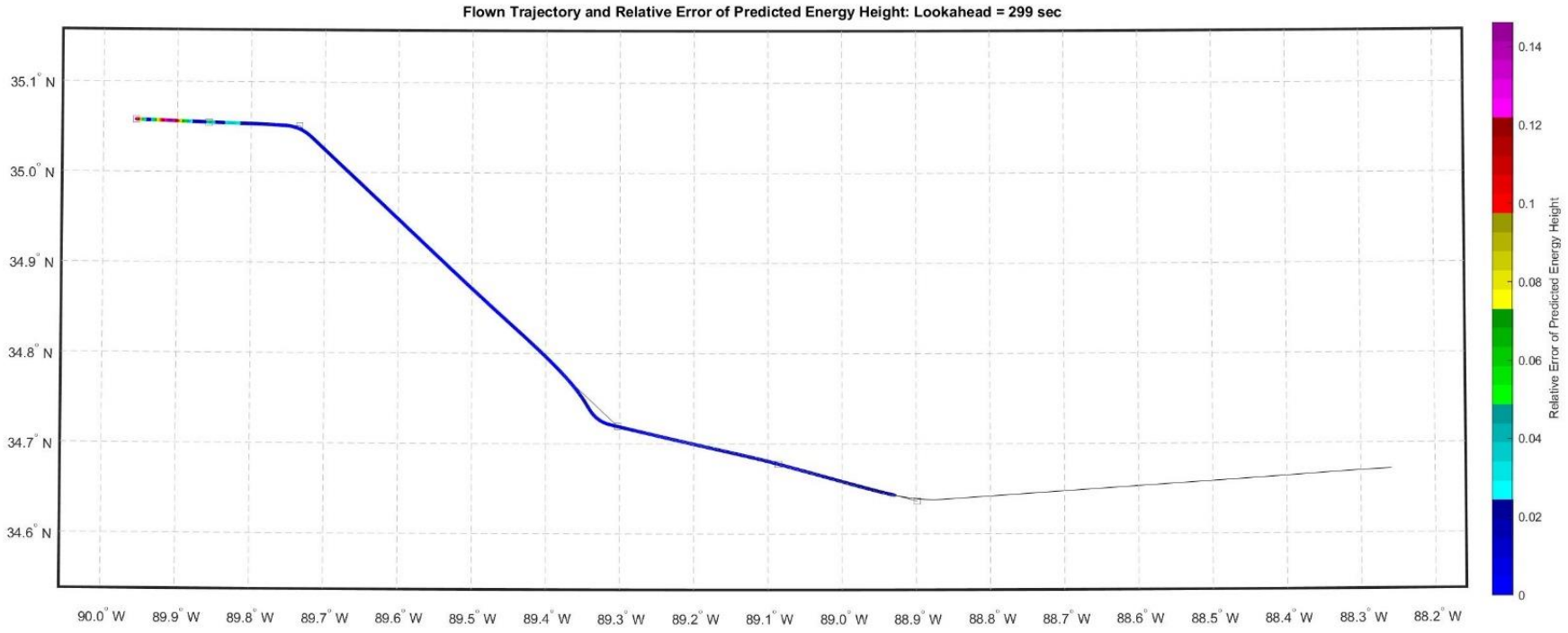

Figure C. 32: VANZE to Runway 27: Lateral Path Color-Coded for Energy Prediction Error for Look-Ahead of 299 Seconds

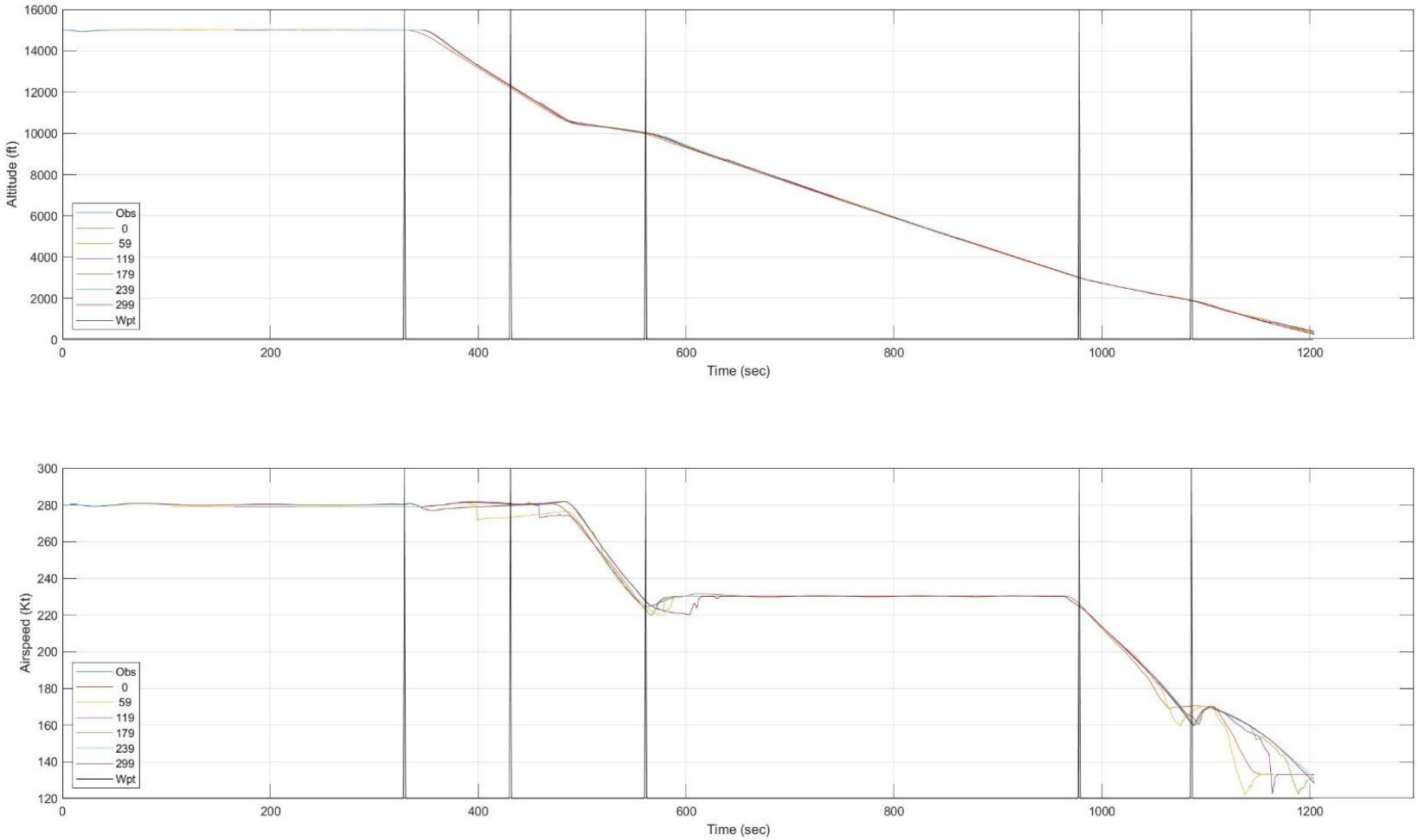

Figure C. 33: VANZE to Runway 27: Time History of Predicted Altitude and Airspeed

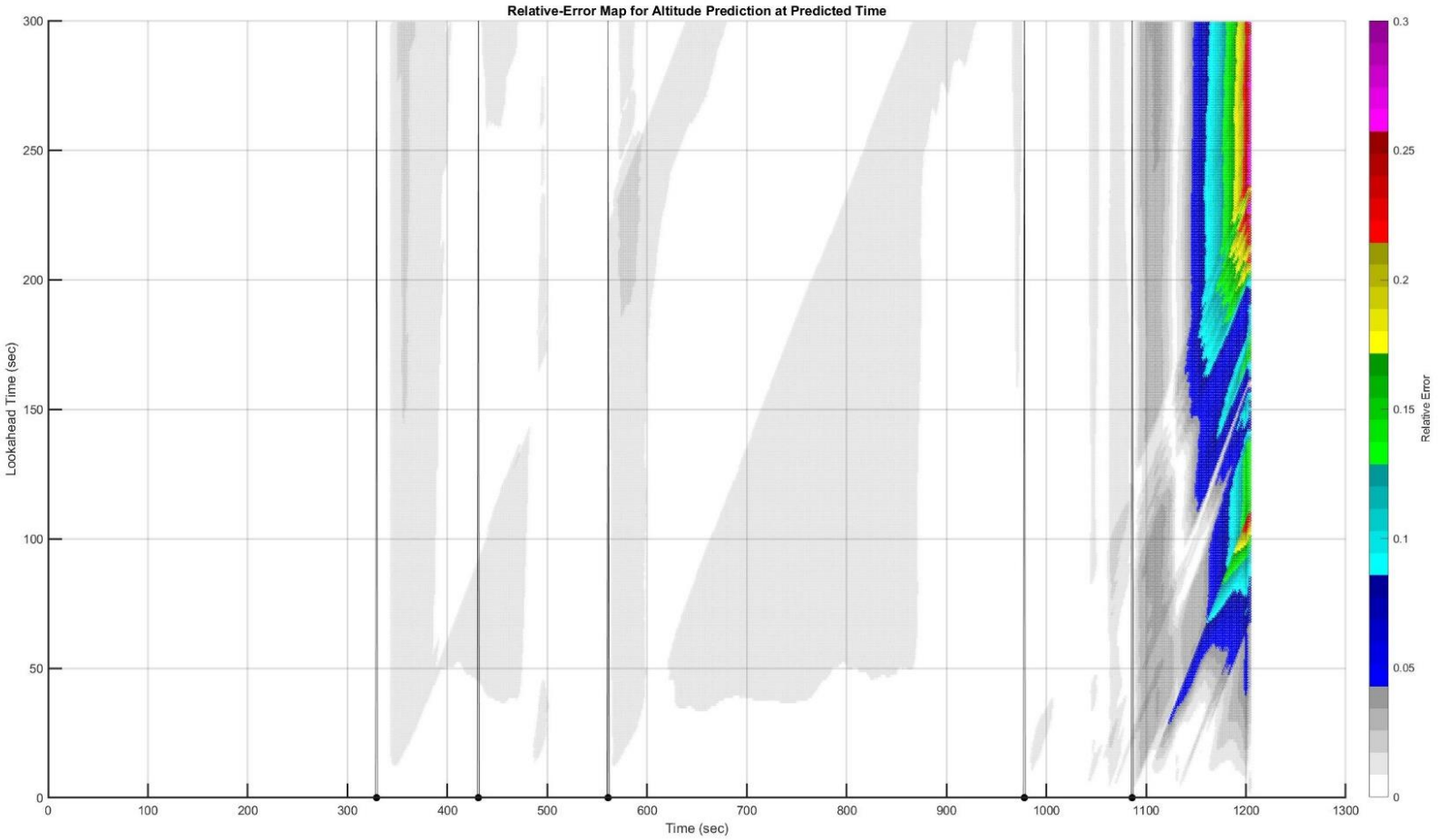

Figure C. 34: VANZE to Runway 27: Heatmap of Altitude Prediction Error (Time is $t + \tau$)

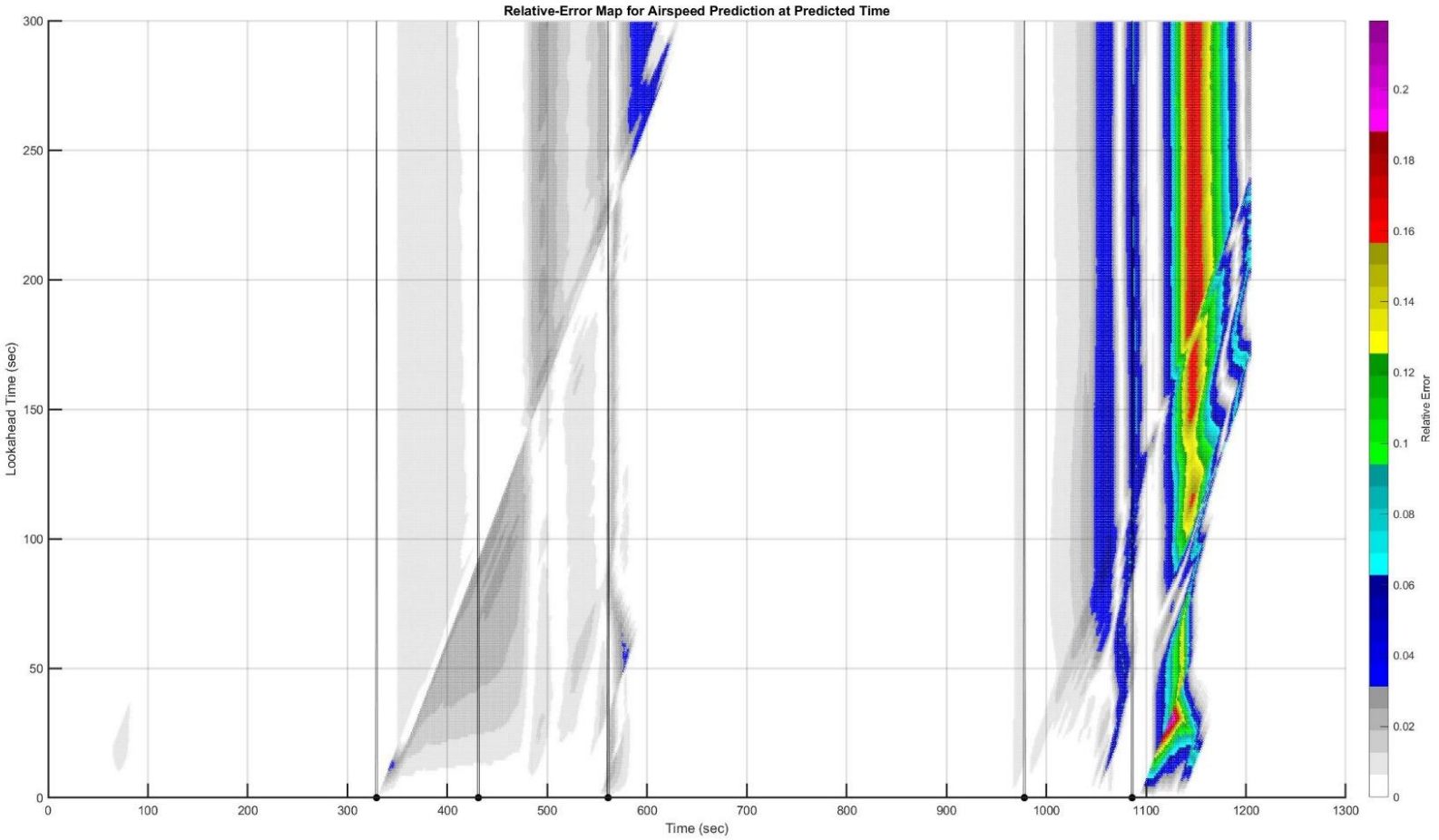

Figure C. 35: VANZE to Runway 27: Heatmap of Airspeed Prediction Error (Time is $t + \tau$)

C.8. Trajectory: VANZE to 36C

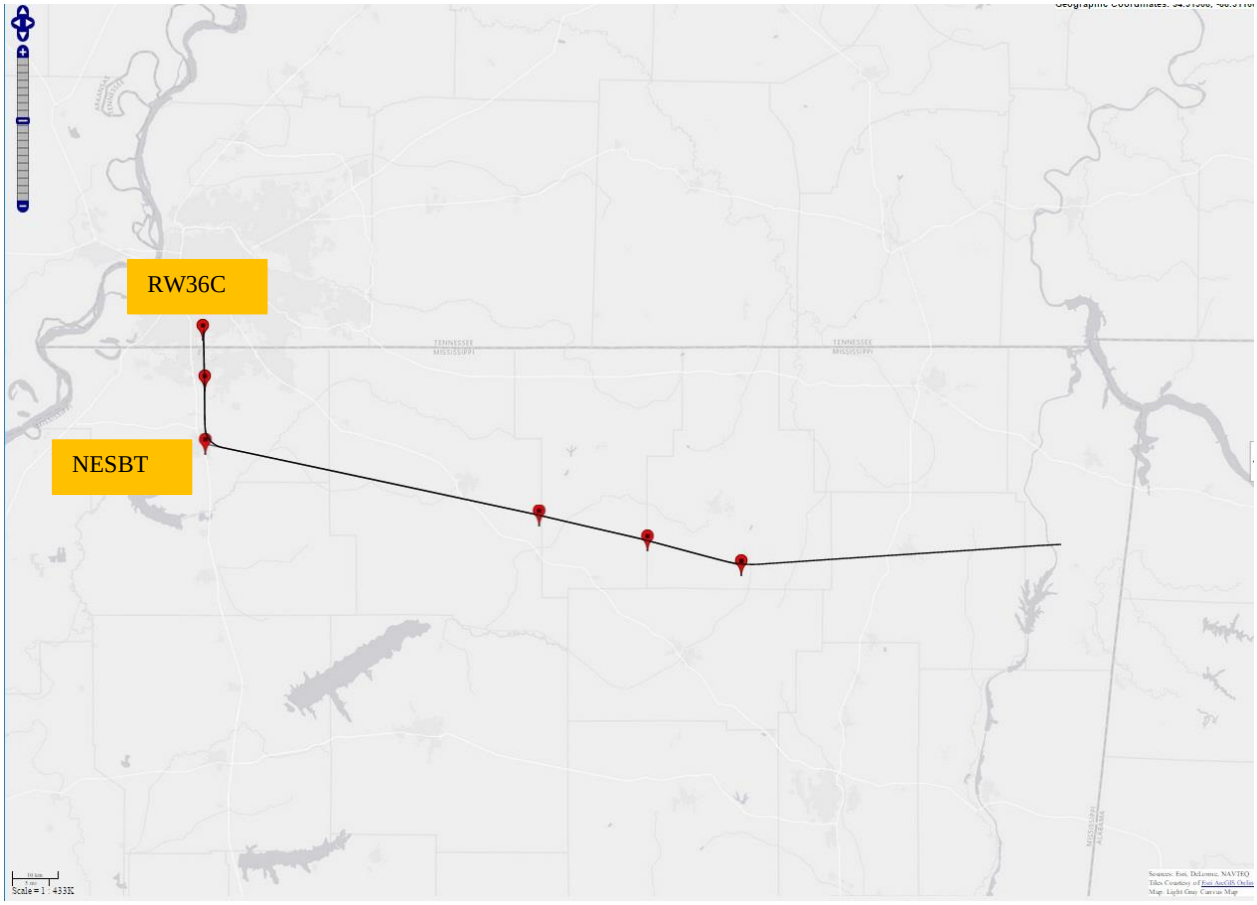

Figure C. 36: VANZE to Runway 36C: Planned and Actual Trajectories (Red markers indicate waypoints)

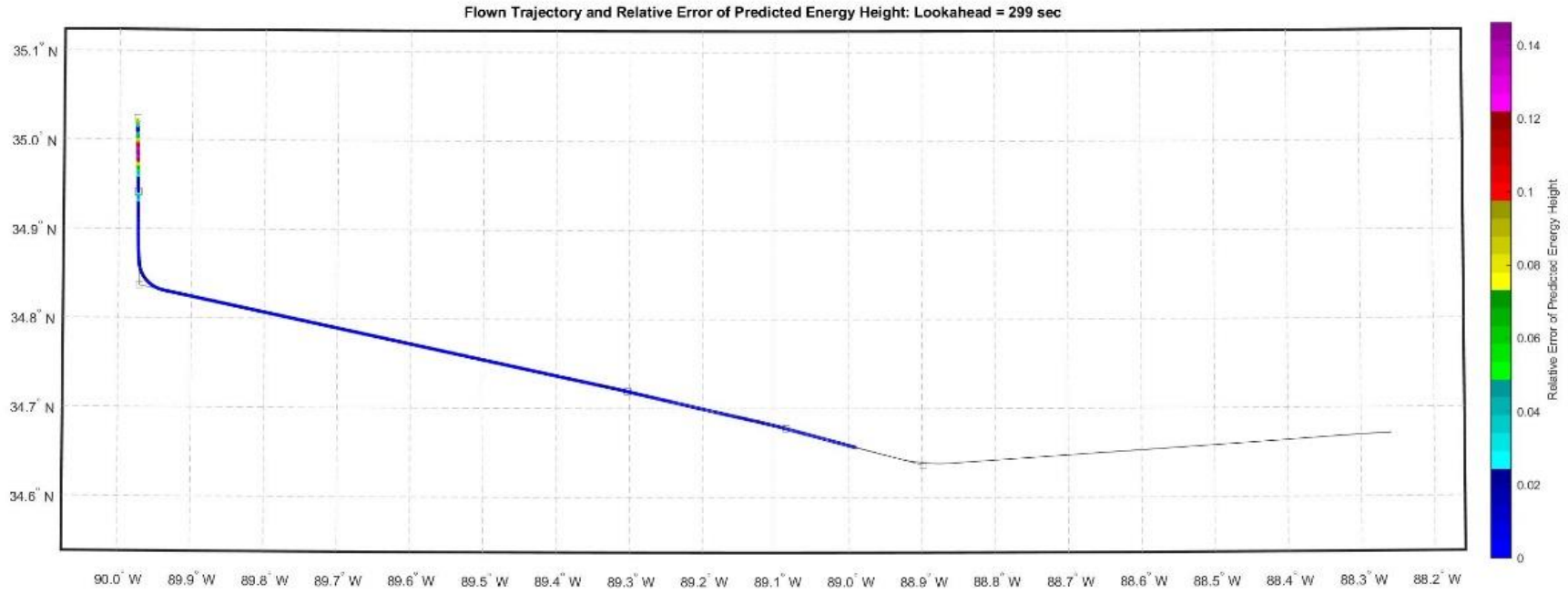

Figure C. 37: VANZE to Runway 36C: Lateral Path Color-Coded for Energy Prediction Error for Look-Ahead of 299 Seconds

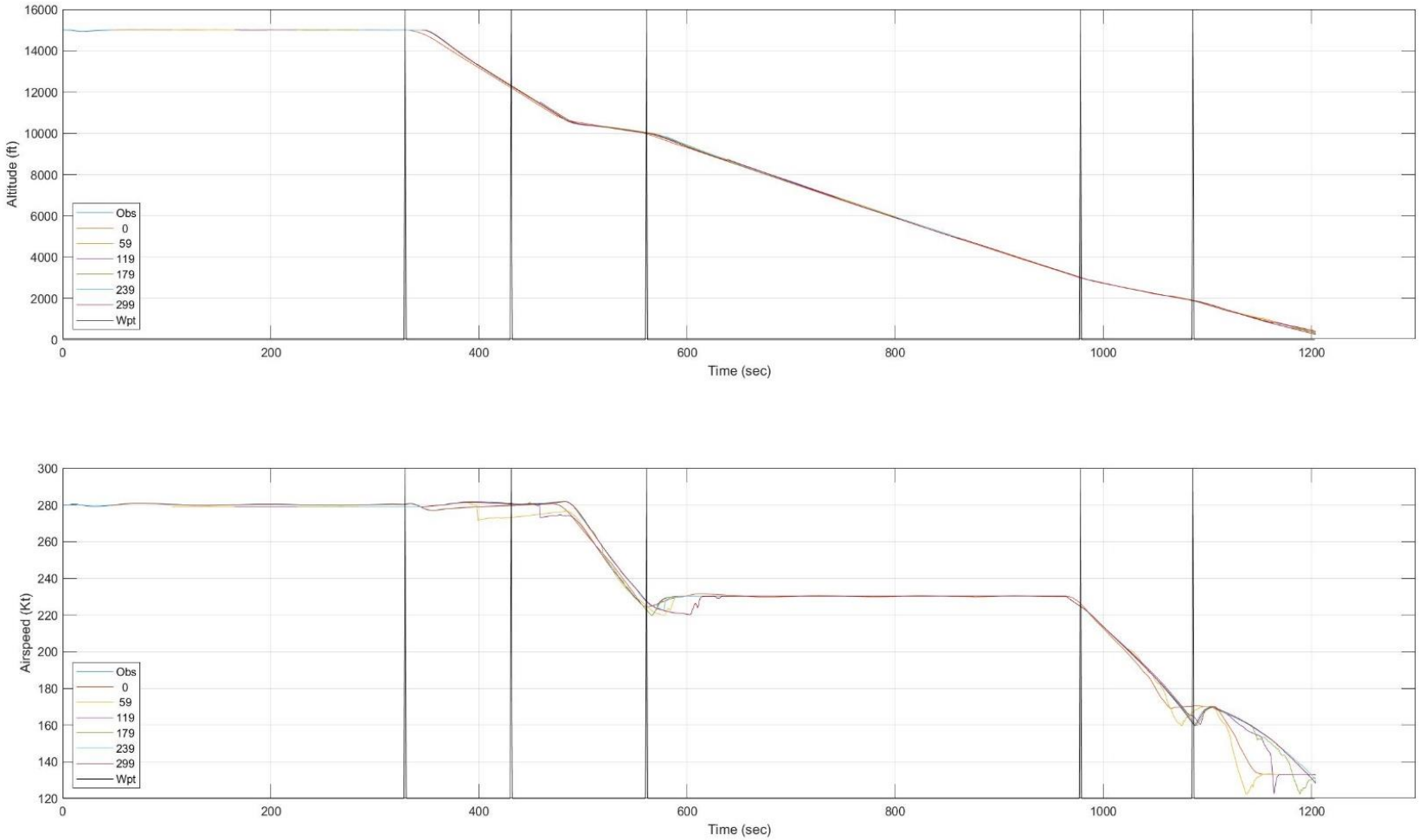

Figure C. 38: VANZE to Runway 36C: Time History of Predicted Altitude and Airspeed

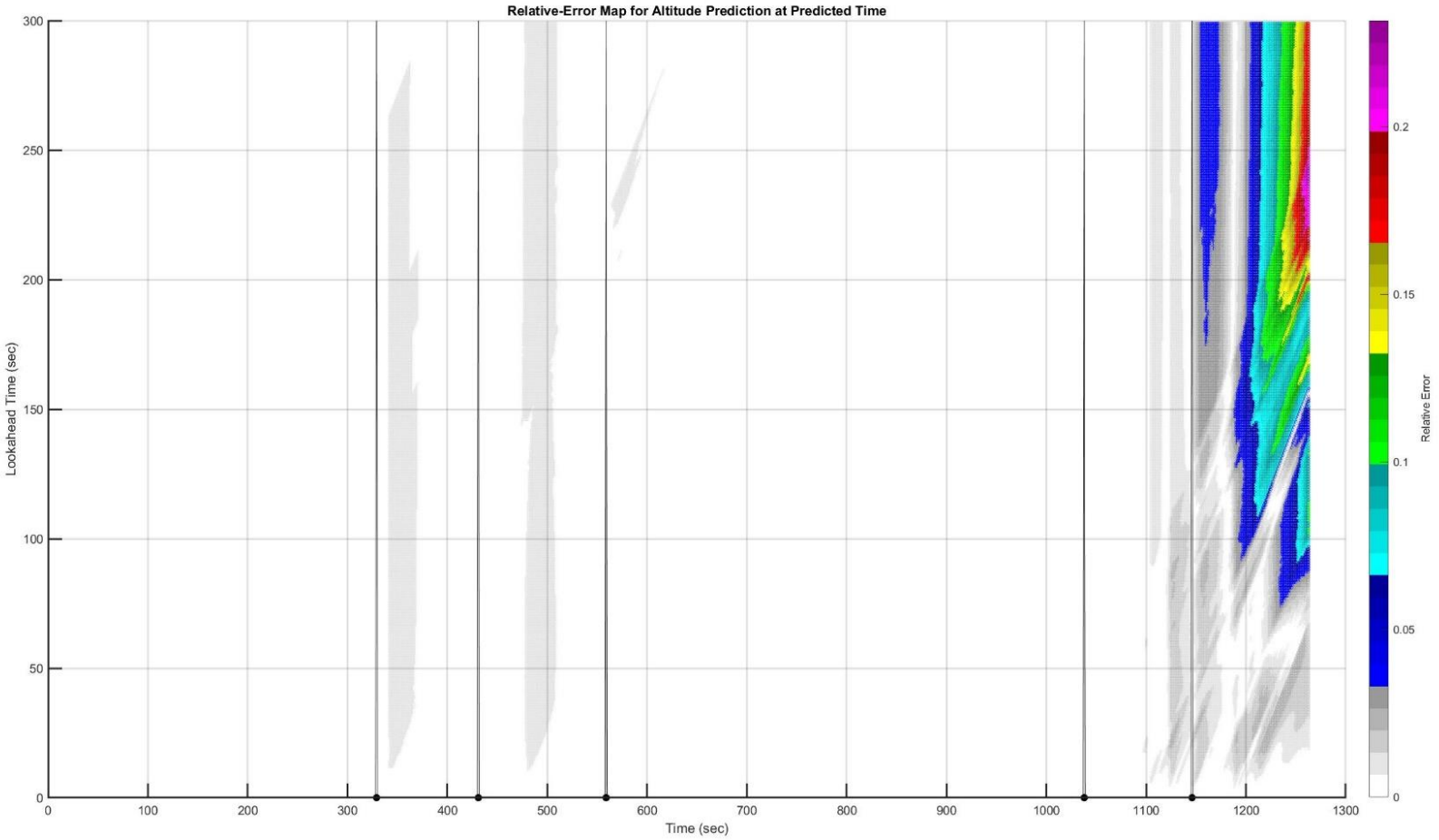

Figure C. 39: VANZE to Runway 36C: Heatmap of Altitude Prediction Error (Time is $t + \tau$)

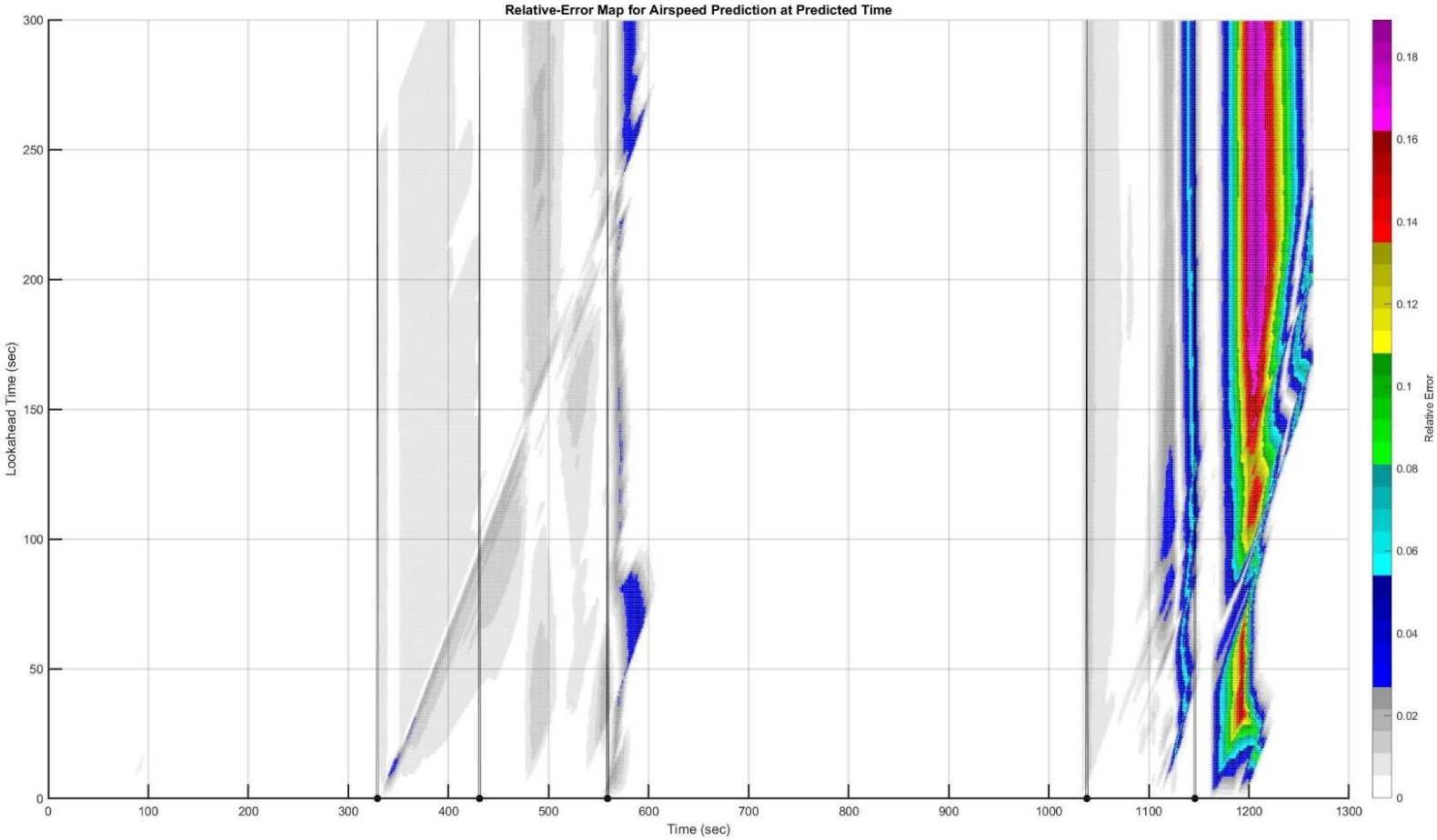

Figure C. 40: VANZE to Runway 36C: Heatmap of Airspeed Prediction Error (Time is $t + \tau$)

C.9. Trajectory: HOBRK to 09

Figure C. 41: HOBRK to Runway 09: Planned and Actual Trajectories (Red markers indicate waypoints)

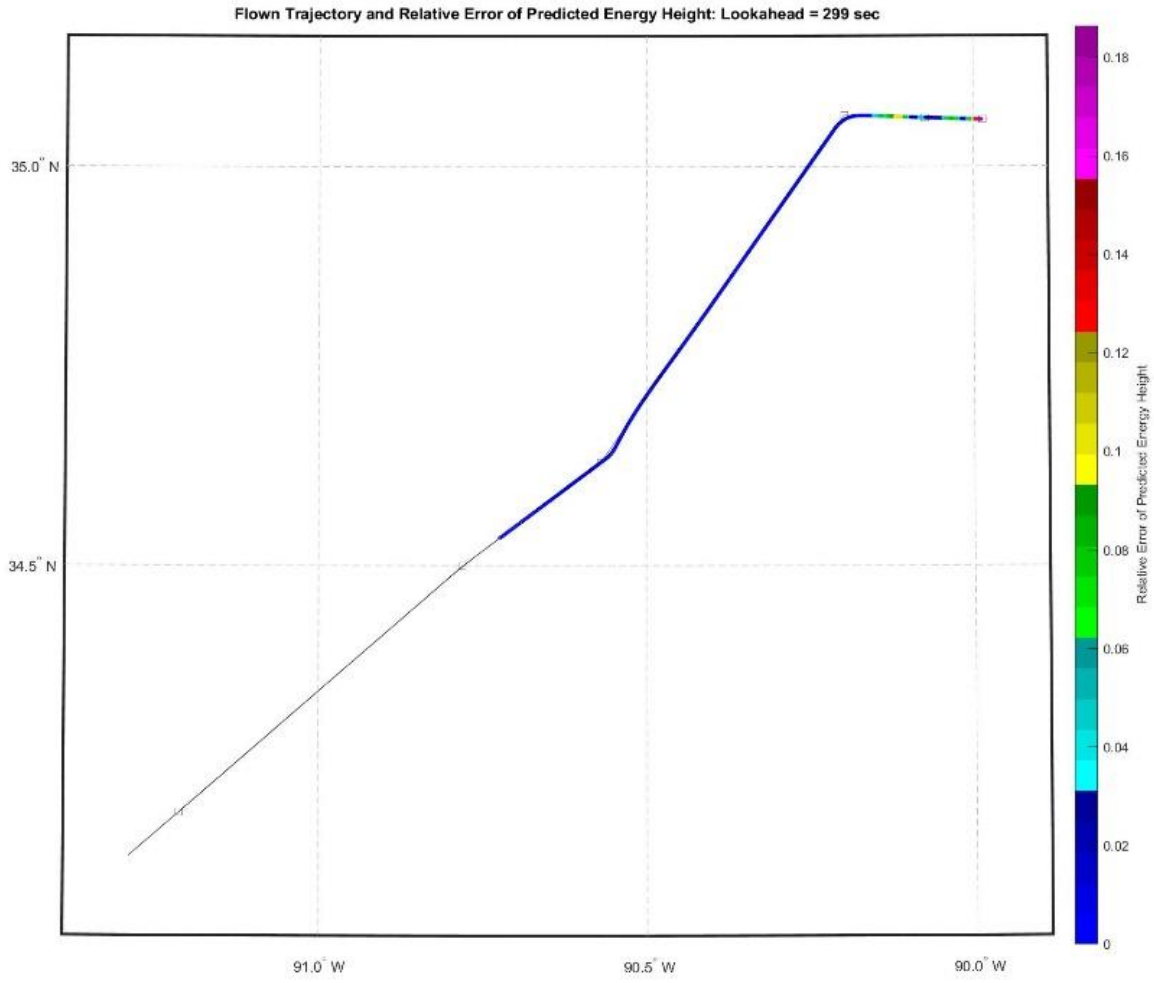

Figure C. 42: HOBRK to Runway 09: Lateral Path Color-Coded for Energy Prediction Error for Look-Ahead of 299 Seconds

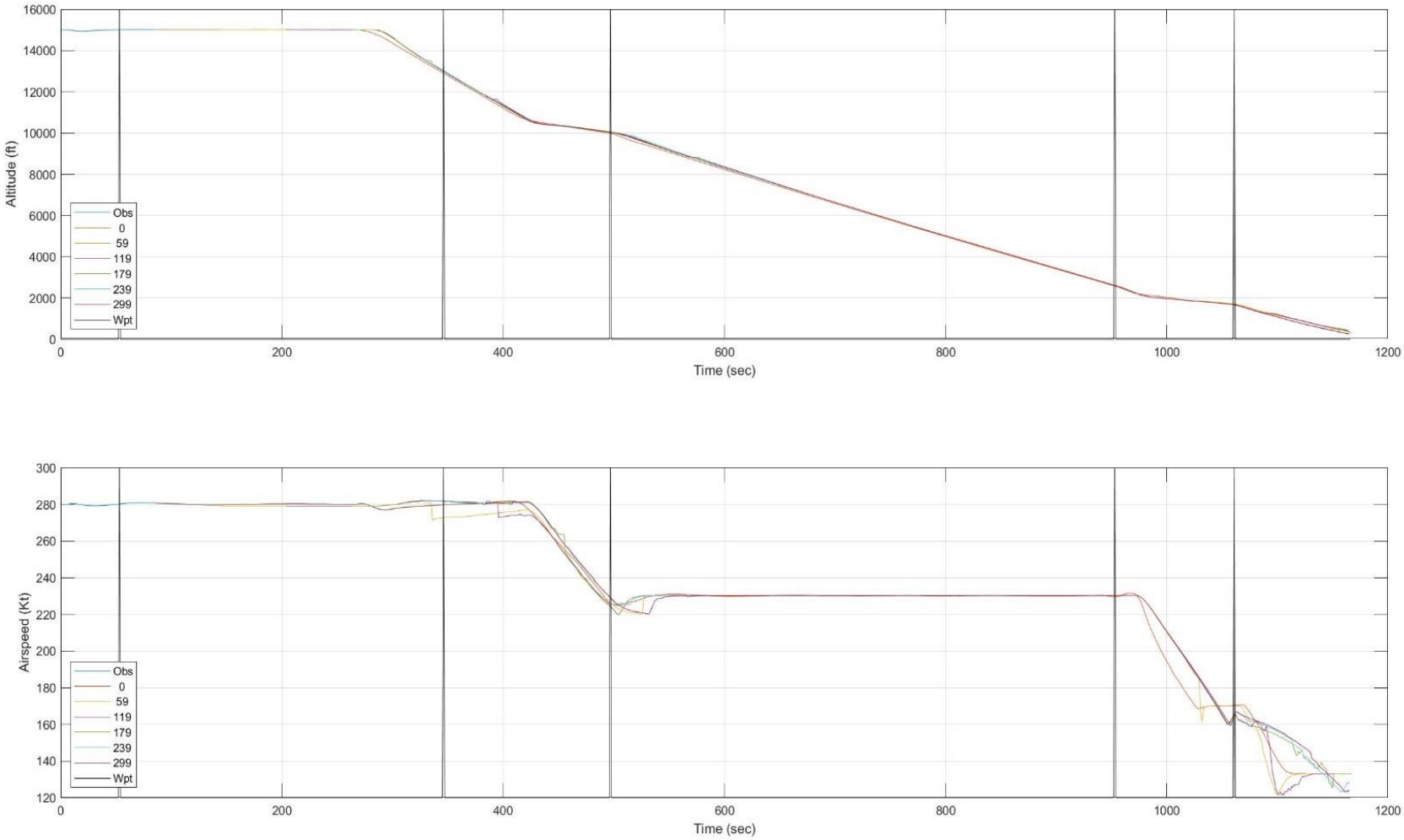

Figure C. 43: HOBRK to Runway 09: Time History of Predicted Altitude and Airspeed

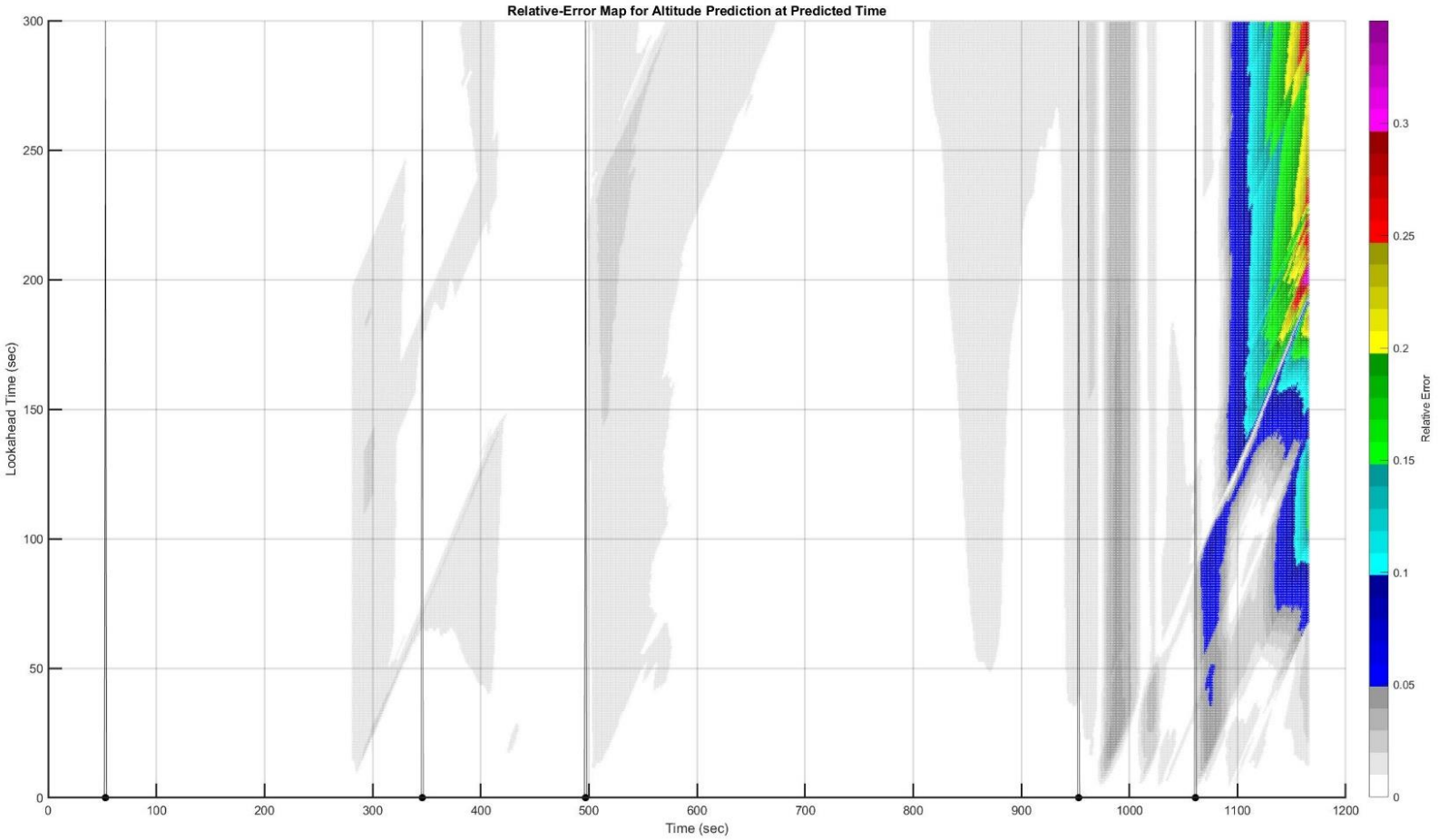

Figure C. 44: HOBRK to Runway 09: Heatmap of Altitude Prediction Error (Time is $t + \tau$)

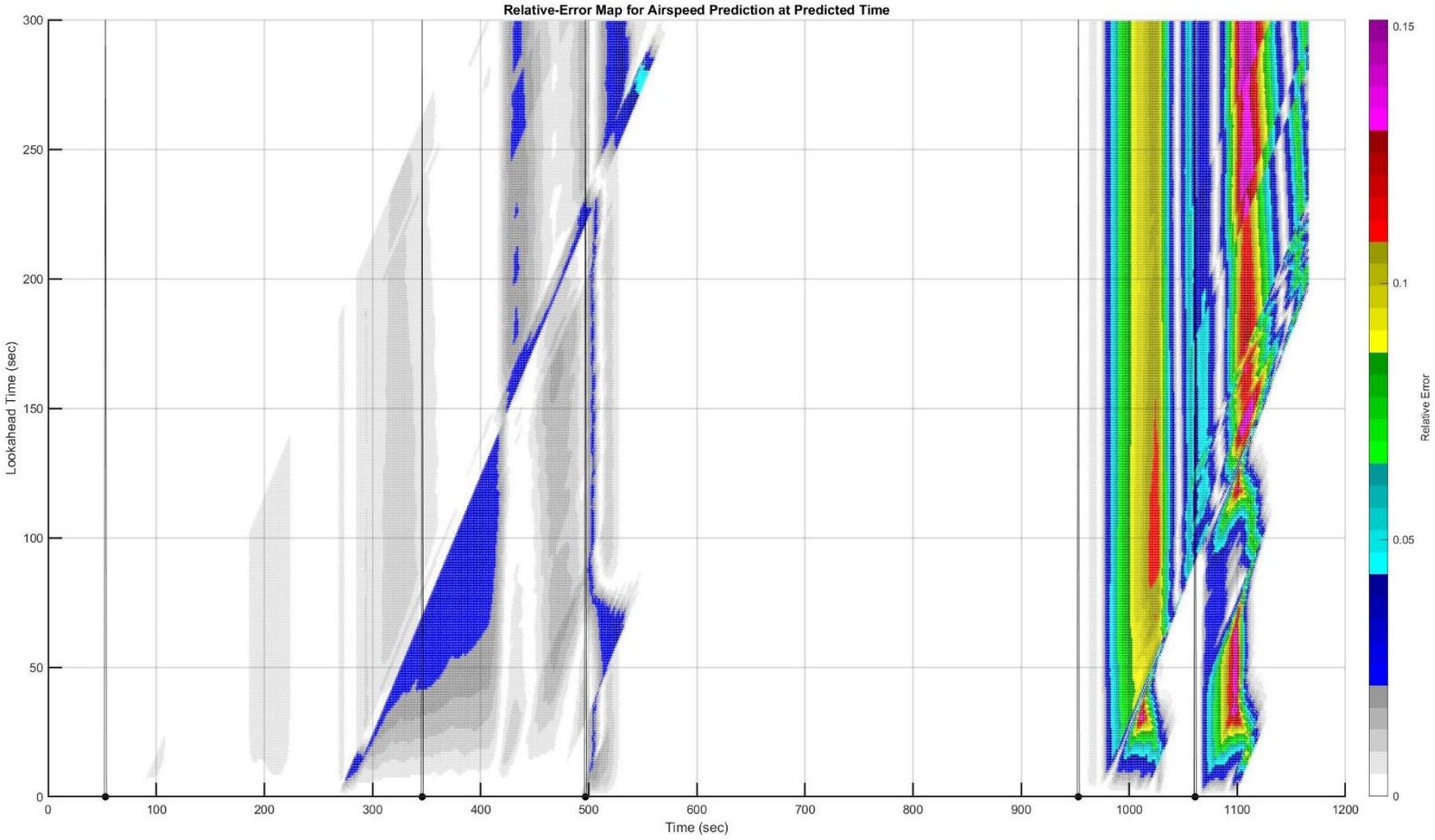

Figure C. 45: HOBRK to Runway 09: Heatmap of Altitude Prediction Error (Time is $t + \tau$)

C.10. Trajectory: HOBRK to 18C

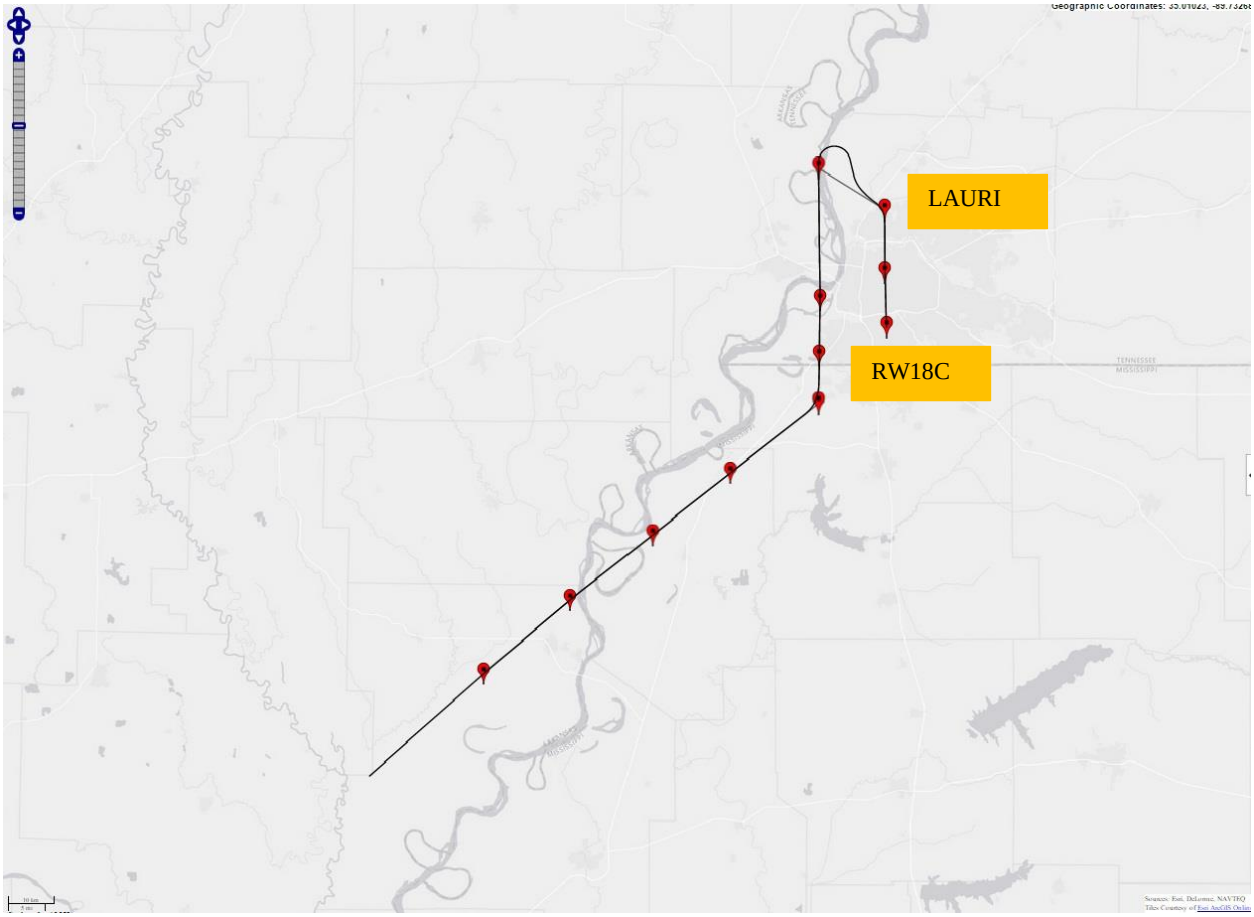

Figure C. 46: HOBRK to Runway 18C: Planned and Actual Trajectories (Red markers indicate waypoints)

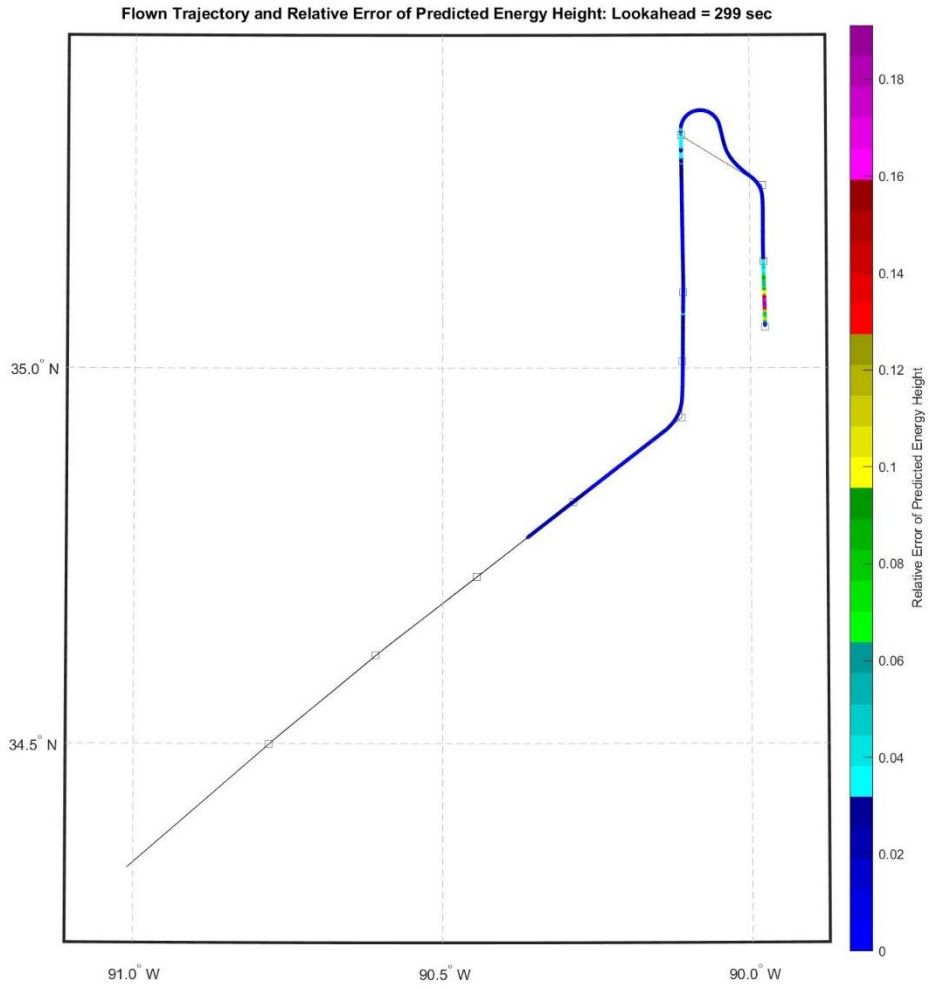

Figure C. 47: HOBRK to Runway 18C: Lateral Path Color-Coded for Energy Prediction Error for Look-Ahead of 299 Seconds

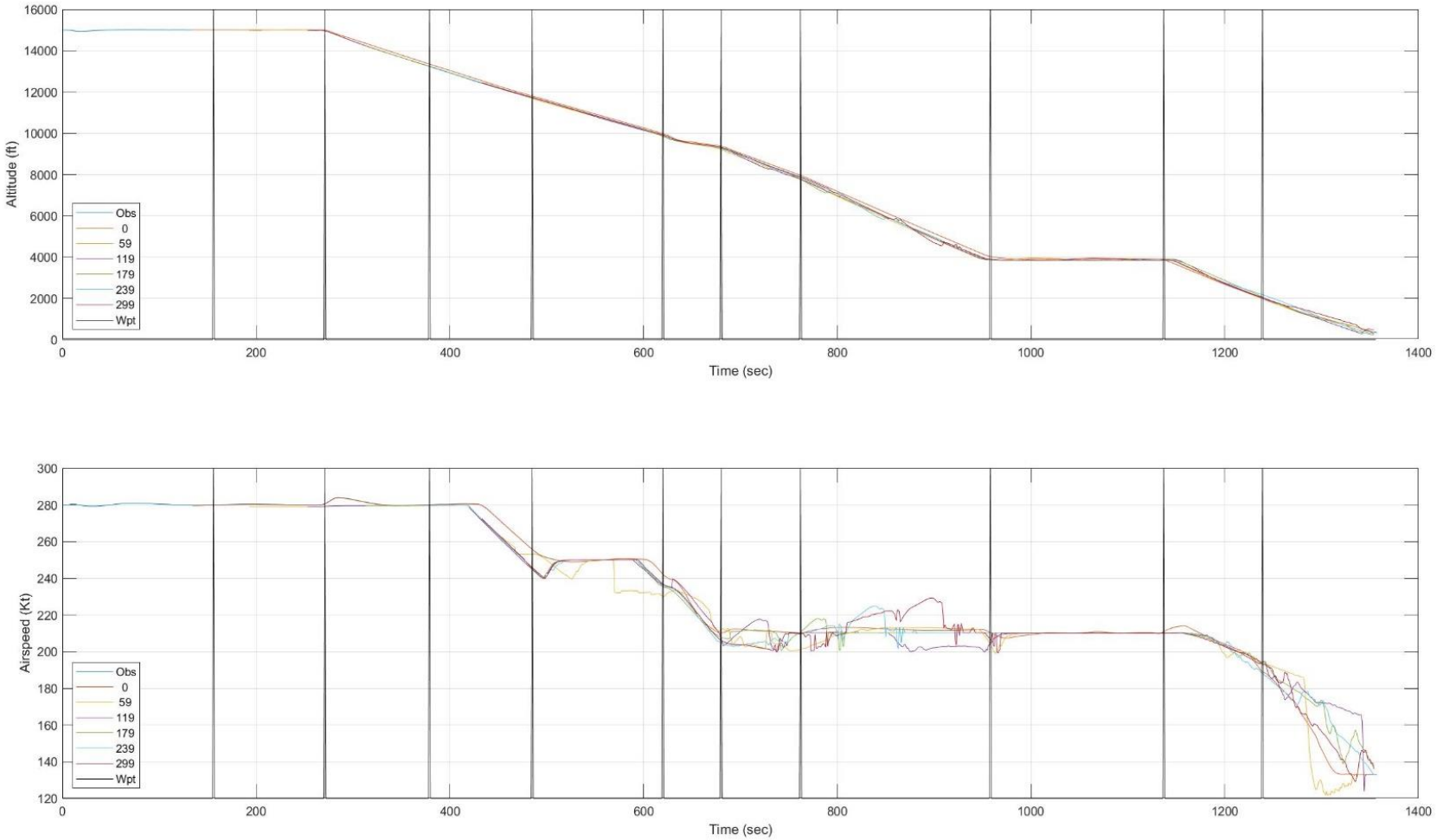

Figure C. 48: HOBRK to Runway 18C: Time History of Predicted Altitude and Airspeed

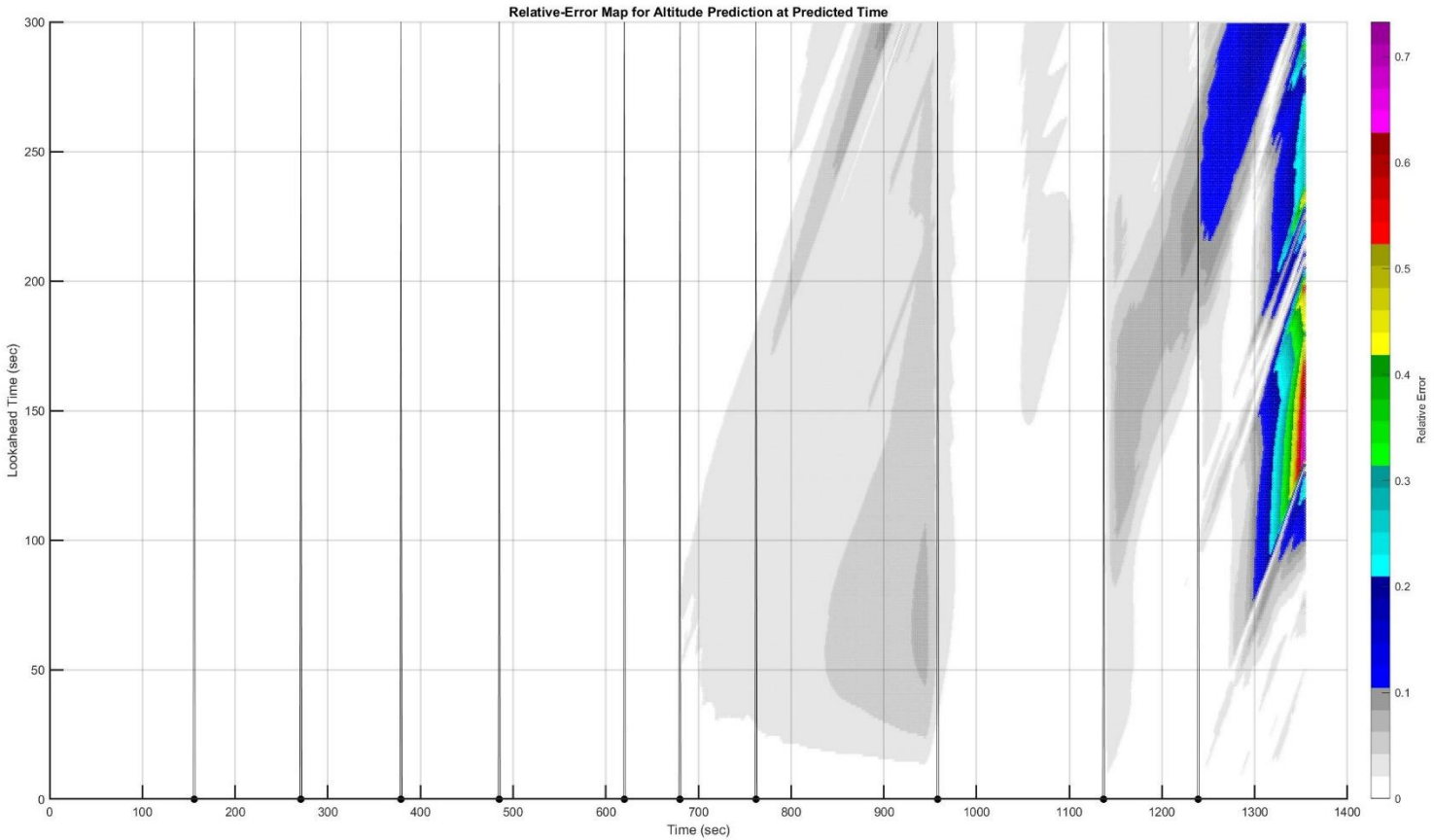

Figure C. 49: HOBRK to Runway 18C: Heatmap of Altitude Prediction Error (Time is $t + \tau$)

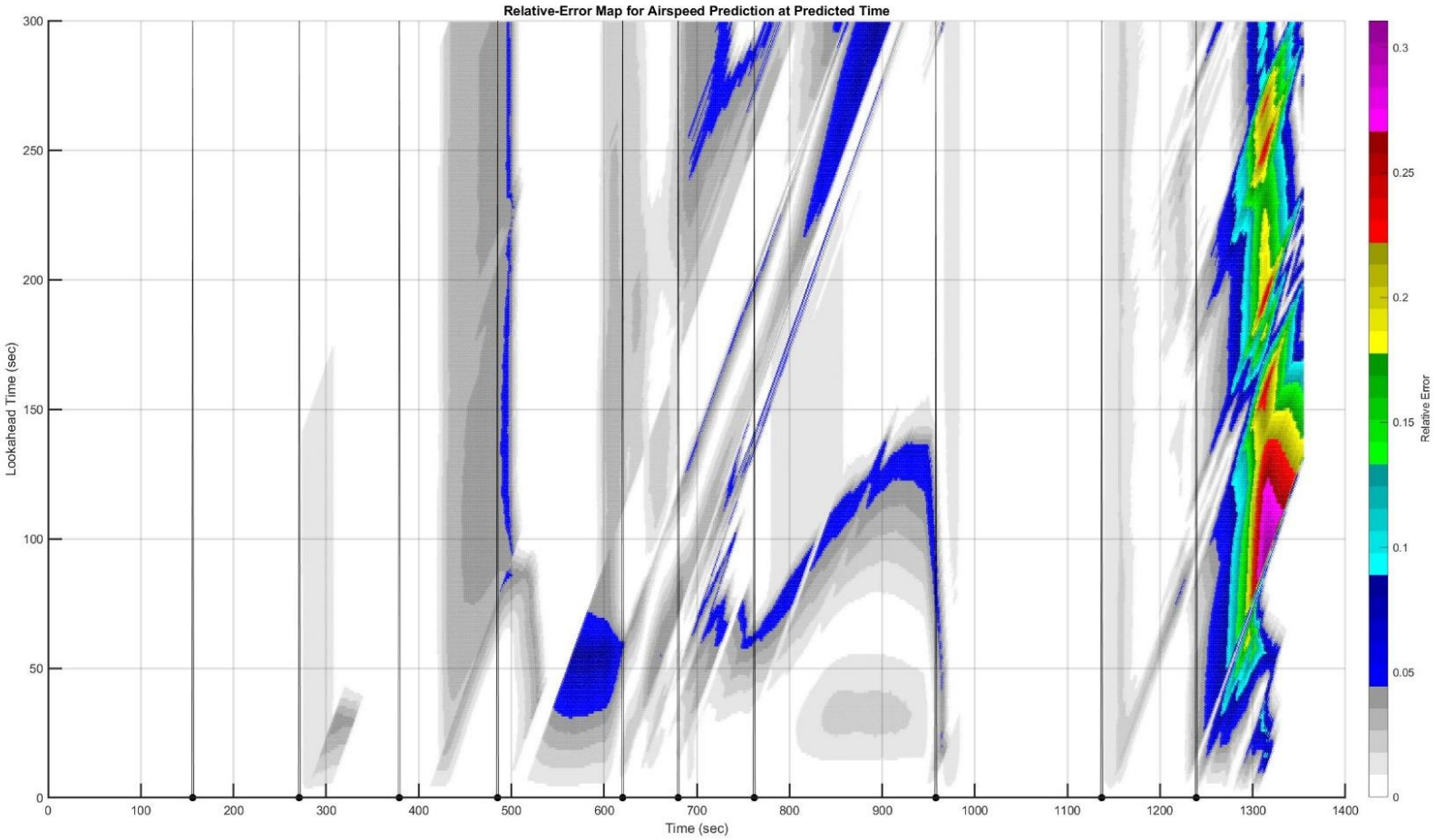

Figure C. 50: HOBRK to Runway 18C: Heatmap of Airspeed Prediction Error (Time is $t + \tau$)

C.11. Trajectory: HOBRK to 27

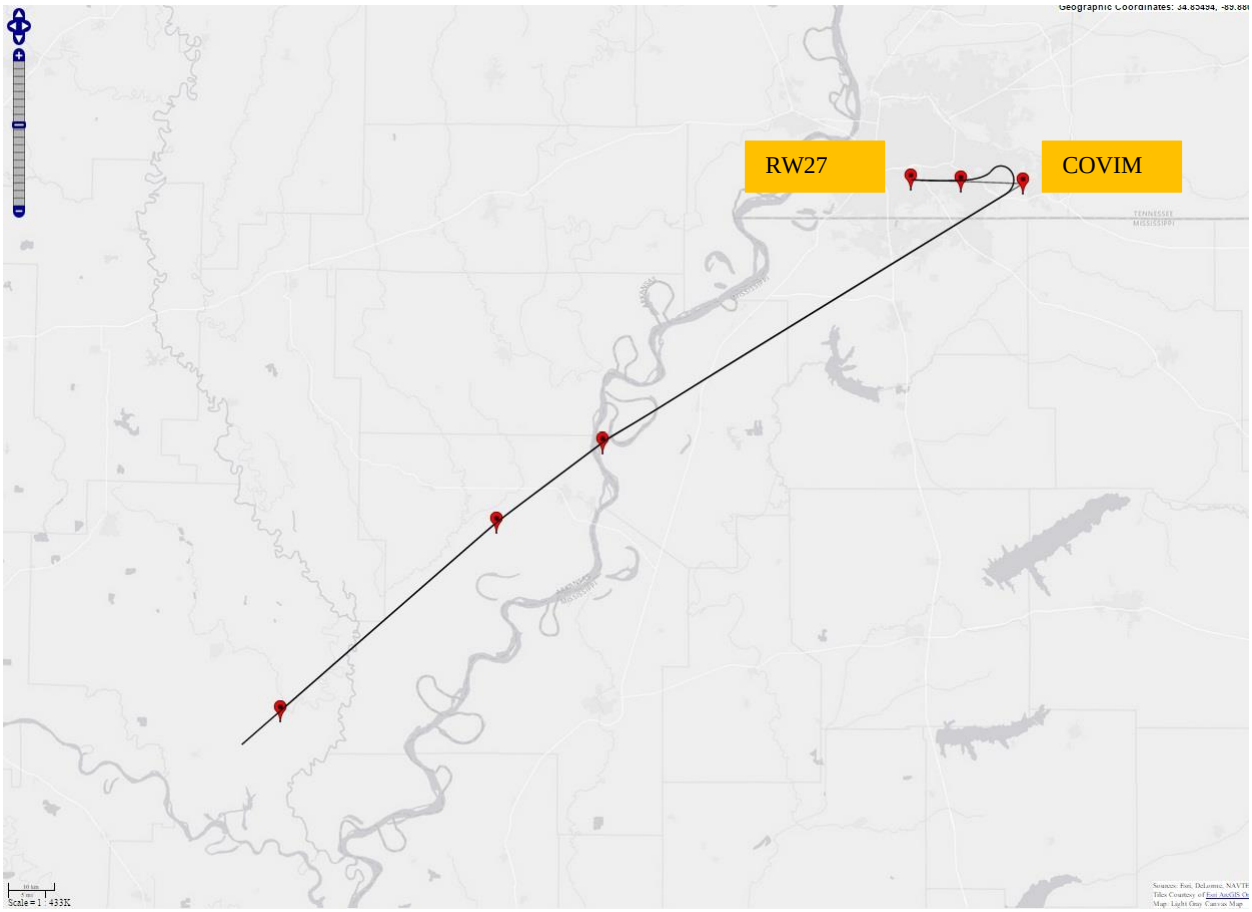

Figure C. 51: HOBRK to Runway 27: Planned and Actual Trajectories (Red markers indicate waypoints)

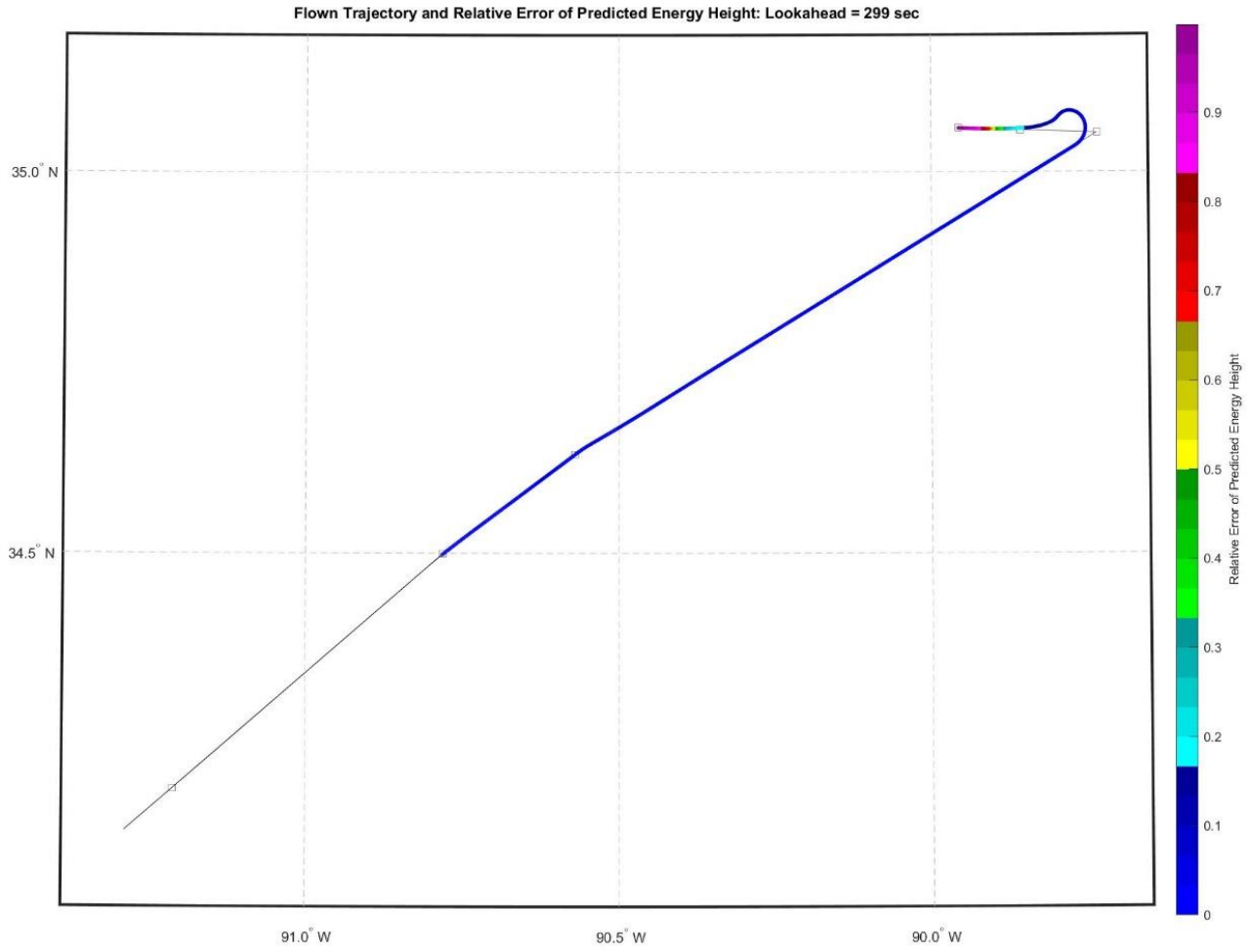

Figure C. 52: HOBRK to Runway 27: Lateral Path Color-Coded for Energy Prediction Error for Look-Ahead of 299 Seconds

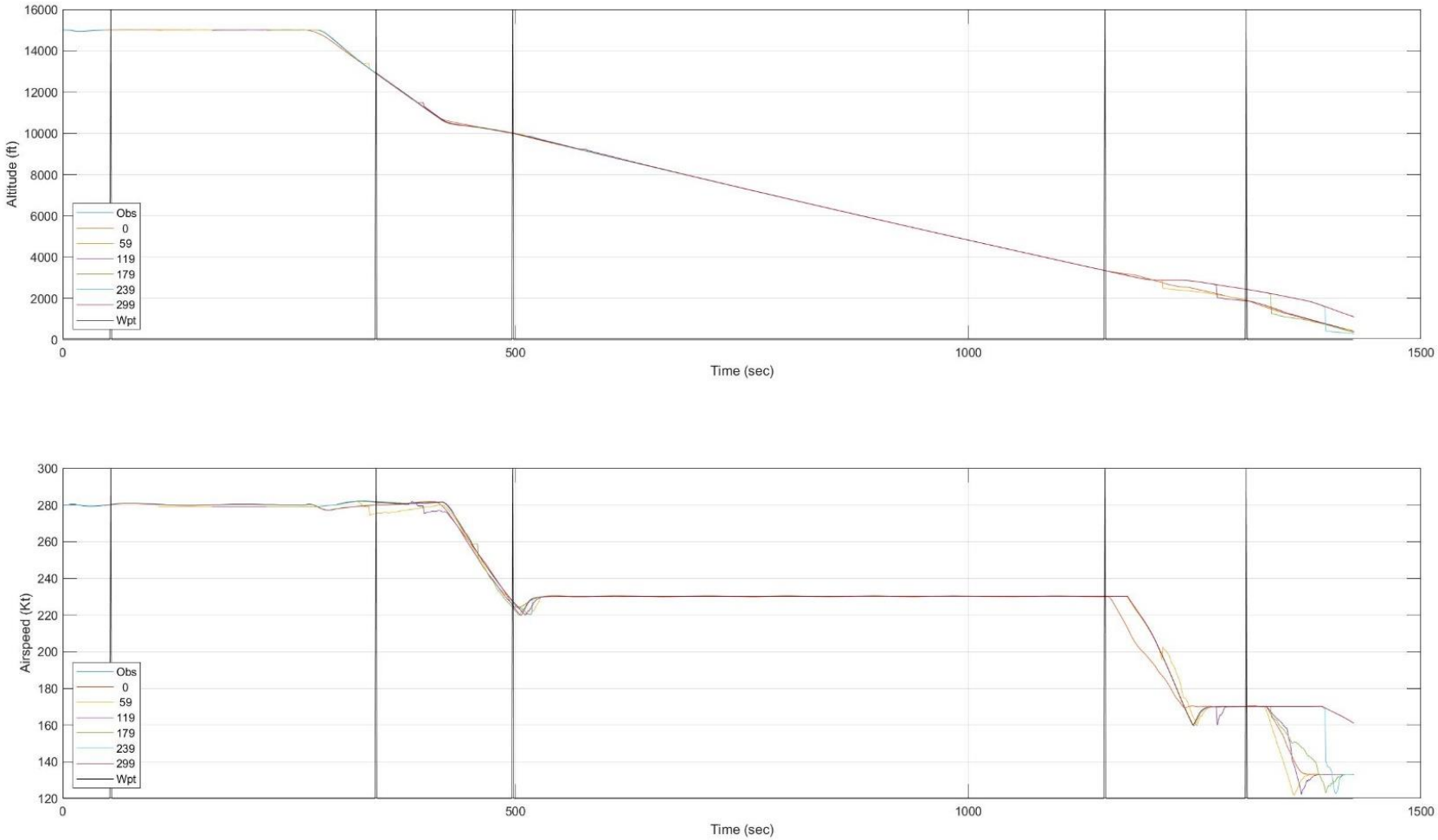

Figure C. 53: HOBRK to Runway 27: Time History of Predicted Altitude and Airspeed

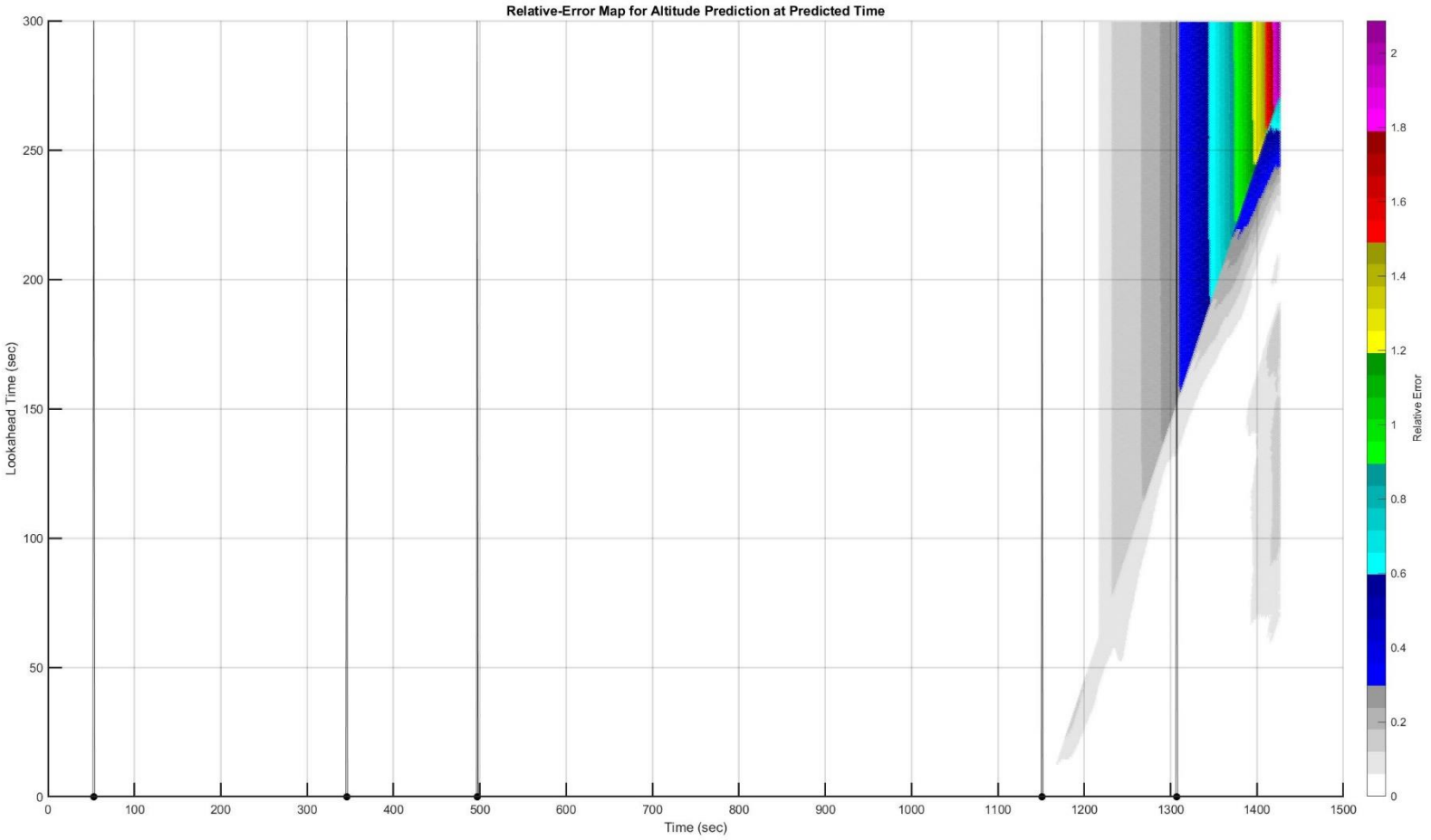

Figure C. 54: HOBRK to Runway 27: Heatmap of Altitude Prediction Error (Time is $t + \tau$)

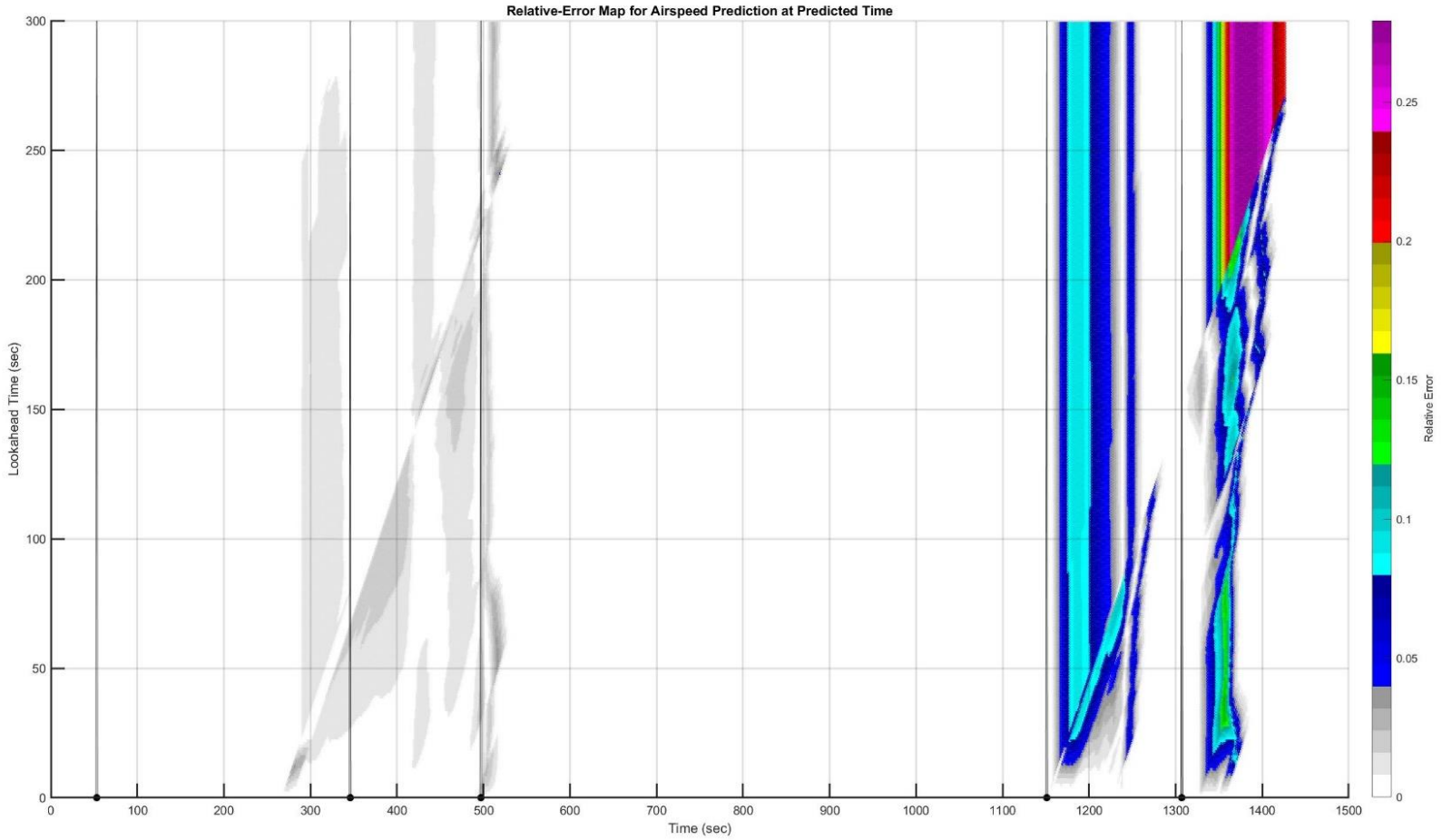

Figure C. 55: HOBRK to Runway 27: Heatmap of Airspeed Prediction Error (Time is $t + \tau$)

C.12. Trajectory: HOBRK to 36C

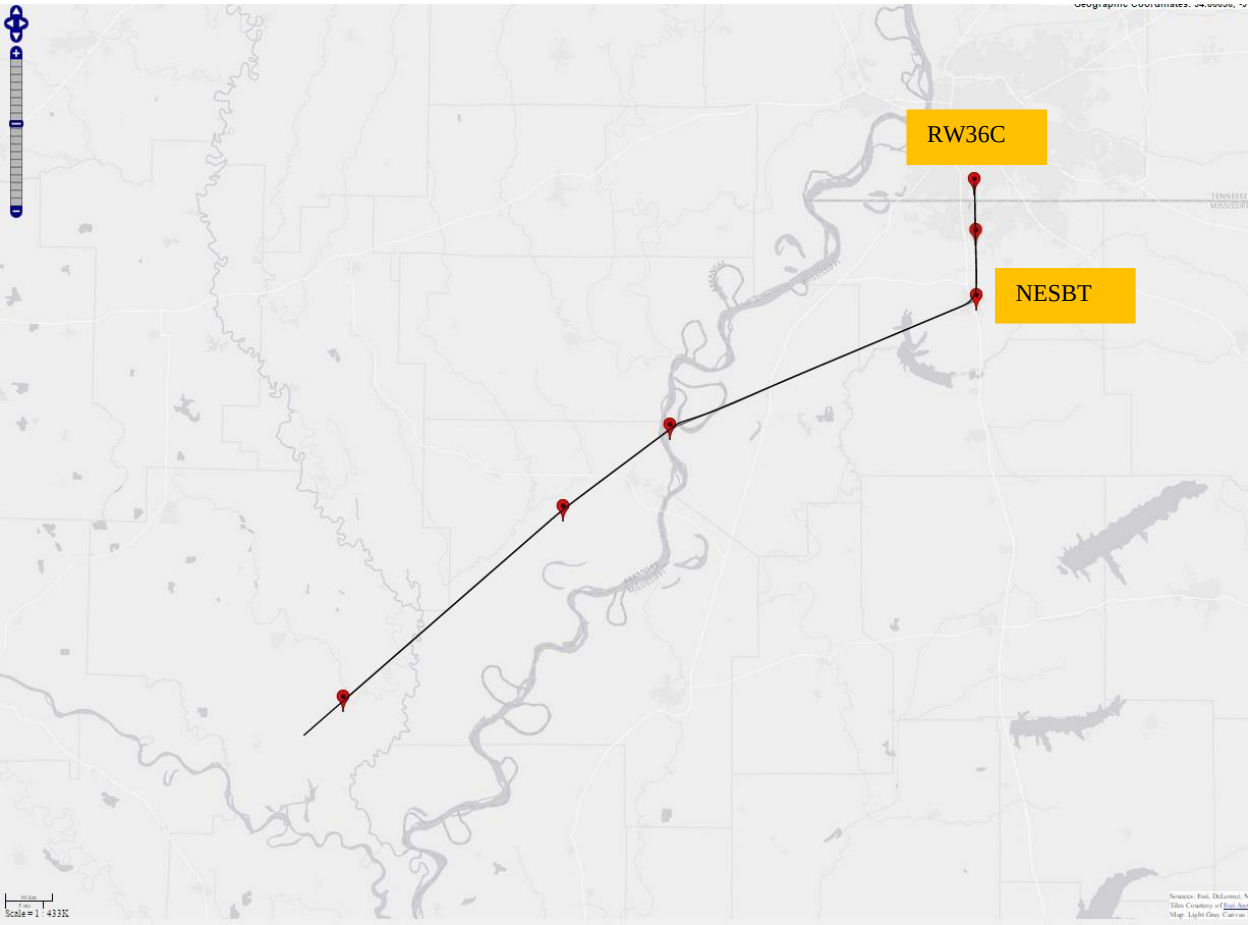

Figure C. 56: HOBRK to Runway 36C: Planned and Actual Trajectories (Red markers indicate waypoints)

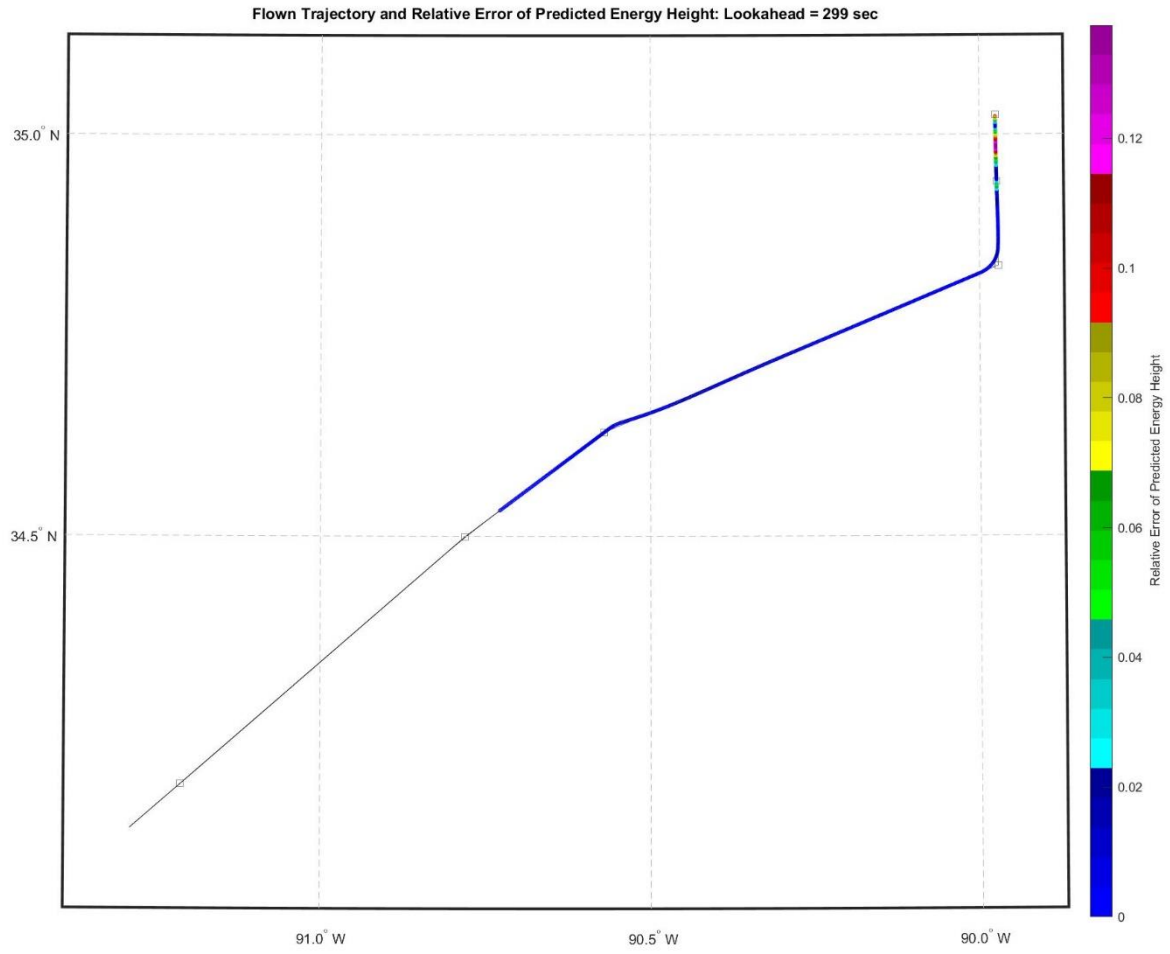

Figure C. 57: HOBRK to Runway 36C: Lateral Path Color-Coded for Energy Prediction Error for Look-Ahead of 299 Seconds

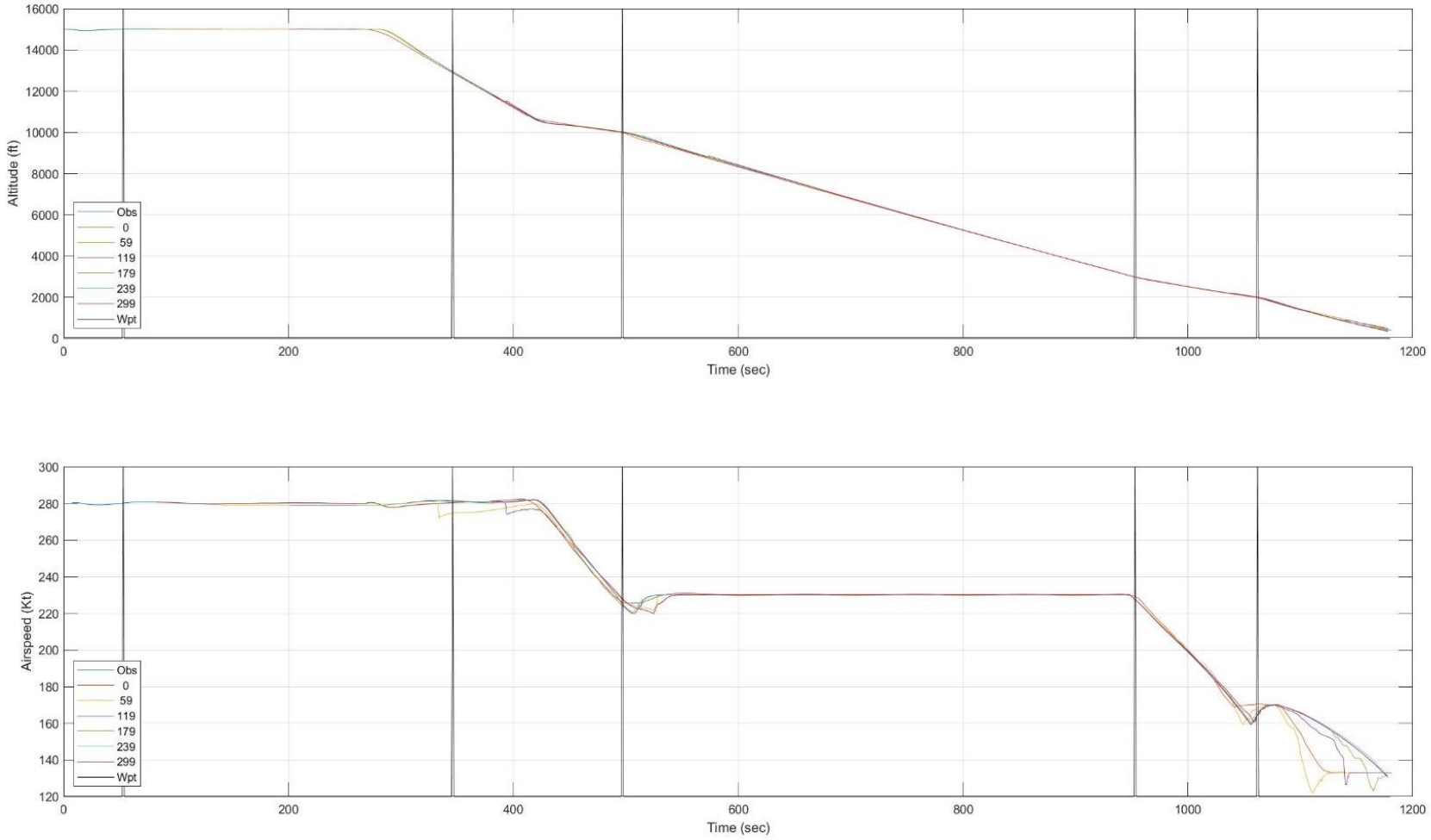

Figure C. 58: HOBRK to Runway 36C: Time History of Predicted Altitude and Airspeed

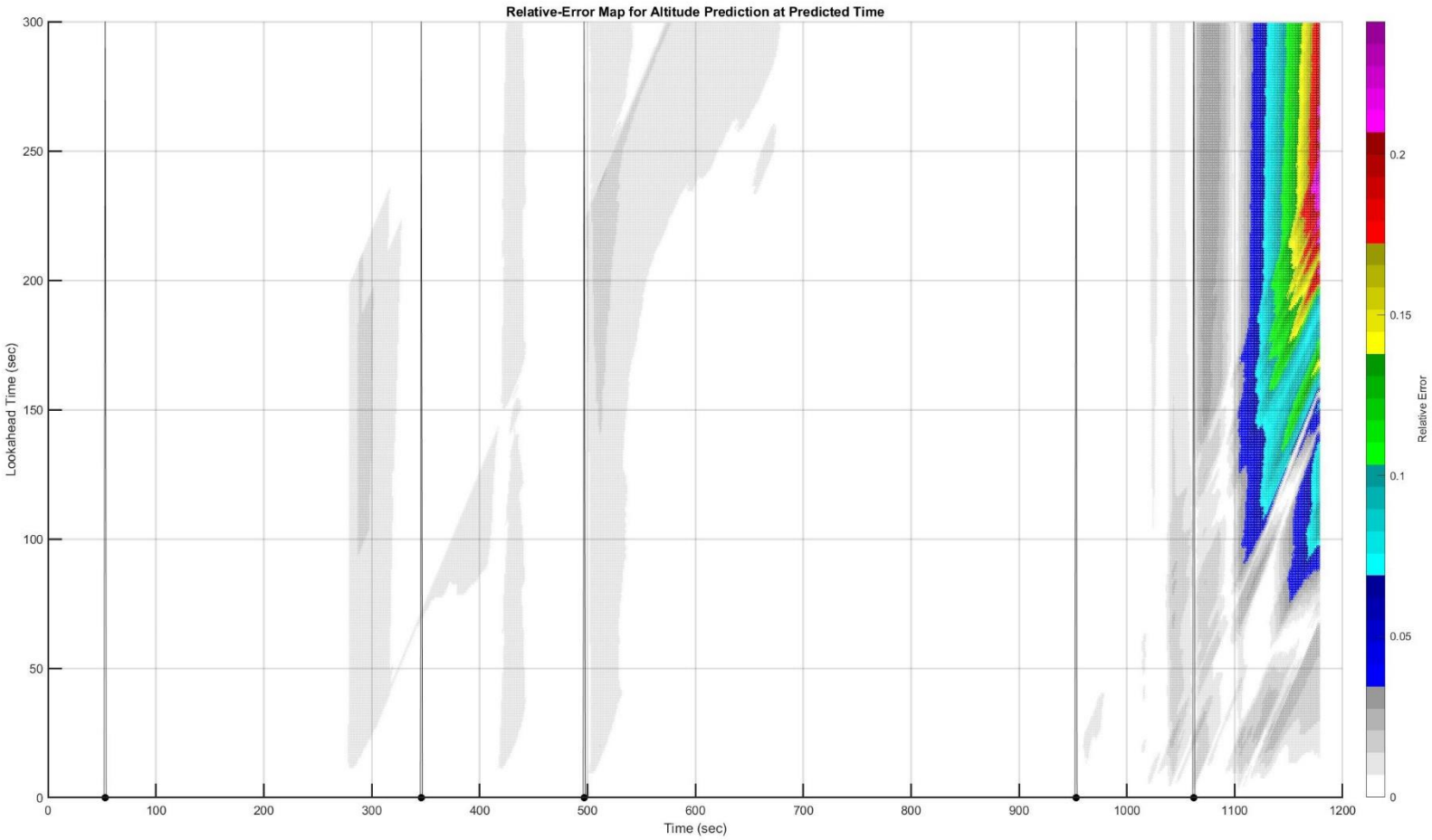

Figure C. 59: HOBRK to Runway 36C: Heatmap of Altitude Prediction Error (Time is $t + \tau$)

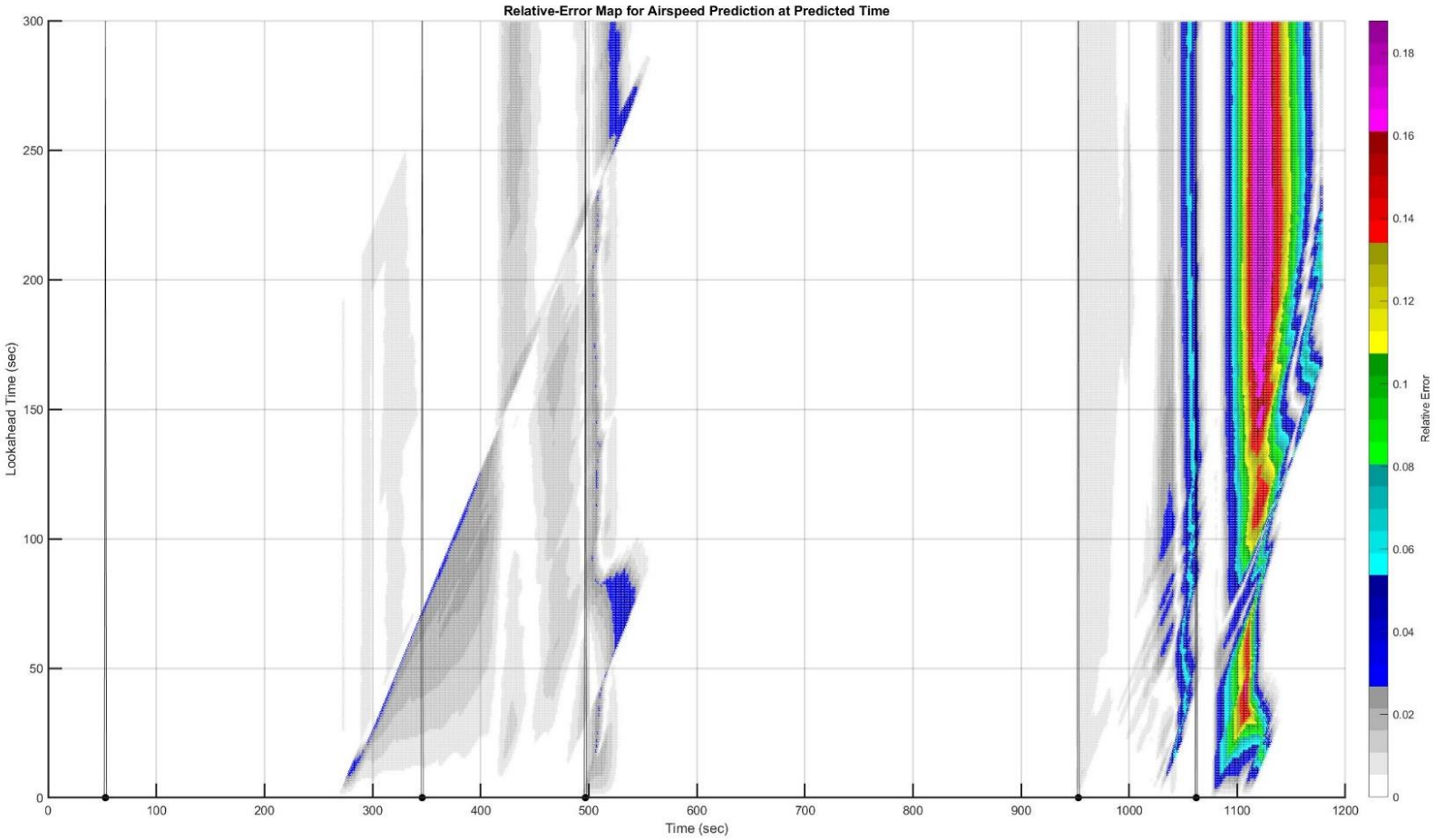

Figure C. 60: HOBRK to Runway 36C: Heatmap of Airspeed Prediction Error (Time is $t + \tau$)

C.13. Trajectory: BRBBQ to 09

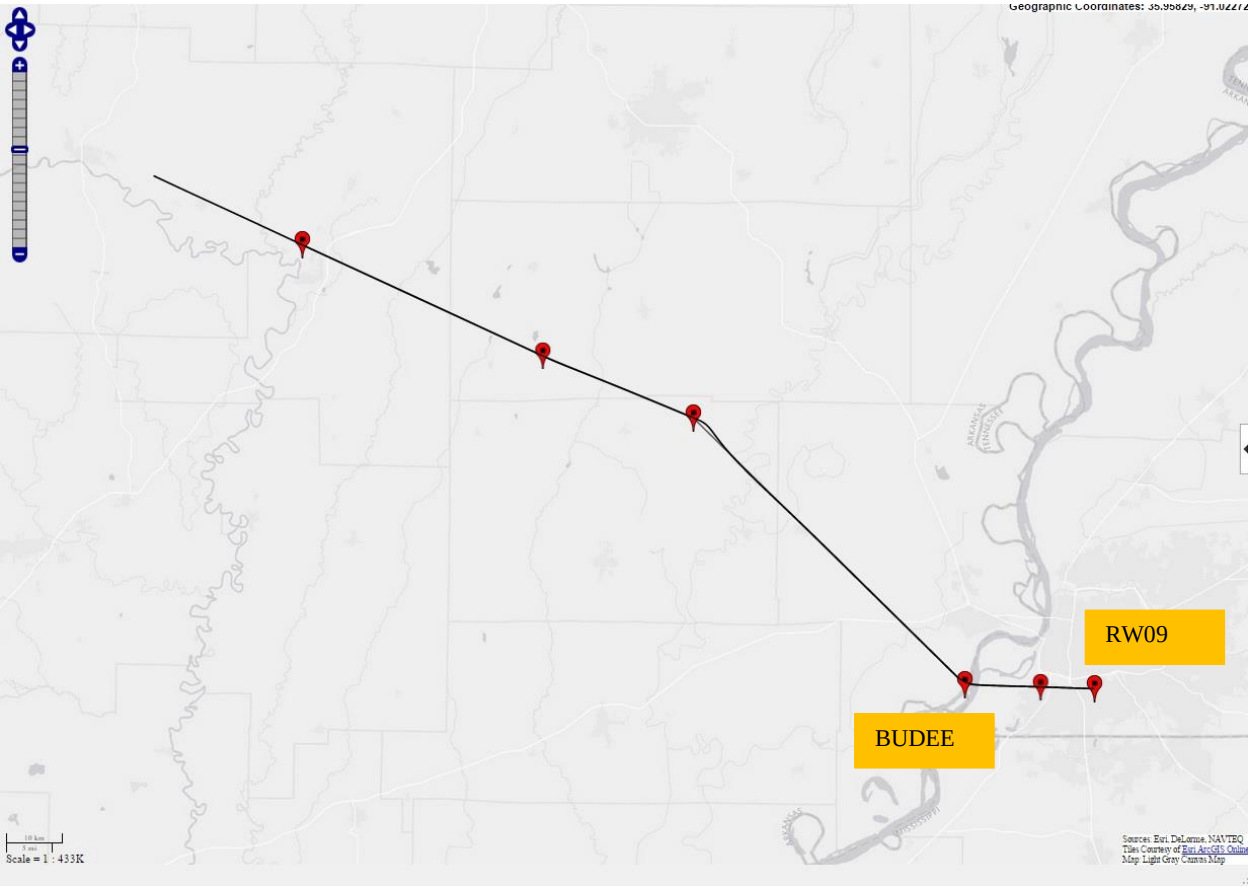

Figure C. 61: BRBBQ to Runway 09: Planned and Actual Trajectories (Red markers indicate waypoints)

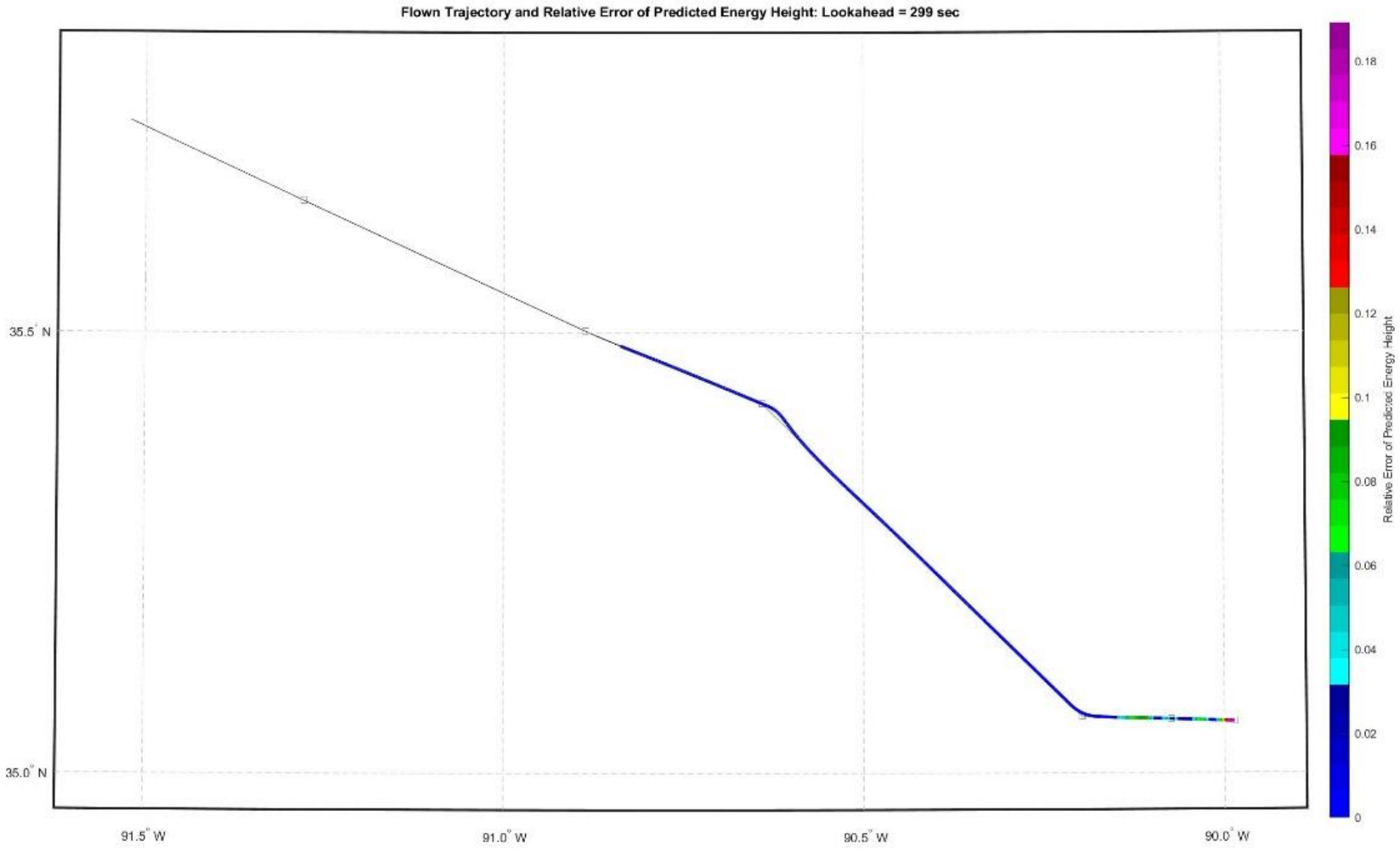

Figure C. 62: BRBBQ to Runway 09: Lateral Path Color-Coded for Energy Prediction Error for Look-Ahead of 299 Seconds

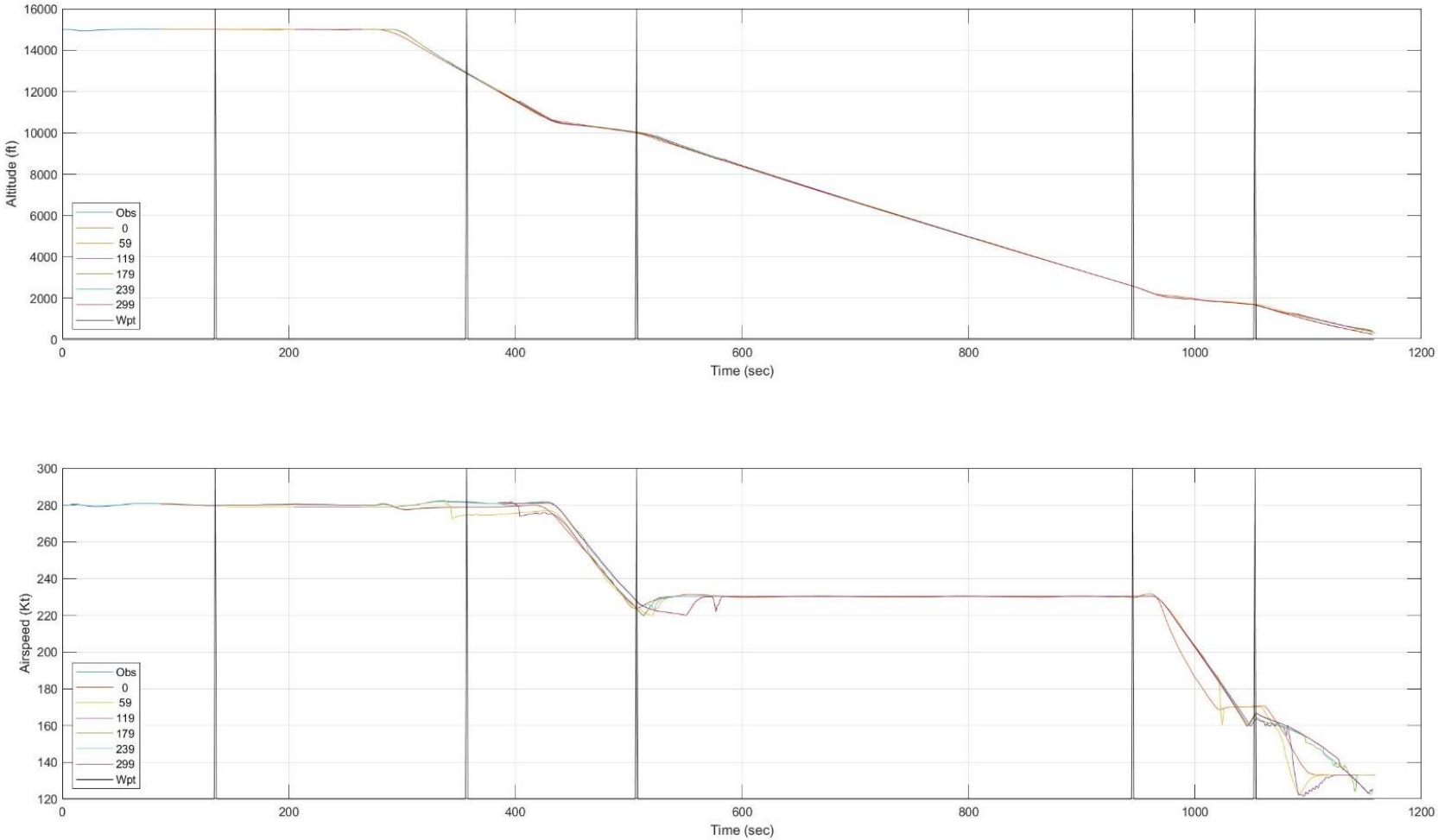

Figure C. 63: BRBBQ to Runway 09: Time History of Predicted Altitude and Airspeed

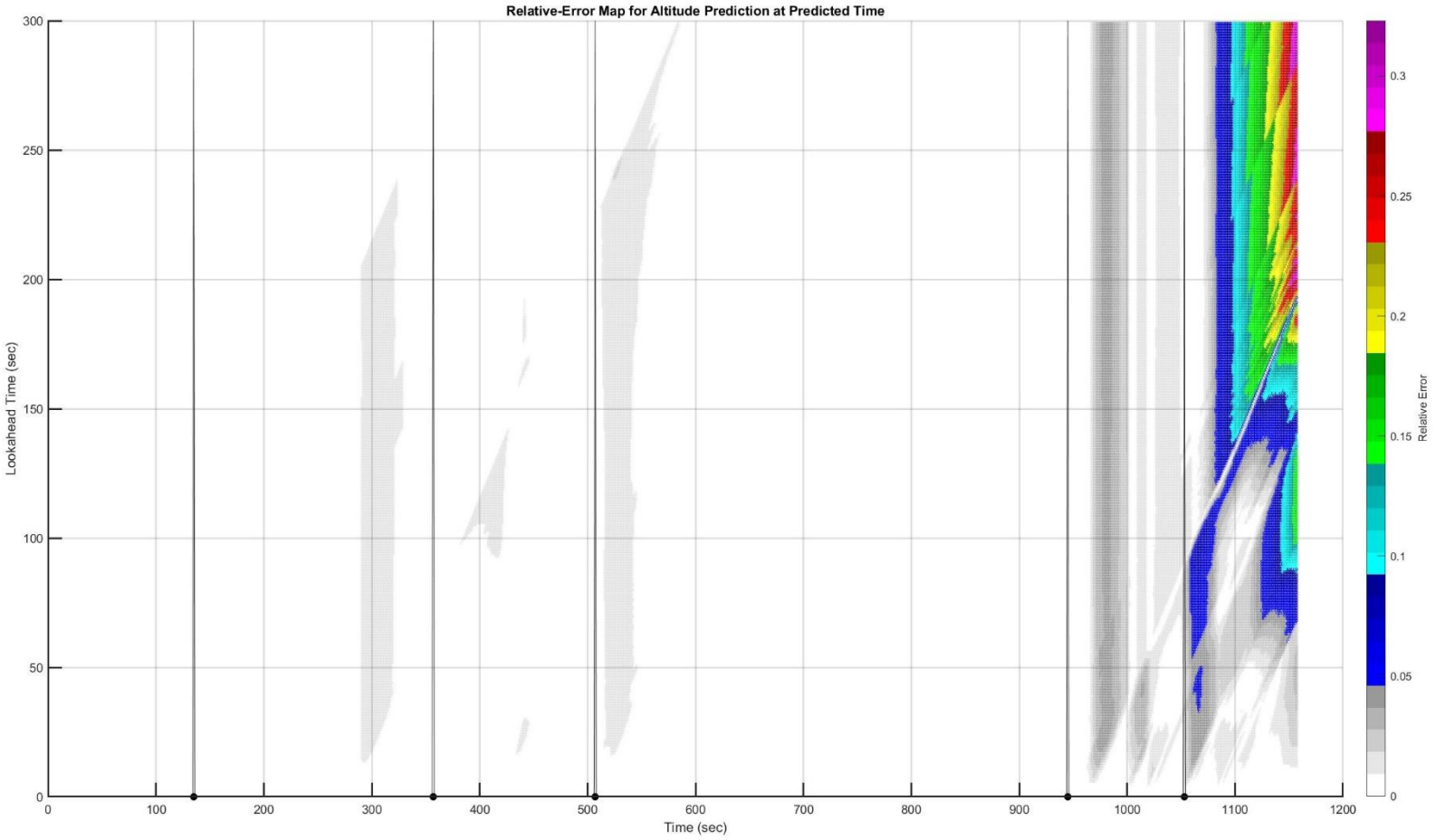

Figure C. 64: BRBBQ to Runway 09: Heatmap of Altitude Prediction Error (Time is $t + \tau$)

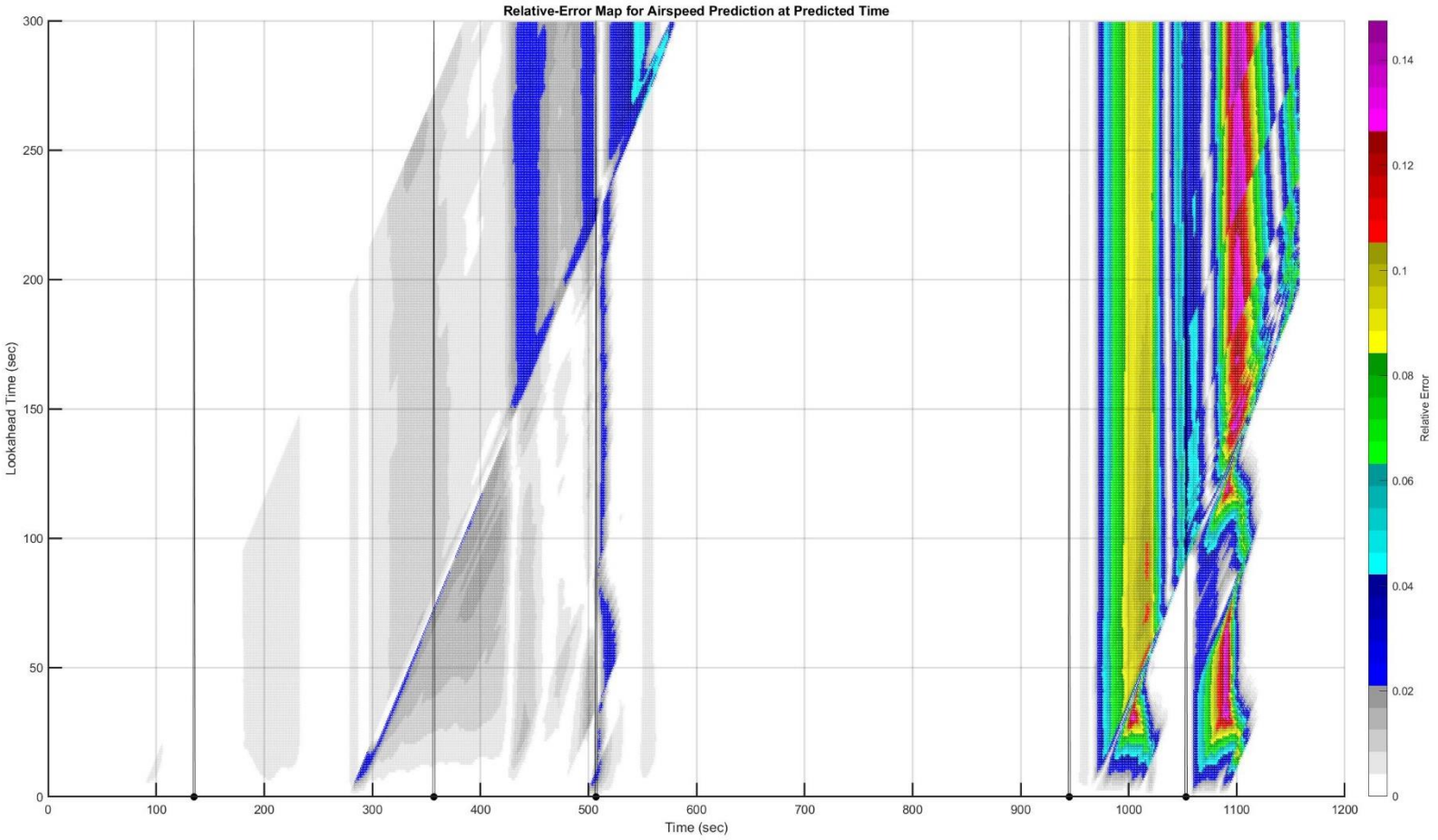

Figure C. 65: BRBBQ to Runway 09: Heatmap of Airspeed Prediction Error (Time is $t + \tau$)

C.14. Trajectory: BRBBQ to 18C

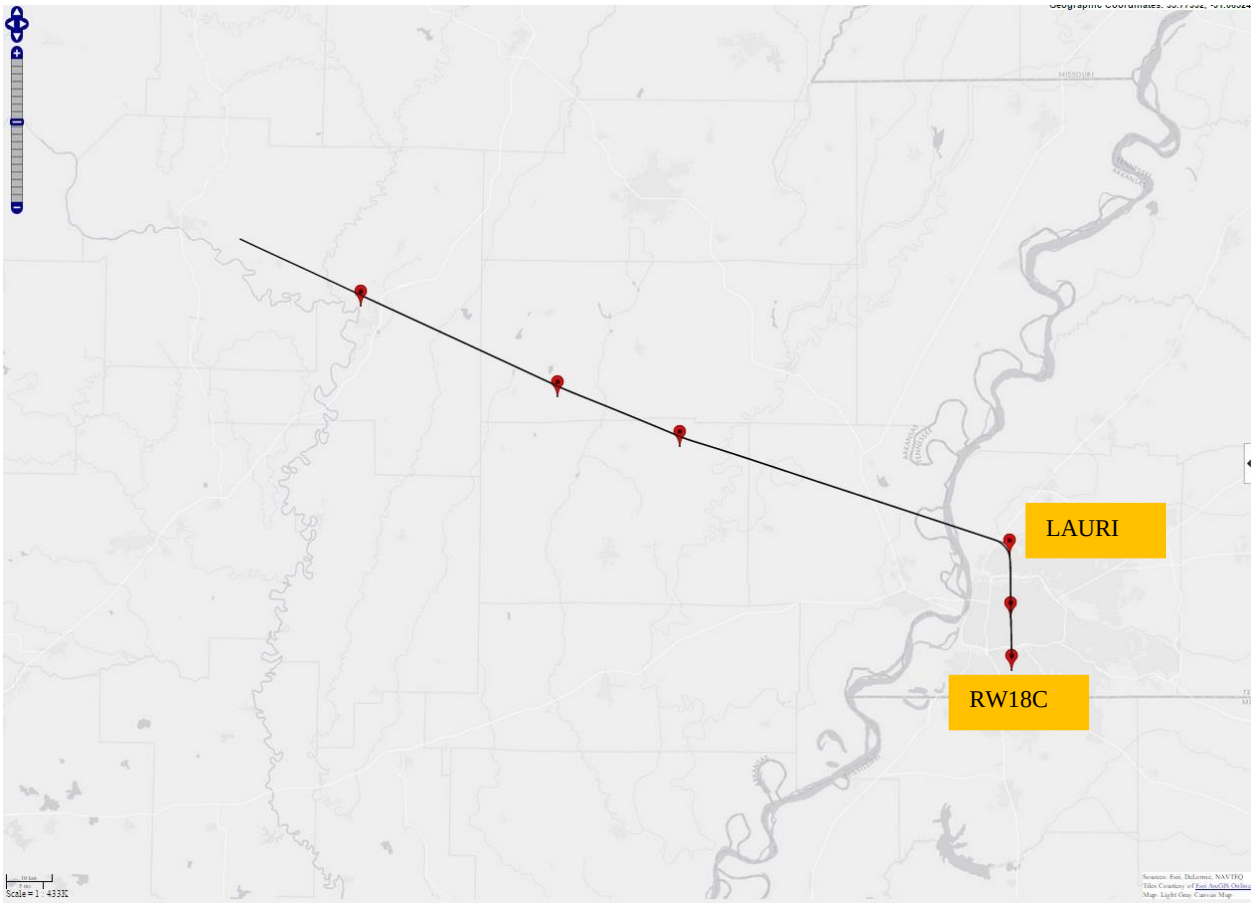

Figure C. 66: BRBBQ to Runway 18C: Planned and Actual Trajectories (Red markers indicate waypoints)

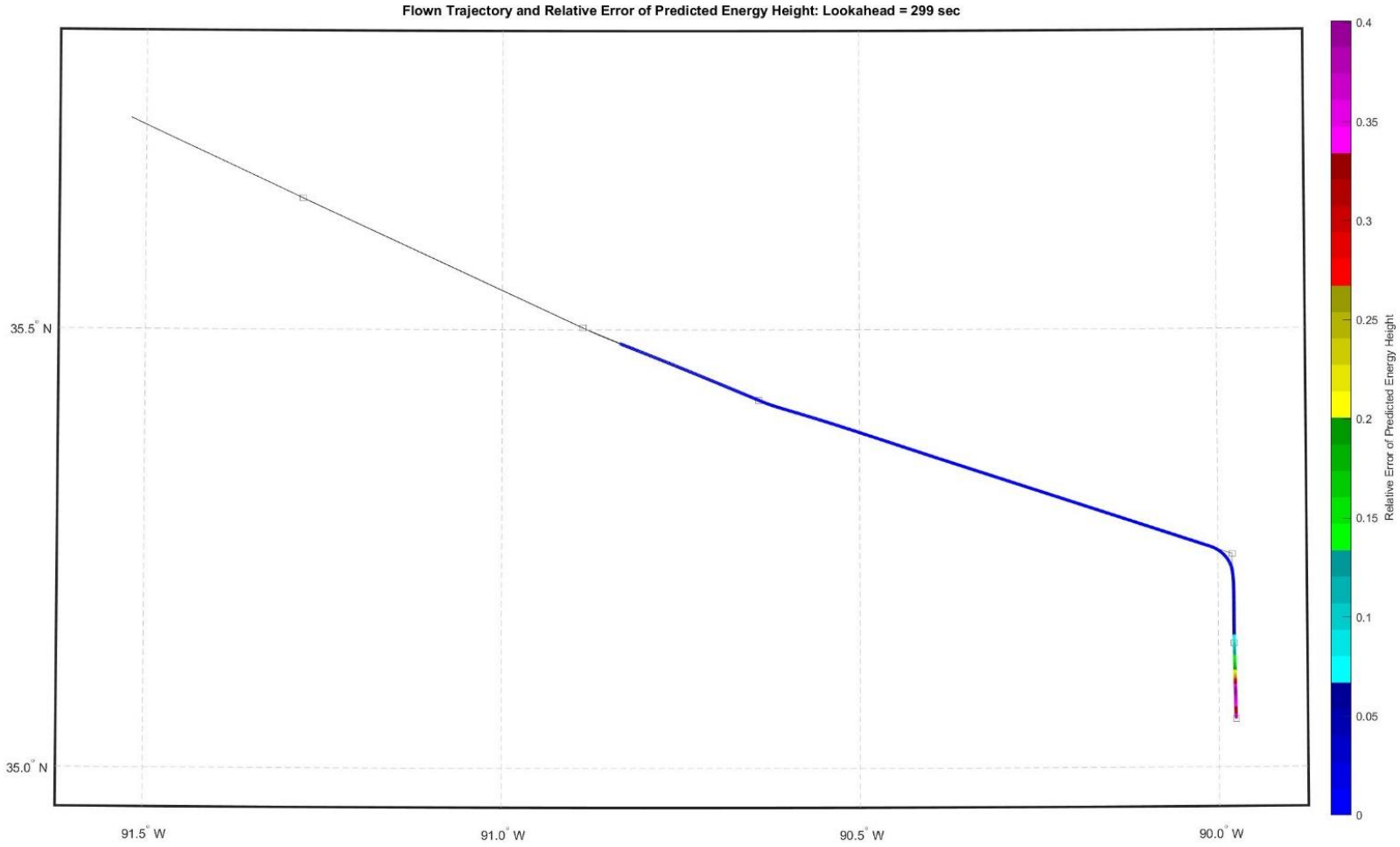

Figure C. 67: BRBBQ to Runway 18C: Lateral Path Color-Coded for Energy Prediction Error for Look-Ahead of 299 Seconds

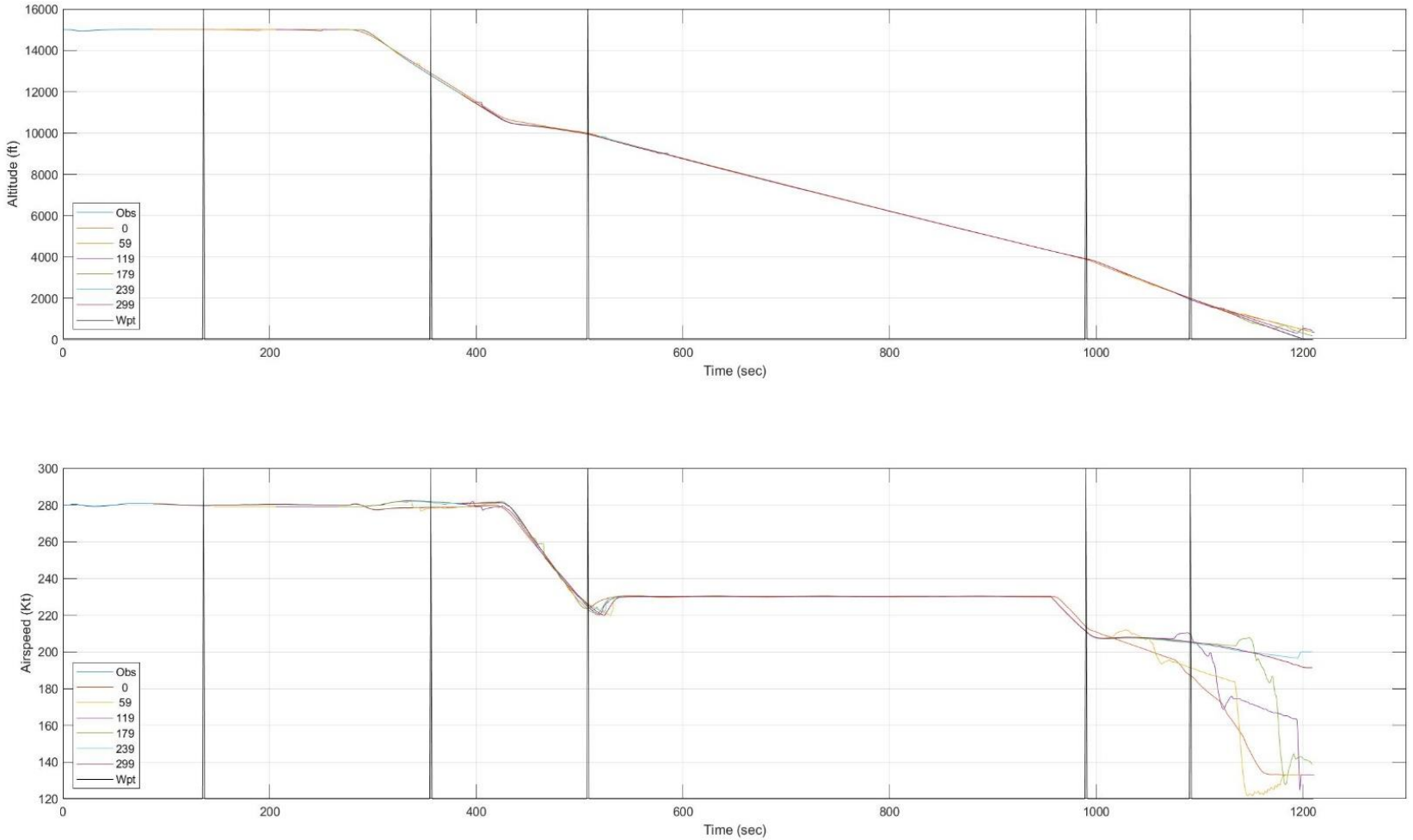

Figure C. 68: BRBBQ to Runway 18C: Time History of Predicted Altitude and Airspeed

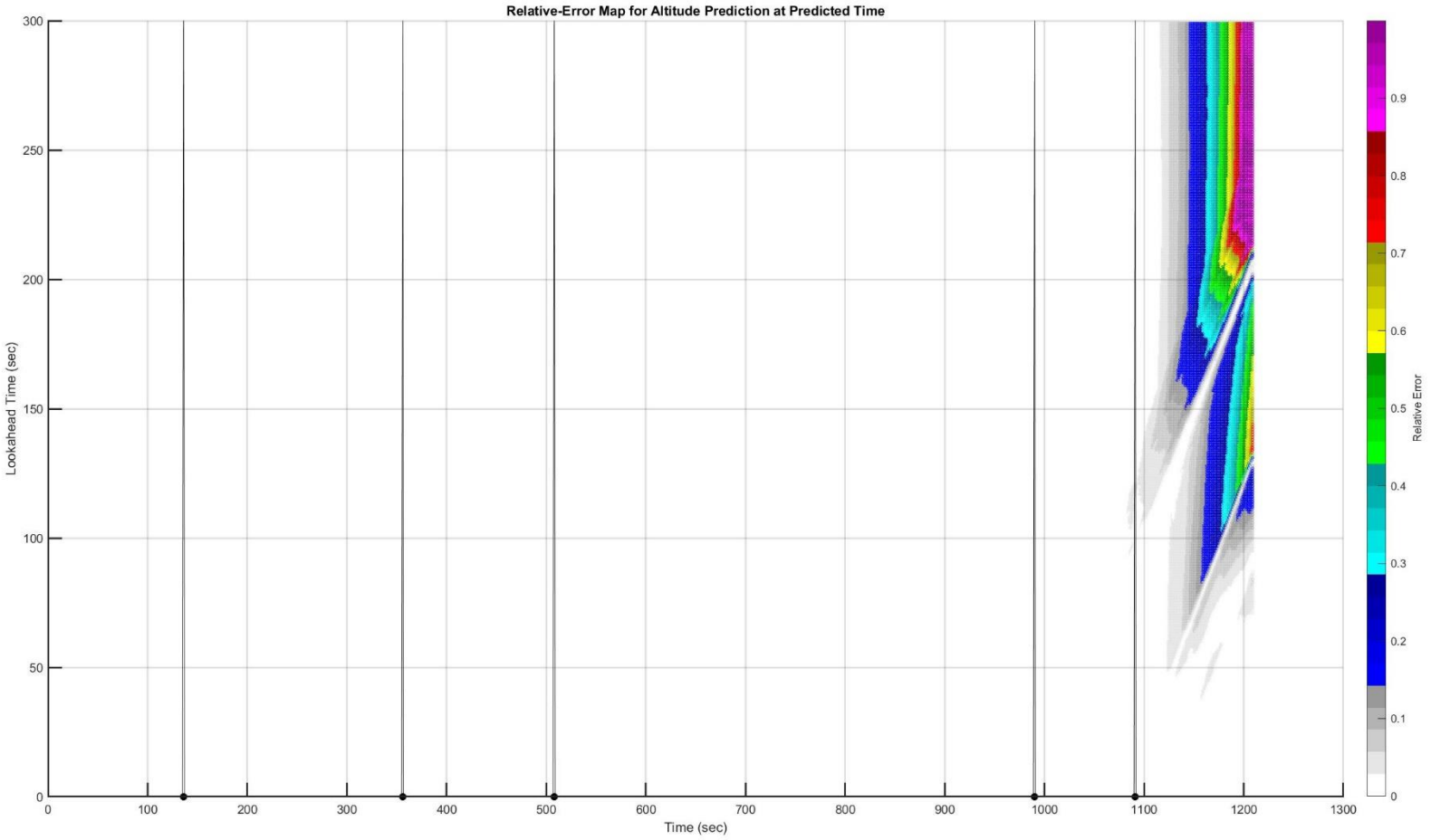

Figure C. 69: BRBBQ to Runway 18C: Heatmap of Altitude Prediction Error (Time is $t + \tau$)

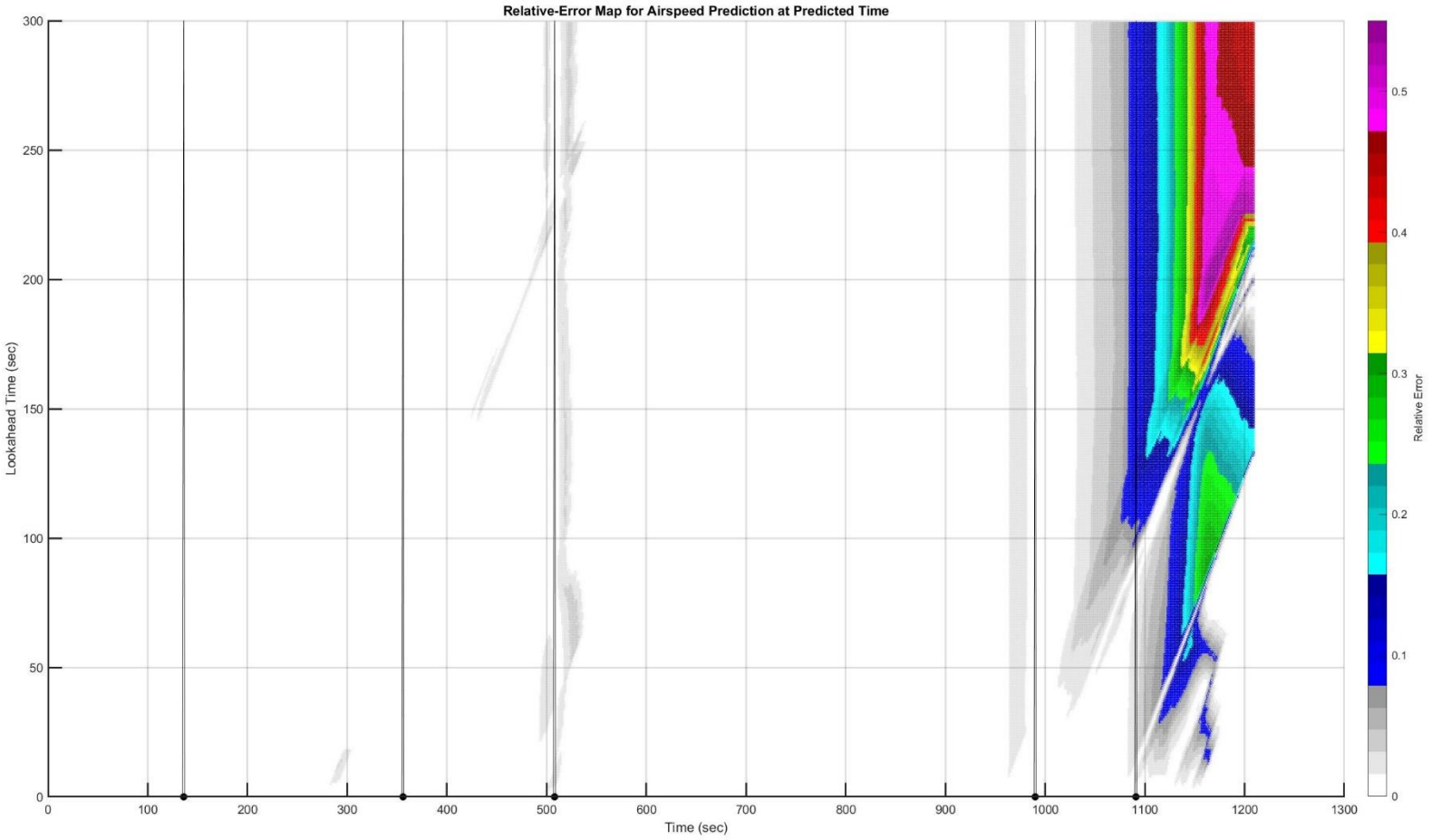

Figure C. 70: BRBBQ to Runway 18C: Heatmap of Airspeed Prediction Error (Time is $t + \tau$)

C.15. Trajectory: BRBBQ to 27

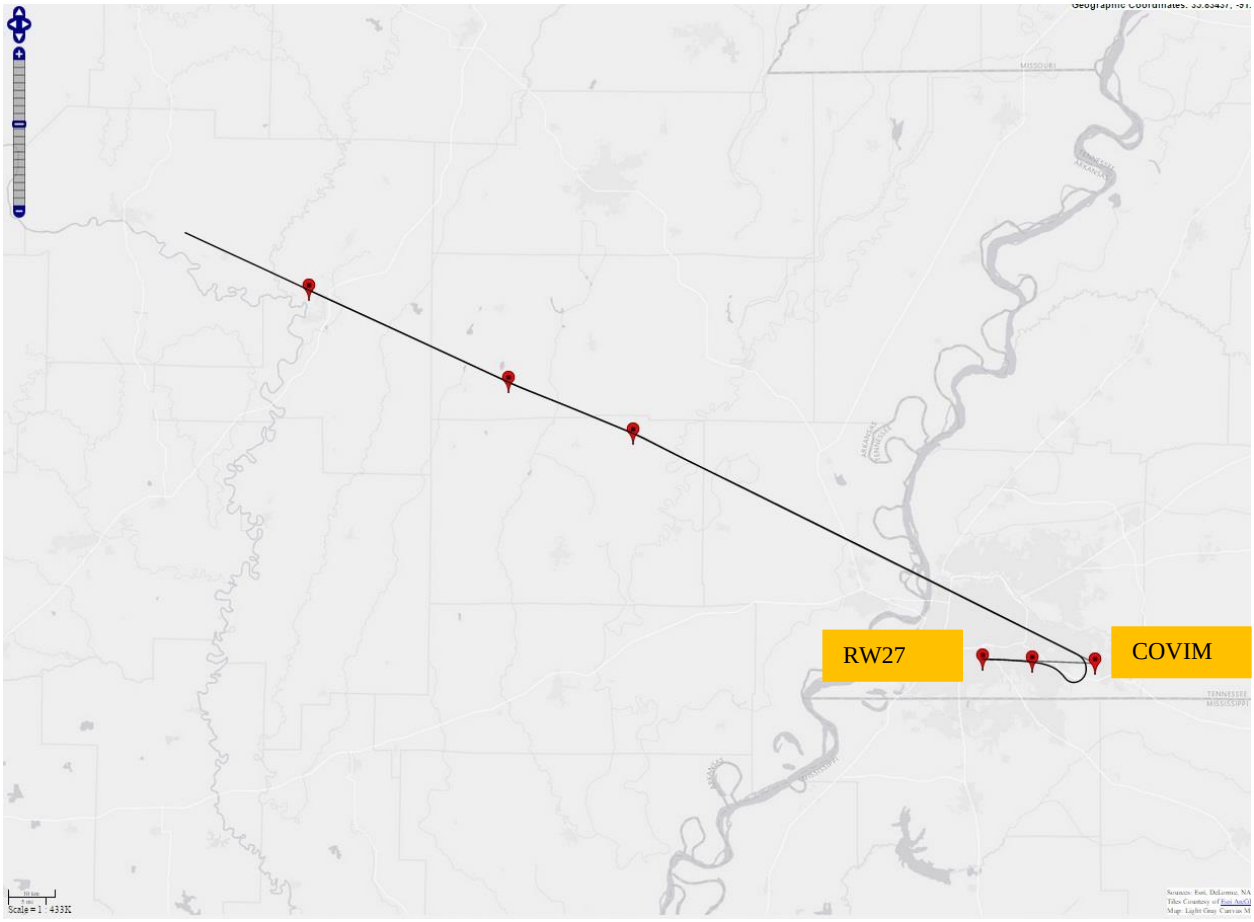

Figure C. 71: BRBBQ to Runway 27: Planned and Actual Trajectories (Red markers indicate waypoints)

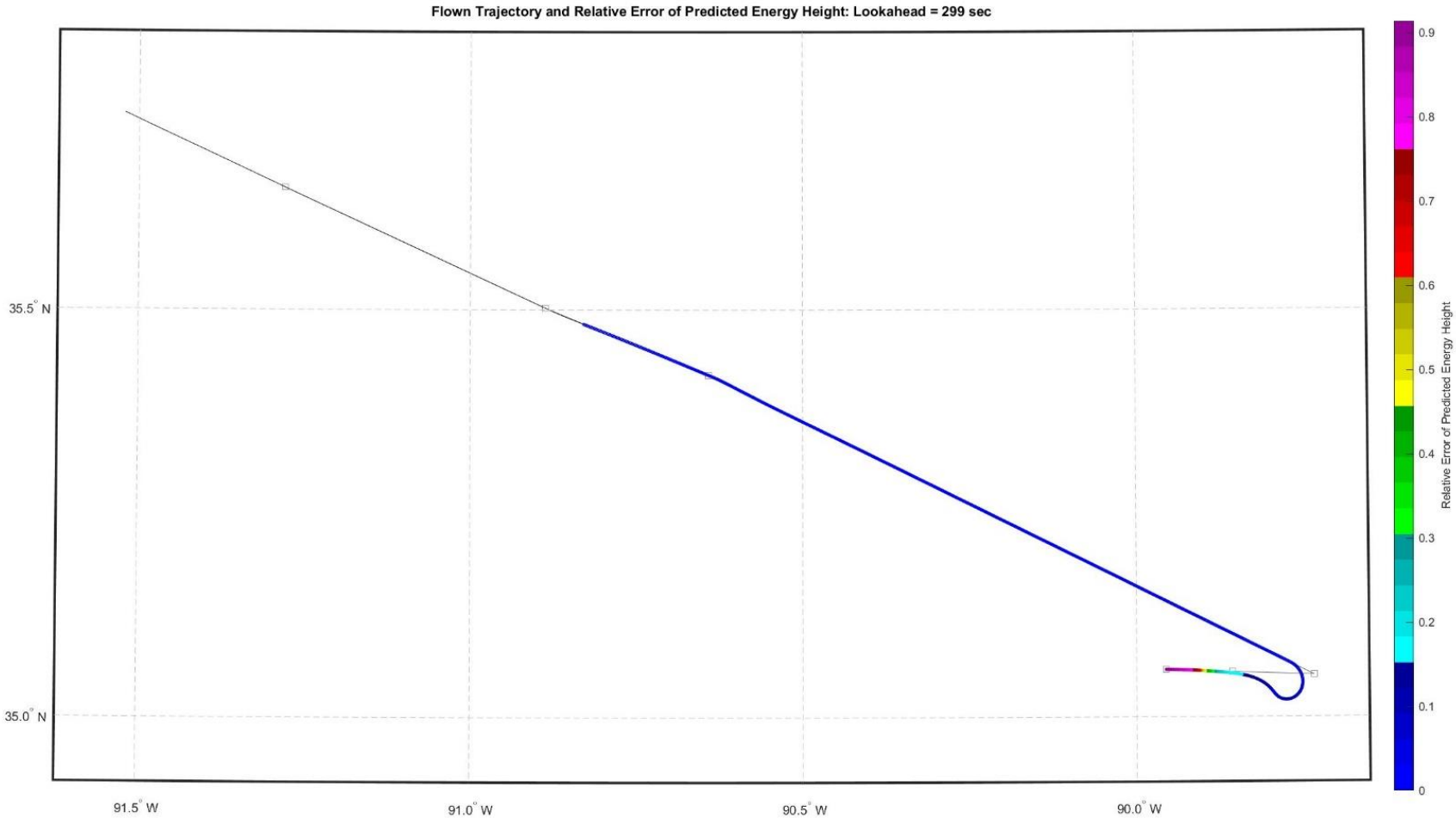

Figure C. 72: BRBBQ to Runway 27: Lateral Path Color-Coded for Energy Prediction Error for Look-Ahead of 299 Seconds

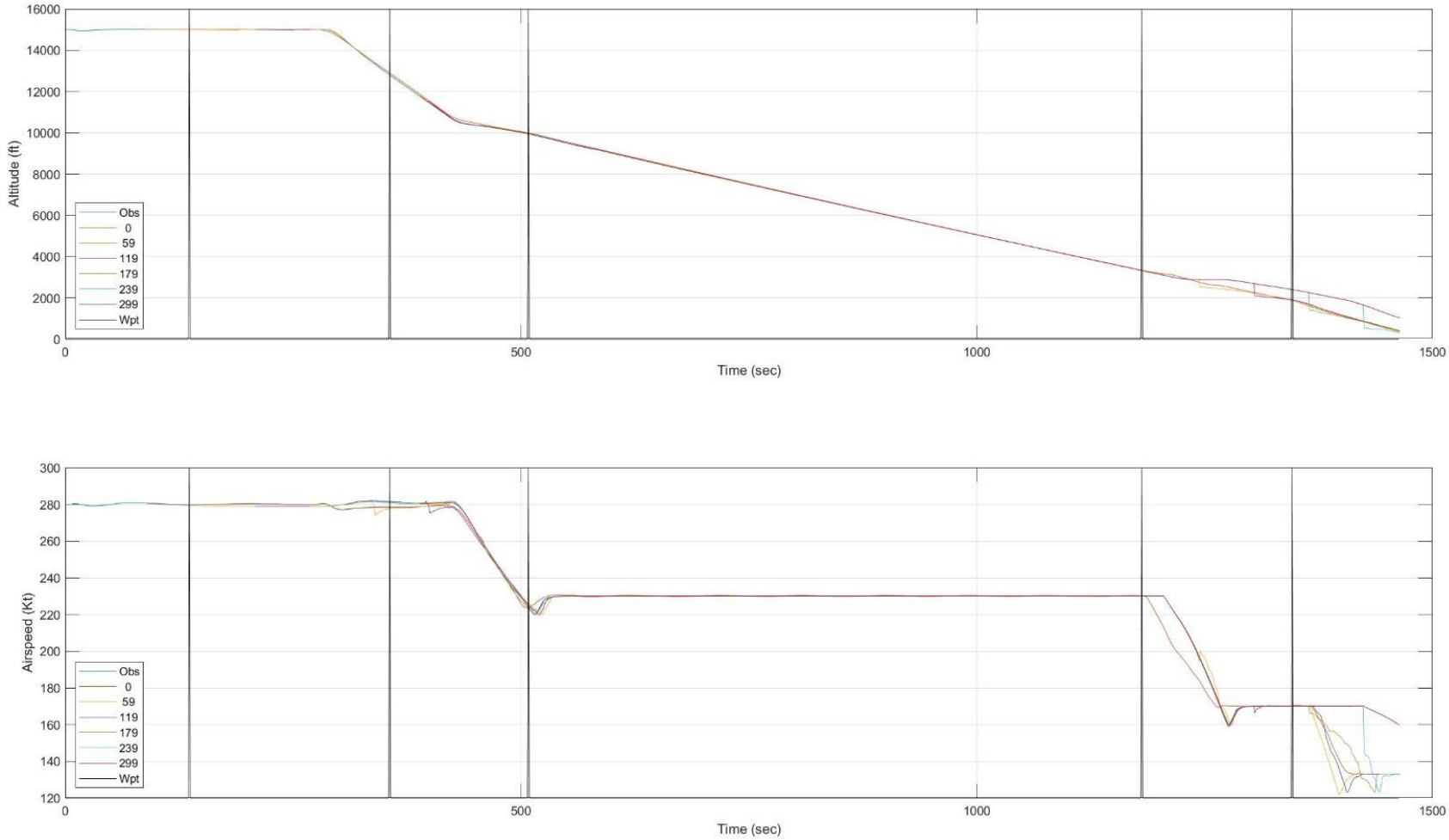

Figure C. 73: BRBBQ to Runway 27: Time History of Predicted Altitude and Airspeed

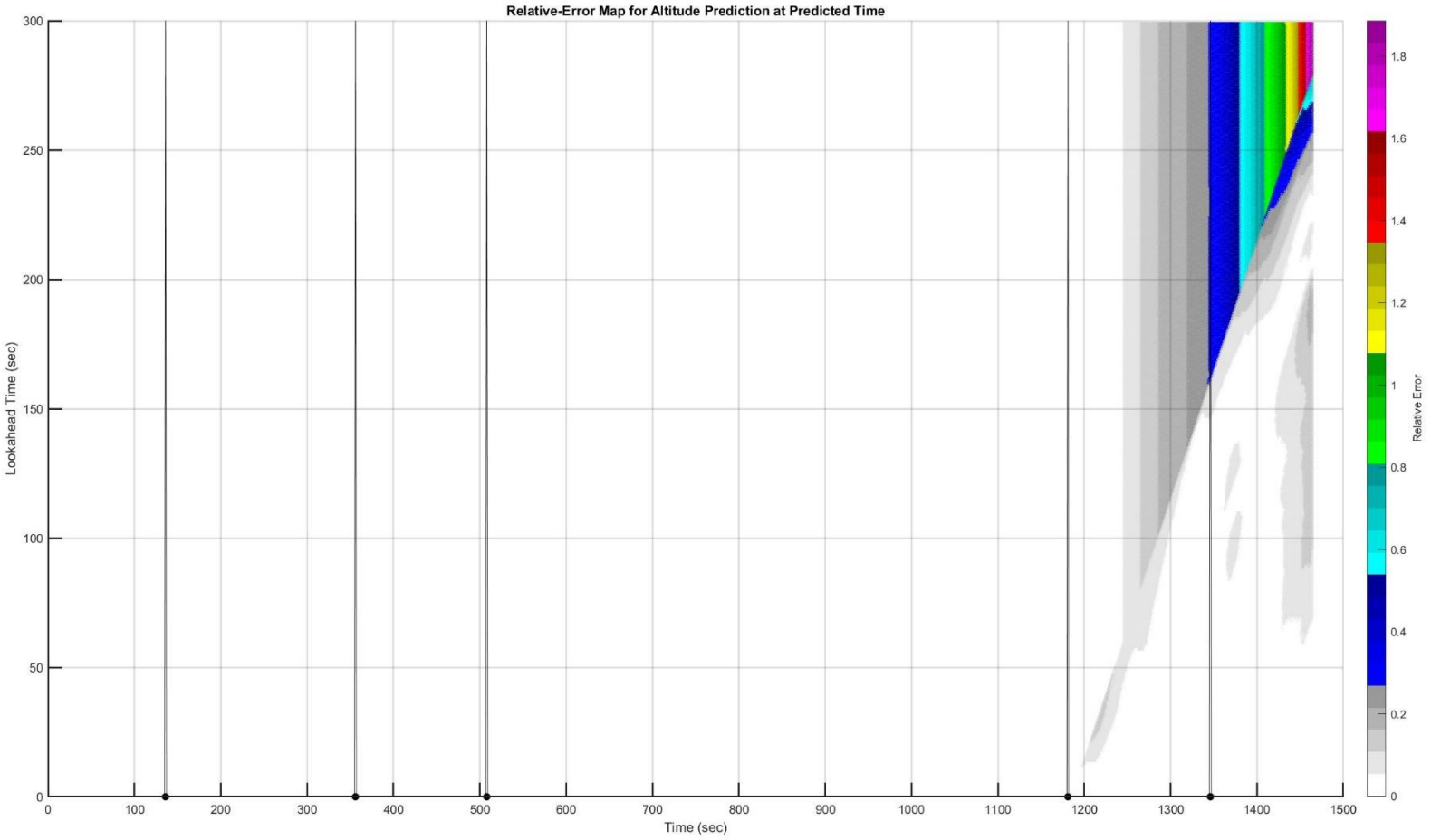

Figure C. 74: BRBBQ to Runway 27: Heatmap of Altitude Prediction Error (Time is $t + \tau$)

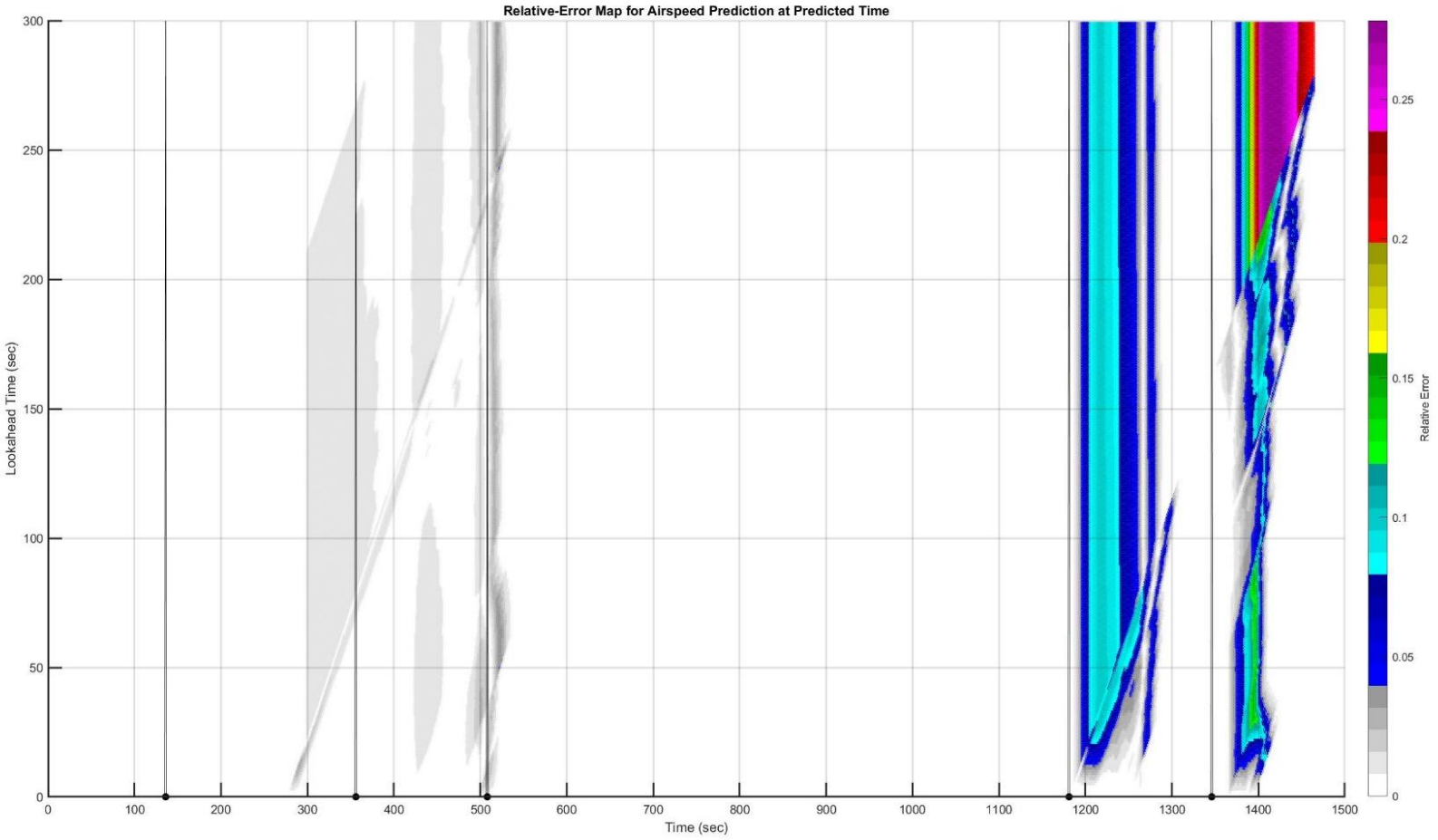

Figure C. 75: BRBBQ to Runway 27: Heatmap of Airspeed Prediction Error (Time is $t + \tau$)

C.16. Trajectory: BRBBQ to 36C

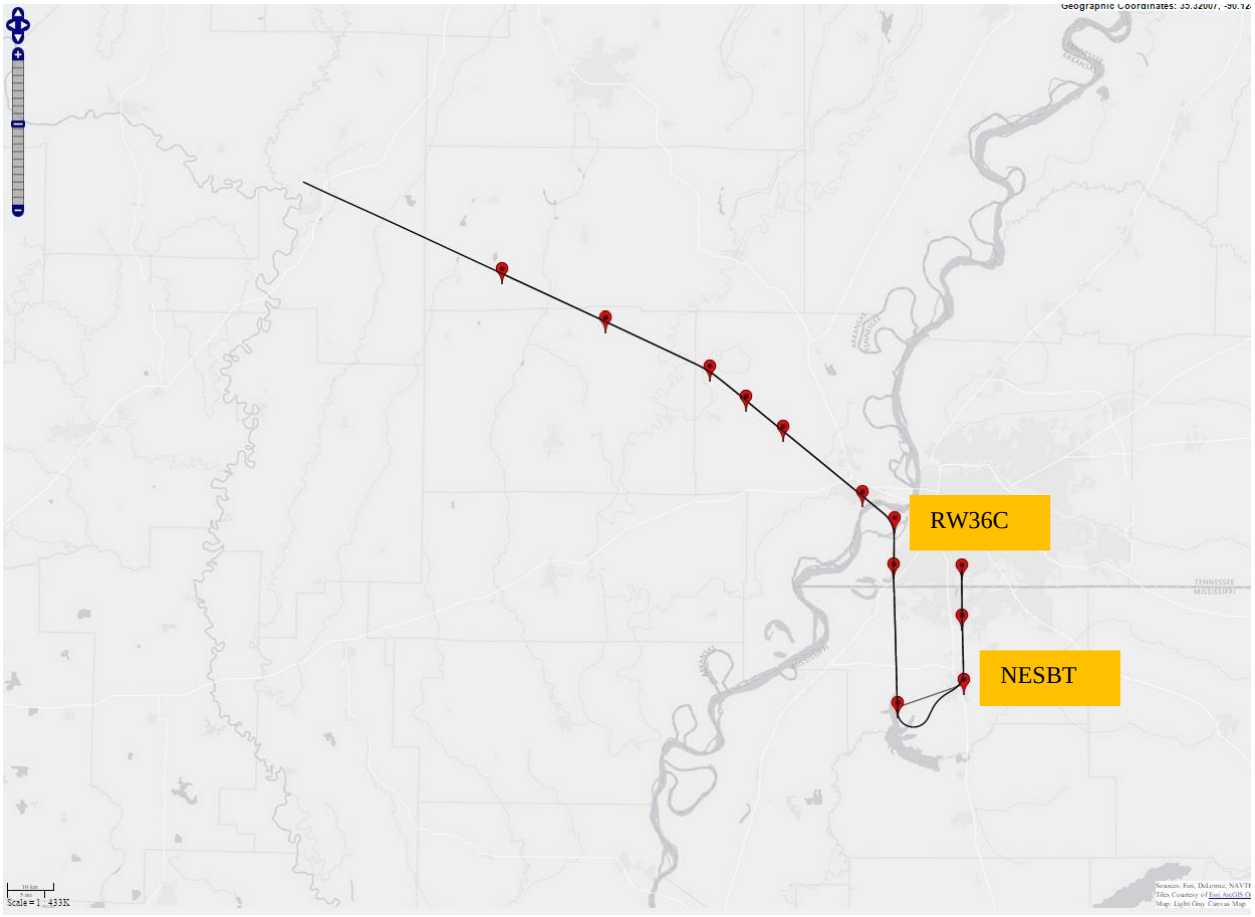

Figure C. 76: BRBBQ to Runway 36C: Planned and Actual Trajectories (Red markers indicate waypoints)

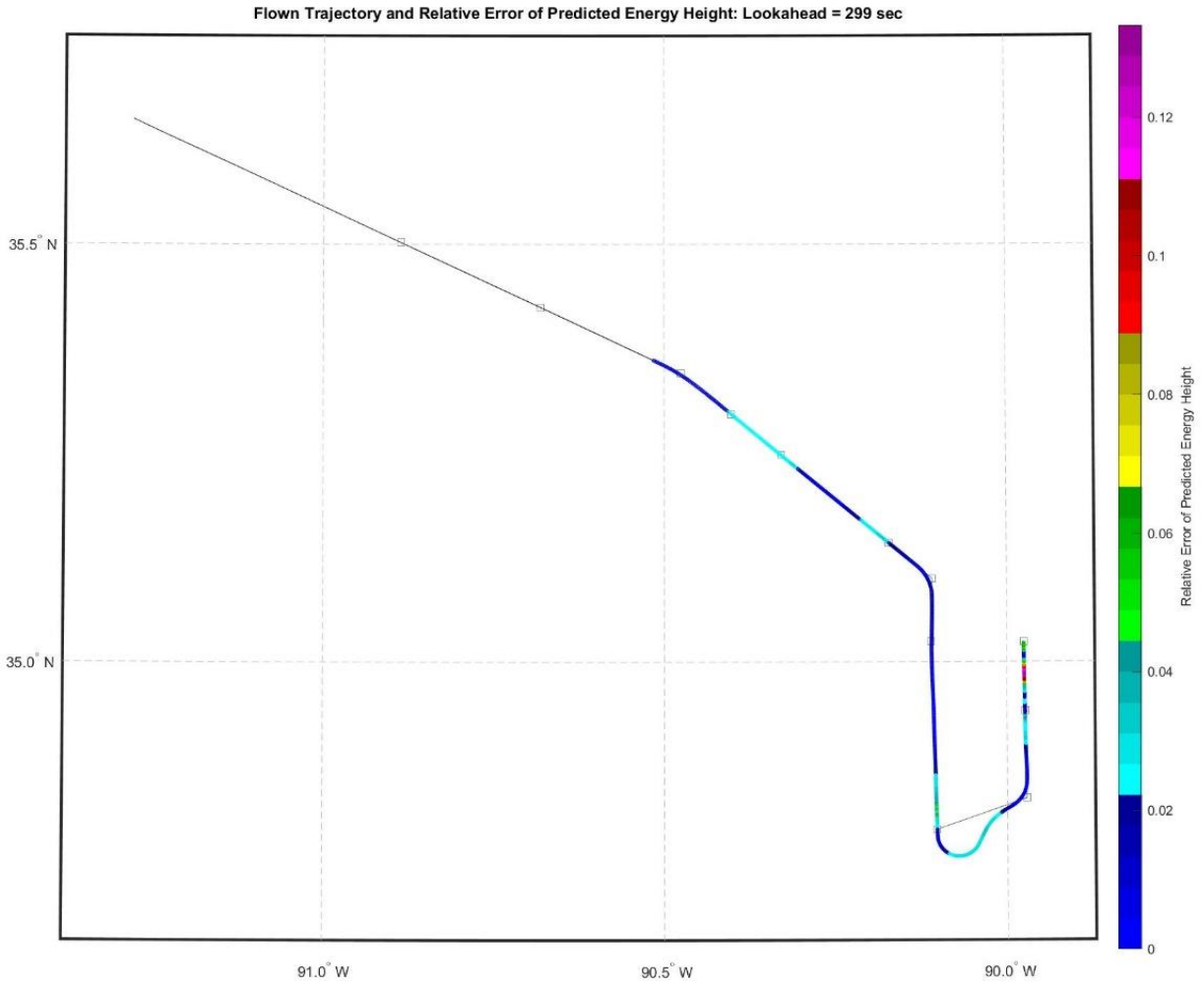

Figure C. 77: BRBBQ to Runway 36C: Lateral Path Color-Coded for Energy Prediction Error for Look-Ahead of 299 Seconds

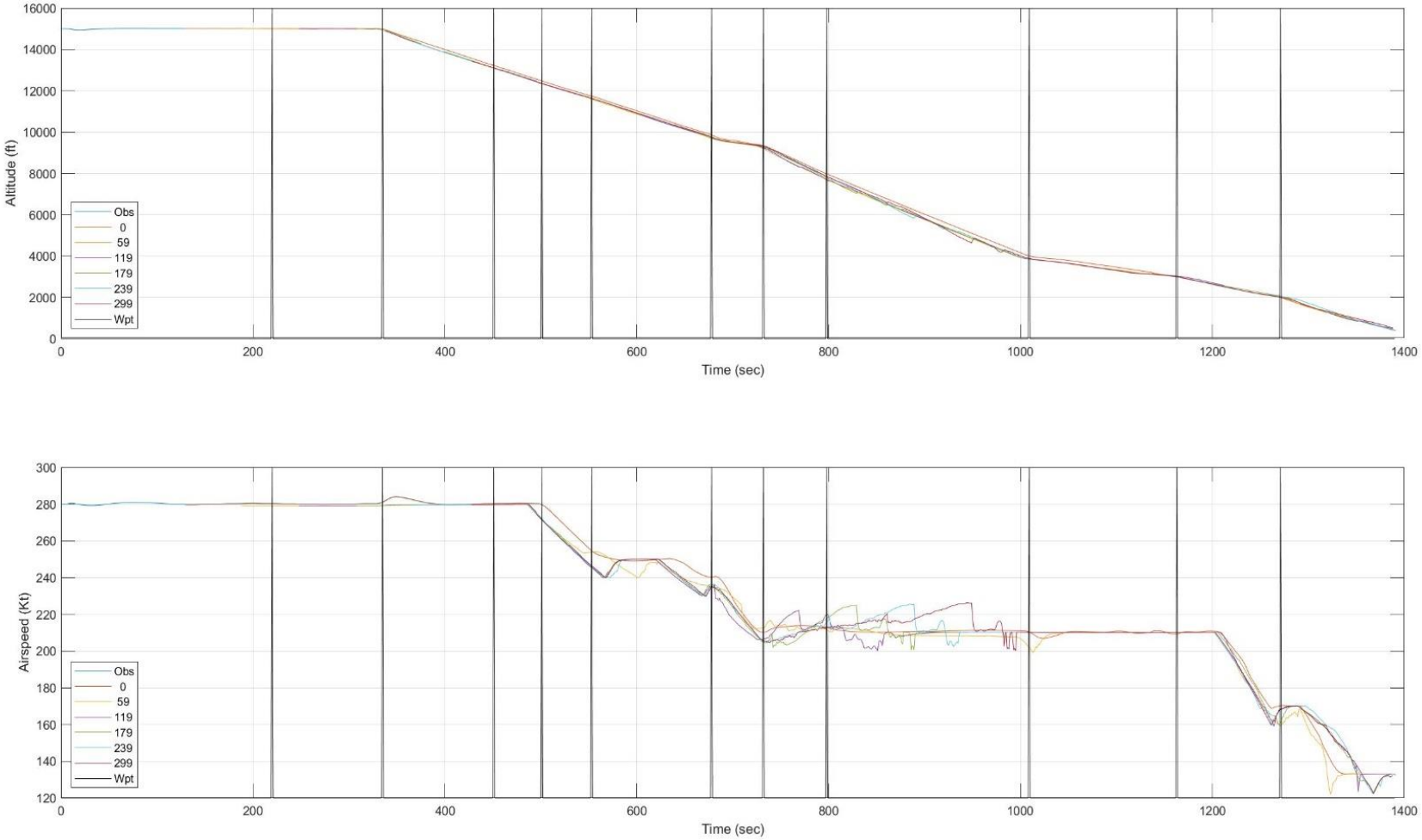

Figure C. 78: BRBBQ to Runway 36C: Time History of Predicted Altitude and Airspeed

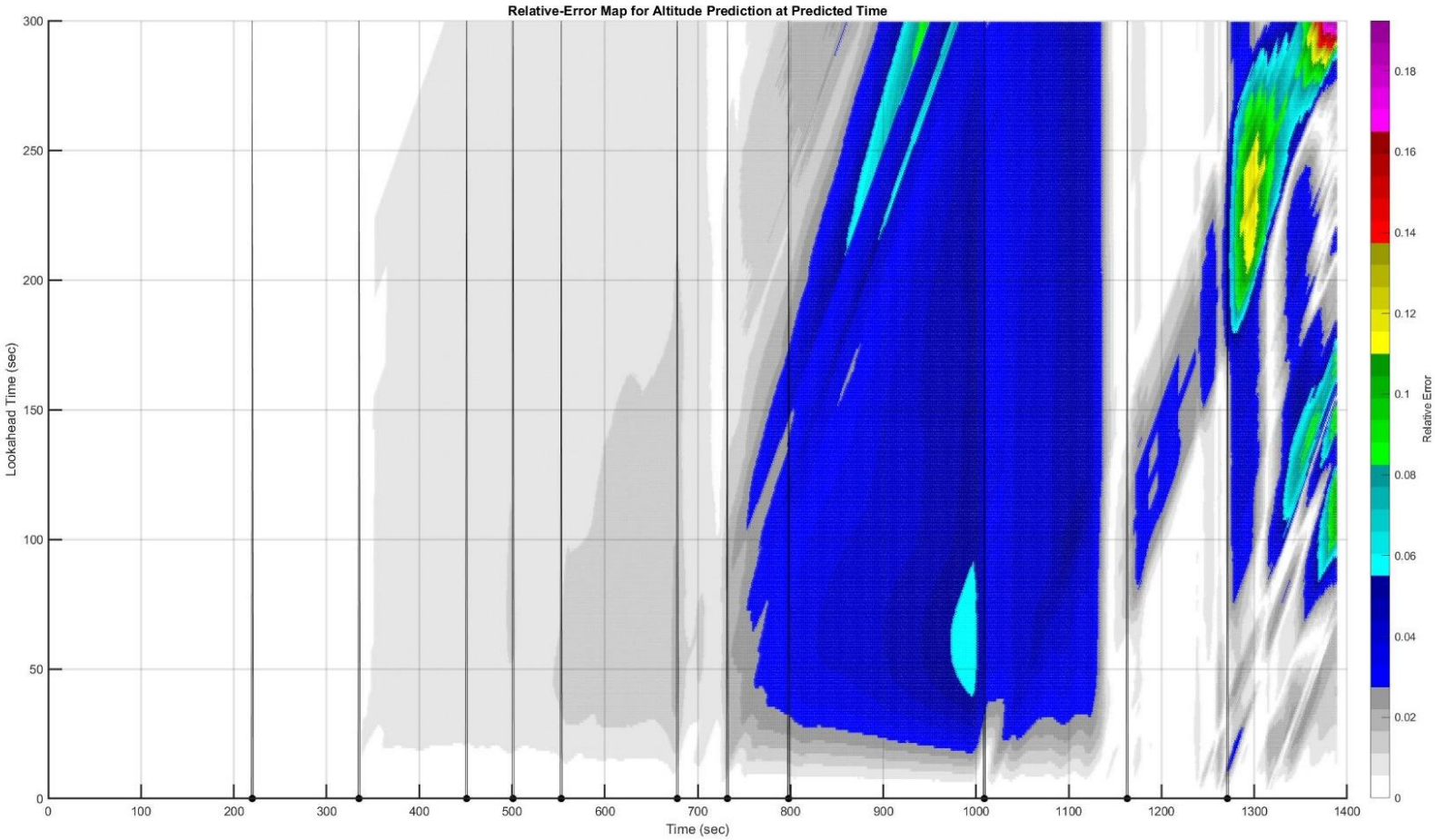

Figure C. 79: BRBBQ to Runway 36C: Heatmap of Altitude Prediction Error (Time is t + □)

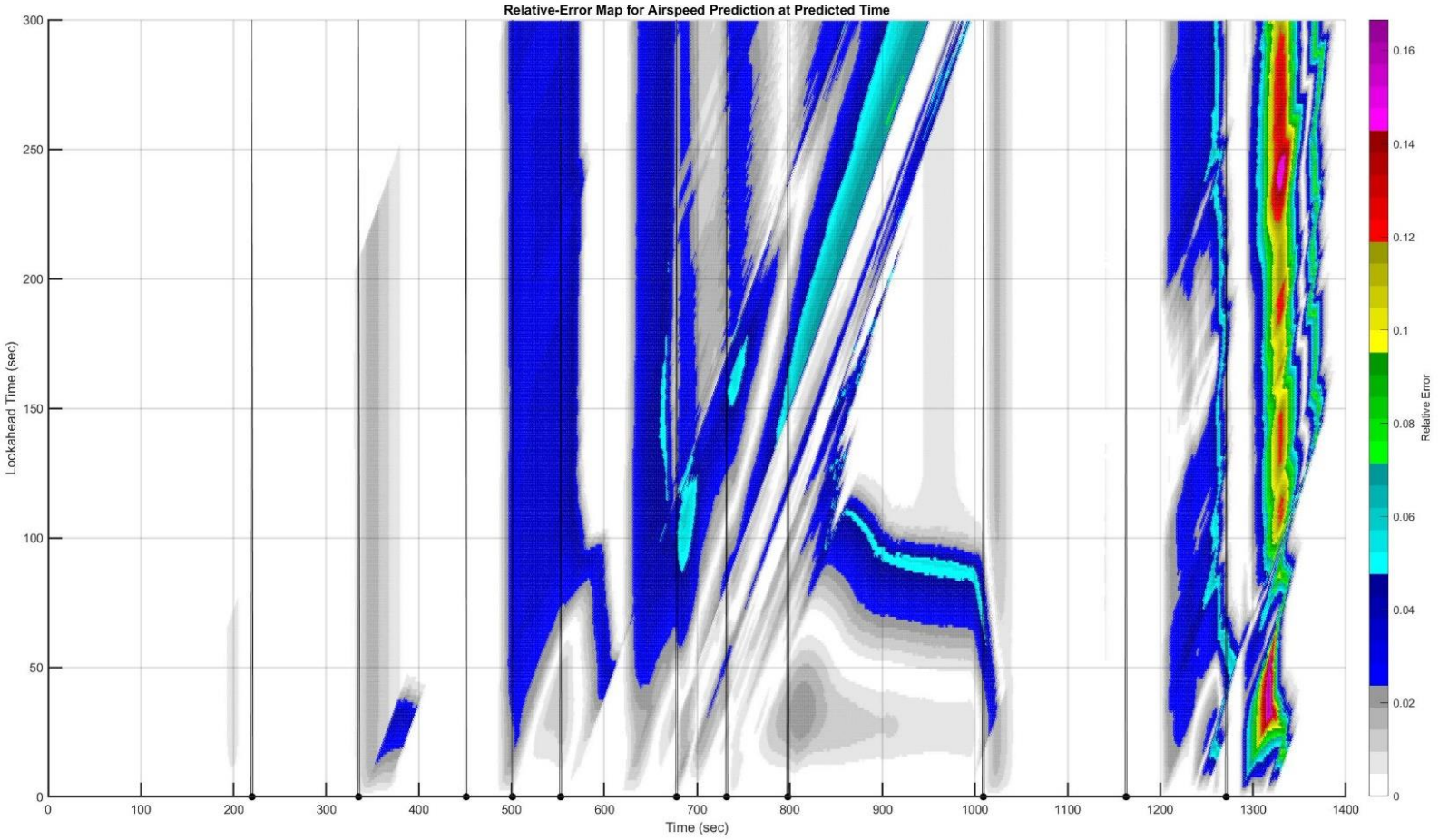

Figure C. 80: BRBBQ to Runway 36C: Heatmap of Airspeed Prediction Error (Time is $t + \tau$)

C.17. Trajectory: HYTHR to 09

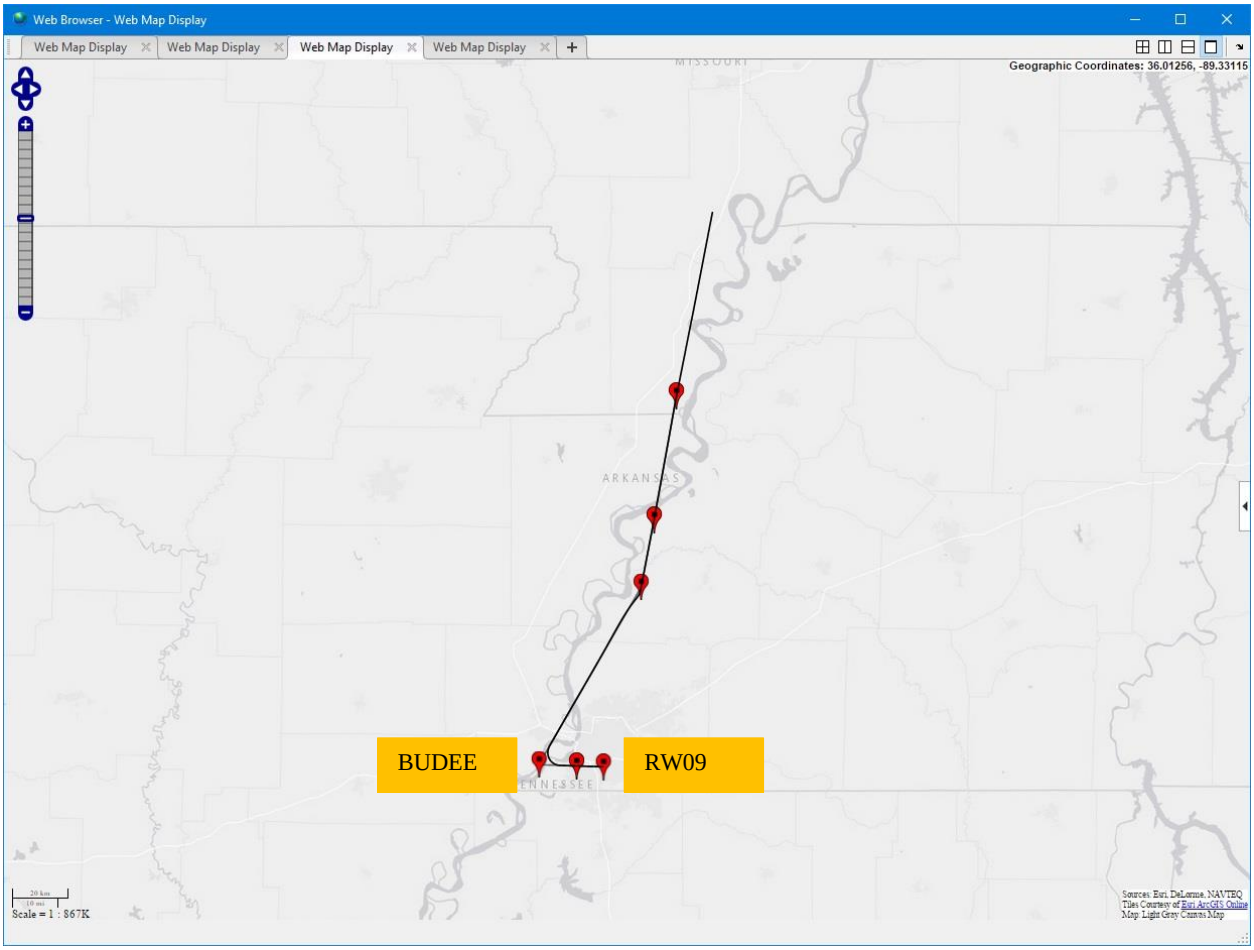

Figure C. 81: HYTHR to Runway 09: Planned and Actual Trajectories (Red markers indicate waypoints)

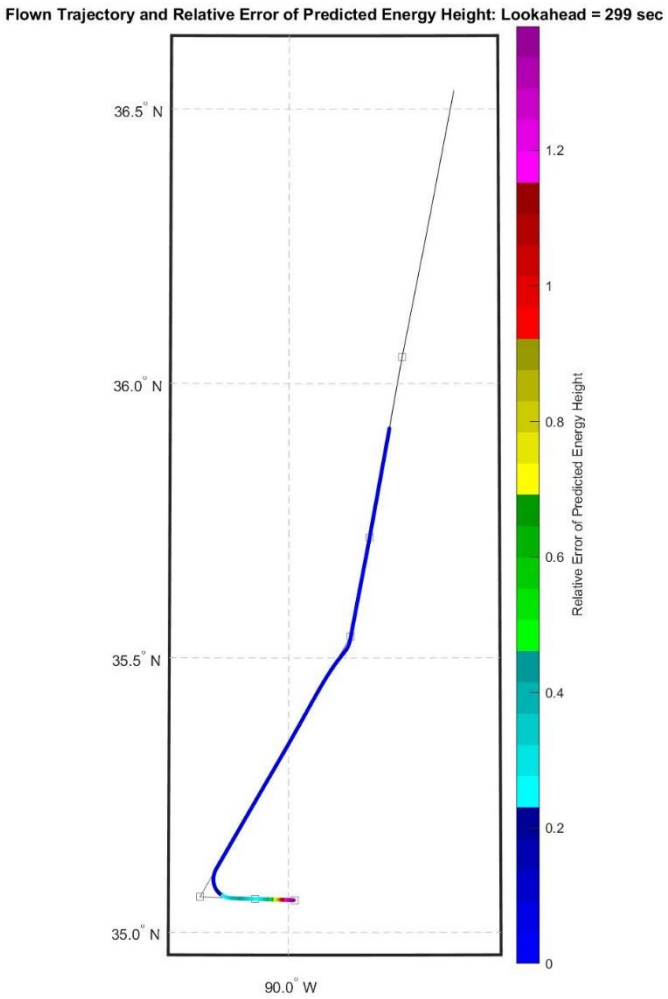

Figure C. 82: HYTHR to Runway 09: Lateral Path Color-Coded for Energy Prediction Error for Look-Ahead of 299 Seconds

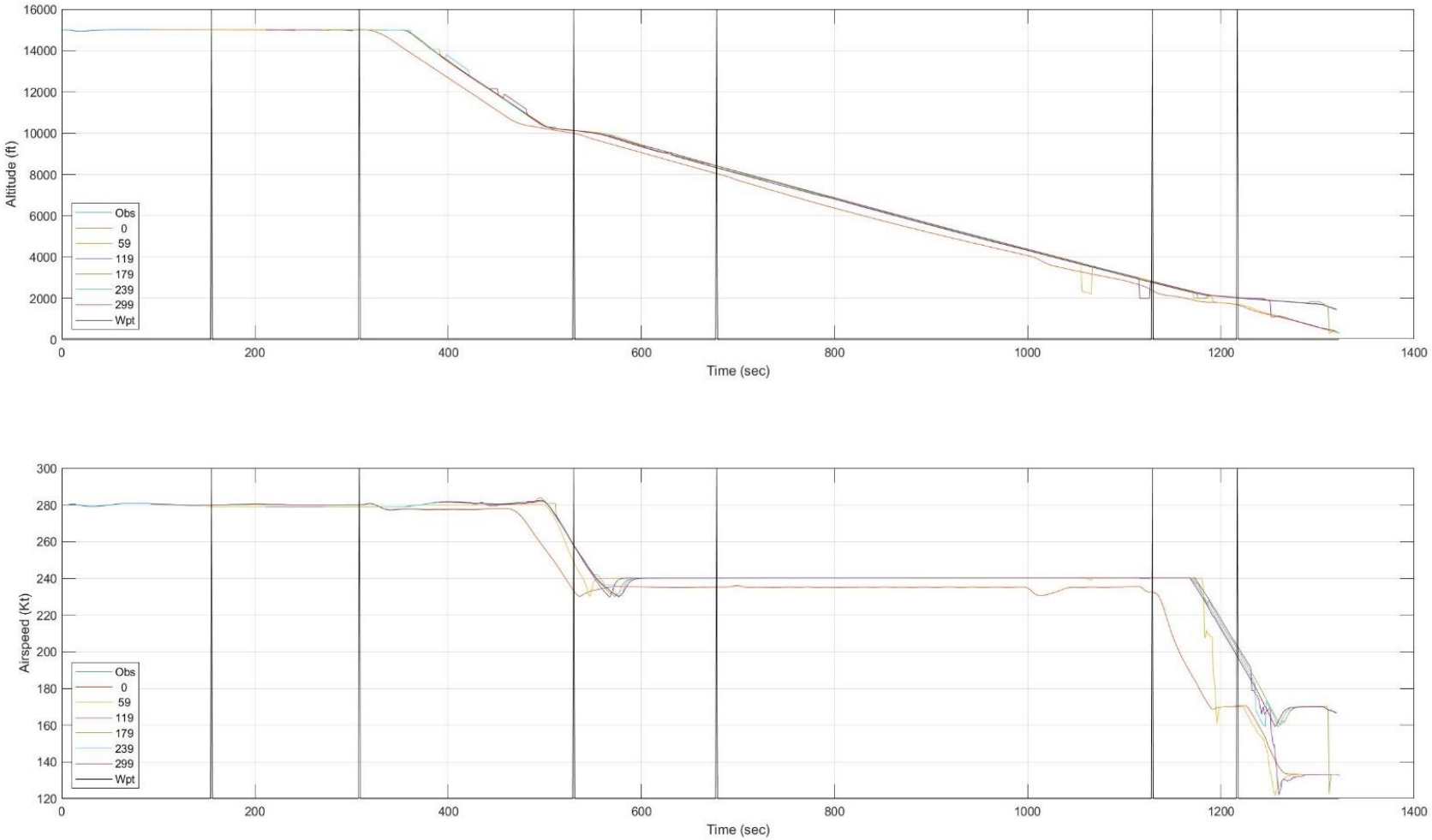

Figure C. 83: HYTHR to Runway 09: Time History of Predicted Altitude and Airspeed

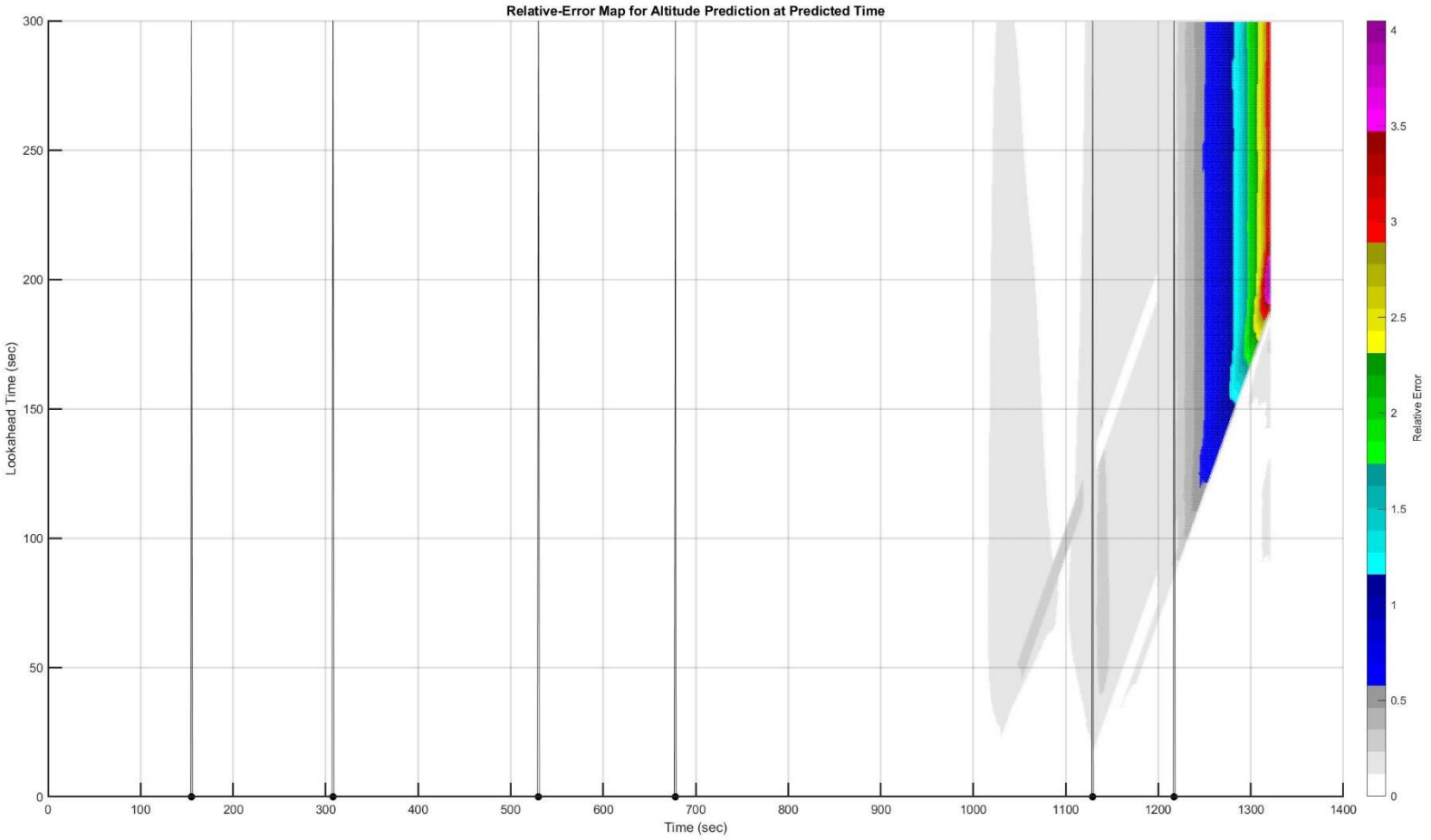

Figure C. 84: HYTHR to Runway 09: Heatmap of Altitude Prediction Error (Time is $t + \tau$)

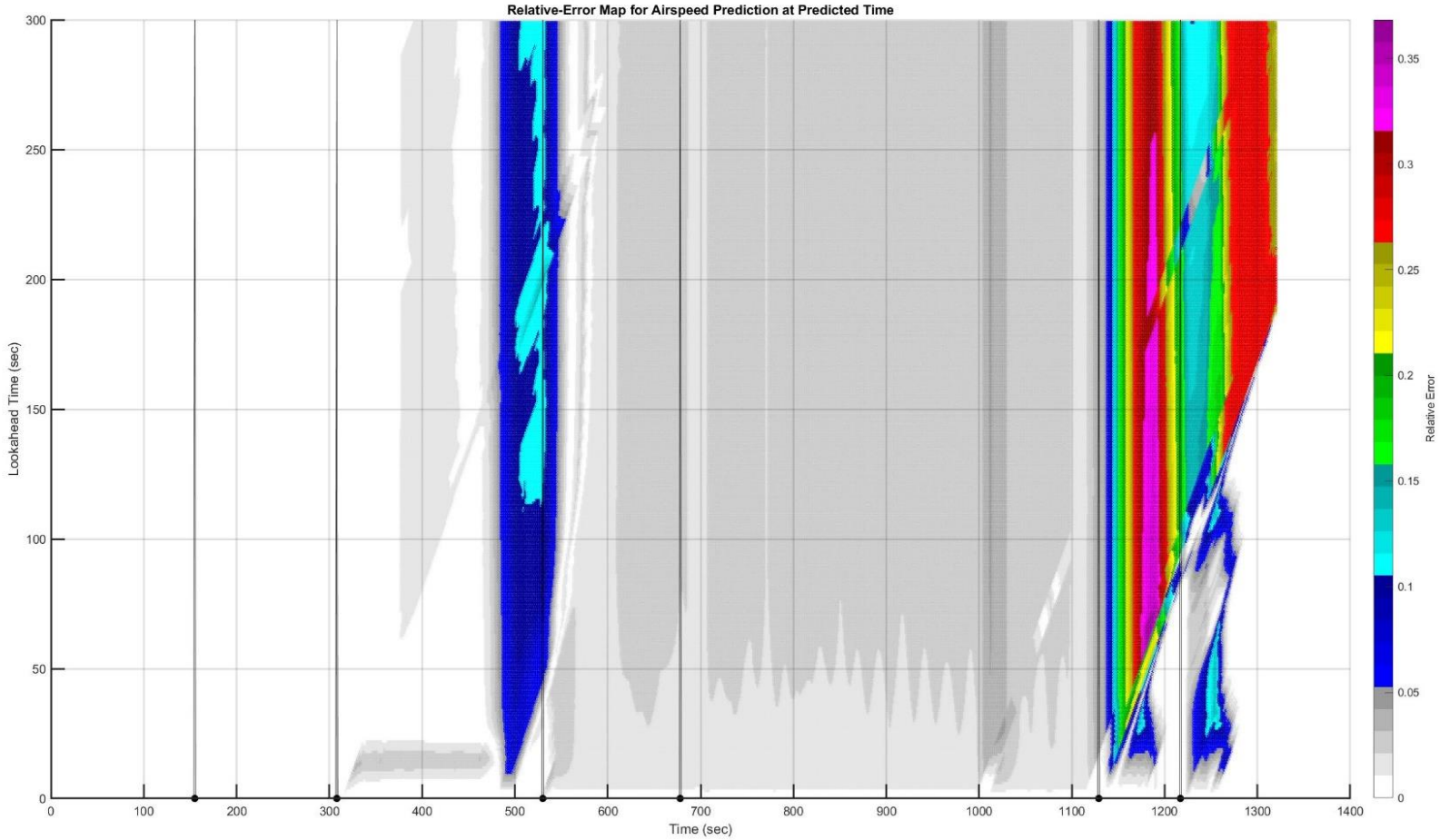

Figure C. 85: HYTHR to Runway 09: Heatmap of Airspeed Prediction Error (Time is $t + \tau$)

C.18. Trajectory: HYTHR to 18C

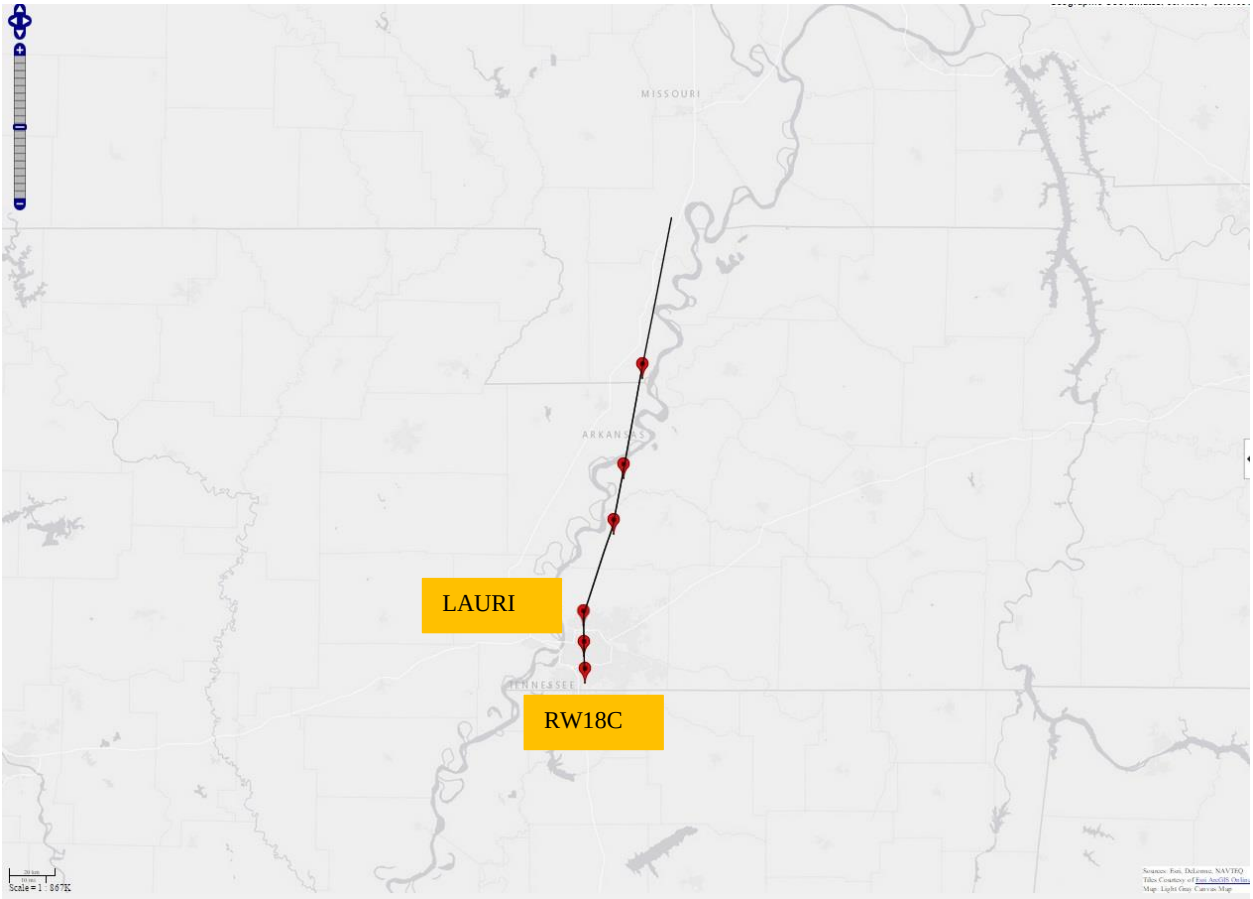

Figure C. 86: HYTHR to Runway 18C: Planned and Actual Trajectories (Red markers indicate waypoints)

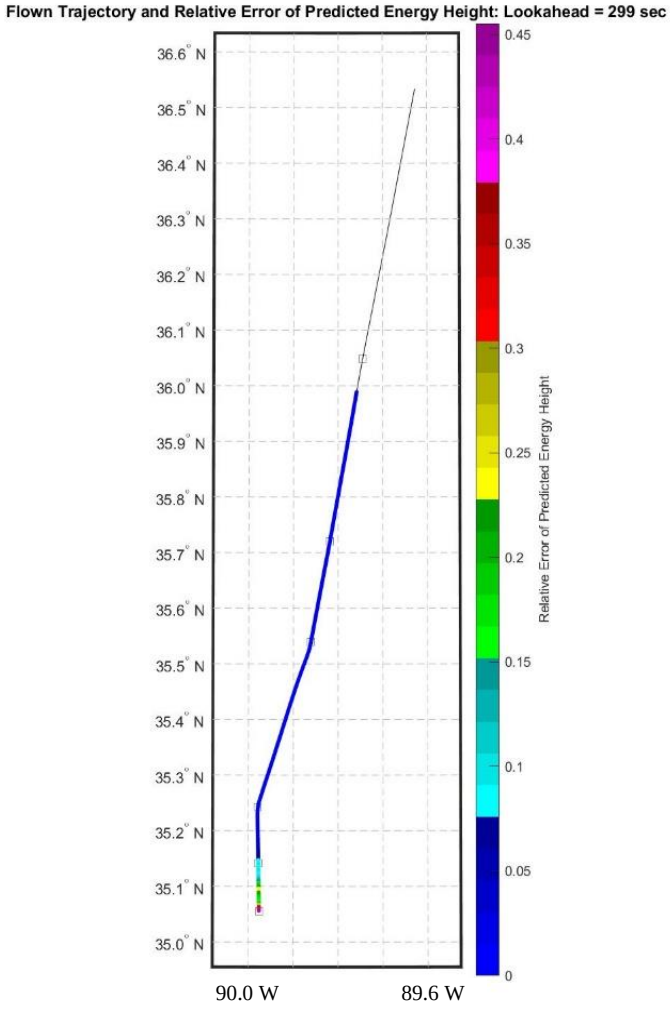

Figure C. 87: HYTHR to Runway 18C: Lateral Path Color-Coded for Energy Prediction Error for Look-Ahead of 299 Seconds

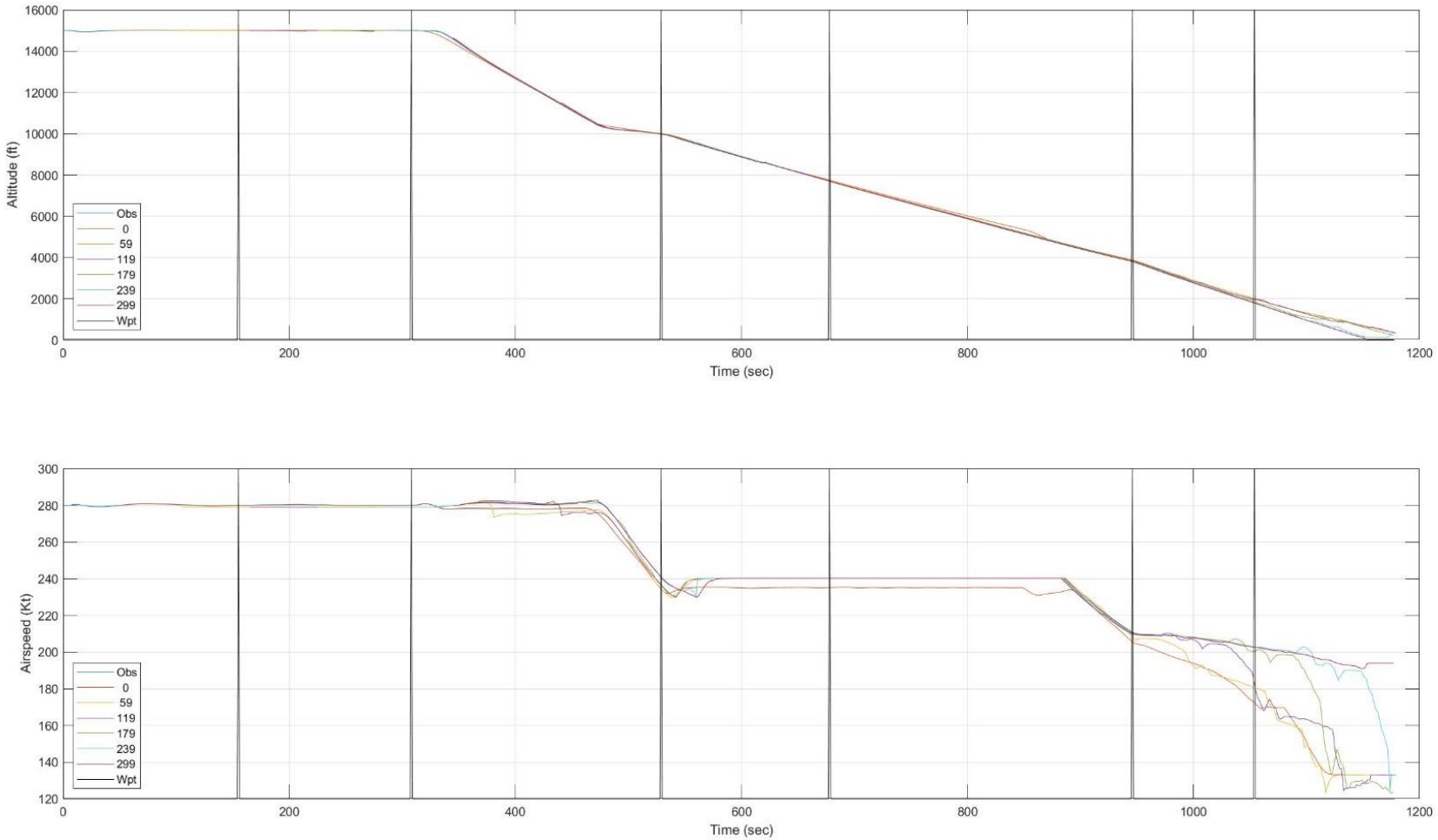

Figure C. 88: HYTHR to Runway 18C: Time History of Predicted Altitude and Airspeed

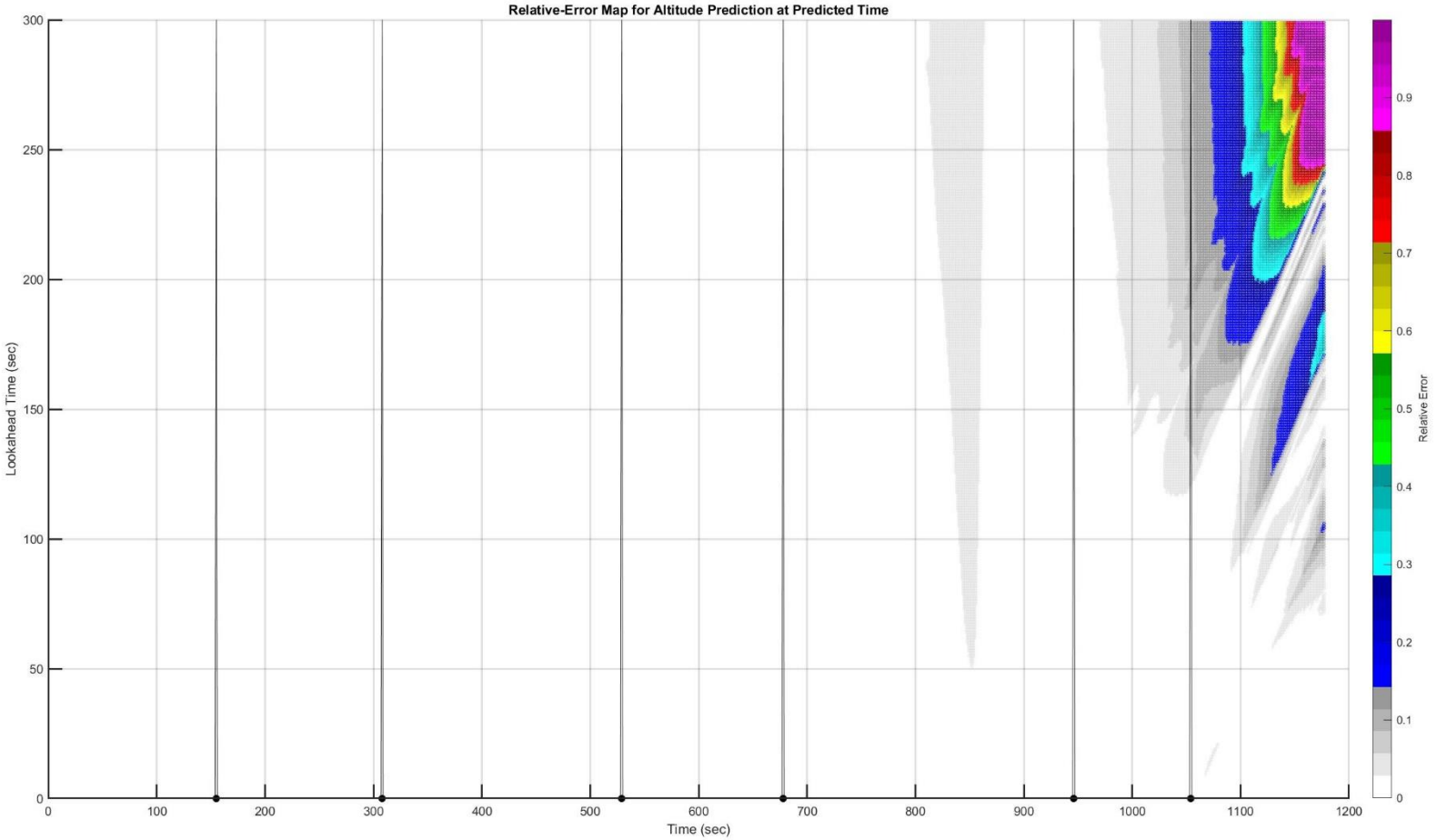

Figure C. 89: HYTHR to Runway 18C: Heatmap of Altitude Prediction Error (Time is $t + \tau$)

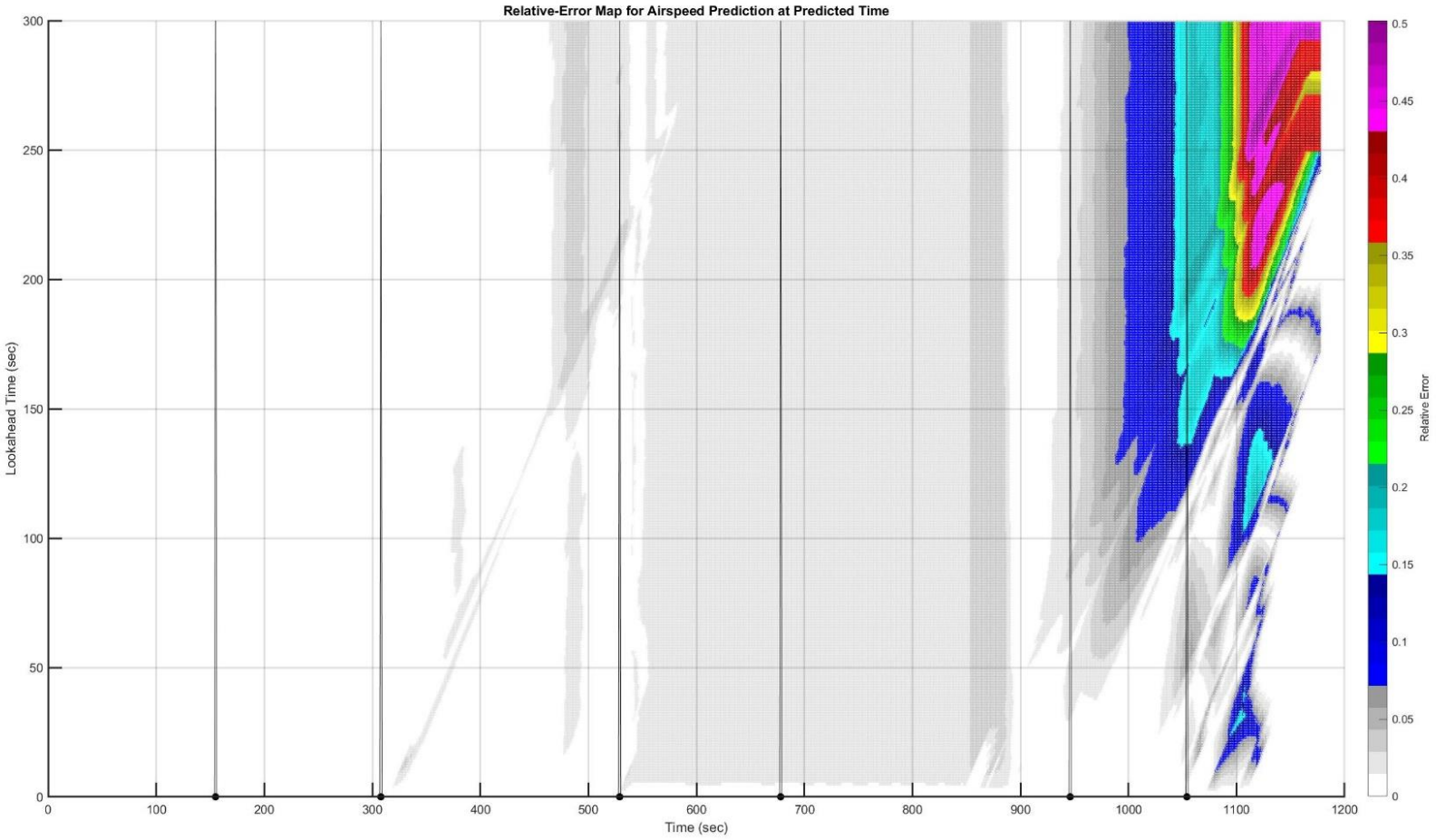

Figure C. 90: HYTHR to Runway 18C: Heatmap of Airspeed Prediction Error (Time is $t + \tau$)

C.19. Trajectory: HYTHR to 27

Figure C. 91: HYTHR to Runway 27: Planned and Actual Trajectories (Red markers indicate waypoints)

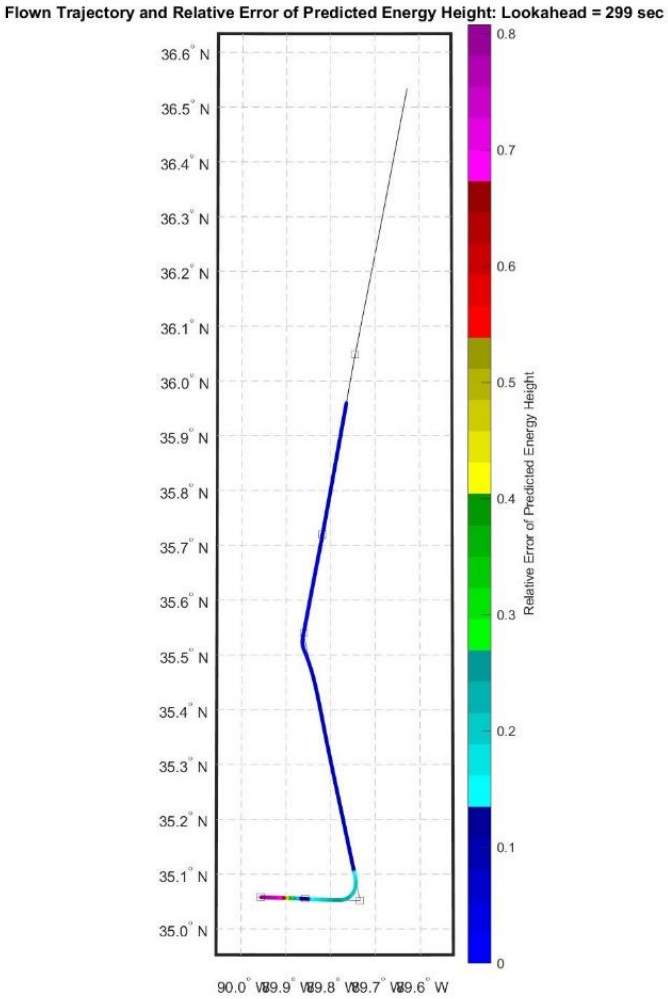

Figure C. 92: HYTHR to Runway 27: Lateral Path Color-Coded for Energy Prediction Error for Look-Ahead of 299 Seconds

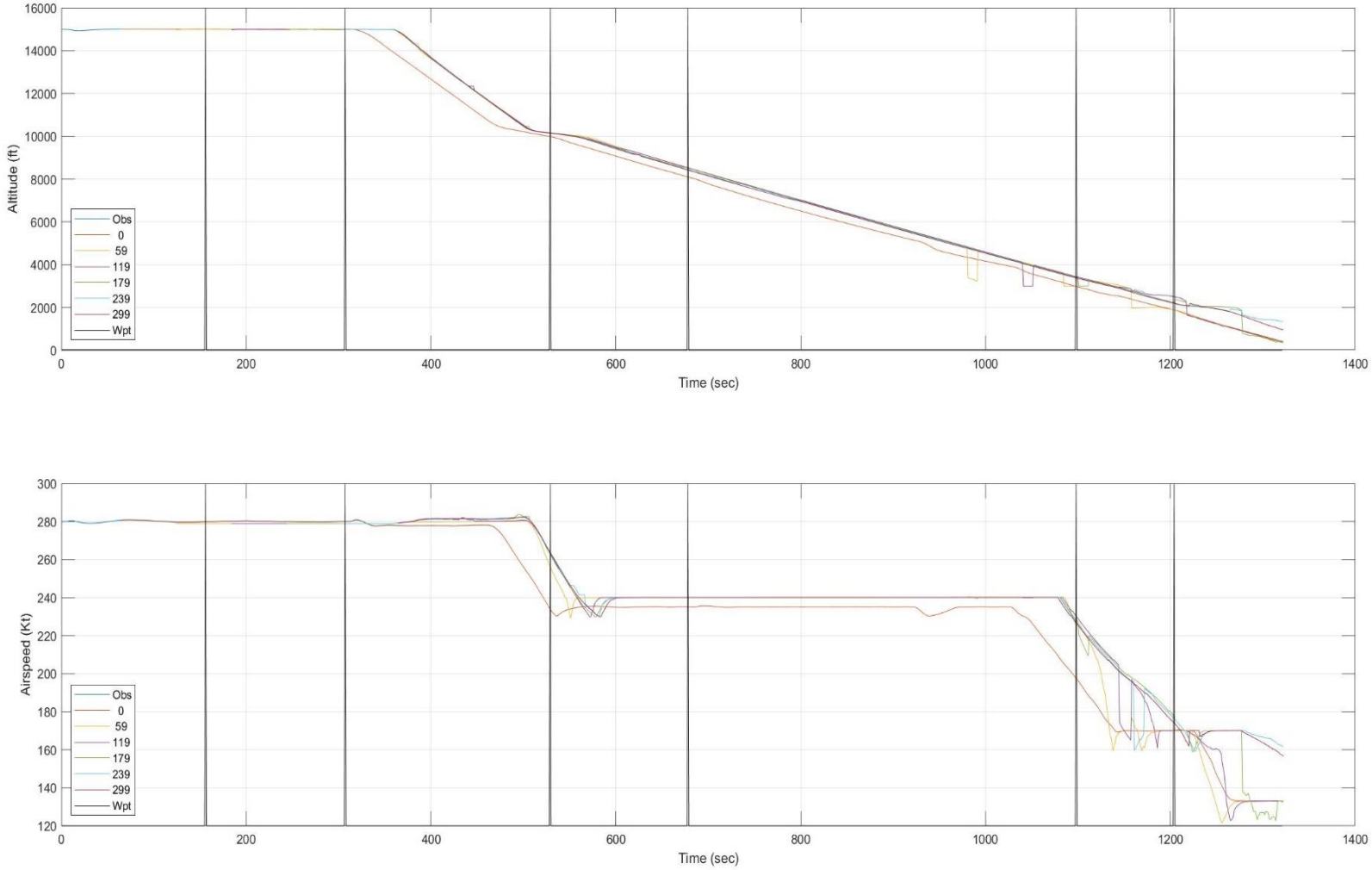

Figure C. 93: HYTHR to Runway 27: Time History of Predicted Altitude and Airspeed

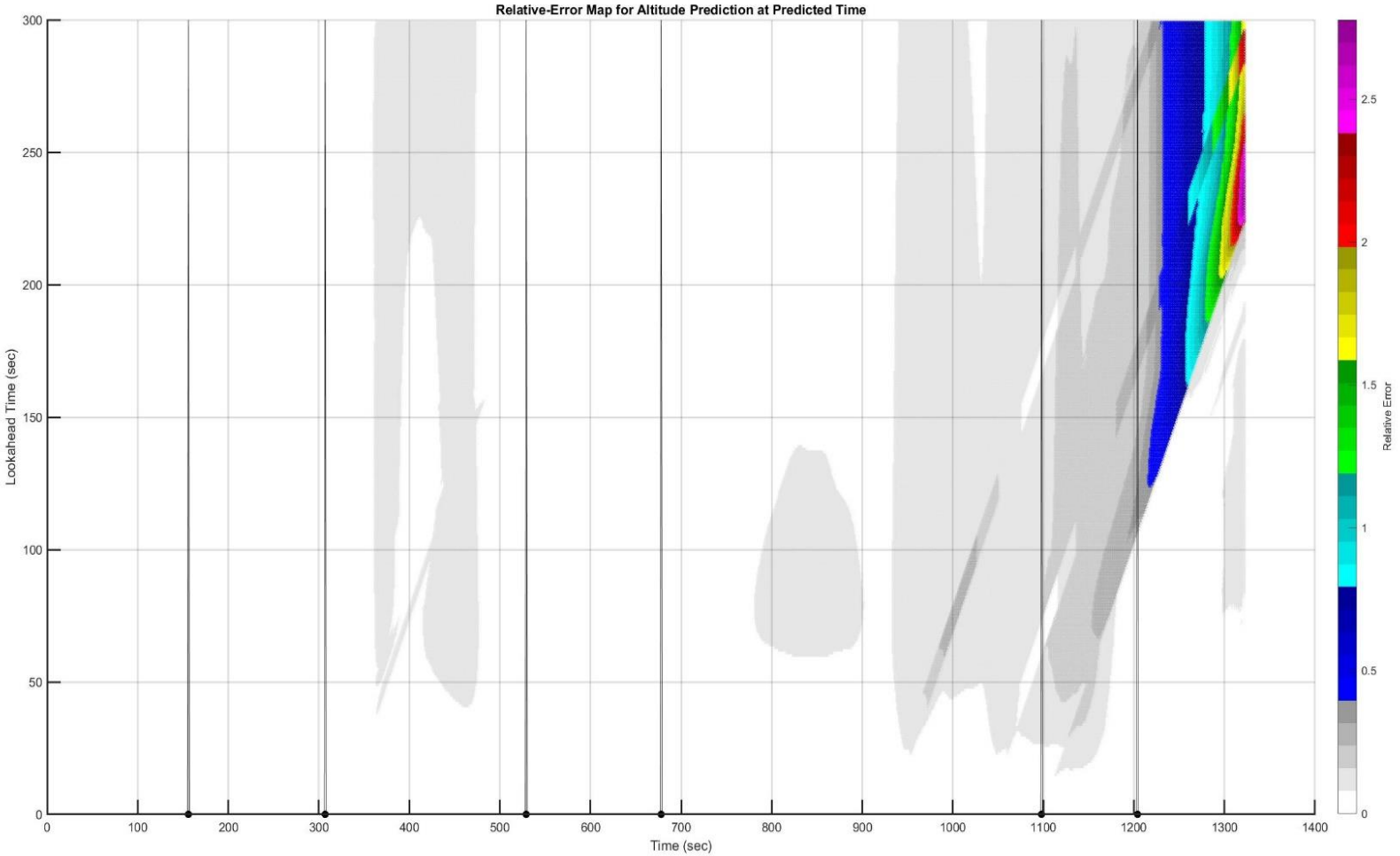

Figure C. 94: HYHTR to Runway 27: Heatmap of Altitude Prediction Error (Time is $t + \tau$)

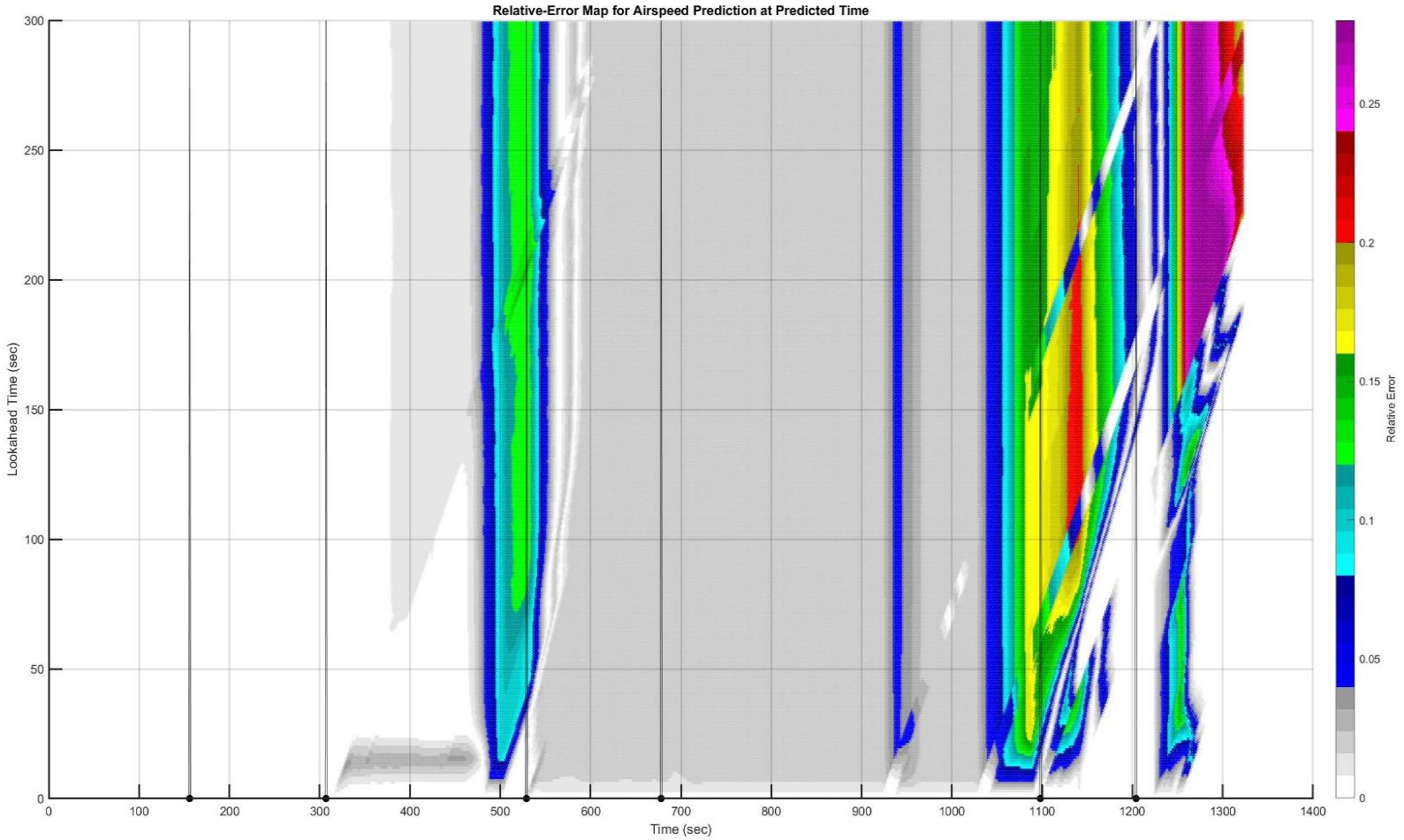

Figure C. 95: HYHTR to Runway 27: Heatmap of Airspeed Prediction Error (Time is $t + \tau$)

C.20. Trajectory: HYTHR to 36C

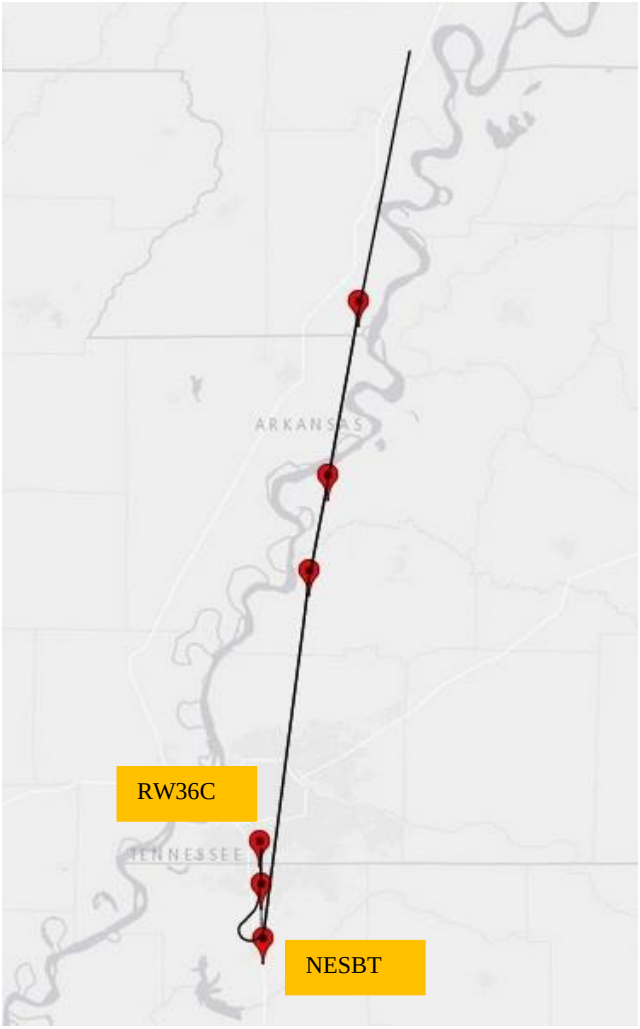

Figure C. 96: HYTHR to Runway 36C: Planned and Actual Trajectories (Red markers indicate waypoints)

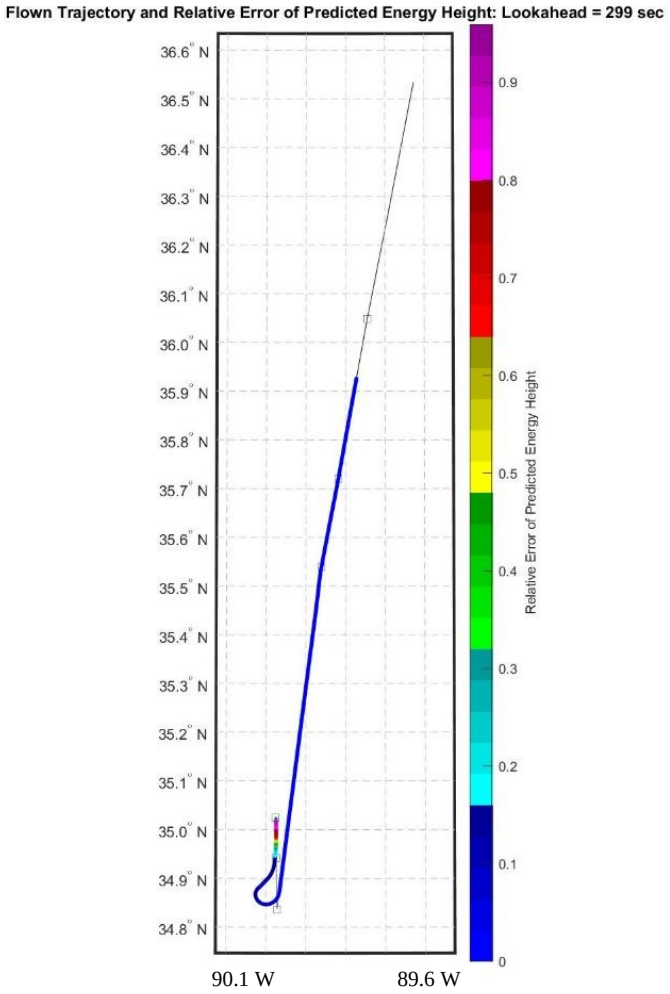

Figure C. 97: HYHTR to Runway 36C: Lateral Path Color-Coded for Energy Prediction Error for Look-Ahead of 299 Seconds

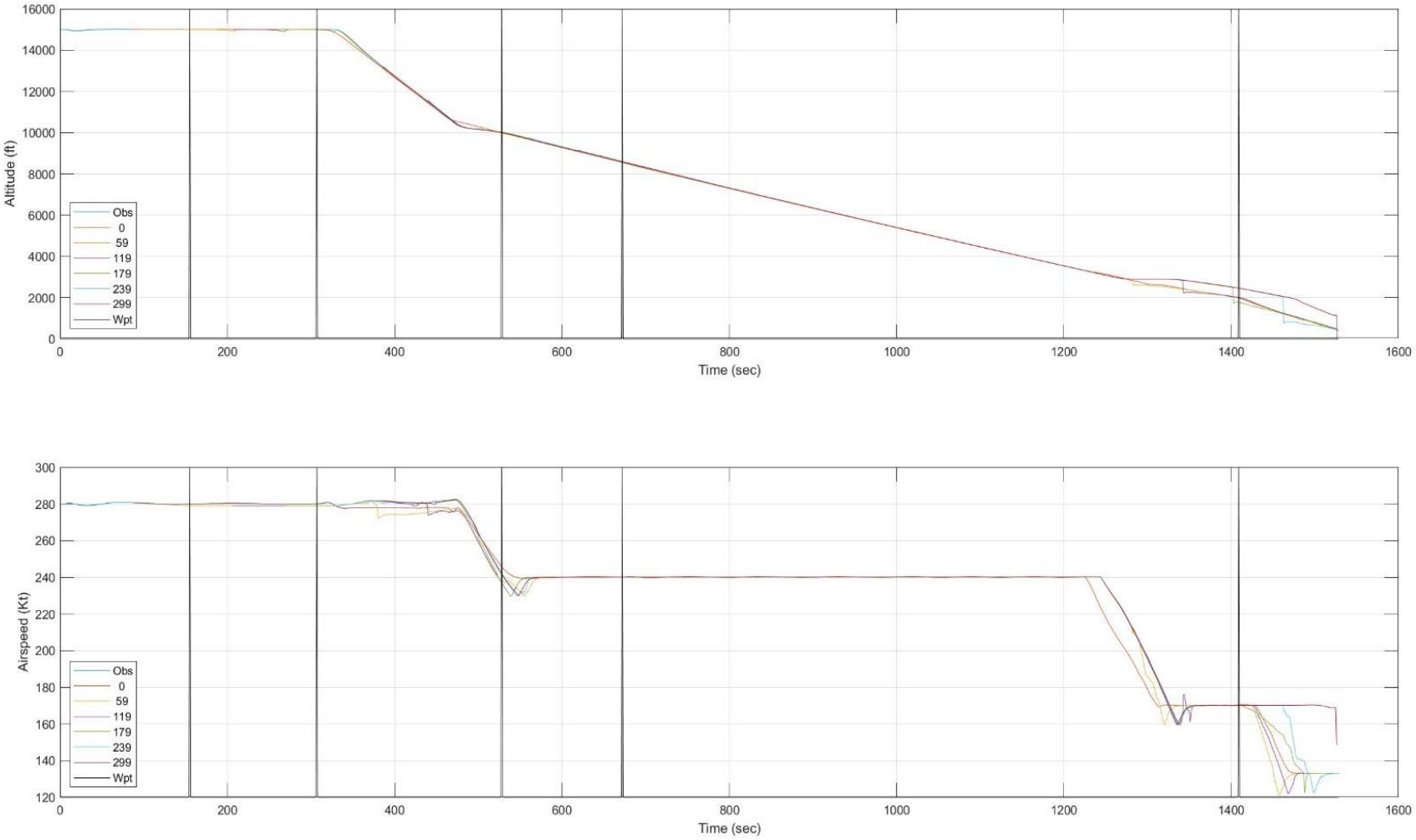

Figure C. 98: HYTHR to Runway 36C: Time History of Predicted Altitude and Airspeed

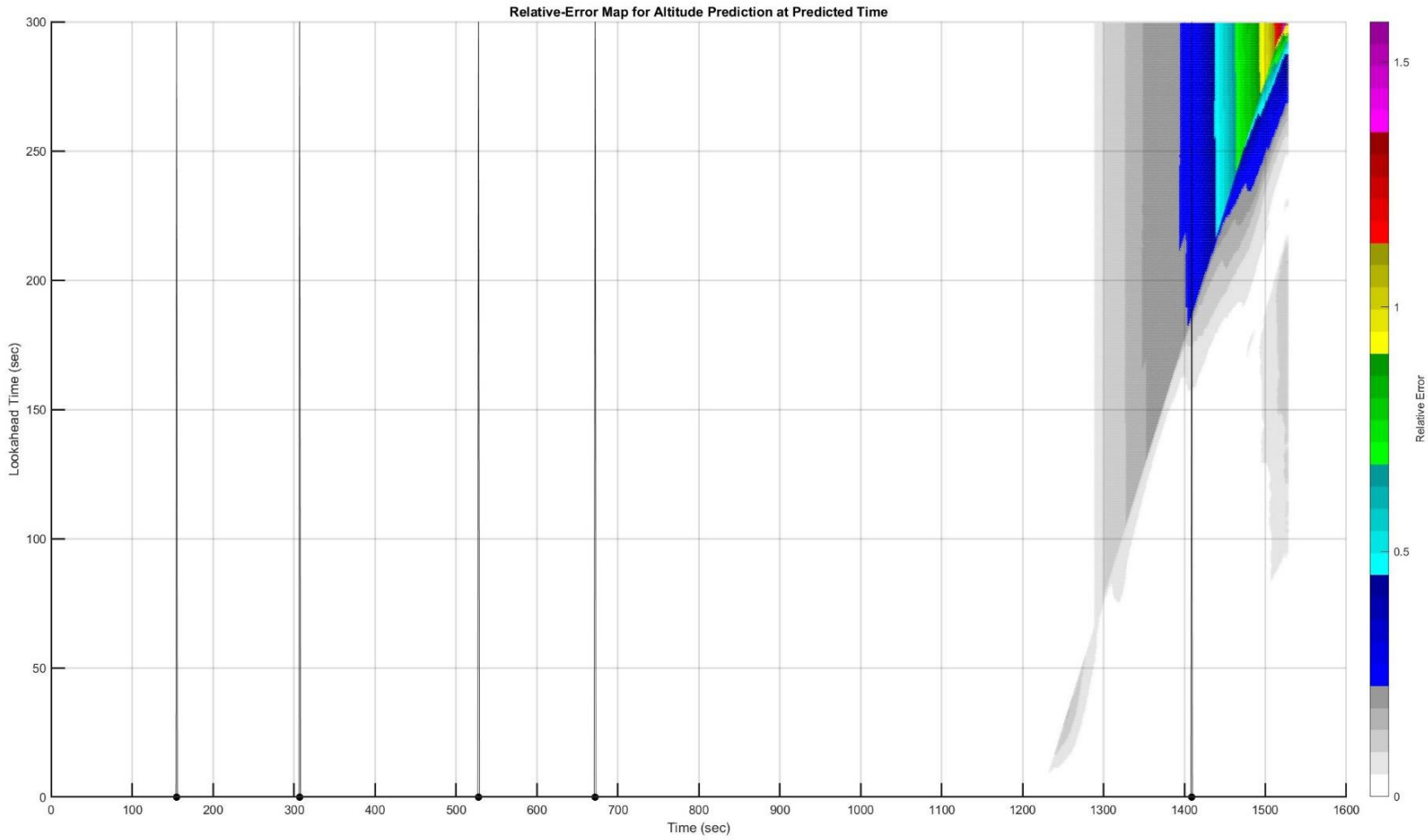

Figure C. 99: HYTHR to Runway 36C: Heatmap of Altitude Prediction Error (Time is $t + \tau$)

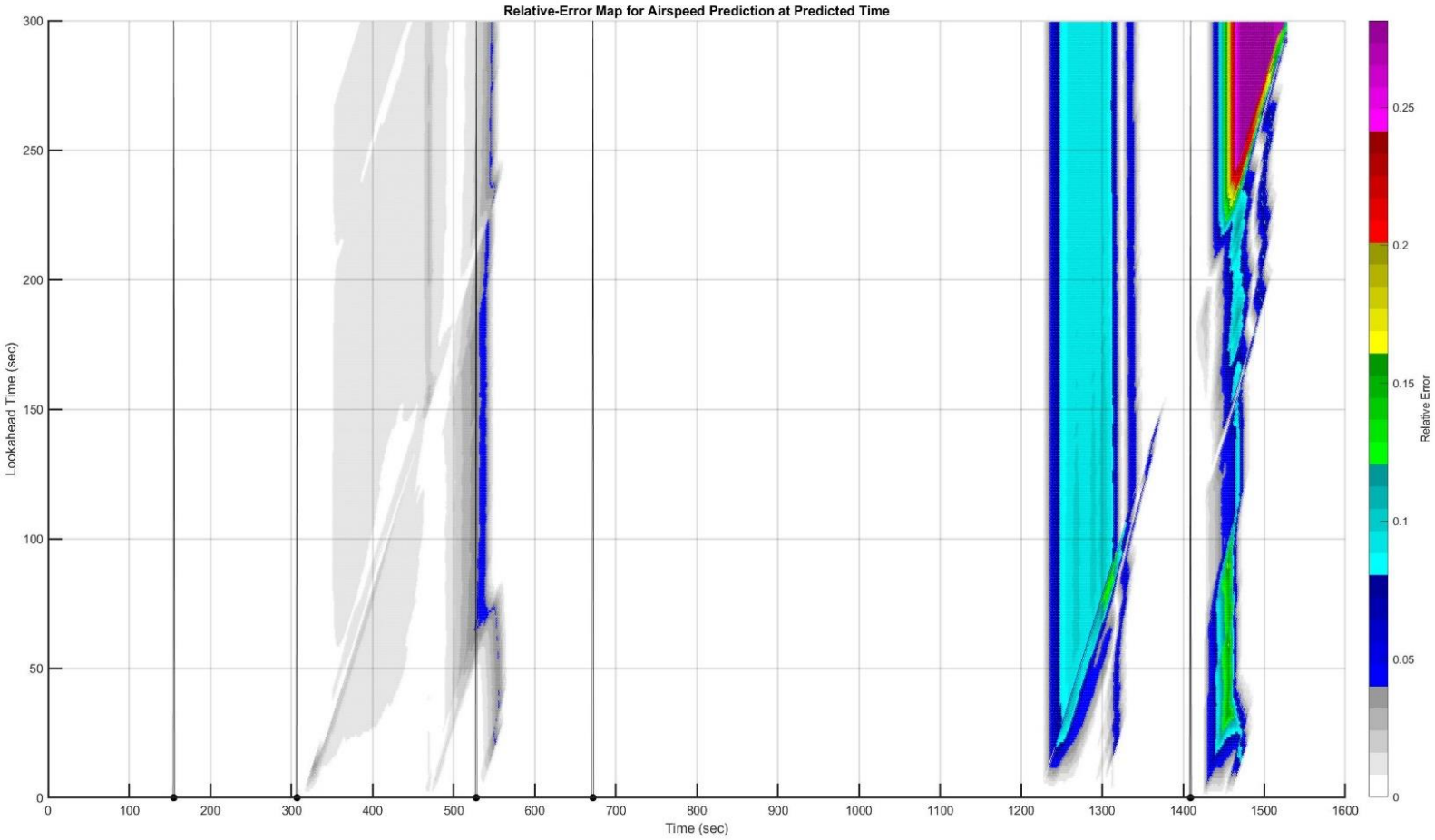

Figure C. 100: HYTHR to Runway 36C: Heatmap of Airspeed Prediction Error (Time is $t + \tau$)

C.21. Trajectory: MONAA to 09

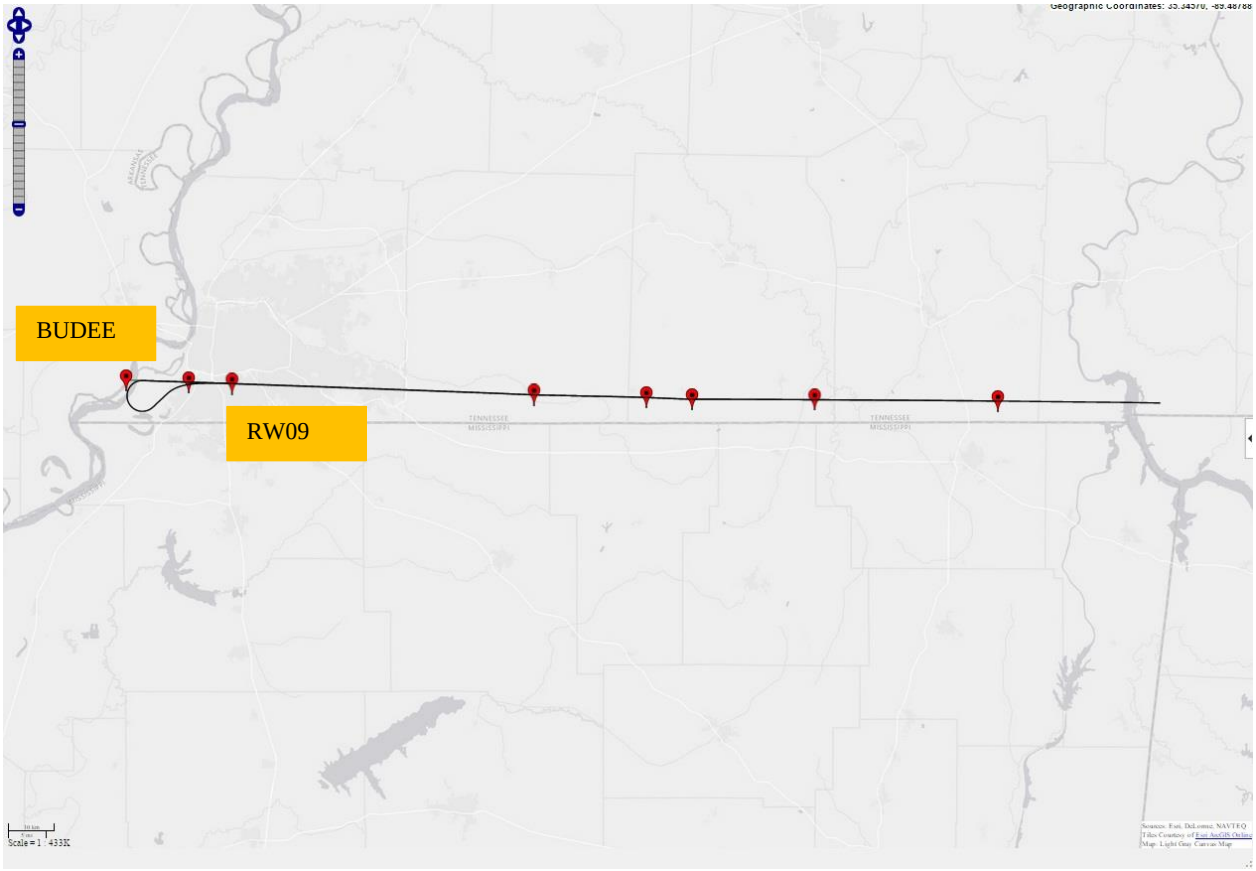

Figure C. 101: MONAA to Runway 09: Planned and Actual Trajectories (Red markers indicate waypoints)

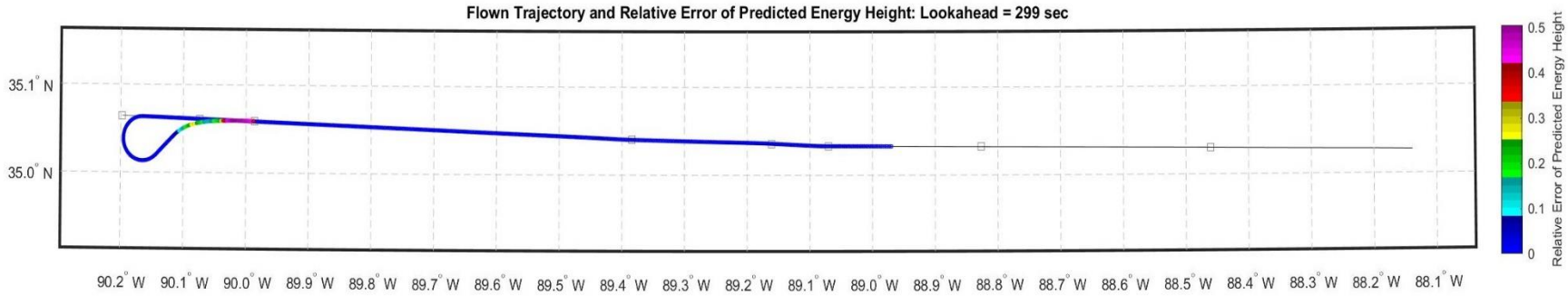

Figure C. 102: MONAA to Runway 09: Lateral Path Color-Coded for Energy Prediction Error for Look-Ahead of 299 Seconds

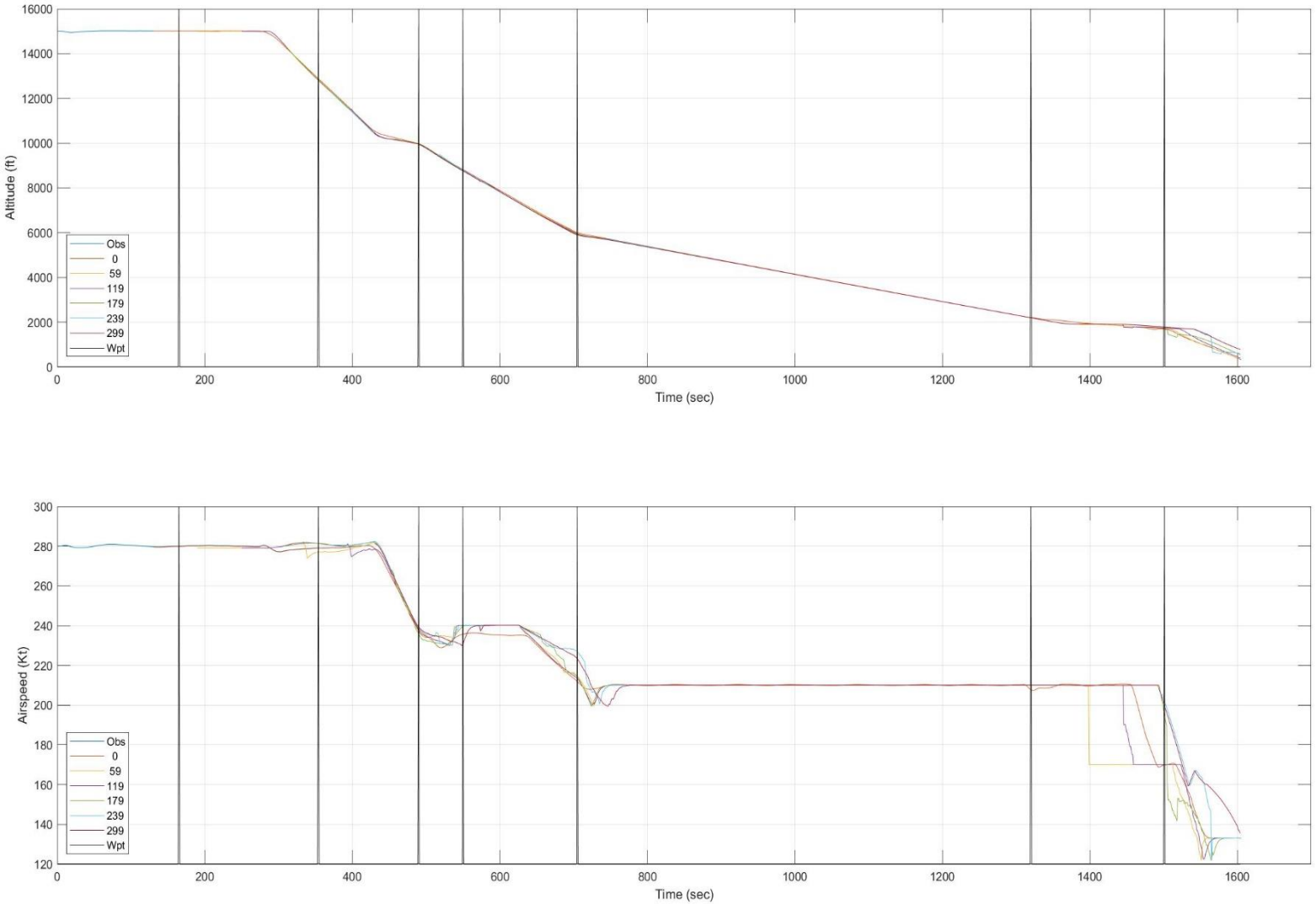

Figure C. 103: MONAA to Runway 09: Time History of Predicted Altitude and Airspeed

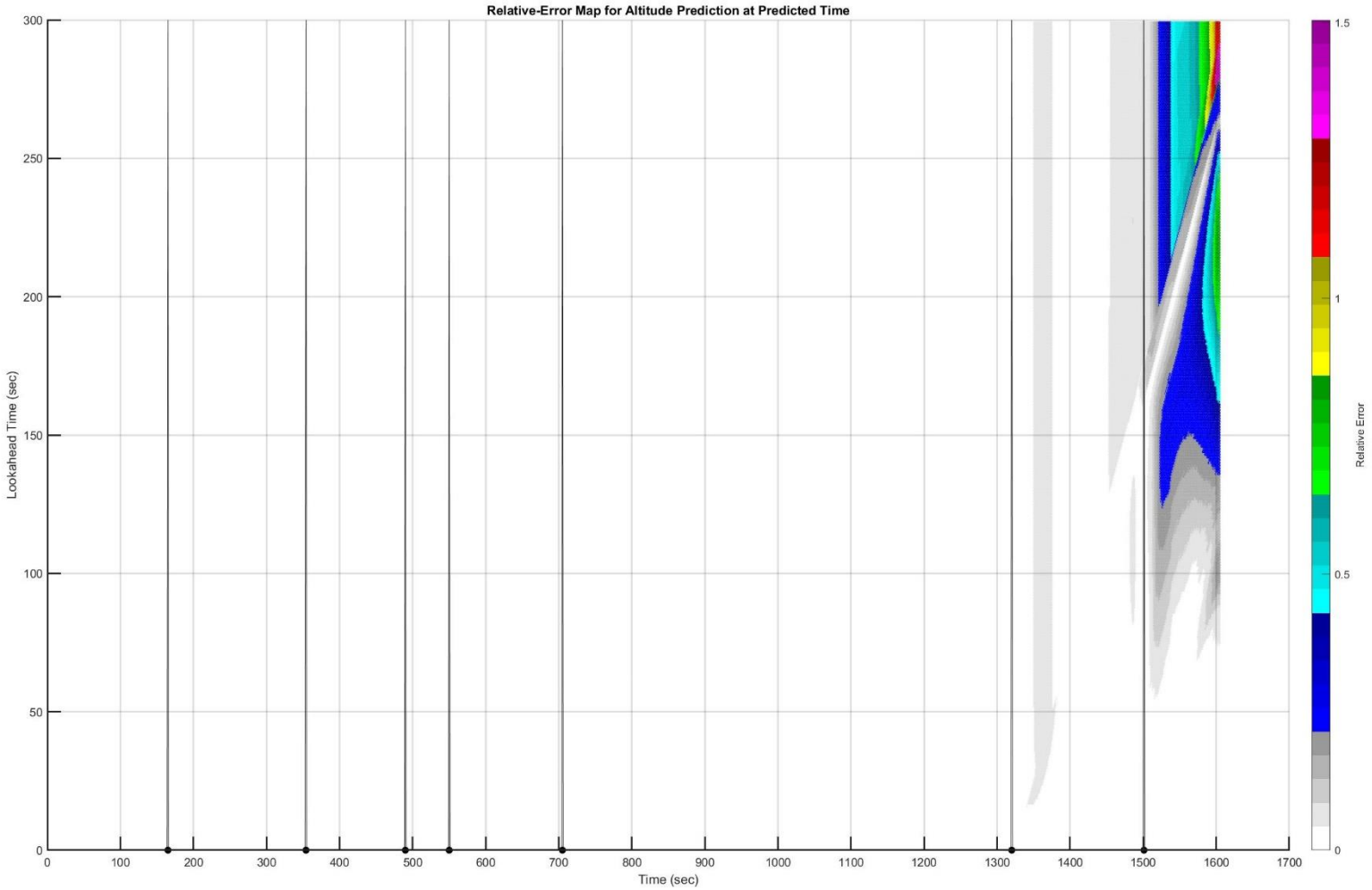

Figure C. 104: MONAA to Runway 09: Heatmap of Altitude Prediction Error (Time is $t + \tau$)

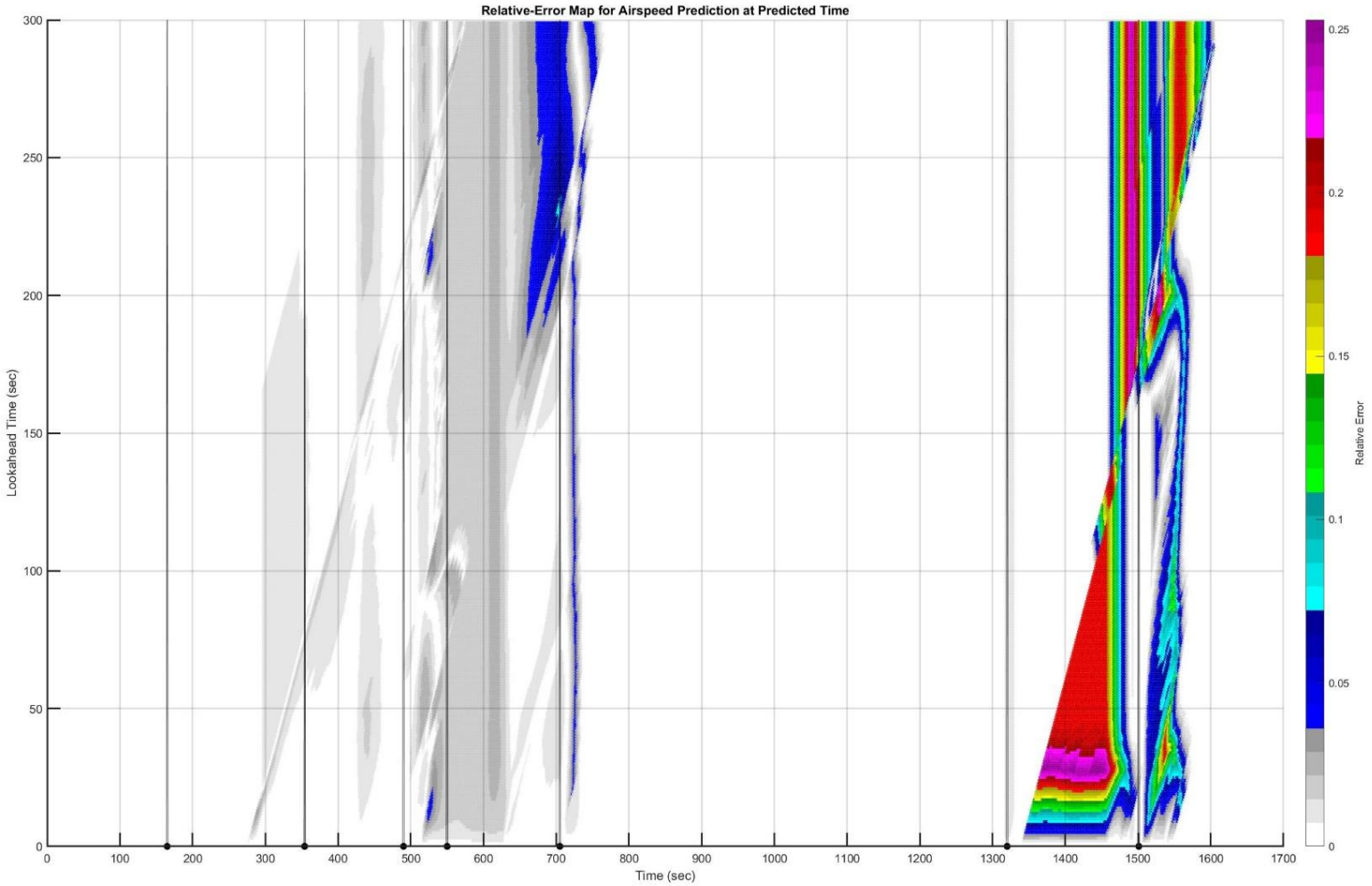

Figure C. 105: MONAA to Runway 09: Heatmap of Airspeed Prediction Error (Time is $t + \tau$)

C.22. Trajectory: MONAA to 18C

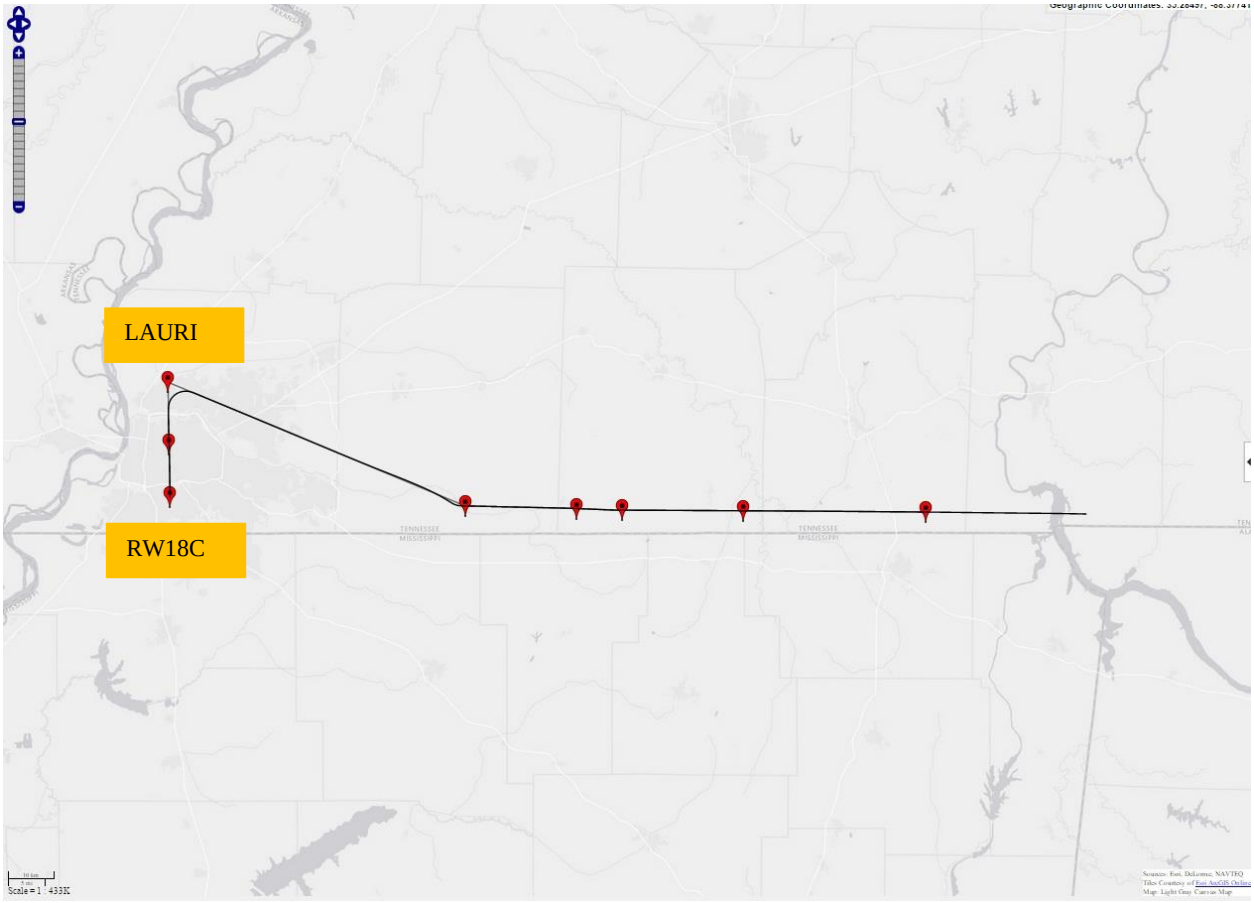

Figure C. 106: MONAA to Runway 18C: Planned and Actual Trajectories (Red markers indicate waypoints)

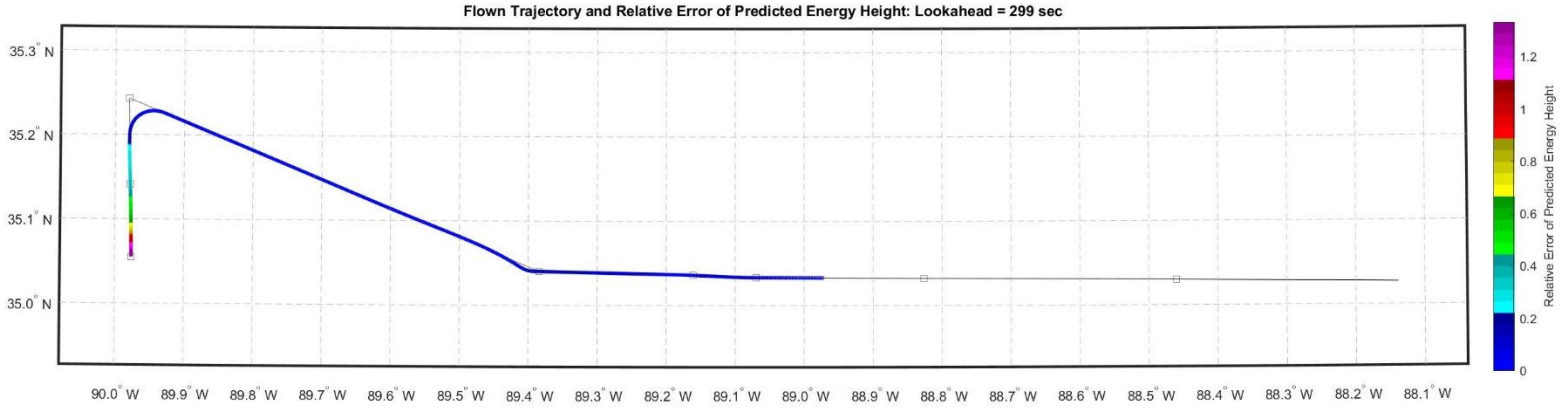

Figure C. 107: MONAA to Runway 18C: Lateral Path Color-Coded for Energy Prediction Error for Look-Ahead of 299 Seconds

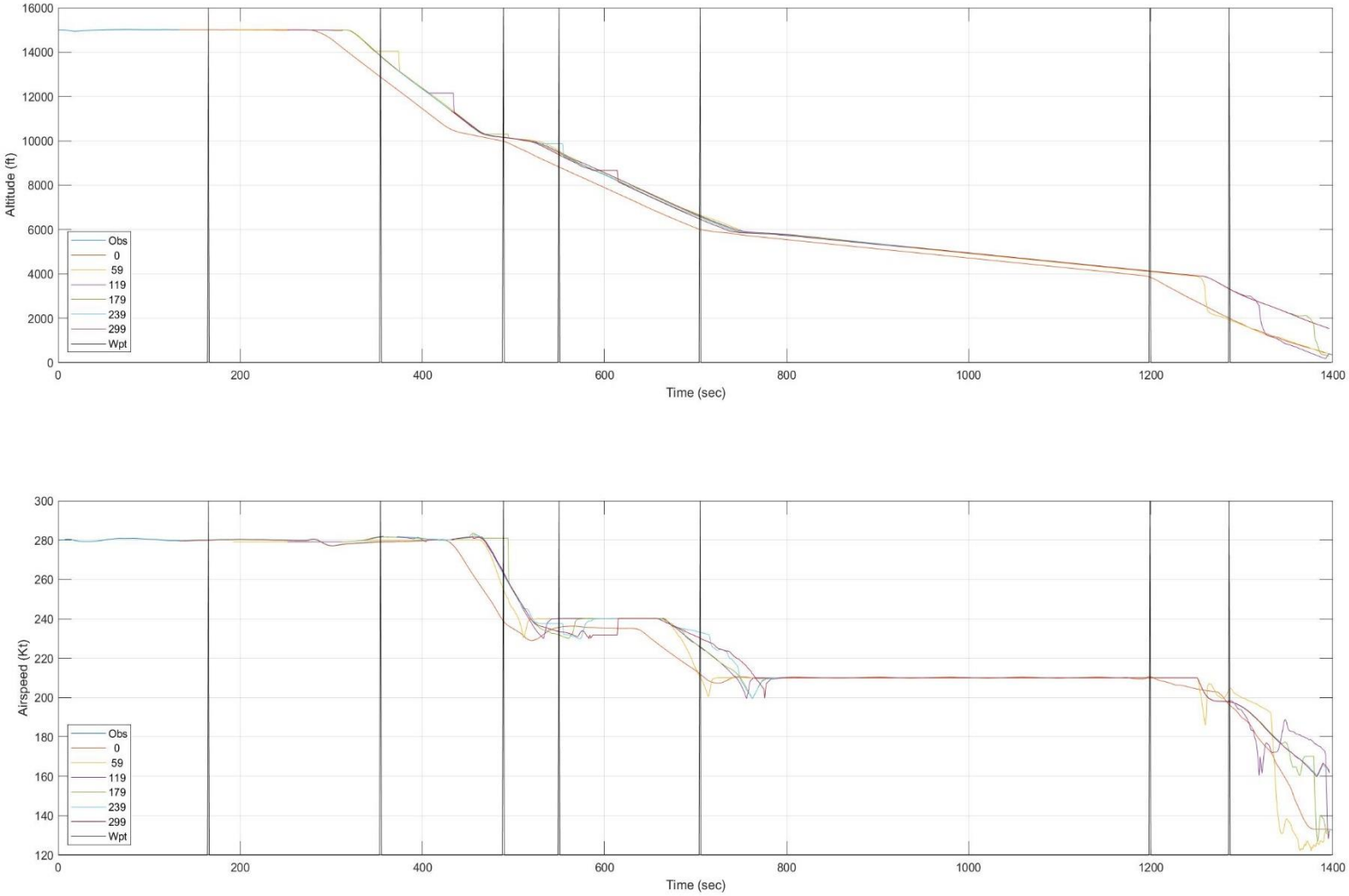

Figure C. 108: MONAA to Runway 18C: Time History of Predicted Altitude and Airspeed

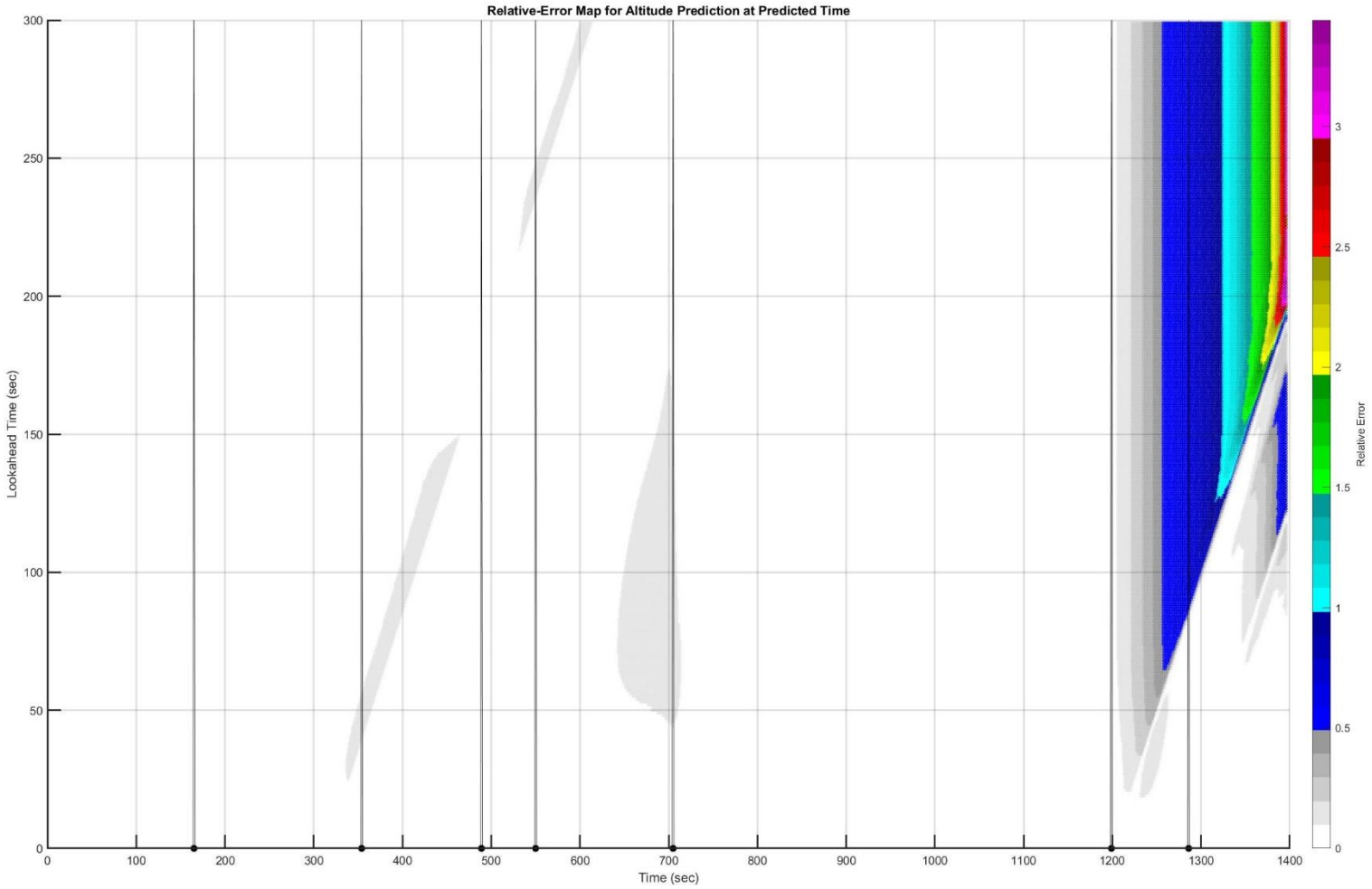

Figure C. 109: MONAA to Runway 18C: Heatmap of Altitude Prediction Error (Time is $t + \tau$)

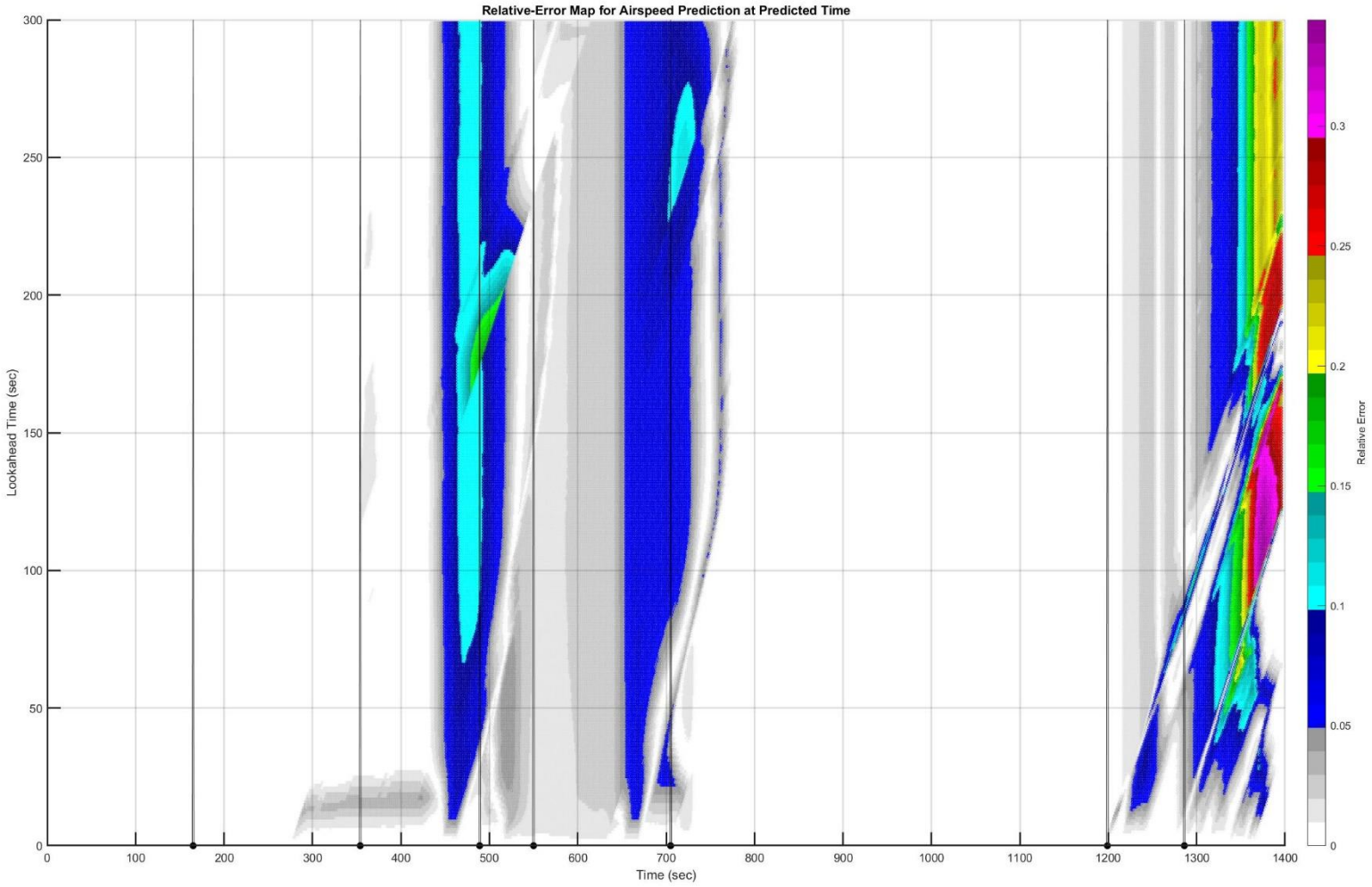

Figure C. 110: MONAA to Runway 18C: Heatmap of Airspeed Prediction Error (Time is $t + \tau$)

C.23. Trajectory: MONAA to 27

Figure C. 111: MONAA to Runway 27: Planned and Actual Trajectories (Red markers indicate waypoints)

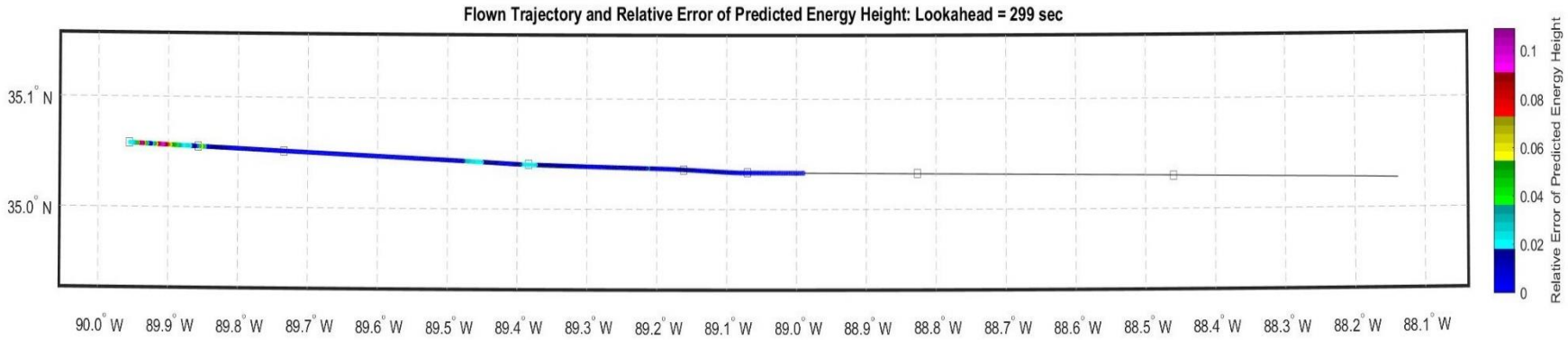

Figure C. 112: MONAA to Runway 27: Lateral Path Color-Coded for Energy Prediction Error for Look-Ahead of 299 Seconds

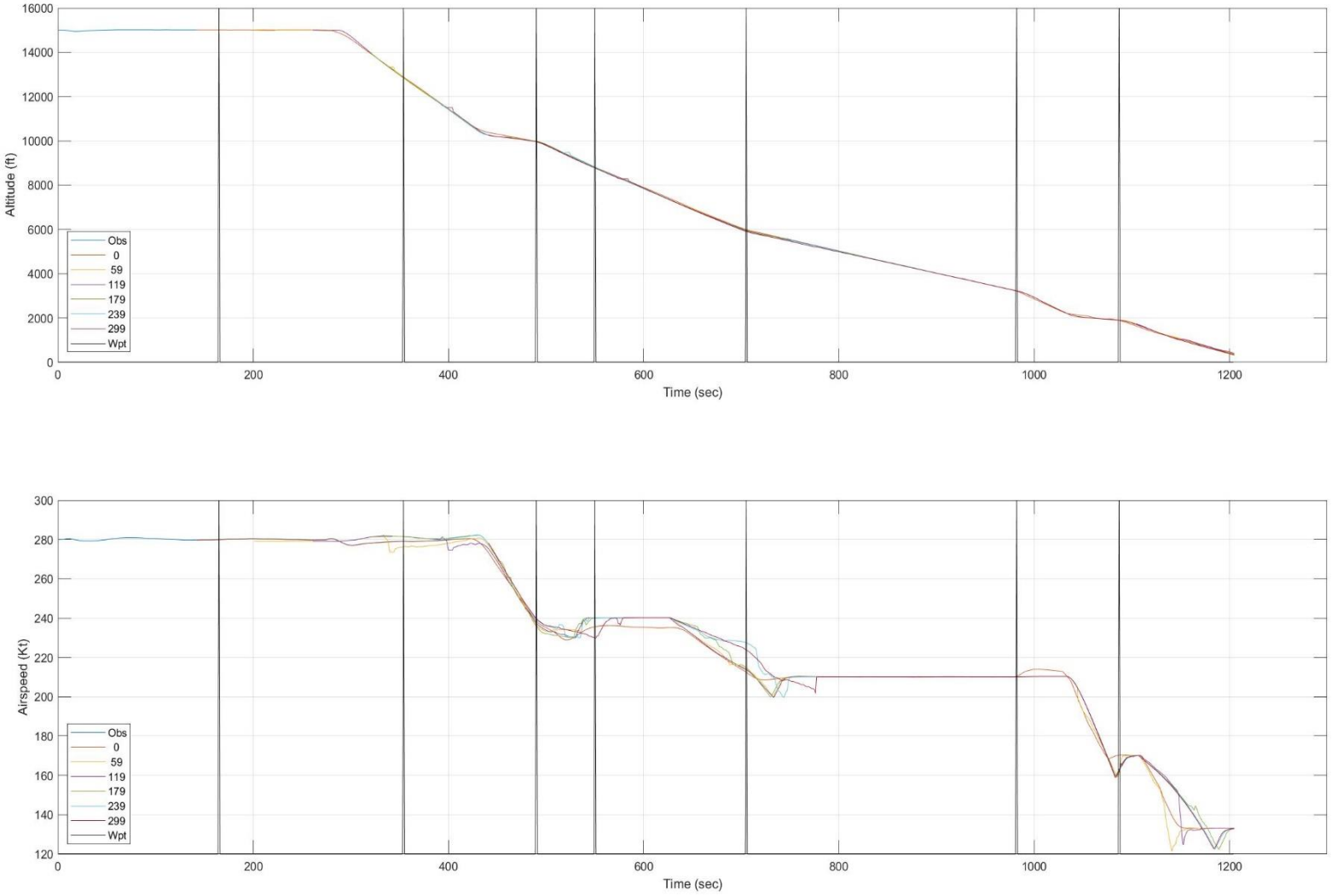

Figure C. 113: MONAA to Runway 27: Time History of Predicted Altitude and Airspeed

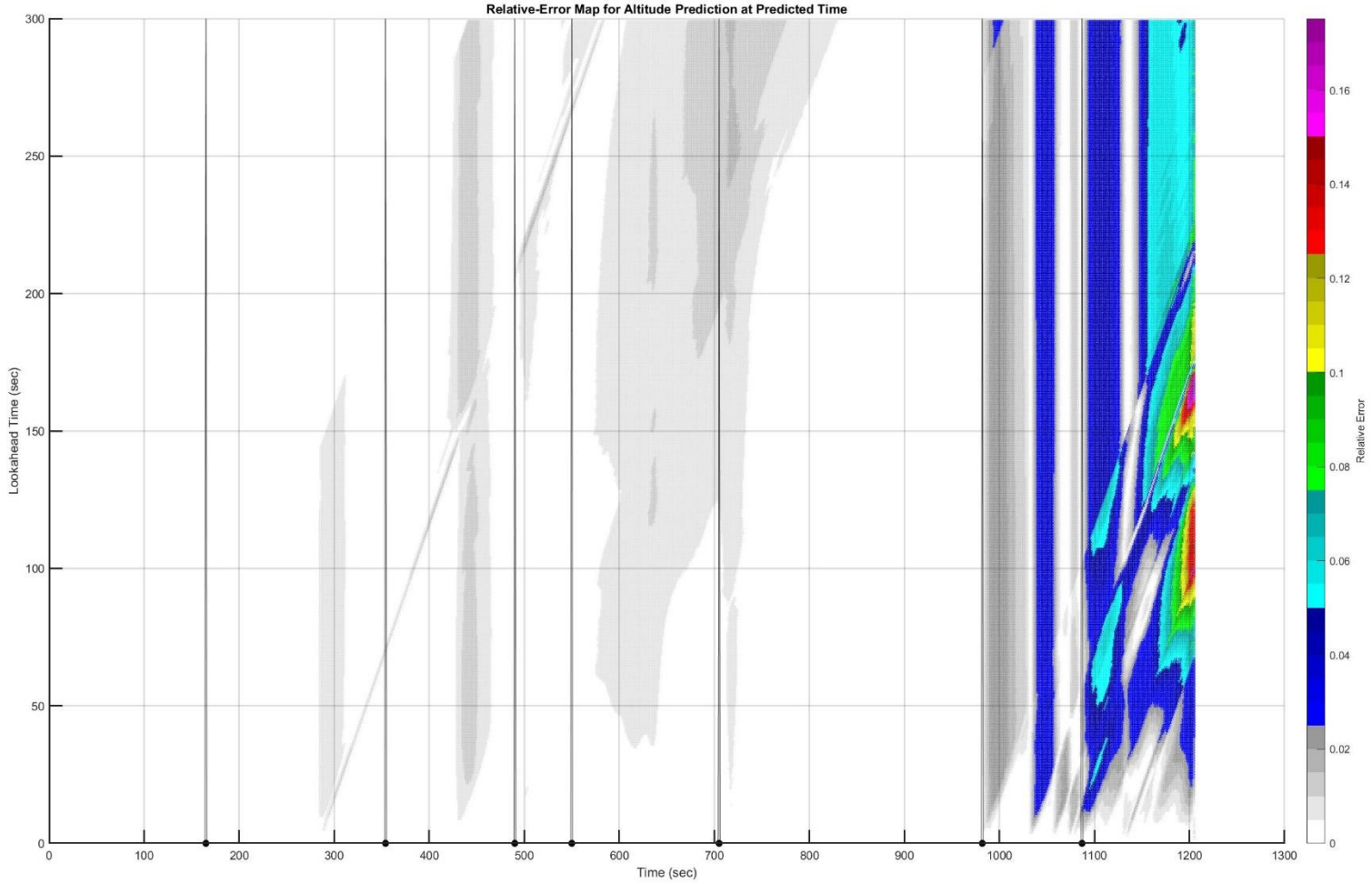

Figure C. 114: MONAA to Runway 27: Heatmap of Altitude Prediction Error (Time is $t + \tau$)

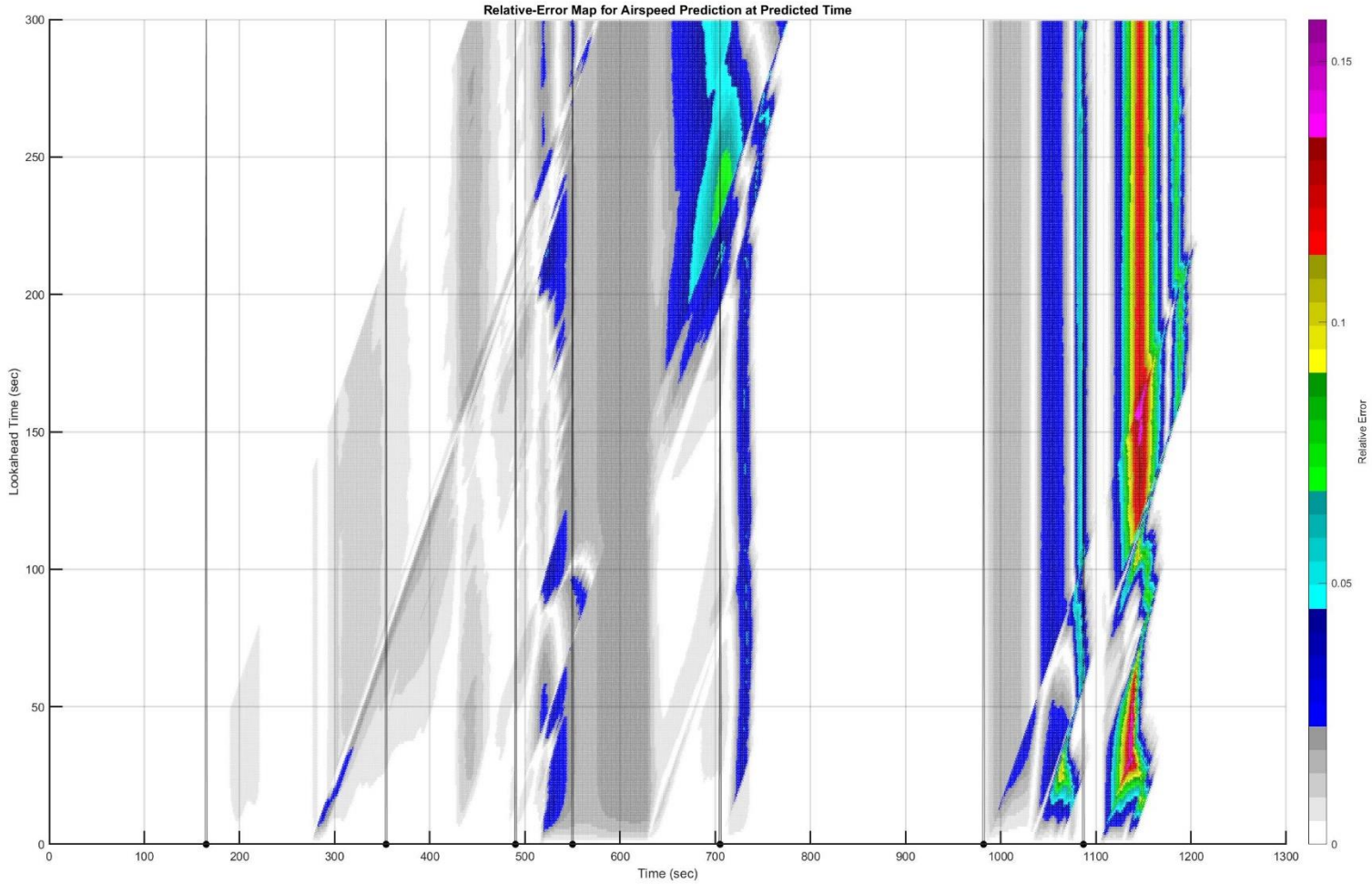

Figure C. 115: MONAA to Runway 27: Heatmap of Airspeed Prediction Error (Time is $t + \tau$)

C.24. Trajectory: MONAA to 36C

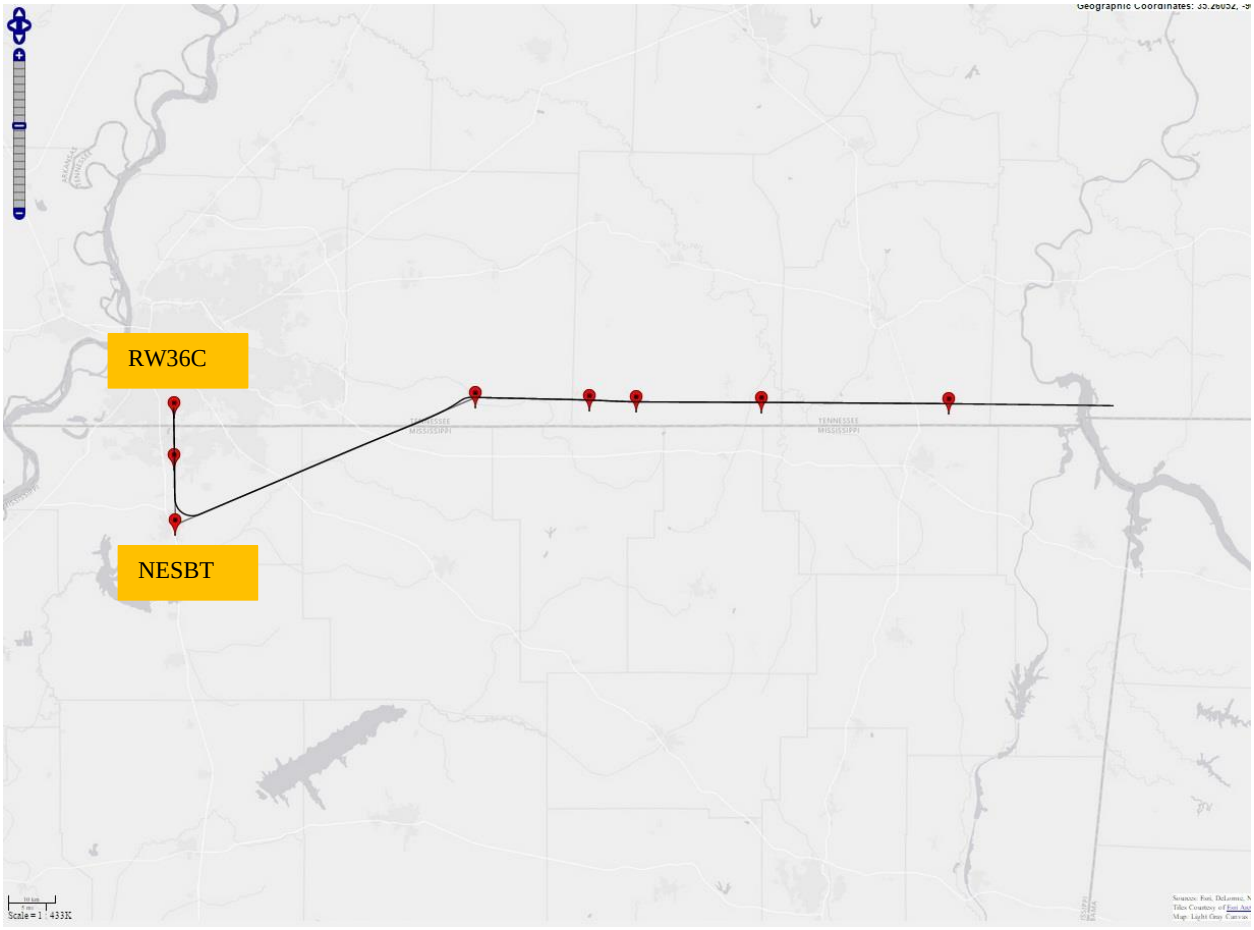

Figure C. 116: MONAA to Runway 36C: Planned and Actual Trajectories (Red markers indicate waypoints)

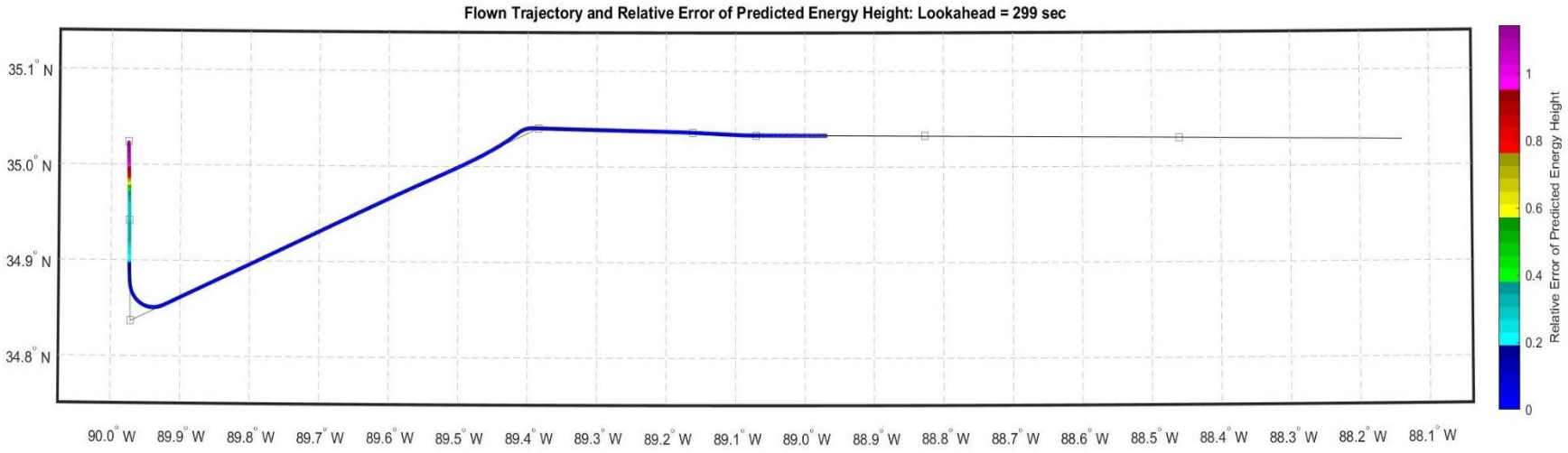

Figure C. 117: MONAA to Runway 36C: Lateral Path Color-Coded for Energy Prediction Error for Look-Ahead of 299 Seconds

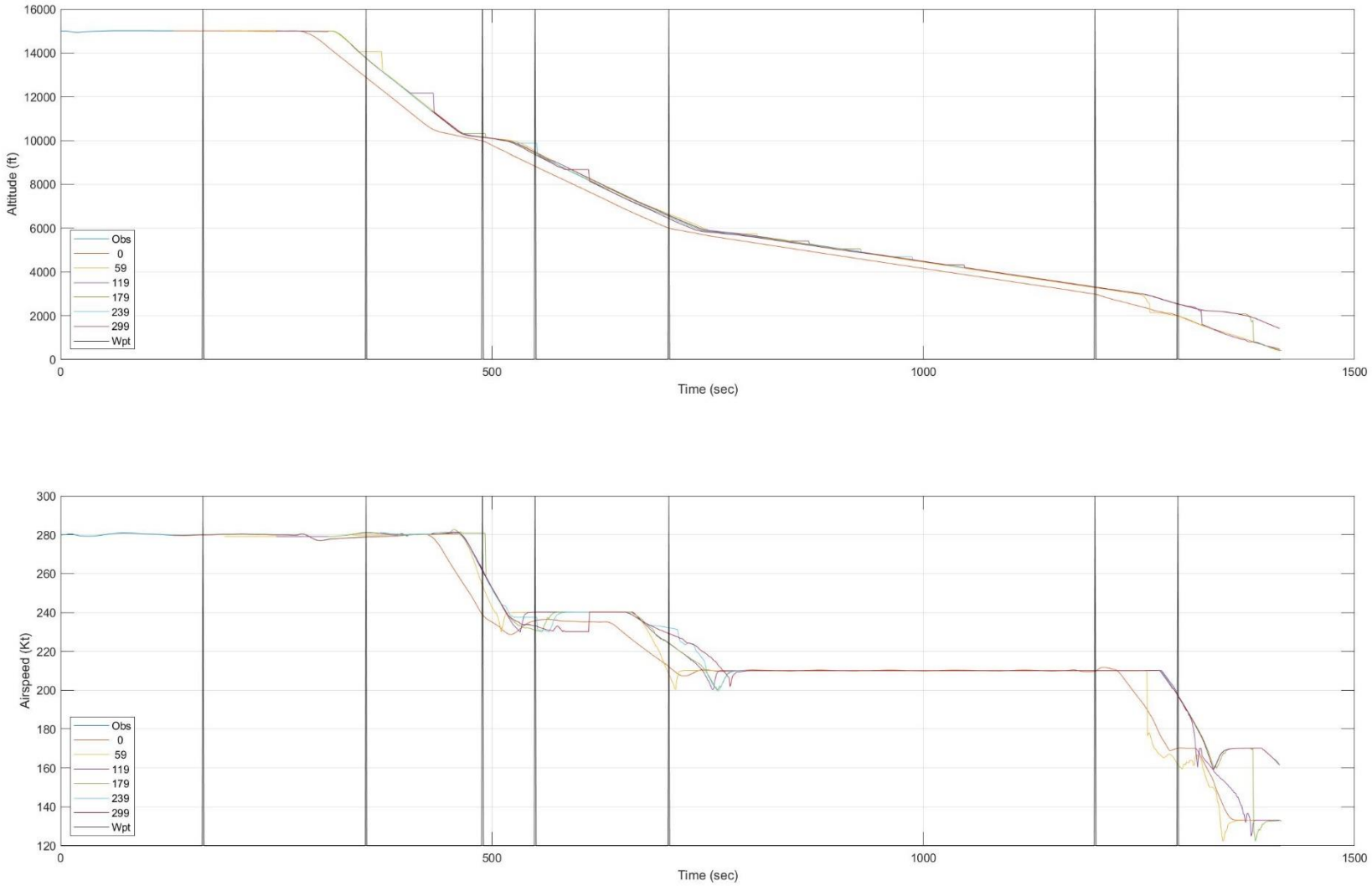

Figure C. 118: MONAA to Runway 36C: Time History of Predicted Altitude and Airspeed

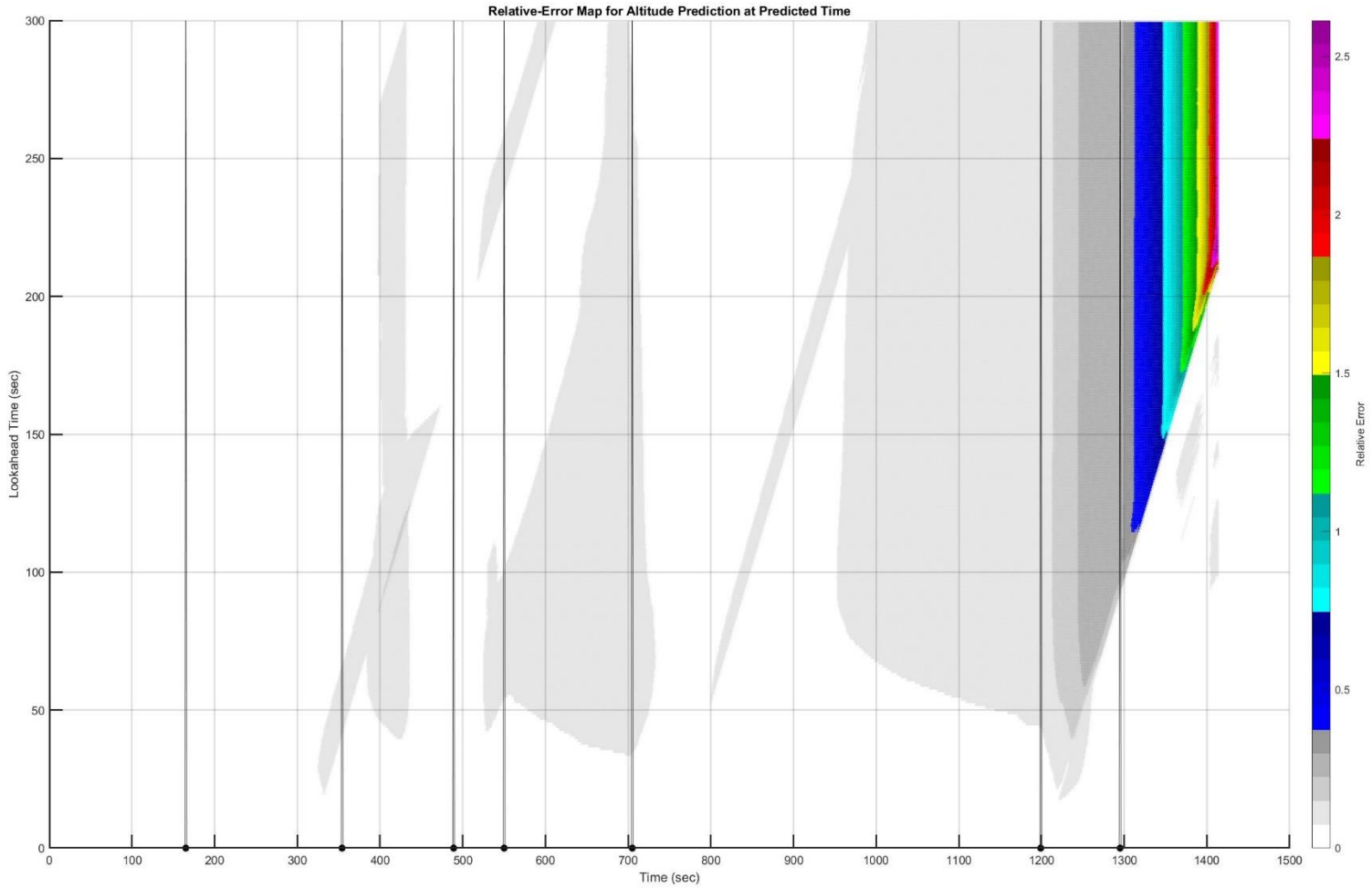

Figure C. 119: MONAA to Runway 36C: Heatmap of Altitude Prediction Error (Time is $t + \tau$)

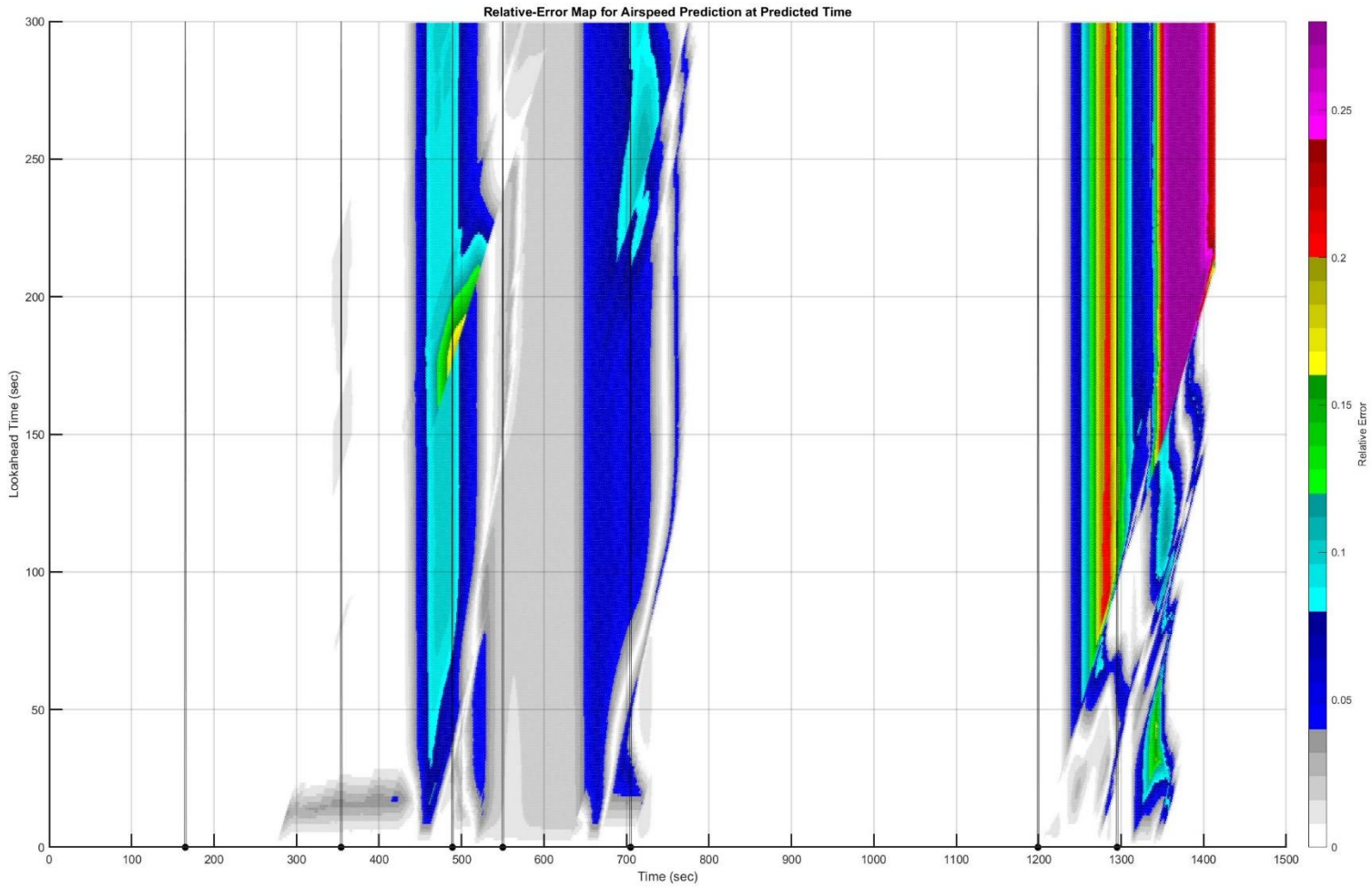

Figure C. 120: MONAA to Runway 36C: Heatmap of Airspeed Prediction Error (Time is $t + \tau$)

C.25. Trajectory: CONDR to 09

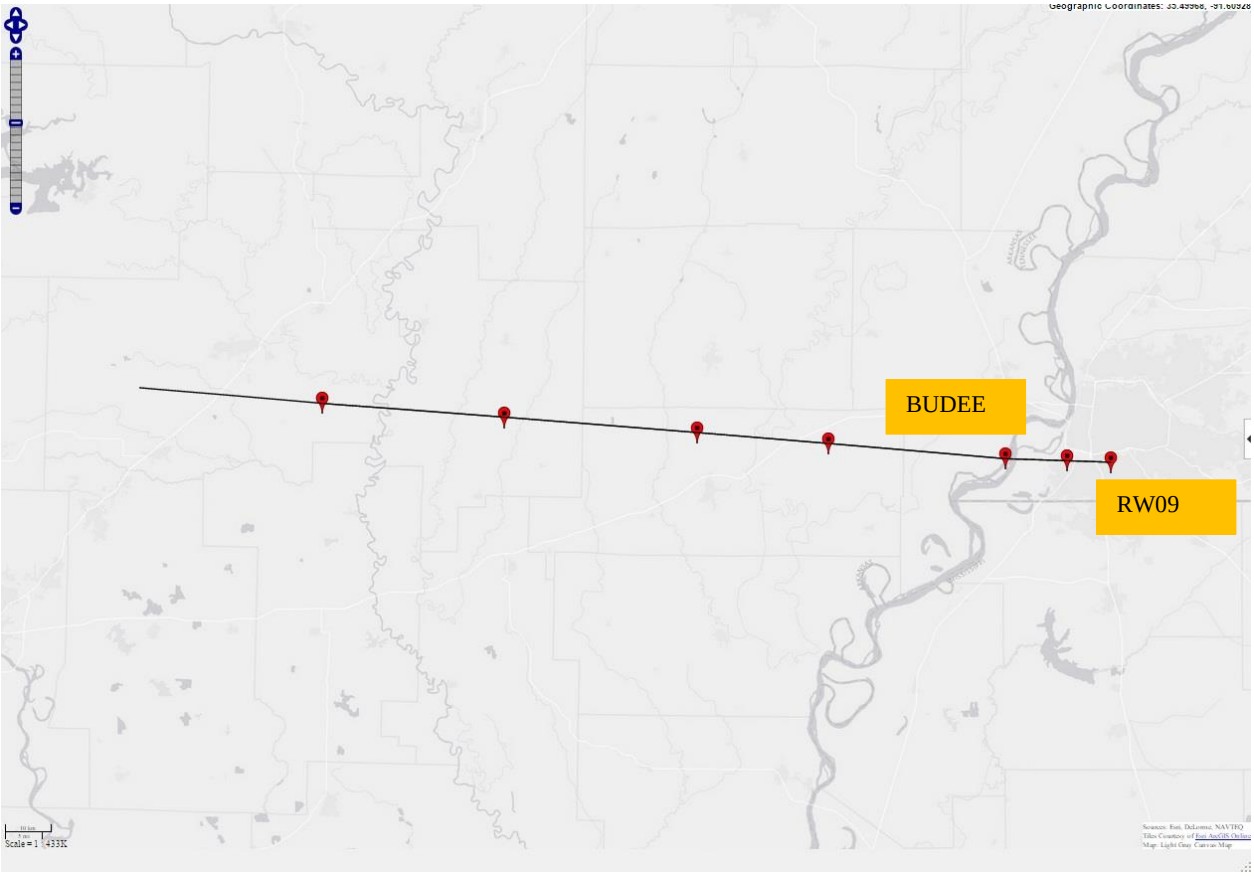

Figure C. 121: CONDR to Runway 09: Planned and Actual Trajectories (Red markers indicate waypoints)

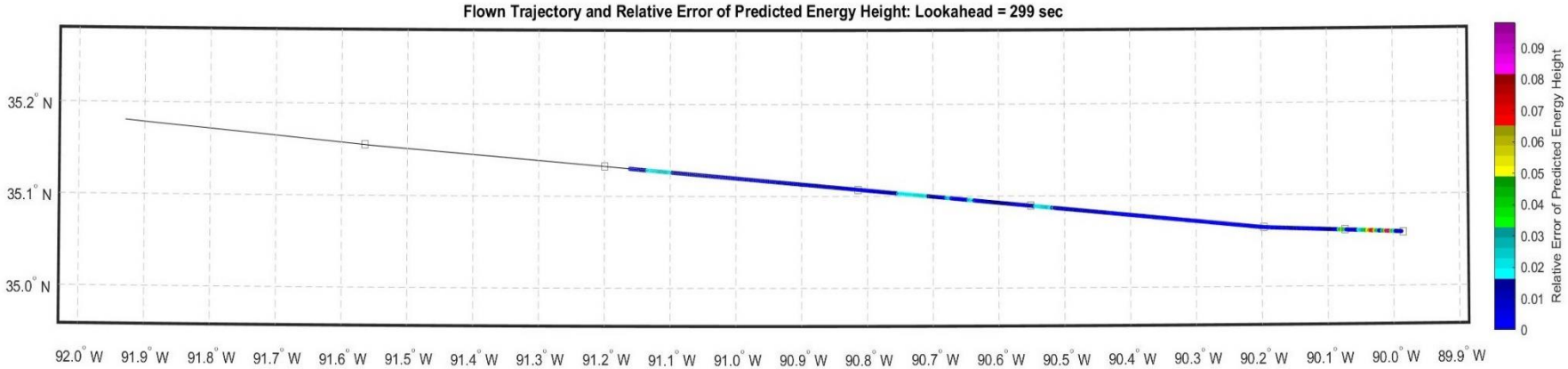

Figure C. 122: CONDR to Runway 09: Lateral Path Color-Coded for Energy Prediction Error for Look-Ahead of 299 Seconds

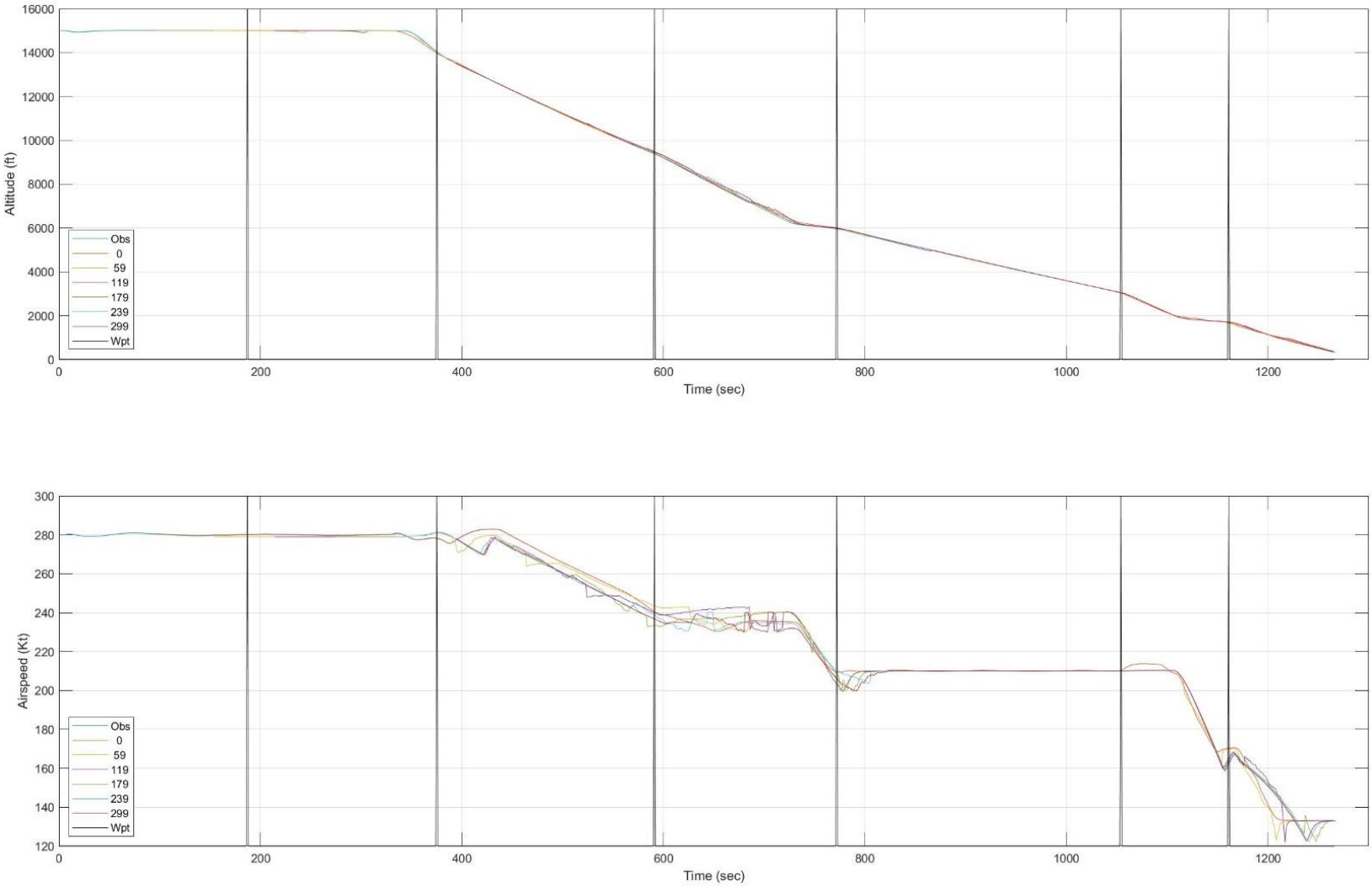

Figure C. 123: CONDR to Runway 09: Time History of Predicted Altitude and Airspeed

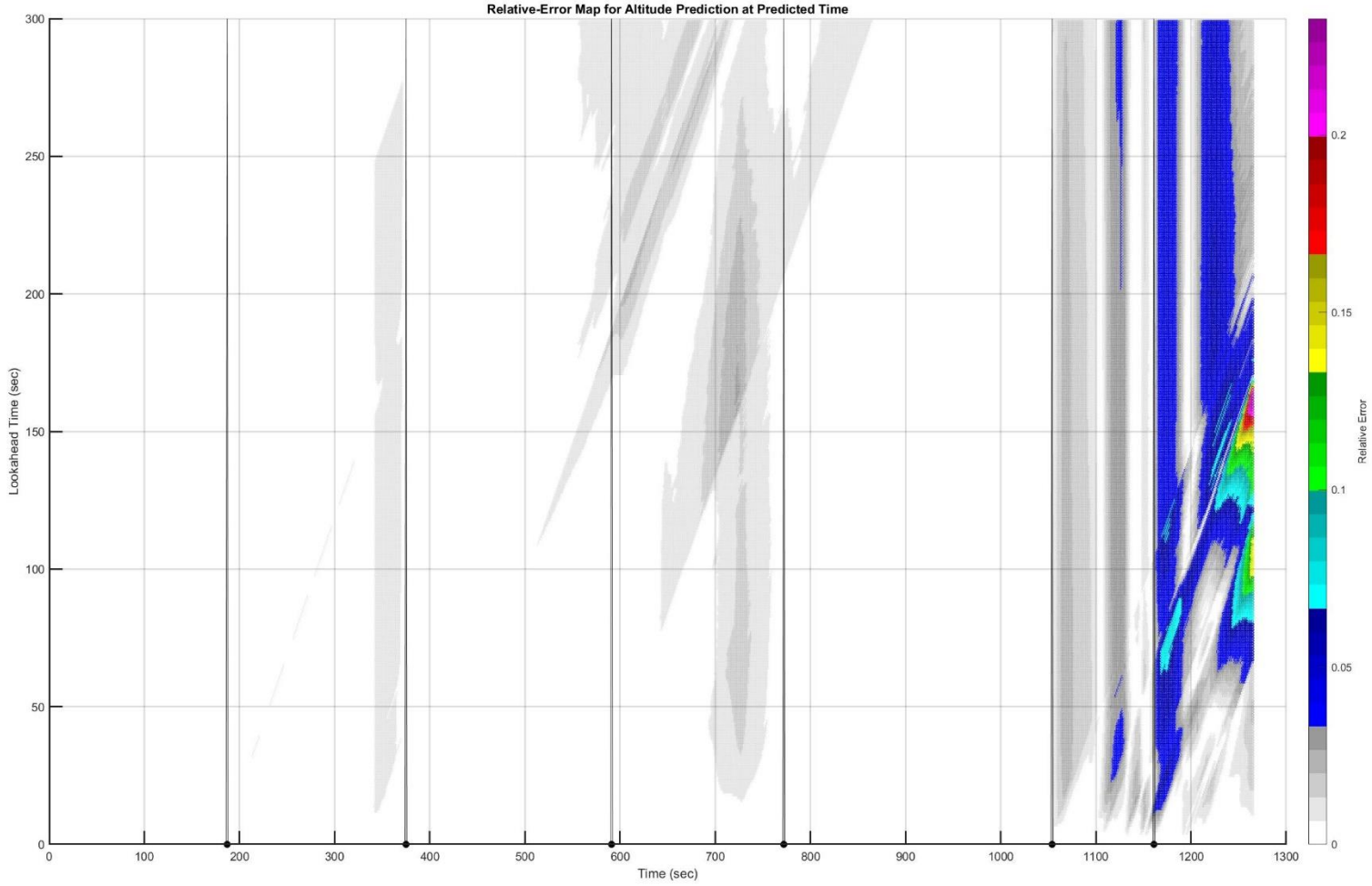

Figure C. 124: CONDR to Runway 09: Heatmap of Altitude Prediction Error (Time is $t + \tau$)

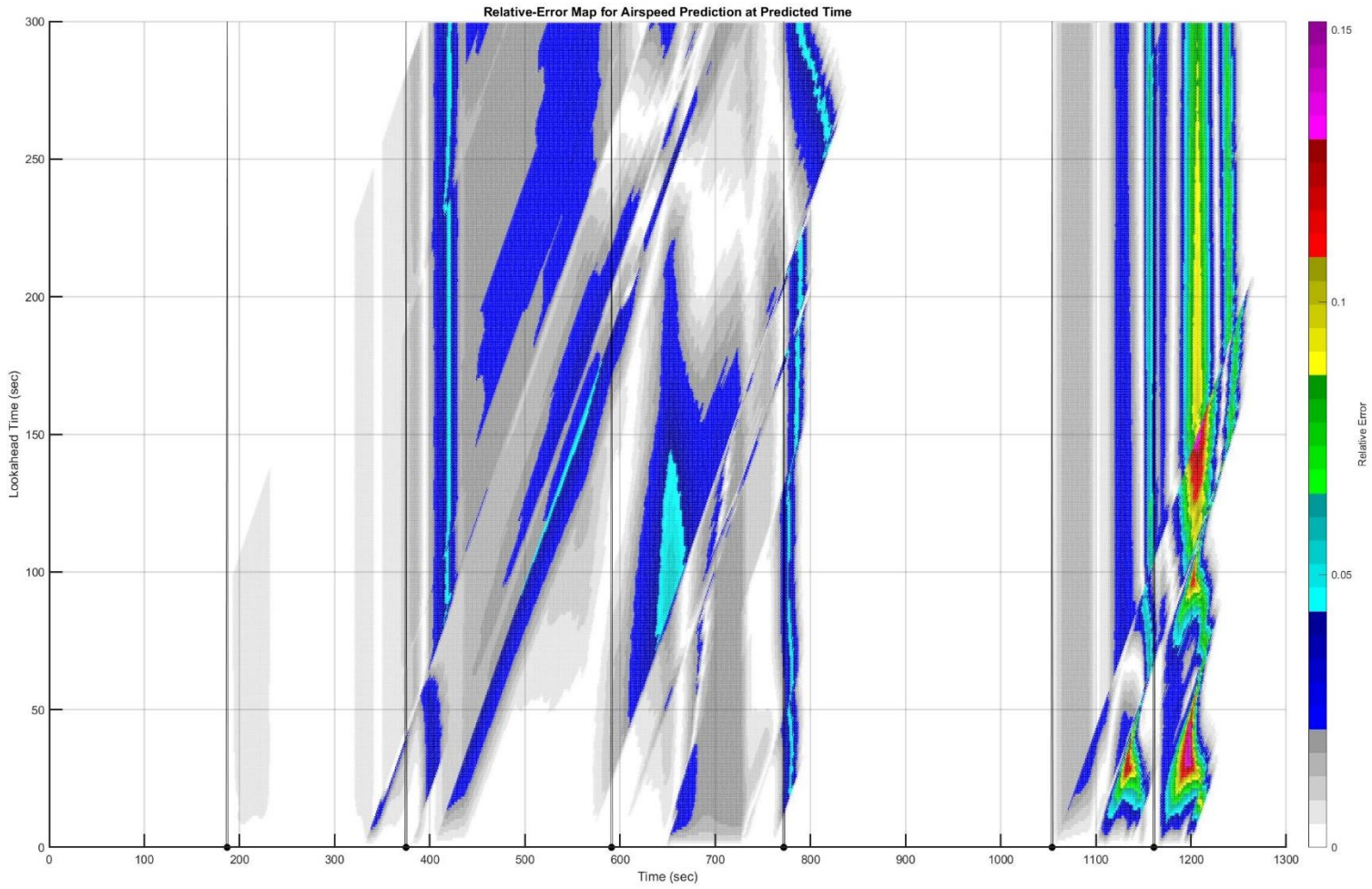

Figure C. 125: MONAA to Runway 09: Heatmap of Airspeed Prediction Error (Time is $t + \tau$)

C.26. Trajectory: CONDR to 18C

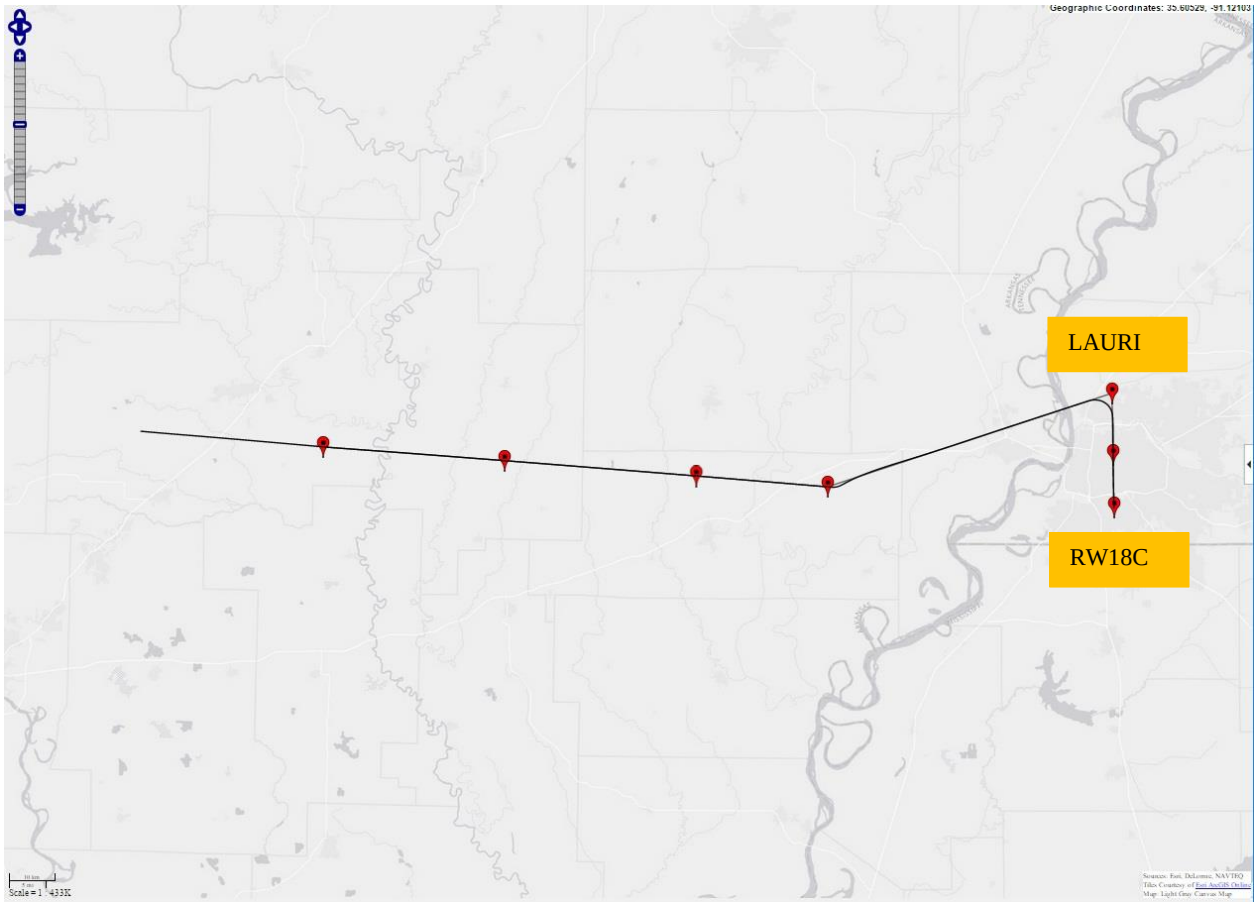

Figure C. 126: CONDR to Runway 18C: Planned and Actual Trajectories (Red markers indicate waypoints)

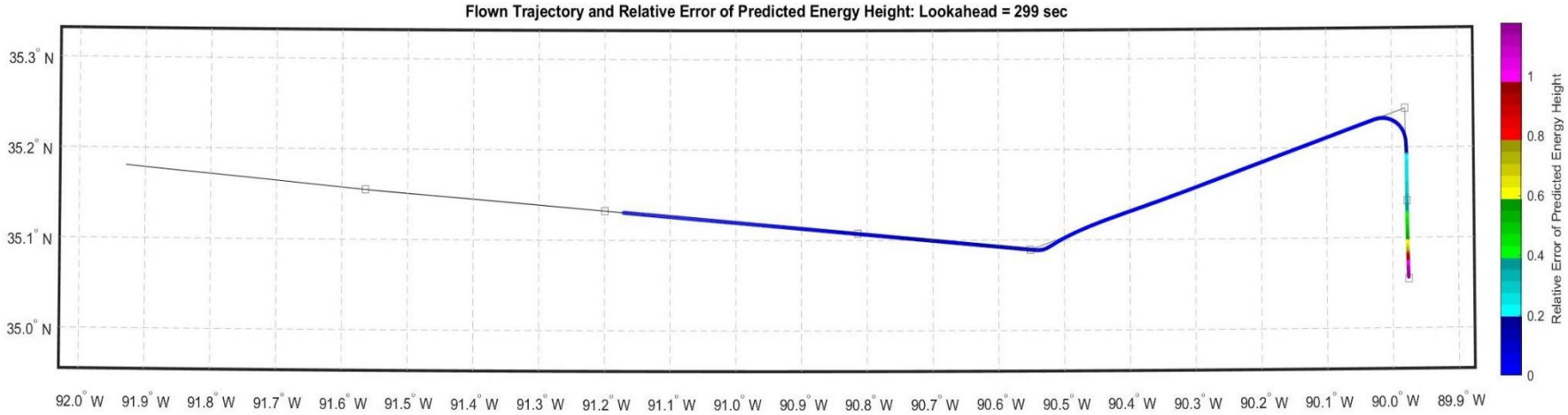

Figure C. 127: CONDR to Runway 18C: Lateral Path Color-Coded for Energy Prediction Error for Look-Ahead of 299 Seconds

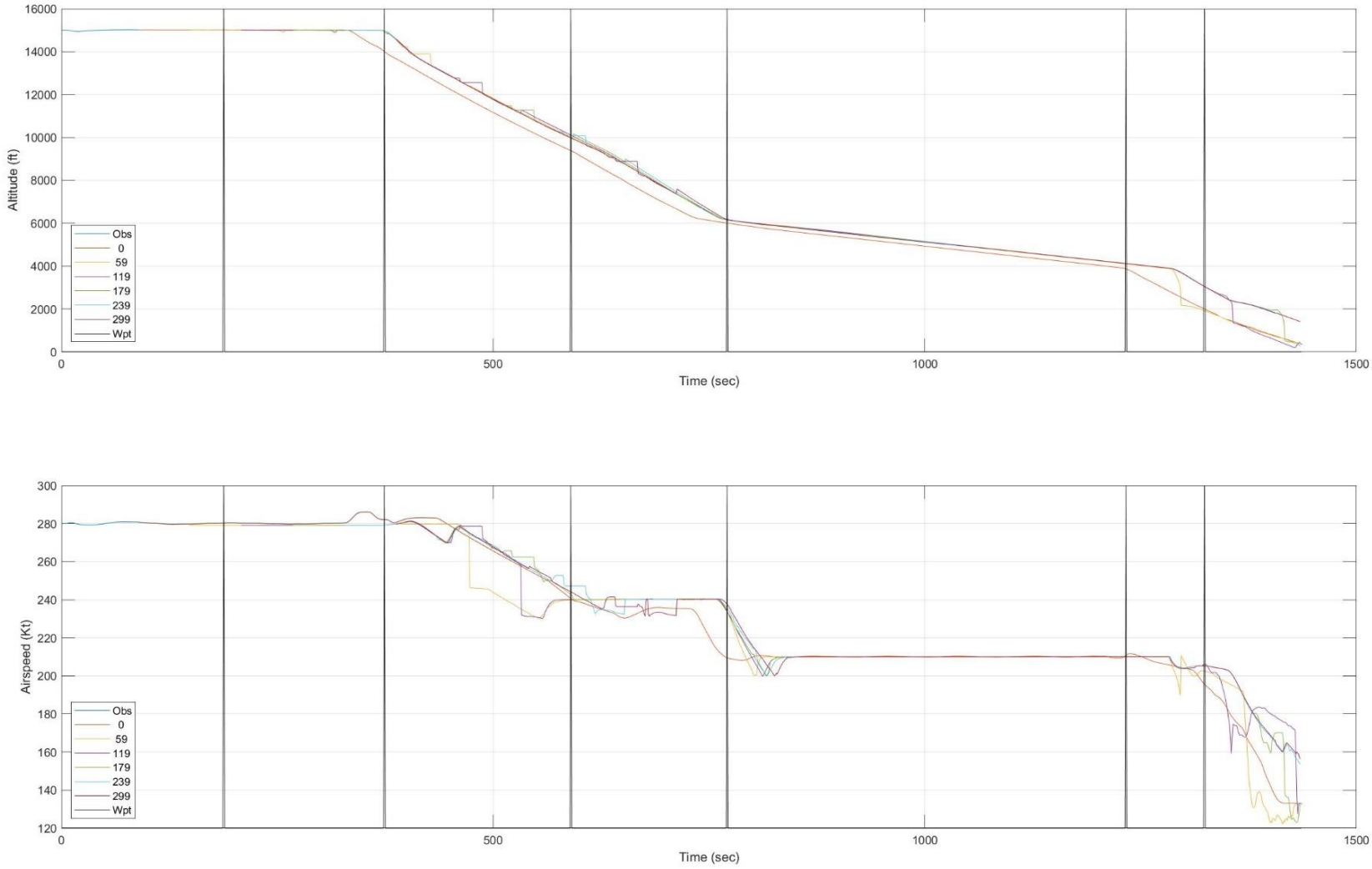

Figure C. 128: CONDR to Runway 18C: Time History of Predicted Altitude and Airspeed

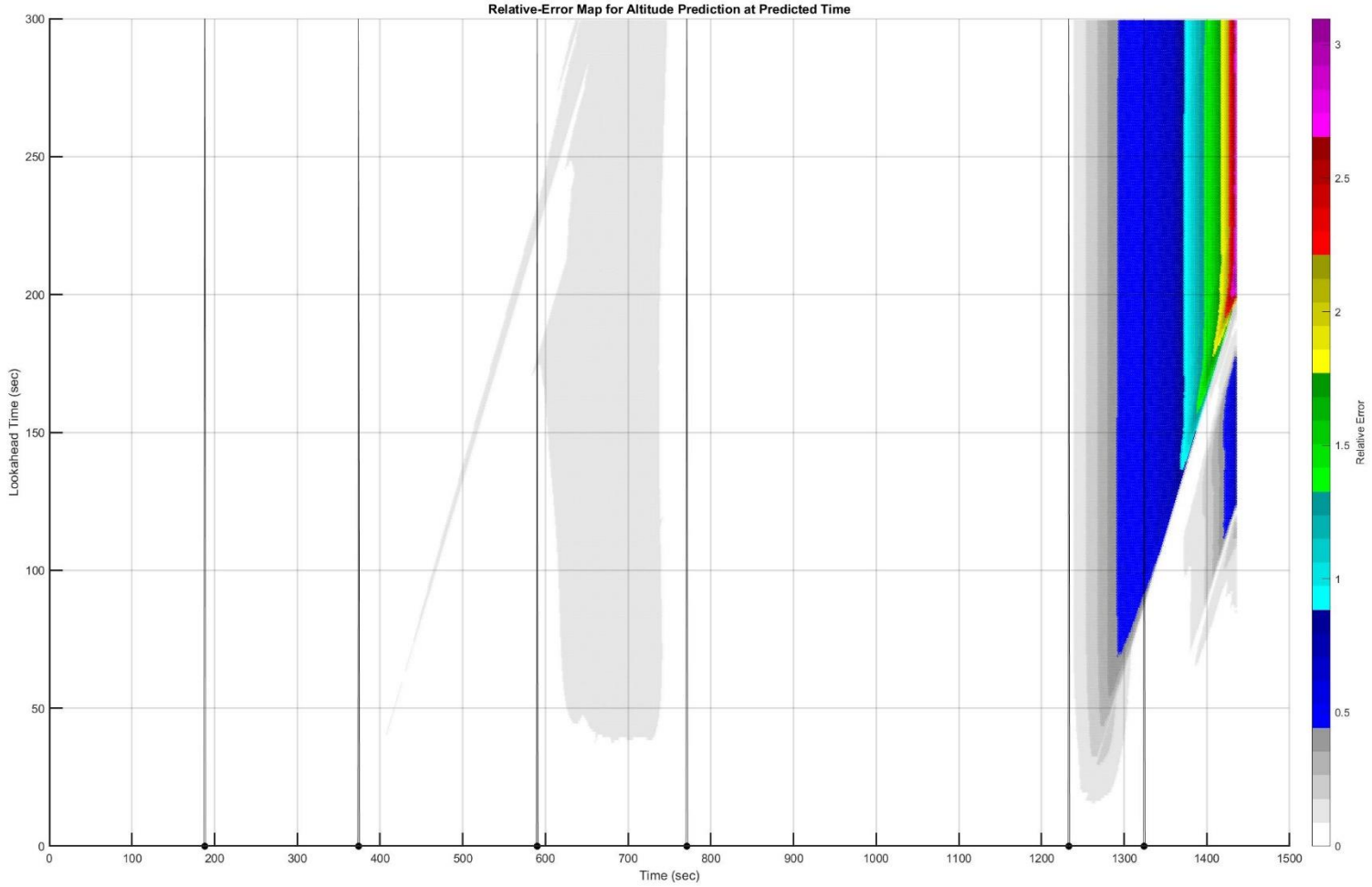

Figure C. 129: CONDR to Runway 18C: Heatmap of Altitude Prediction Error (Time is $t + \tau$)

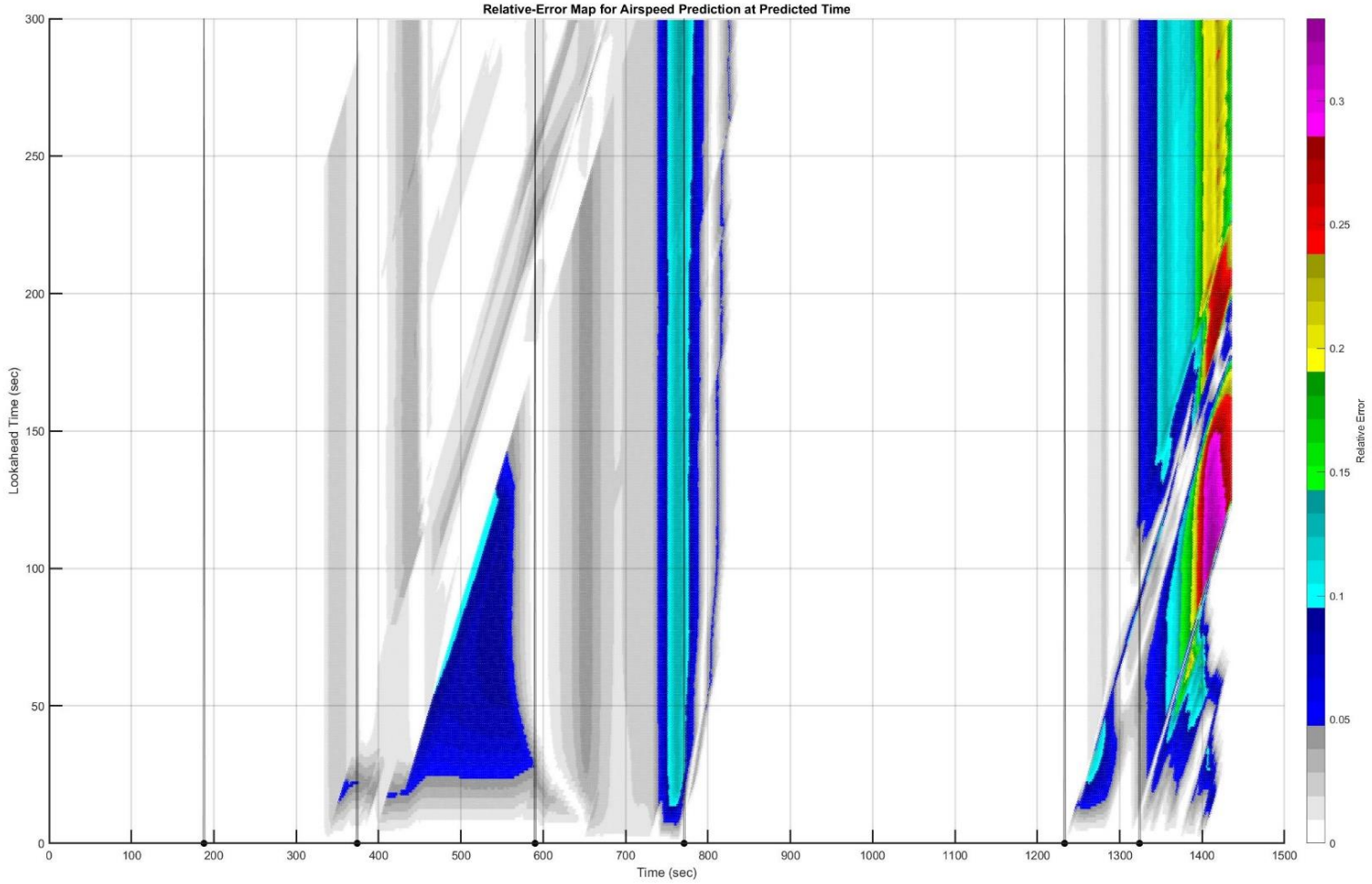

Figure C. 130: CONDR to Runway 18C: Heatmap of Airspeed Prediction Error (Time is $t + \tau$)

C.27. Trajectory: CONDR to 27

Figure C. 131: CONDR to Runway 27: Planned and Actual Trajectories (Red markers indicate waypoints)

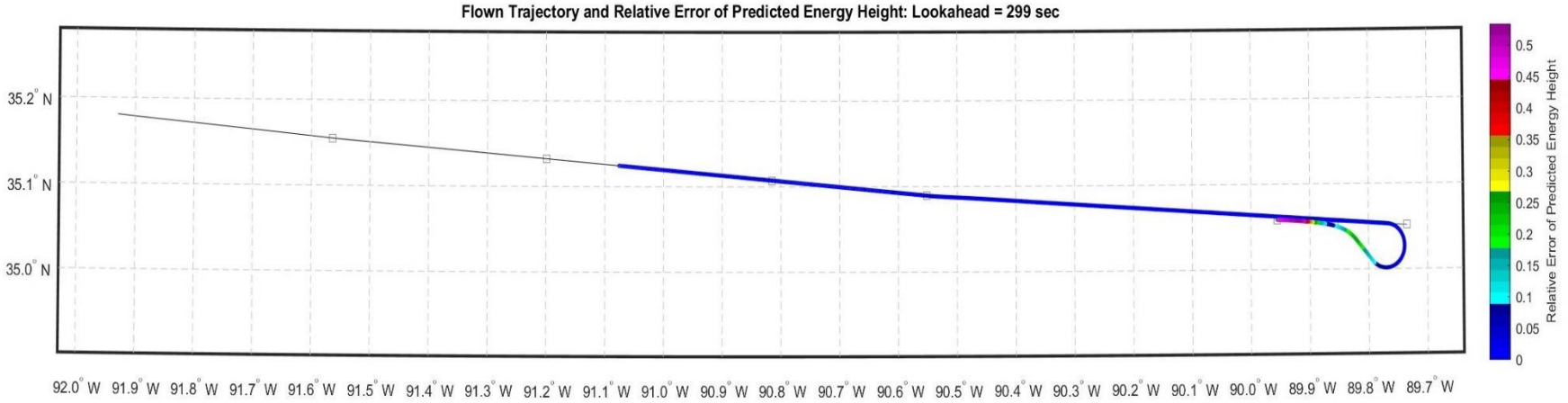

Figure C. 132: CONDR to Runway 27: Lateral Path Color-Coded for Energy Prediction Error for Look-Ahead of 299 Seconds

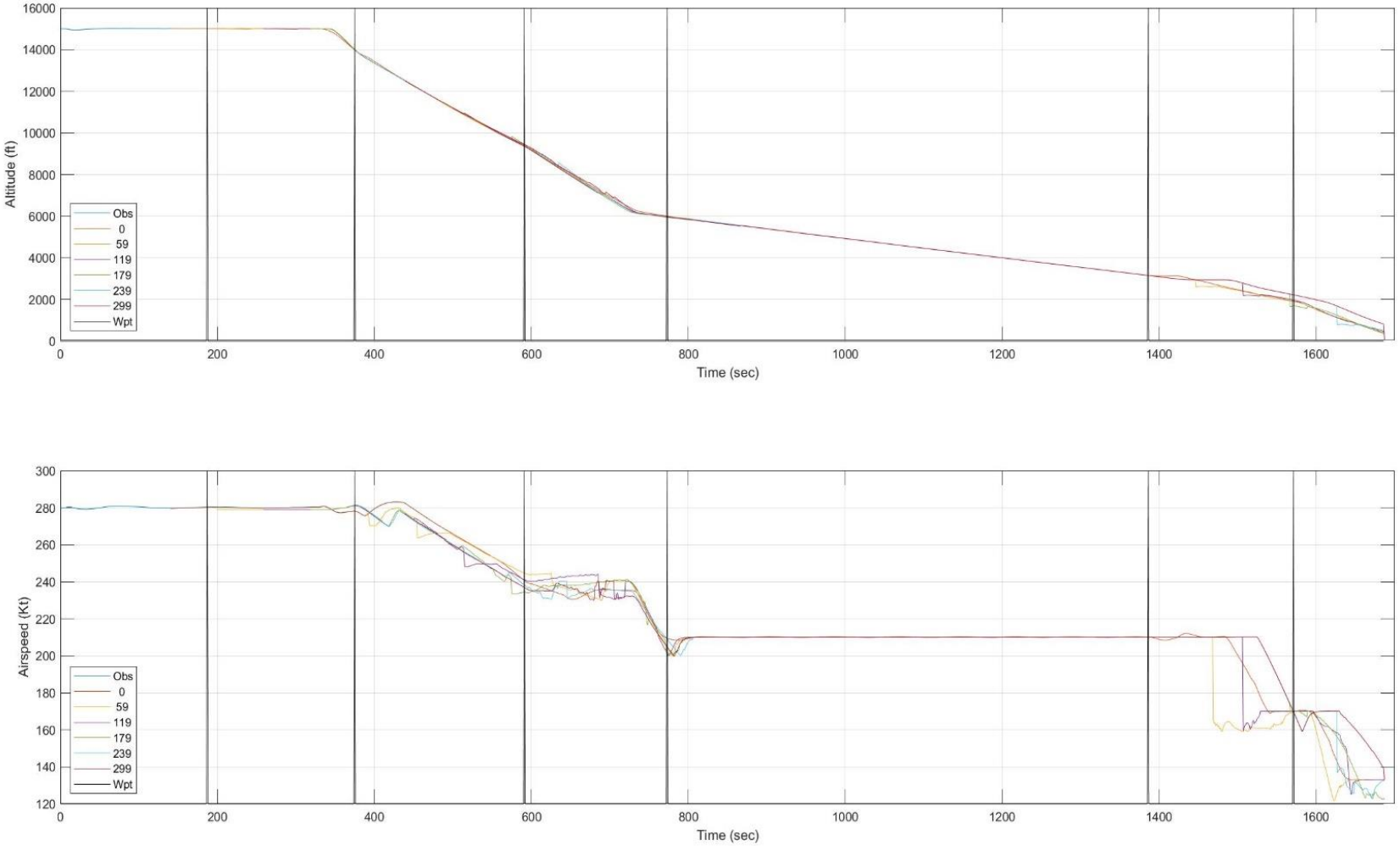

Figure C. 133: CONDR to Runway 27: Time History of Predicted Altitude and Airspeed

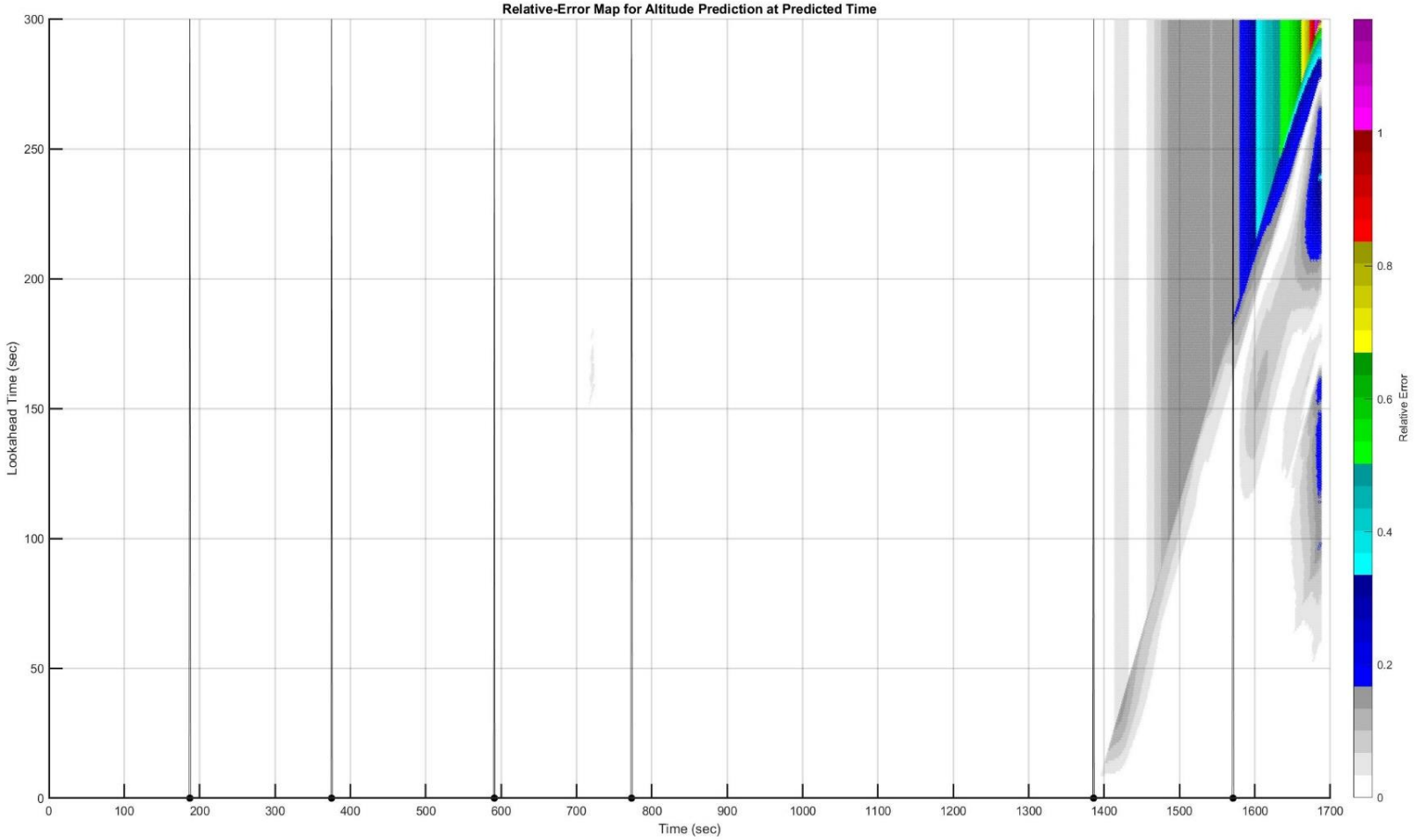

Figure C. 134: CONDR to Runway 27: Heatmap of Altitude Prediction Error (Time is $t + \tau$)

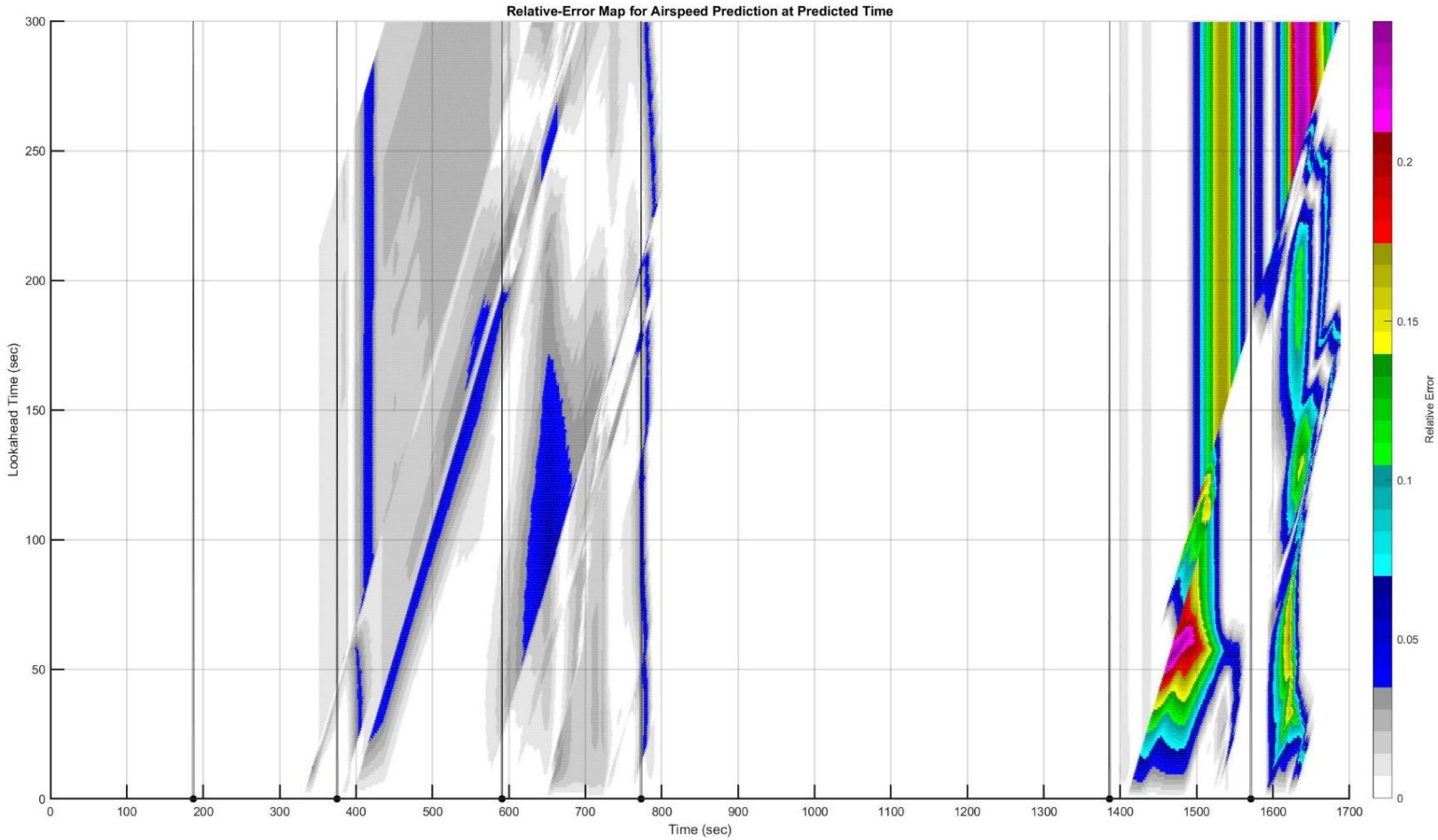

Figure C. 135: MONAA to Runway 27: Heatmap of Airspeed Prediction Error (Time is $t + \tau$)

C.28. Trajectory: CONDR to 36C

Figure C. 136: CONDR to Runway 36C: Planned and Actual Trajectories (Red markers indicate waypoints)

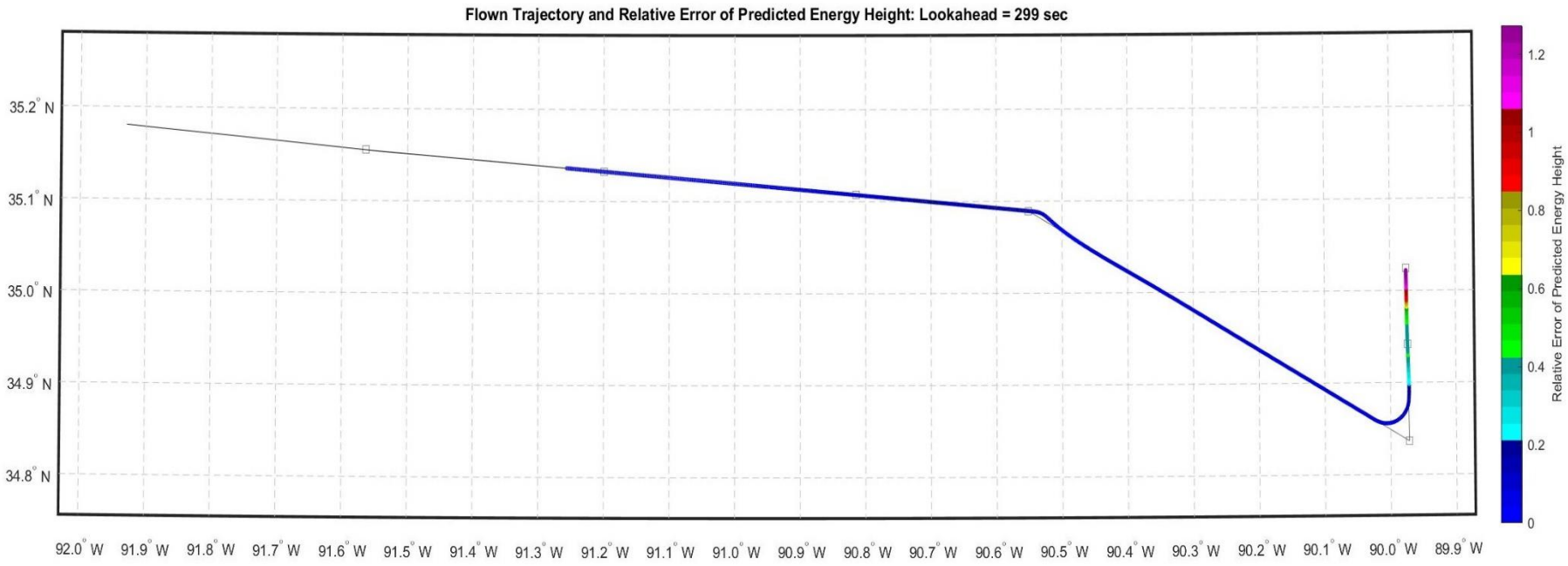

Figure C. 137: CONDR to Runway 36C: Lateral Path Color-Coded for Energy Prediction Error for Look-Ahead of 299 Seconds

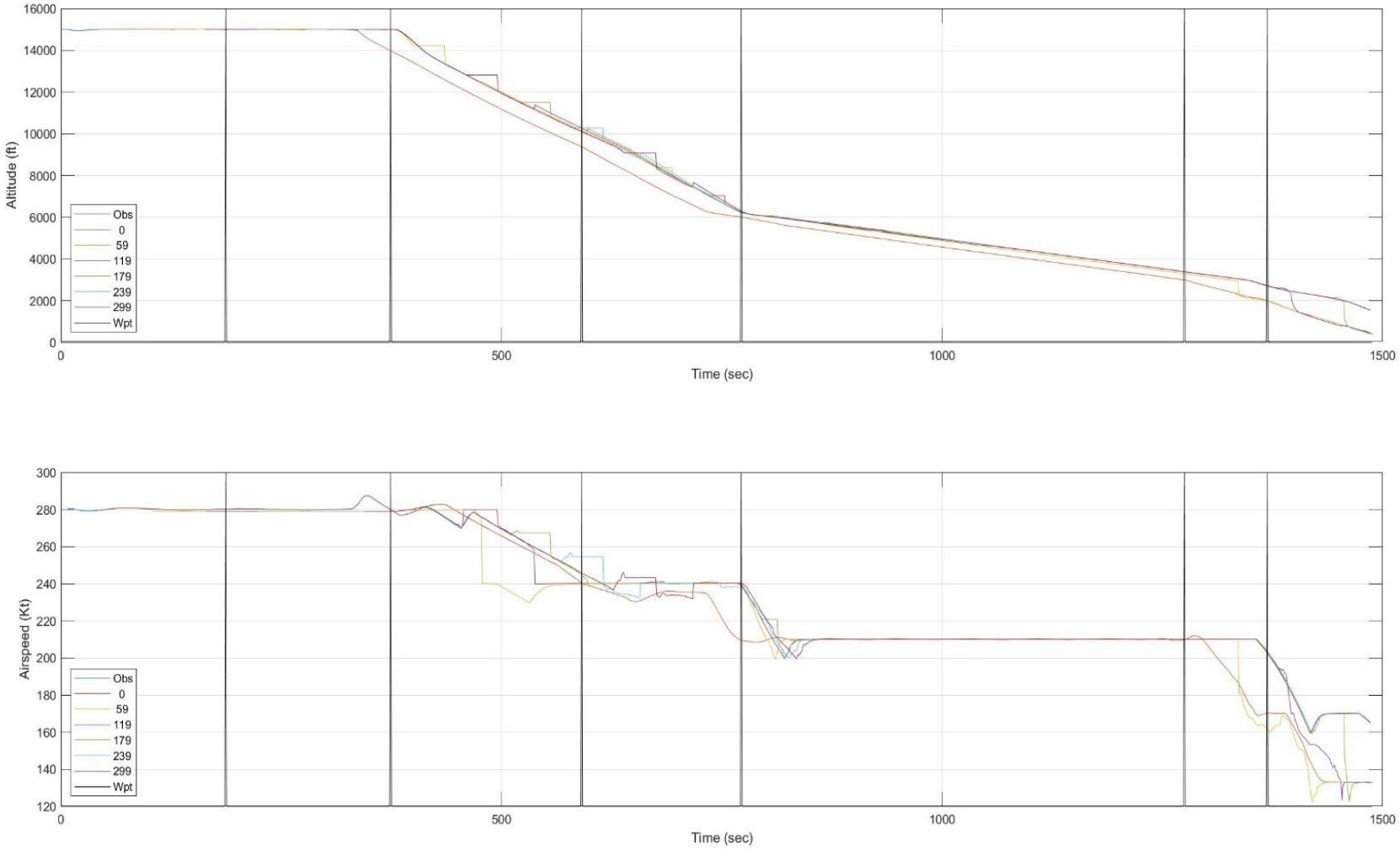

Figure C. 138: CONDR to Runway 36C: Time History of Predicted Altitude and Airspeed

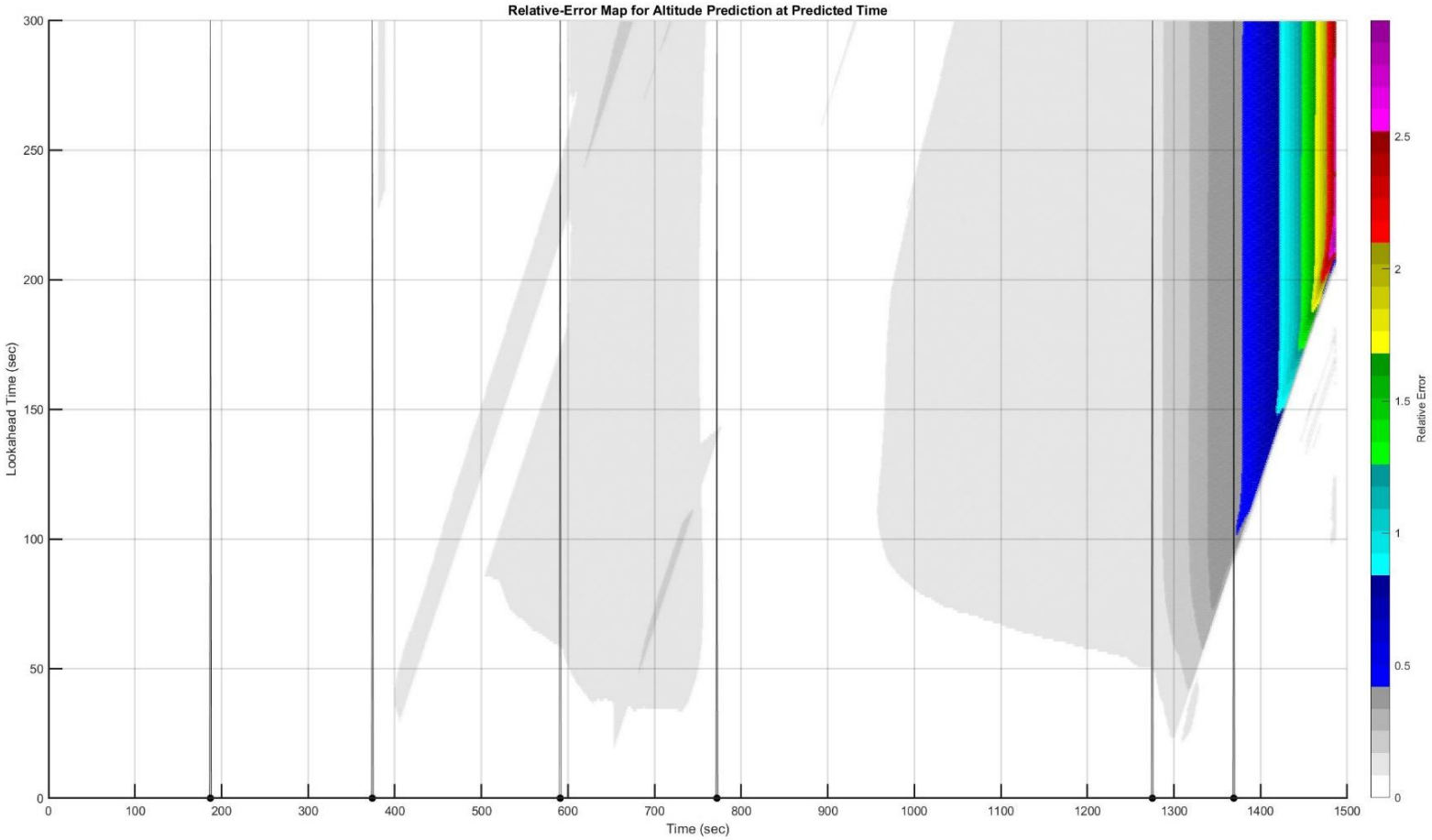

Figure C. 139: CONDR to Runway 36C: Heatmap of Altitude Prediction Error (Time is $t + \tau$)

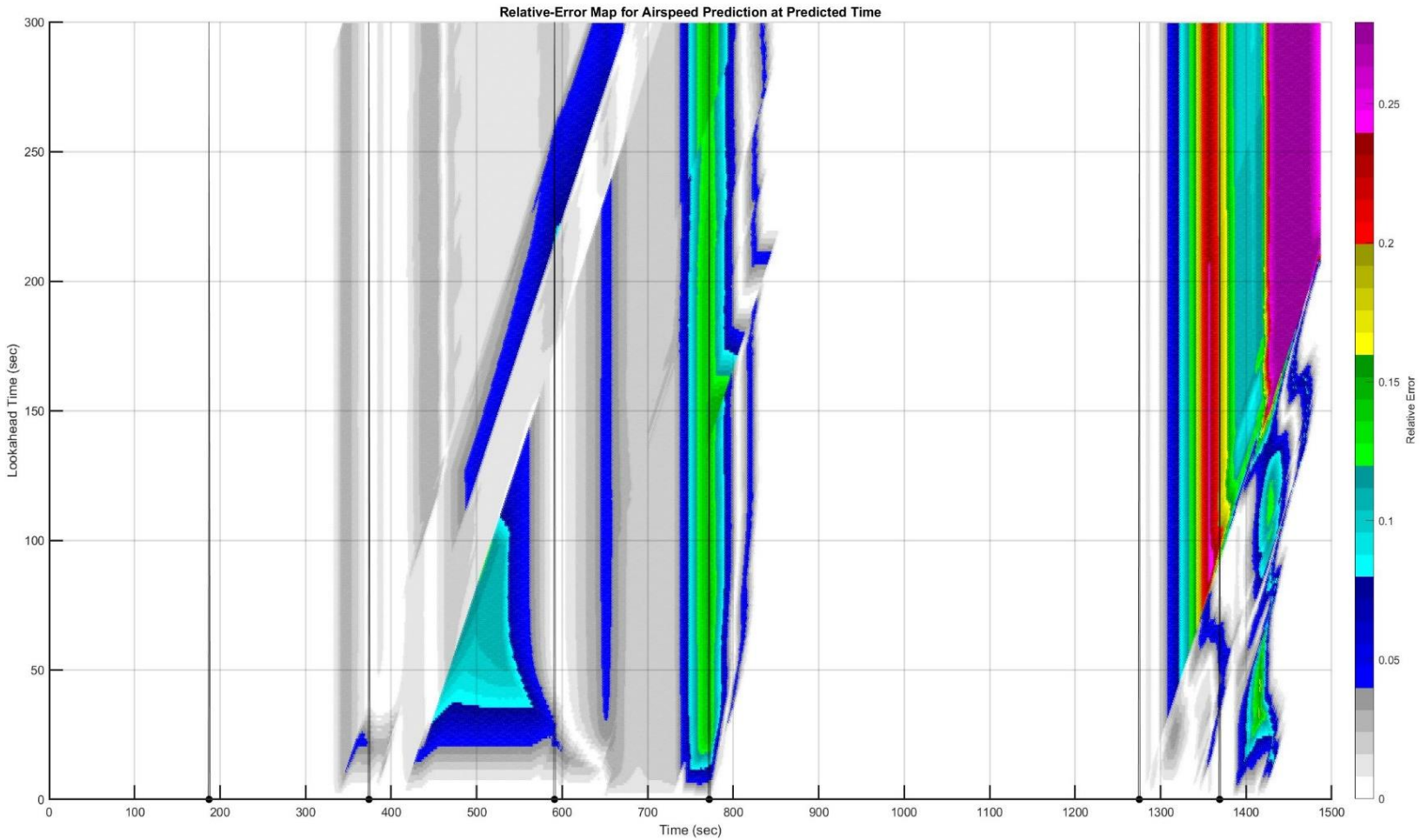

Figure C. 140: CONDR to Runway 36C: Heatmap of Airspeed Prediction Error (Time is $t + \tau$)

REPORT DOCUMENTATION PAGE

Form Approved
OMB No. 0704-0188

1. REPORT DATE *(DD-MM-YYYY)*
1-07-2019

2. REPORT TYPE
Technical Memorandum

3. DATES COVERED *(From - To)*

4. TITLE AND SUBTITLE

CASPEr: An Approach to Characterize the Performance of Onboard Airplane Energy State and Automation Mode Prediction Functions

5a. CONTRACT NUMBER

5b. GRANT NUMBER

5c. PROGRAM ELEMENT NUMBER

6. AUTHOR(S)

Torres-Pomales, Wilfredo

5d. PROJECT NUMBER

5e. TASK NUMBER

5f. WORK UNIT NUMBER
340428.04.90.07.07

7. PERFORMING ORGANIZATION NAME(S) AND ADDRESS(ES)

NASA Langley Research Center
Hampton, VA 23681-2199

8. PERFORMING ORGANIZATION REPORT NUMBER
L-21036

9. SPONSORING/MONITORING AGENCY NAME(S) AND ADDRESS(ES)

National Aeronautics and Space Administration
Washington, DC 20546-0001

10. SPONSOR/MONITOR'S ACRONYM(S)
NASA

11. SPONSOR/MONITOR'S REPORT NUMBER(S)
NASA-TM-2019-220289

12. DISTRIBUTION/AVAILABILITY STATEMENT

Unclassified-
Subject Category 03
Availability: NASA STI Program (757) 864-9658

13. SUPPLEMENTARY NOTES

14. ABSTRACT

The Commercial Aviation Safety Team (CAST) has identified a set of safety enhancements to mitigate the risks of loss of control in-flight (LOC-I) accidents and incidents involving commercial transport airplanes. In support of this, NASA has been developing technologies intended to enhance flight crew awareness of airplane systems, attitude, and energy state. This report describes preliminary ideas for a methodology to assess the goodness of onboard airplane energy state and automation mode prediction functions. The methodology is intended to contribute to the goal of moving these prediction technologies to the readiness level required for transition to industry and reduce the technology certification risks. In addition, this report describes a simulation-based approach named CASPEr (Characterization of Airplane State Prediction Error) to characterize the performance of these predictive functions over a wide range of operational conditions. The first exploratory version of this approach is described. The bulk of the report documents the initial results of tests to characterize the performance of an airplane trajectory prediction function. Future reports will give additional performance characterization results for this function and a complete description of the proposed methodology to assess such functions.

15. SUBJECT TERMS

Airplane Trajectory; Prediction Performance; Simulation; Situational Awareness; State Prediction

16. SECURITY CLASSIFICATION OF:			17. LIMITATION OF ABSTRACT	18. NUMBER OF PAGES	19a. NAME OF RESPONSIBLE PERSON
a. REPORT	b. ABSTRACT	c. THIS PAGE			STI Help Desk (email: help@sti.nasa.gov)
U	U	U	UU	248	19b. TELEPHONE NUMBER *(Include area code)* (757) 864-9658